Kansas Geological Survey

Detection and Characterization of the Distribution of Mineral Intrusion in the Great Bend Prairie Aquifer, South-Central Kansas

by

Glenn W. Garneau

Kansas Geological Survey Open-File Report 95-35
June 1995

GEOHYDROLOGY

KANSAS GEOLOGICAL SURVEY
OPEN-FILE REPORT 1995-35

Detection and Characterization of
the Distribution of Mineral Intrusion
in the Great Bend Prairie Aquifer,
South-central Kansas

by

Glenn W. Garneau

Disclaimer

The Kansas Geological Survey does not guarantee this document to be free from errors or inaccuracies and disclaims any responsibility or liability for interpretations based on data used in the production of this document or decisions based thereon. This report is intended to make results of research available at the earliest possible date, but is not intended to constitute final or formal publications.

Kansas Geological Survey
1930 Constant Avenue
University of Kansas
Lawrence, KS 66047-3726

TABLE OF CONTENTS

Acknowledgements and foreword. I would like to thank Robert W. Buddemeier for his excellent leadership and guidance as the Principle Investigator for the Mineral Intrusion Project at the Kansas Geological Survey (KGS). The Mineral Intrusion Project is funded by the Kansas Water Office and is a collaborative effort of the KGS and the Big Bend Groundwater Management District (GMD5). Special thanks also go to David P. Young of the KGS for his meticulous collection -- within the heart of the "Stafford Triangle" -- of excellent data that contributed to this thesis. I would also like to thank Don Whittemore, Marios Sophocleous, and Hillel Rubin (visiting scientist) of the KGS who have reviewed and participated in project developments. Other staff of the KGS who have contributed their expertise are Jim Butler, John Doveton, Al Macfarlane, and Mark Schoneweis. Persons who have provided insightful review and guidance are the past and present members of my thesis advisory committee: Ernie Angino, Carl McElwee, Antonis Koussis, and Don Steeples; staff of the GMD5: Sharon Falk (manager) and Dan Zehr (geologist); and the one who most encouraged me to take this new career direction: Sylvie Rueff.

I consider myself to be extremely fortunate to have been able to participate in this important research and development effort. This effort follows over 15 years of experience in the development and application of digital image processing methods at the NASA Jet Propulsion Laboratory. These applications ranged from the multispectral analysis of the rings of Saturn and Uranus to the atmospheric dynamics of Jupiter and Neptune[1]. This experience has allowed me to bring a fresh approach to what has been described as "one of the most difficult log analysis problems facing geologists"[2]. A new approach to the "shaly-sand" log analysis problem precludes the dogmatic methods that were developed for other applications and in an era before digital signal processing. While the approach presented here may not be universally applicable, I hope that it will encourage others to examine alternative approaches to water quality assessment using down-hole logging methods for environmental applications.

---

[1]AAAS *Science* **206**:4421 cover; **212**:4491 p.165; **215**:4532 p.532; **246**:4936 p.1431.
[2]AAPG Continuing Education Course Notes CE Note 31, 1990, *Log Evaluation of Shaly Sandstones: A Practical Guide*, by G. B. Asquith.

LIST OF FIGURES and TABLES

Abstract. An *ad hoc* procedure to determine ground-water quality from analysis of electromagnetic induction (EM) logs was developed to detect and assess the distribution of mineral intrusion into the Great Bend Prairie aquifer. The cross correlation between the EM and natural gamma-ray logs from a freshwater well was optimized (based on empirical statistics) to reduce variations on the EM log due primarily to the presence of clay minerals. The EM log correction method avoids the necessity for determination of variations of aquifer porosity or cation-exchange capacity for detailed log analysis of porewater conductance.

The correction method was applied to logs collected from a network of monitoring wells in the aquifer. The corrected EM logs (units of millisiemens per meter, mS/m) were calibrated to chloride concentration (mg/L) based on a highly significant linear-regression relationship (R=0.99) between the chlorinity of well-water samples and the median values of the corrected EM log for the screened intervals of the wells sampled.

The derived freshwater-saltwater transition zone profiles were processed by curve-fitting techniques to develop objective, quantitative estimates of key characteristics such as the saturated thicknesses of the usable fresh and unusable salt water (at the 500 mg/L chloride interface). The curve-fits also allowed incomplete aquifer transition zone profiles to be completed to the base of the aquifer by extrapolation. The transition zone characteristics provide a database for regionalization of saltwater distribution and for monitoring changes of the distribution at both local and regional scales.

Other applications of complete transition zone profiles include integration to determine and map the aquifer total salt load and to adjust measured fluid levels for the effects of variable density at monitoring sites. The adjusted fluid levels were used to map the equivalent fresh-water potentiometric surface and to map the distribution of vertical environmental-water head gradients within the aquifer. The profiles were also applied to calibrate a range of transverse dispersivity values for a conceptual model of solute transport. Comparisons of the model solutions with observed saltwater distribution indicates possible sources and

mechanisms of mineral intrusion at regional and local scales. The relevance of these applications to the apparent steady-state distribution of salt water is discussed in terms of development of a salt budget for the Great Bend Prairie aquifer.

INTRODUCTION AND BACKGROUND

Salt water intrudes into the Great Bend Prairie aquifer where the shallow alluvial aquifer is in contact with Permian bedrock formations containing evaporites such as halite and anhydrite (Figure 1). This is east of a north-south line approximately coincident with U.S. Highway 281 in south-central Kansas. The Mineral Intrusion Project of the Kansas Geological Survey and the Big Bend Groundwater Management District No. 5 (GMD5) is an investigation to determine the extent and rate of salt water intrusion into the eastern half (approximately 1800 sq mi) of GMD5 (Figure 2). Major objectives of the project are to develop appropriate methods and to collect sufficient data to determine the present salt distribution and to monitor changes of salt water in the aquifer for groundwater management decision making purposes. A complete statement of project objectives and approach is presented by Buddemeier et al. (1992).

This thesis represents a compilation of the contributions by the author to previously published mineral intrusion project status and data open-file reports (Buddemeier et al., 1993; Young et al., 1993; Buddemeier et al., 1994). In addition, this thesis presents further methods development and applied data analyses with discussion. The remainder of this introduction also includes a brief discussion of previous geohydrologic studies that are relevant to the intrusion of salt water into the Great Bend Prairie aquifer. A discussion of the distribution of clay in the aquifer is also of particular interest to both the distribution of salt water and the methods development for shaly-sand log analysis.

The method of log analysis developed by this thesis represents an *ad hoc* procedure to determine vertical water quality distribution from monitoring wells. This method, adapted from standard digital image processing techniques, exploits the inherent cross correlation between gamma-ray and electromagnetic induction logs. Application of this method avoids the traditional empirical log analysis techniques which require detailed *a priori* knowledge of aquifer porosity and/or clay mineralogy. The new log analysis method reduces the background noise or "shaly-sand"

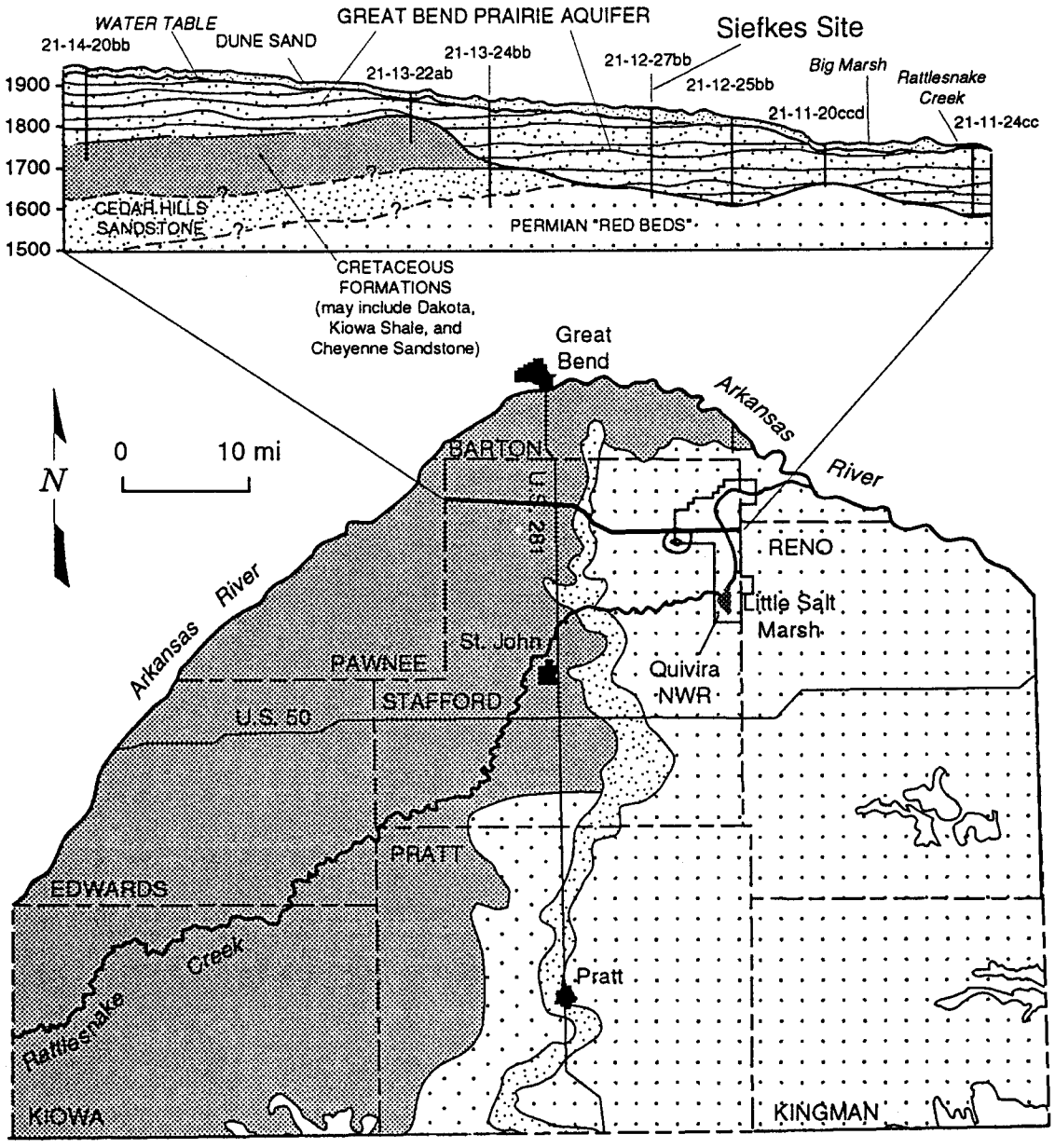

Figure 1. Location map and hydrogeologic setting. The Great Bend Prairie aquifer, a Quaternary alluvial deposit in South-Central Kansas, overlies the salt-containing Cedar Hills and other Permian formations. In the west, Permian formation brines are confined by the Cretaceous Dakota formation, but in the east, saltwater is free to mix upward and contaminate the overlying freshwater aquifer.

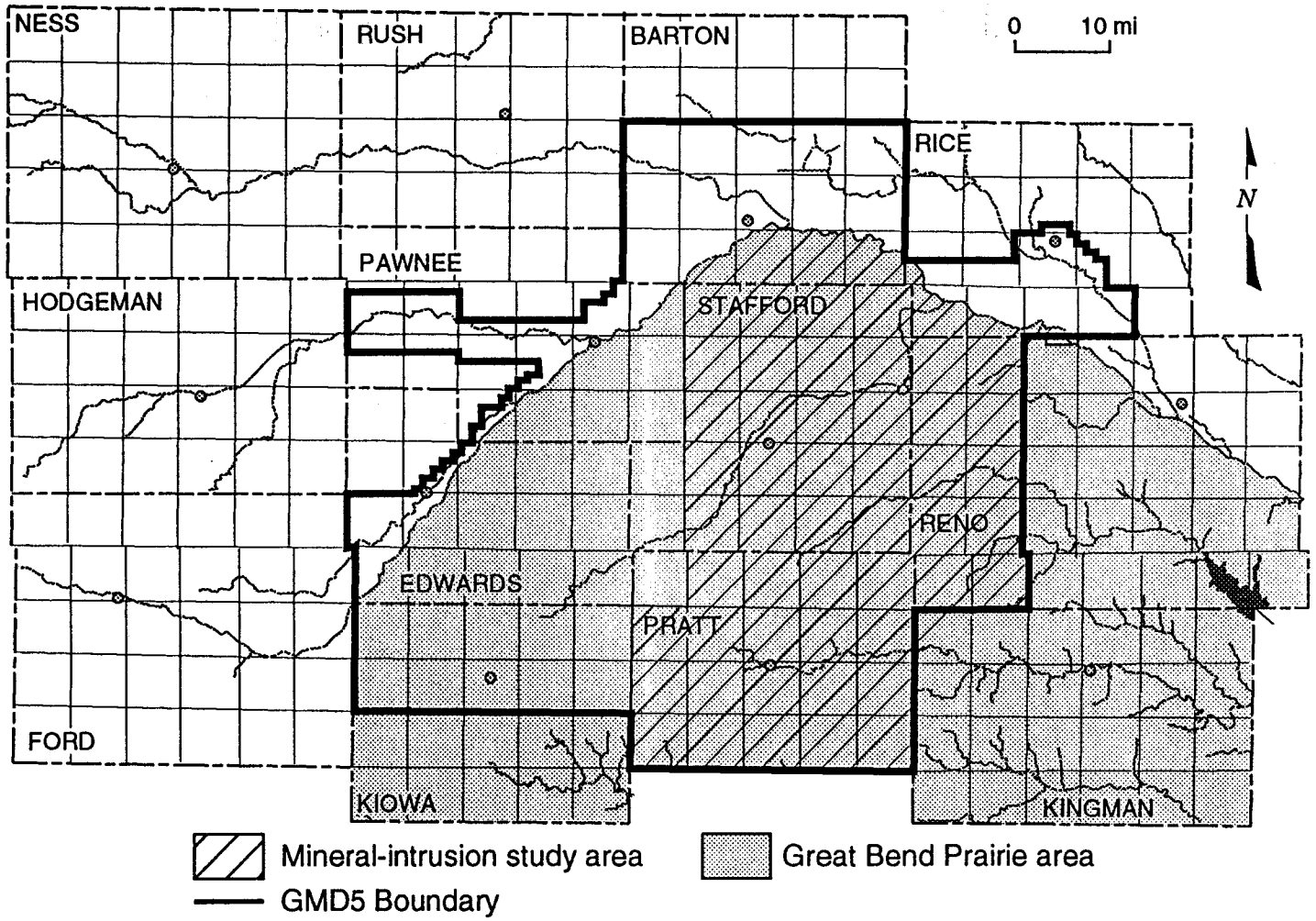

Figure 2. Map of the Big Bend Groundwater Management District (GMD5) showing the major features of the region and the area of primary interest to this study.

effects that confound ground-water quality resolution at levels corresponding to the transition from fresh to brackish water.

Curve-fitting techniques are applied to the processed logs (1) to estimate the freshwater-saltwater interface (defined as the 500 mg/L chloride level closest to the depth of the bedrock); (2) to complete the missing portion of log profiles at sites where the logging probe does not reach bedrock depth; and (3) to reduce the large volume of data represented by the processed logs to a manageable dataset that defines the freshwater-saltwater transition characteristics. The dataset of transition zone characteristics establishes a baseline reference with which to compare future measurements in order to detect and quantify temporal changes in the freshwater-saltwater distribution.

Regionalization of the freshwater-saltwater interface is accomplished by trend surface analysis through multiple regression of the elevations of the interface with elevations of the water table and bedrock surfaces. The results of the log analysis procedures are summarized in tabular form and the study area is mapped showing the percent of aquifer saturated thickness occupied by saline water exceeding 500 mg/L chloride.

This thesis also uses three applications to further analyze the freshwater-saltwater profiles derived from the methods developed herein. These three applications share a common and important element -- the analysis of the distribution of solute mass intruding into the aquifer. The first application integrates the vertical chloride concentration profiles to map the distribution of mass in the aquifer relative to a source brine with a chloride concentration of 42,000 mg/L. The second application uses the mass distribution to make adjustments for the effects of variable density on monitoring well fluid-level measurements, and to map the density-adjusted potentiometric surfaces and vertical head gradients. The third application experiments with a recently developed solute transport model -- an analytical model of advective and dispersive transport that considers solute-mass distribution within boundary layers. Each of these applications provides important input toward the future development of a comprehensive salt budget for the aquifer. The results of these applications are summarized with regard to implications for the apparent

regional steady-state distribution of salt water. However, results from monitoring the freshwater-saltwater transition zone near a seasonally pumped irrigation well show local upward penetration of saline water into the fresh-water portion of the aquifer. These observations and other freshwater-saltwater observations are summarized in appendices to this thesis.

Great Bend Prairie Aquifer

The Great Bend Prairie aquifer, part of the High Plains aquifer system, is a shallow (usually less than 300 ft thick from land surface to bedrock), alluvial aquifer of Quaternary age (2.0 ma to present). Groundwater resources of the Great Bend Prairie aquifer are managed by the Big Bend Groundwater Management District No. 5 (GMD5) by authorization under the Kansas Groundwater Management District Act of 1972 subject to the regulations of the Division of Water Resources and the Chief Engineer. The GMD5, created in 1978, adopted a policy of safe-yield management primarily through well-spacing requirements for the Great Bend Prairie aquifer (Jenkins, 1983; Smith, 1989).

Previous studies have been conducted to understand and quantify the critical geohydrologic parameters which govern the flow and availability of ground water in the Great Bend Prairie aquifer. The GMD5 and the KGS cooperatively constructed a monitoring well network in the eastern half of the GMD5. Cobb (1980) described the first several well-nest sites, located roughly on township corners (every six mi), usually with wells screened in the upper and lower alluvial aquifer and one well screened in the bedrock. The network of wells at 52 sites (Figure 3) allows sampling of ground water from different aquifer levels, measurement of fluid levels, hydraulic testing of the aquifer (slug and pumping tests), and geophysical well logging.

The intrusion of salt water into the Great Bend Prairie aquifer complicates the already difficult requirements of safe-yield management of ground-water resources in the GMD5. Salt water intruding into the aquifer from below reduces the fresh-water saturated thickness and thus limits the

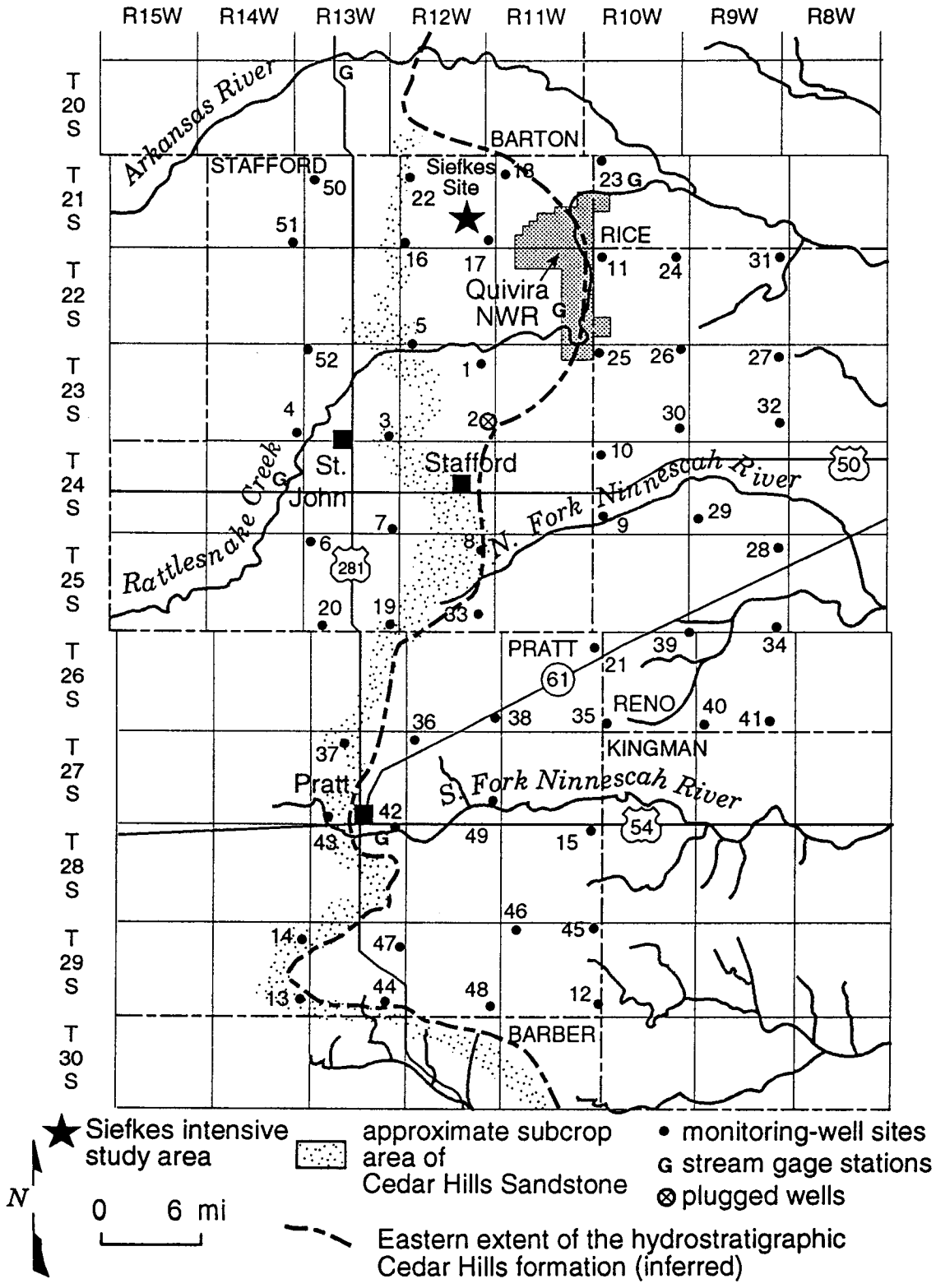

Figure 3. Observation wells and other physical features in the area of the KGS/GMD5 monitoring-well network.

usable resource to the upper part of the aquifer. Additionally, by pumping fresh water from the upper aquifer, an upward flow of salt water can be induced, further reducing the resource. Any enhanced flow of salt water into surface and shallow ground waters threatens municipal, agricultural, domestic, and wildlife resources. Currently, the GMD5 has established a moratorium on the development of new irrigation wells within much of the study area to prevent possible degradation of the fresh-water resource. The GMD5 management is particularly interested in obtaining any information on mineral intrusion processes that would warrant any changes to this policy.

Geology and geohydrology of the study area

Large areas of the south-central plains states of the U.S.A. are underlain by sediments of Permian age (230 ma) containing evaporites deposited in shallow, hypersaline environments (Johnson, 1981). Figure 4 is a paleogeographic map indicating the extent of Permian basin evaporite deposition that includes the study area. The evaporites, primarily halite with lesser amounts of anhydrite, occur as massive beds to isolated crystals and as major to minor cementing agents in these formations (Jordan and Vosburg, 1963; Holdoway, 1978). Several other studies have been and are currently being conducted to examine the various mechanisms and controls by which Permian evaporites are dissolved and flow into shallow ground and surface waters in other areas of the south-central plains (Morton, 1986; Gustavson, et al., 1980; Gustavson, et al., 1994; Richter et al. 1990).

Underlying the alluvium forming the Great Bend Prairie aquifer are sedimentary bedrock formations of Cretaceous age (65 to 145 ma) and Permian age (230-285 ma) (see Figure 1). A general stratigraphic column for the mineral intrusion study area is shown on Figure 5. During the hiatuses between deposition of the alluvium, Cretaceous, and Permian formations, subaerial exposure and erosion produced the subcropping bedrock pattern shown on Figure 1. Sophocleous and Stern (1993) have generated a topographic map of the bedrock surface from available well

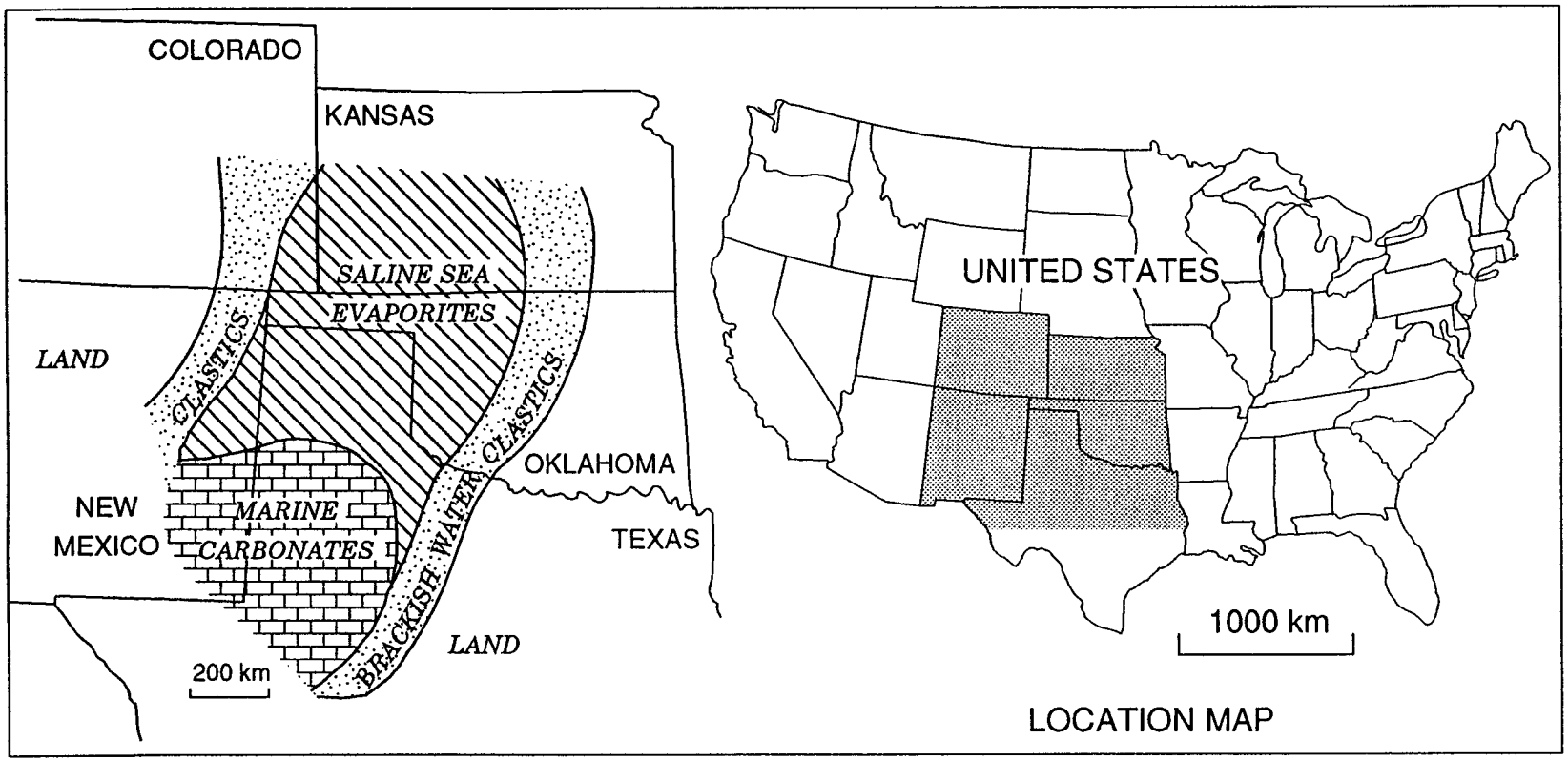

Figure 4. Paleogeographic map showing deposition of evaporite facies during the Permian (after Johnson, 1981).

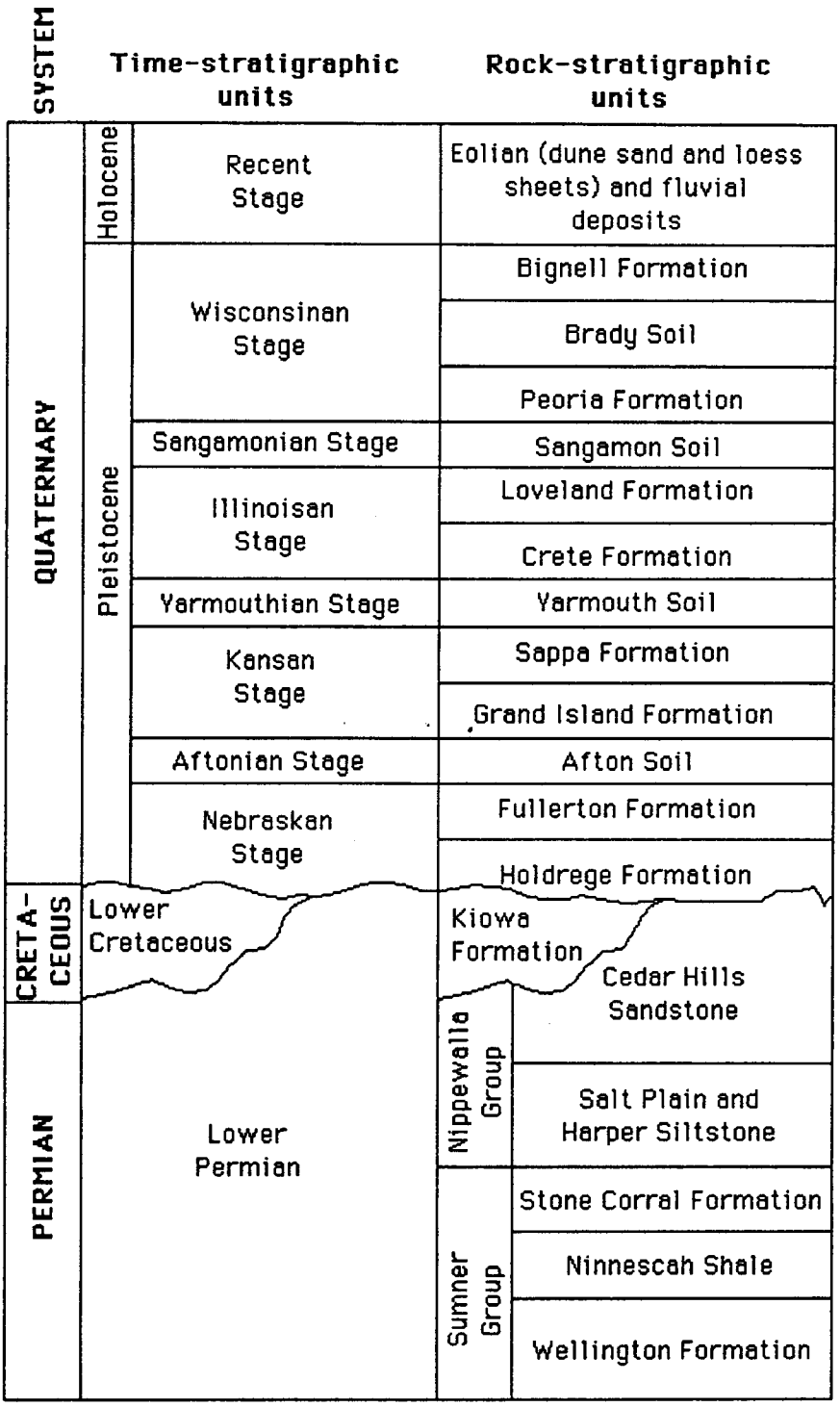

Figure 5. General stratigraphy of the mineral intrusion study area.
After: Fader and Stullken (1978); Bayne and O'Connor (1968).

control data (Figure 6). The bedrock topographic map shows the paleo-drainage system that developed on the bedrock with a general west to east flow pattern. The paleo-valleys, now filled with the alluvium forming the aquifer, may serve as possible collection areas or as drainage paths for salt water because of the greater density of the salt water compared to fresh water. Periods of subaerial exposure also probably resulted in weathering of the bedrock surfaces. The depth of the weathered surfaces depends on the length of exposure, topographic position, and the presence of easily weathered materials such as evaporites.

The geohydrology of the Quaternary Great Bend Prairie aquifer is described by Layton and Berry (1973) and Fader and Stullken (1978). The alluvial aquifer is composed of unconsolidated fluvial (streams), lacustrine (lakes and marshes), and eolian (wind) deposits of gravel, sand, silt, and clay. Gravel and coarse sand deposits represent stream channel and bar lateral accretion surfaces (Collinson, 1986). Fluvial deposits of fine sand, silt, and clay occur between the channels as levee, crevasse splay, and overbank flood deposits (Collinson, 1986). Fine-grained sediments can also accumulate as abandoned channel plugs and thus form thick, lens-shaped bodies of limited lateral extent (Hallam, 1981). Figure 7 shows the three-dimensional geometry of a characteristic sequence of alluvial deposits of fluvial origin.

Lacustrine deposits of fine-grained sediments form lens-shaped bodies of great lateral extent compared to thickness and often contain organic material such as peat (Allen and Collinson, 1986). The lacustrine environment of deposition on the Great Bend Prairie would today be represented by the Big and Little Salt Marshes located within the Quivira National Wildlife Refuge shown on Figure 3.

Eolian deposits are typically represented by fine-grained dune sand and loess (silt) (Welch and Hale, 1987). Dune sand, from sources along the Arkansas River, and loess deposits currently form a veneer over much of the Great Bend Prairie (Fader and Stullken, 1978). Three other major loess deposits are described in central Kansas representing the Loveland, Peoria, and Bignell formations (Bayne and O'Connor, 1968). Thicknesses of the usually sheet-like loess deposits in south-central Kansas are vague and can

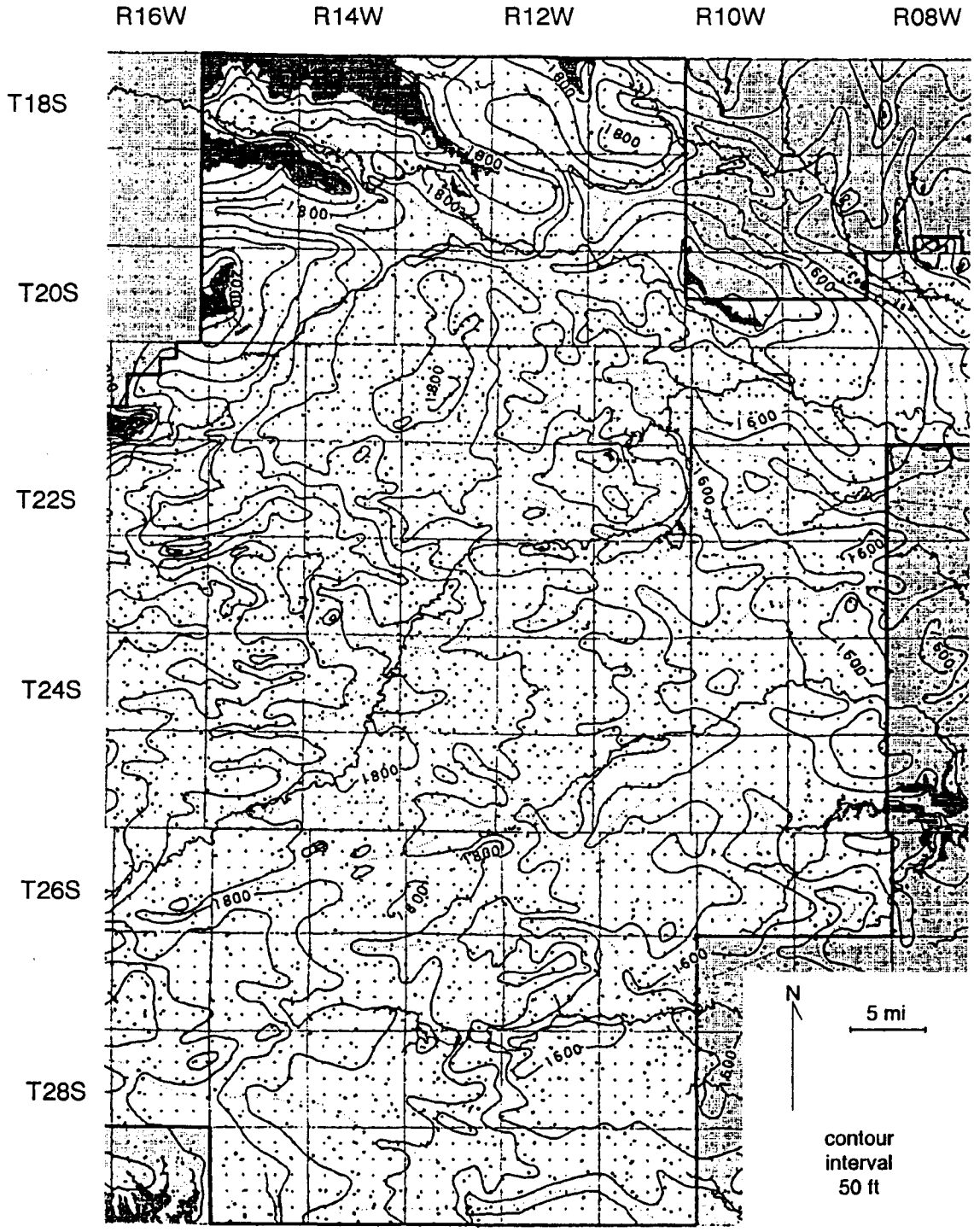

Figure 6. Topographic map of the bedrock surface below the mineral intrusion study area. Detail from map produced by Sophocleous and Stern (1994).

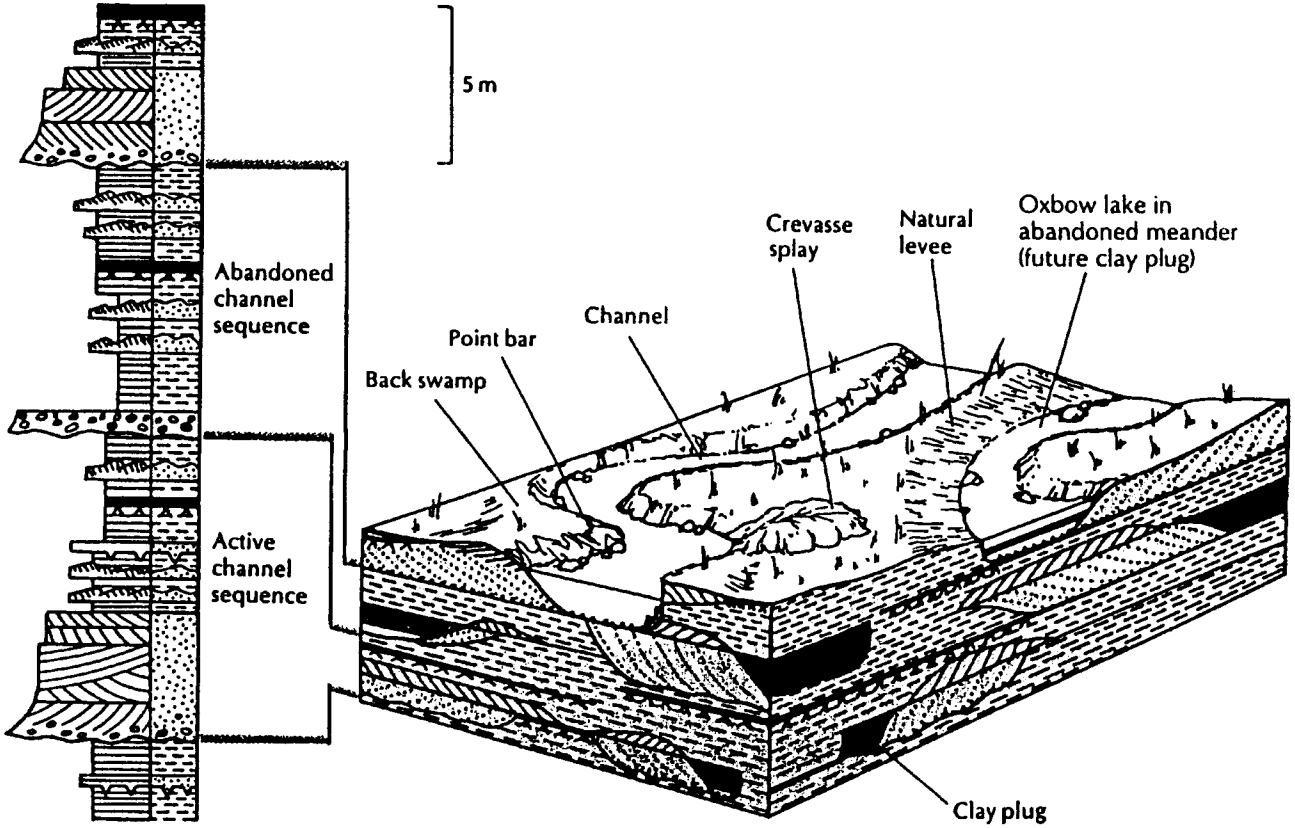

Figure 7. Three-dimensional geometry of alluvial aquifer deposits of fluvial origin (after Hallam, 1981). Clay-rich layers are commonly discontinuous on both depositional (clay plugs) and erosional (active channel) contacts.

be expected to be highly variable from reworking by erosion (Welch and Hale, 1987). Minor air-fall and reworked deposits of volcanic ashes have been detected in the alluvium with possible sources from eruptions in California, Wyoming, and New Mexico (Ward et al., 1993; Boellstorff, 1976).

Extensive clay layers have also developed in the Great Bend Prairie aquifer as the products of soil formation. Paleosols of Quaternary age in central Kansas include the Afton, Yarmouth, Sangamon, and Brady Soils (Bayne and O'Connor, 1968). Caliche horizons, usually associated with soil formation (Allen, 1974), are included on several well driller's lithologic logs and indicate the presence of paleosols (Stullken and Fader, 1976; Buddemeier et al., 1993; Gillespie and Hargadine, 1994). Thickness of clay layers developed from soil formation depend on the climate, length of time of soil development, and the nature of the parent material (Collinson, 1986). As with the loess deposits mentioned above, information on paleosol thickness and extent within the Great Bend Prairie aquifer is vague and incomplete.

The thickness of major clay layers can be determined roughly from well driller's lithologic logs or more precisely by geophysical methods. Signatures from natural gamma-rays emitted by radioactive isotopes of potassium, uranium, and thorium (K, U, Th), which are concentrated in clay minerals, can be detected on wire-line gamma-ray well logs. Rosner (1988) inferred a general relationship between gamma-ray emission rate and alluvial lithology for the Great Bend Prairie aquifer. Figure 8 shows that a detection rate of 50 or less counts-per-second (cps) corresponds to a clay-free sand and gravel interval and a count rate of 100 or greater cps corresponds to a clay-rich interval. Gamma-ray logging probes are commonly calibrated to the reference standards of the American Petroleum Institute to standardize the response of different detectors. However, the comparative count rate between different probes is of only minor import to this study. More important is the result indicating uniformity of gamma-ray log response to lithology. This result implies that log analysis procedures can be generalized for the entire study area.

Rosner (1988) subdivided the alluvium into a general three-layered stratigraphy using the analog gamma-ray logs from the network of

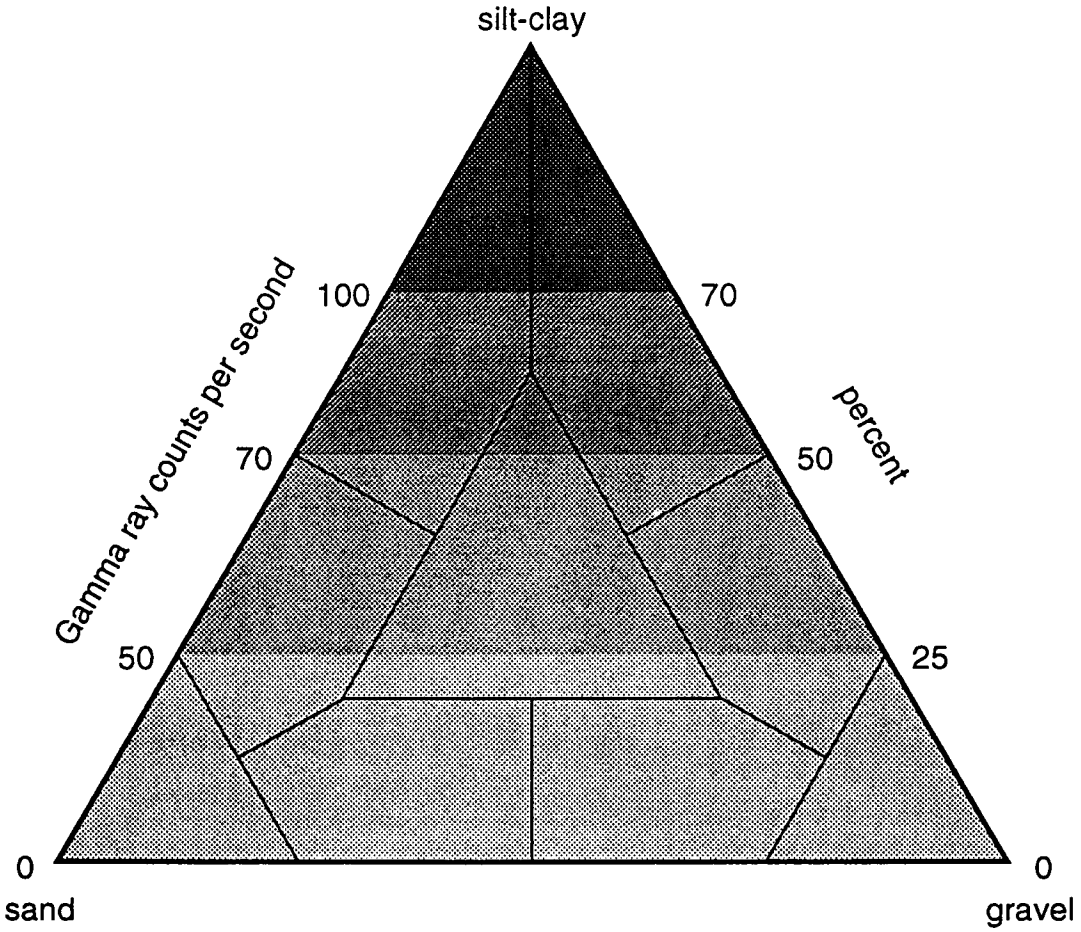

Figure 8. Lithologic ternary diagram for alluvial sediments of Great Bend Prairie after (Rosner, 1988).

monitoring wells. On top of the bedrock is a sequence of sand and gravel layers that is generally separated from an upper sand and gravel sequence by a silt and clay-rich layer of varying thickness. This three-layered description of the aquifer may tend to give the impression that ground water flow is effectively segregated or confined to layers of high hydraulic conductivity throughout the Great Bend Prairie aquifer. However, because of the several possible silt and clay-rich horizons deposited or pedogenically formed in the Great Bend Prairie alluvium (as discussed above), the ubiquitous presence of at least one thick, mid-depth silt and clay-rich layer should be expected. Furthermore, individual layers should not be considered continuous on more than a local scale because of difficulty in correlation from site to site and the fact that fine-grained layers are often discontinuous due to both depositional and erosional contacts (Figure 7).

The configuration and distribution of clay layers within the Great Bend Prairie aquifer are important factors to consider since these low-permeability horizons can control the vertical movement and distribution of solutes in the ground water. Salt water, seeping from the bedrock, can be effectively confined below an extensive clay layer. Conversely, in a situation where the salt water is flushed downward, such as in an area where salt has become enriched in the soil, the denser salt water can become perched on top of a clay layer. Alternating sand and clay layers can also influence the vertical and lateral macrodispersion of solute within an aquifer (Desbarats, 1990).

Young (1992) summarized the geohydrologic evidence for the interconnectedness of the Permian formations and overlying Great Bend Prairie aquifer. Salt water, primarily Na-Cl (halite) type, from dissolution of cements in the clastic red-bed Permian Cedar Hills Sandstone and Salt Plain Formation, seeps into the alluvial Great Bend Prairie aquifer in areas of direct connection between the Permian bedrock and the aquifer. The sudden increase of chloride concentration in ground and stream waters immediately east of the contact between the Permian strata and the aquifer is evidence for the natural source of salt water in this region (Cobb, 1980). The sudden increase also indicates that west of this contact the Cretaceous

strata (probably Kiowa shale) serve as an aquitard by generally confining the salt water within the Permian strata. Figure 3 shows the approximate position of the Cedar Hills Sandstone subcrop based on the map of Fader and Stullken (1978). Figure 3 also shows the approximate position of the eastern edge of the hydrostratigraphically-defined Cedar Hills Sandstone based on the map of Macfarlane et al. (1993). The two positions generally match up except in the northern part of the study area where the hydrostratigraphic unit extends much farther to the east than the original unit. This indicates that the northern part of the aquifer is in contact with a much larger surface area of sandy Permian units than the southern part.

Previous studies of stream-aquifer interactions on the Great Bend Prairie have been conducted for the Rattlesnake Creek watershed (Sophocleous, 1992; Sophocleous and McAllister, 1990; Sophocleous and Perkins, 1992) and the South Fork of the Ninnescah River (Moya, 1985; Gillespie and Hargadine, 1994). These studies have shown that these tributaries to the Arkansas River are gaining streams -- streams that rely on ground water to maintain a baseflow throughout their reaches during most years. Because the Rattlesnake and Ninnescah are gaining streams, the upward flow and discharge of ground water to the stream can cause salt water to flow upwards from the lower part of the aquifer and also discharge into the stream (Cobb, 1980; McElwee, 1984). The rapid increase in the salinity of Rattlesnake Creek immediately east of the contact of the alluvial aquifer and the Permian bedrock is evidence for this salt-water up-coning phenomenon (Sophocleous, 1992). Intermittent reaches of the South Fork of the Ninnescah River are also degraded by salt water discharging to the stream (Gillespie and Hargadine, 1994).

The localized discharge of saline ground water from the Great Bend Prairie aquifer to reaches of the South Fork of the Ninnescah River was investigated by Gillespie and Hargadine (1994). The authors suspected that the saline water originates from a possible zone of salt dissolution in the Permian Ninnescah Shale approximately 600 ft below land surface. Salt dissolution within the Permian bedrock formations can cause subsidence and collapse producing conduits for the potential upward flow of saline water. Dissolution and collapsed zones are frequently the source of salt

water discharge to the surface or near-surface in many parts of the Permian Basin (Johnson, 1981). Instances of subsidence and catastrophic collapse (sinkholes) associated with salt dissolution, in and around the Great Bend Prairie, have been reported by Walters (1978) and Whittemore (1993).

A summary of the available information on geohydrologic characteristics of both the Great Bend Prairie aquifer and the underlying bedrock formations has been compiled by Buddemeier et al. (1994). That report contains tables giving values for permeability or hydraulic conductivity determined from core samples, slug tests, pumping tests, and numerical modeling. The values can vary widely depending on location and the analysis performed, yet the contrast is typically at least an order of magnitude between the aquifer and the underlying bedrock.

The available information on ground water geochemistry from samples obtained from the monitoring well network has been summarized by Whittemore (1993) and is mapped on Figure 9. The geochemical survey shows the trend of increasing salinity with depth and the general distribution of salt water, primarily of Na-Cl type, in the upper and lower alluvial aquifer and the upper (10 to 20 ft) bedrock. These data have provided a basis for correlations between electromagnetic induction logs and water quality in the preliminary development of the methods described in this thesis and reported by Young et al. (1993).

Other possible sources and pathways of mineral intrusion into the Great Bend Prairie aquifer include abandoned boreholes, oil-field brines, and the evaporative enrichment of salt in shallow or poorly drained soils. Isolated instances of mineral intrusion from Permian brine and oil-brine leakage at storage facilities and insufficiently plugged or cased boreholes, and from soil-salt enrichment have been identified by Whittemore (1993 and pers. comm.). Whittemore (1993) was able to distinguish various brine types by using geochemical indices such as bromide-chloride ratios. All of these other possible sources are probably only a relatively minor contributor to the overall distribution of chloride in the Great Bend Prairie aquifer. However, the vertical distribution of chloride at a particular site can be complicated due to multiple sources and pathways.

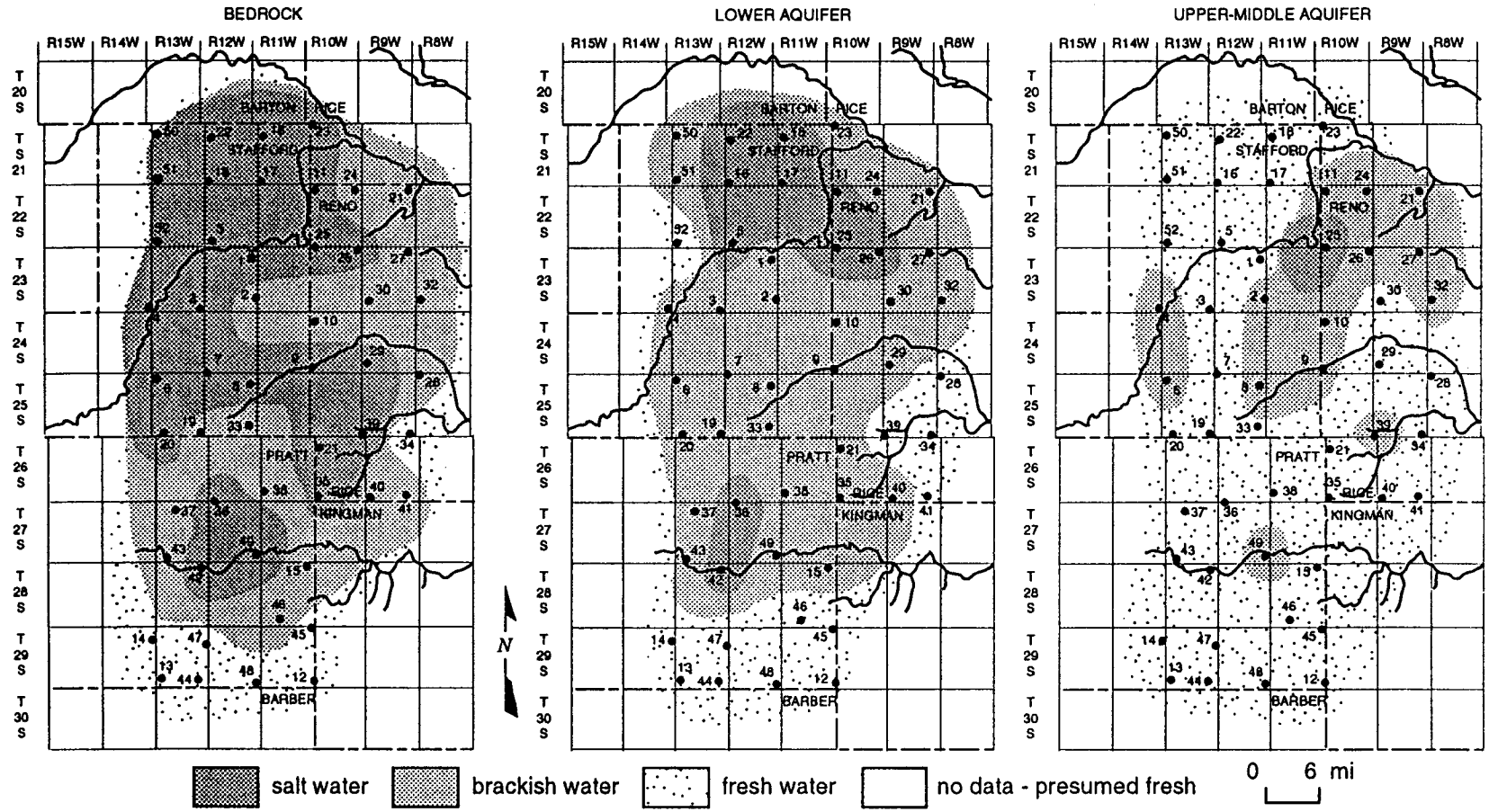

Figure 9. Maps showing catergories of groundwater quality based on conductiviity measurements at the numbered monitoring network sites; wells are identified as fresh (less than 1000 µS, or less than about 550 mg/l total dissolved solids (TDS)), brackish (1000-10000 µS, or 550-6000 mg/l, or saline (greater than 10000 µS or 6000 mg/l TDS). Boundaries are for purposes of illustration only. A: Bedrock (Permian) wells; B: Deep wells in the Great Bend Prairie Aquifer; C: Shallow and intermediate-depth wells. From Buddemeier et al., 1992.

Wireline log analysis in saltwater intrusion applications

Electrical and electromagnetic (EM) geophysical methods have been used extensively in oil exploration and increasingly in hydrogeologic applications (Gaither, 1994). Numerous empirical procedures have been developed to evaluate the results of EM surface and downhole surveys and to distinguish between the contributions of solid and liquid phase constituents to the EM observations. Of particular interest to this study is the analysis of the so-called "shaly-sand" problem--the variation of EM measurements caused by changes of the electrical properties of the background lithologic environment independent of pore fluid characteristics (Worthington, 1985). The background variations are caused by changes in mineralogy; particularly the presence of clay minerals with high cation-exchange capacities (hence the term "shaly-sand"). The superposition of lithologic background "noise" often confounds resolution in the critical region of transition from usable fresh to unusable salt water on electrical logs. The ability to reduce the variable background lithologic signal is of great importance for the accurate determination of water quality in mineral intrusion applications.

Traditional EM log analysis procedures are generally based on the empirical Archie (1942) formation factor relationship. The dimensionless formation factor (F) is defined for a uniform granular reservoir with a bulk conductivity (C_o) fully saturated with a fluid of uniform specific conductance (C_w) as

$$F = \frac{C_w}{C_o} \qquad (1).$$

The relationship is also further generalized for variable pore geometry characteristics as

$$F = \frac{a}{n^m} \qquad (2)$$

where: a is a pore geometry coefficient (usually assumed to equal 1 or $a < 1$ for intergranular and $a > 1$ for carbonates or fracture type porosity); n is the porosity; and m is a formation cementation factor (Kwader, 1985).

When the reservoir is not uniform, such as a sandstone with intercalated shales, equation (1) can be rearranged to include an additive term to account for variations of bulk formation conductivity. The excess conductivity of the clay minerals is represented by a shaly-sand term S so that

$$C_o = \frac{C_w}{F} + S \qquad (3).$$

The shaly-sand term approaches zero for a clean or clay-free sand and also becomes insignificant when compared to large values of C_w. Worthington (1985) classified the various methods of the shaly-sand term evaluation used for the determination of water saturation levels in applications for the hydrocarbon exploration industry. These methods can be grouped into two classes: one that calculates S based on the relative amount of clay present in the matrix--a volume of shale (V_{sh}); and one that is based on the ionic double-layer phenomenon of clay minerals. The first class requires that an independent determination of the matrix clay fraction be made. The other class requires *a priori* knowledge of the formation clay mineralogy so as to estimate the cation-exchange capacity to in turn estimate an appropriate S value.

Natural gamma-ray logs have been used to estimate the volume of shale (V_{sh}) for a formation. A gamma-ray index (I_{gr}) is determined by normalizing the gamma-ray log (GR_{log}) to the empirically determined maximum (GR_{max}) and minimum (GR_{min}) log values

$$I_{gr} = \frac{GR_{log} - GR_{min}}{GR_{max} - GR_{min}} \qquad (4).$$

The volume of shale is then estimated by applying still other empirically derived lithologic relationships, such as this example for unconsolidated Tertiary rocks (Dresser Atlas, 1979)

$$V_{sh} = 0.083[2^{(3.7*I_{gr})} - 1.0] \quad (5).$$

The determination of clay mineral electrical properties requires lab analysis of aquifer samples to determine a possible value for cation-exchange capacity. Cation-exchange capacity can vary widely from 5 to 15 meq/100g for kaolinites and from 100 to 150 meq/100g for vermiculites with overlapping ranges in between these value ranges for illites, chlorites, and montmorillonites (Domenico and Schwartz, 1990). The wide range of possible values makes estimation and application of an appropriate S value extremely difficult and often impractical.

Limitation of traditional shaly-sand techniques, *vis-a-vis* the determination of a continuously variable C_w (and thus water quality) in hydrogeologic applications, occurs because of the necessity of assuming a constant C_w as a calibration point for the other environmental parameters (porosity variables: n, a, and m) which must be estimated empirically on a site-by-site basis. The application of the various empirical shaly-sand methods is further limited by the complex interrelationships of the continuously variable porosity parameters. This level of uncertainty can exceed the total range of water quality values encountered in the formation (Worthington, 1976). Log analysis methods developed for oil exploration can therefore only resolve water quality variations corresponding to a level of thousands of mg/L chloride. In many environmental investigations, such as mineral intrusion into the Great Bend Prairie aquifer, water quality variations at the level of a few hundred mg/L of chloride need to be resolved.

This discussion of traditional log analysis methods demonstrates that alternative techniques for the determination of the vertical distribution of groundwater salinity must be developed for EM logging methods when complete *a priori* knowledge of the vertical distribution of porosity and or clay mineralogy within a formation is lacking. Gaither (1994) suggested that new analytical techniques need to be developed to perform log analysis in environmental investigations when the central assumptions used in hydrocarbon investigations are invalid. The central assumptions

in oil and gas exploration were designed to determine reservoir water saturation levels. These assumptions become invalid or tenuous at best in most environmental applications because water saturation is 100 percent. At this extreme value, general assumptions tend to break down and thus produce spurious results.

The high resolution requirements of environmental applications are discussed by Hallenburg (1992), who indicates that the spatial resolution of electrical tools should be comparable to the resolution provided by gamma-ray detectors for direct correlations between log types. The high resolution self-potential (SP) technique has been used successfully for the determination of water quality in geohydrologic applications (Alger, 1966). However, SP logging is limited to uncased boreholes because of the requirement of direct electrode contact with the formation. Therefore, the use of focused-induction EM methods in plastic-cased (PVC) boreholes is required to provide both the depth of investigation and vertical resolution necessary for detailed log analysis of water quality in unconsolidated aquifers.

Focused-induction logging probes have a series of coils which create an electro-magnetic field when current flows through them that is focused into the adjacent formation. This electro-magnetic field induces a secondary electro-magnetic field in the formation. The logging probe measures the strength of the secondary field as an indicator of the conductive capacity of the formation. The conductive capacity of the formation depends to some extent on the conductance of the solid matrix but primarily depends on the conductance of the pore fluids permeating the matrix. The importance of the volume of pore fluids (as a function of porosity) and connectivity of the pores to the formation conductivity is indicated by the Archie (1942) formation factor relationships (equations 1 and 2).

The "shaly-sand" problem is also present on focused-induction logs when variations in the conductance of the solid matrix are not overwhelmed by the conductivity of the pore fluid. These variations are especially apparent at low ionic concentrations of the pore fluid and thus often confound the resolution of the transition from usable fresh to

brackish water in aquifers. The following section presents a new method by which these variations are ameliorated for the preparation of continuous vertical water-quality profiles for the Great Bend Prairie aquifer.

METHODS DEVELOPMENT

Well logging

This investigation used a Century Geophysics UL-1000 data logger, portable drawworks, and a model 9510 combination natural gamma-ray and four-coil focused-induction logging probe. The radius of investigation of the electromagnetic induction is focused at 16 in (40 cm). Well logs were collected following the manufacturer's specifications: allowing the probe to equilibrate with the borehole fluid temperature for at least 30 min and logging at a rate of approximately 30 ft/min at 0.1 ft sampling intervals.

The monitoring-well sites typically have two wells screened in the alluvial aquifer: one in the upper aquifer and one near the base of the aquifer. Most sites also have a well screened in the bedrock. The Mineral Intrusion Project constructed two new wells in 1993 near an irrigation well at the Siefkes Intensive Study Site (Figure 3) -- one screened in the bedrock and one screened near the base of the aquifer (Buddemeier et al., 1993). The new wells were installed to monitor local changes in the freshwater-saltwater transition zone in direct response to irrigation pumping during the summer months.

The monitoring well network (Figure 3) was logged during March and April 1993--prior to the onset of the normal summer irrigation season before any possible changes to the freshwater-saltwater distribution were induced by high-volume pumping. Sites in the northern part of the study area, where the major salt-water intrusion problems exist (Buddemeier et al., 1993), were logged approximately monthly through the summer.

A drift of the baseline EM log response became apparent when comparisons were made between the initial set of logs and logs collected subsequently from the same sites. Figure 10A is an example that shows that the EM log drift is a simple offset in the signal independent of changes in the signal strength. Figure 10B shows the systematically upward EM log drift compared to the minor random fluctuations of the gamma-ray log. Because the drift is a simple, signal-independent offset, it is subtracted to cancel the offset and set the baseline response equal to the initial set of

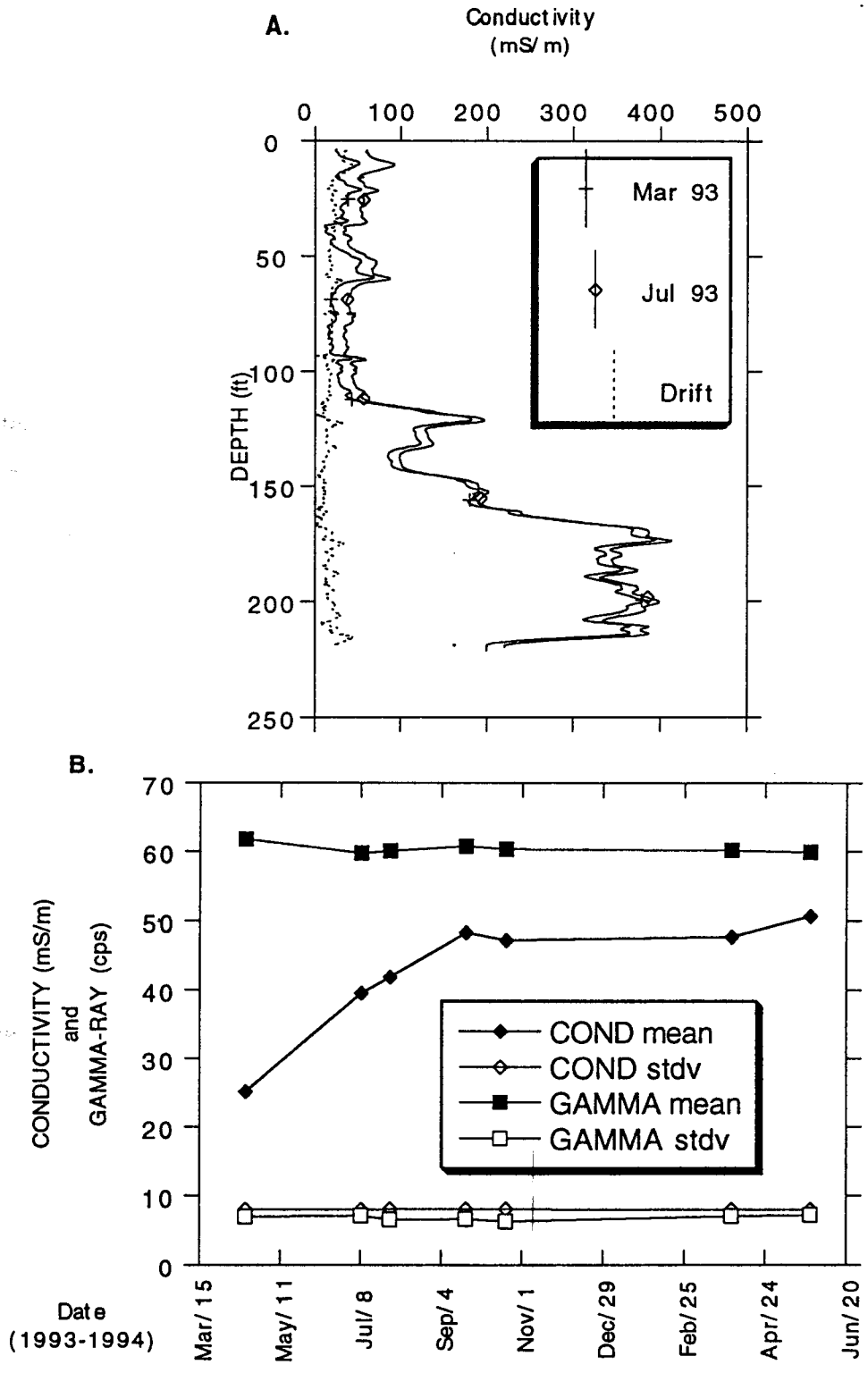

Figure 10. EM log drift. (A) Drift is constant independent of changes in signal strength at site 18. (B) Drift relative to minor random fluctuations of GR log.

logs. The drift offset was interpolated for logs collected between the points shown on Figure 10B by assuming a constant drift rate between dates.

Logs collected at site 50 (Figure 3) were selected to both measure the EM baseline drift and to provide statistics for the development of the lithologic ("shaly-sand") signal correction described subsequently in this thesis. Site 50 was chosen because it is west (and upgradient) of the region of salt-water intrusion (coincident with the contact of the subcropping Permian formations and the aquifer) and because of the ease of logging vehicle access. Site 50 has uniformly fresh water (approximately 40 mg/L chloride) throughout the saturated thickness of the aquifer: chloride = 37 mg/L in the upper and 42 mg/L in the middle well (Whittemore, 1993); and is expected to remain fresh in the foreseeable future.

GR and EM log cross correlation

Figure 11A shows the positive cross-correlation between the GR and EM logs from site 50 at the zeroth lag or sample offset. The cross correlation is due to the independent response of both logs to the presence of clay minerals in the aquifer. This cross correlation suggested that changes on the EM log due to lithologic variations may be reduced by subtracting some level of the processed GR log. The lithologic correction would exploit the inherent cross correlation to reduce the variations on the EM logs that are unrelated to changes of ground-water salinity. As was discussed in the Introduction to this thesis, a shaly-sand correction applied to the EM logs from all monitoring well sites would improve resolution of changes in ground-water salinity as well as estimates of total salt mass compared to the uncorrected logs.

The GR log used for the cross-correlation analysis is a five-log average using all of the GR logs collected at site 50 during 1993. The logs were averaged to improve the signal-to-noise ratio associated with the stochastic process of gamma-ray emission and detection. The cross correlation indicates a close spatial correspondence between both the GR and EM logs and lithologic changes at a site with uniformly fresh water. Comparable levels of cross correlation ($R > 0.7$ using single GR logs) were

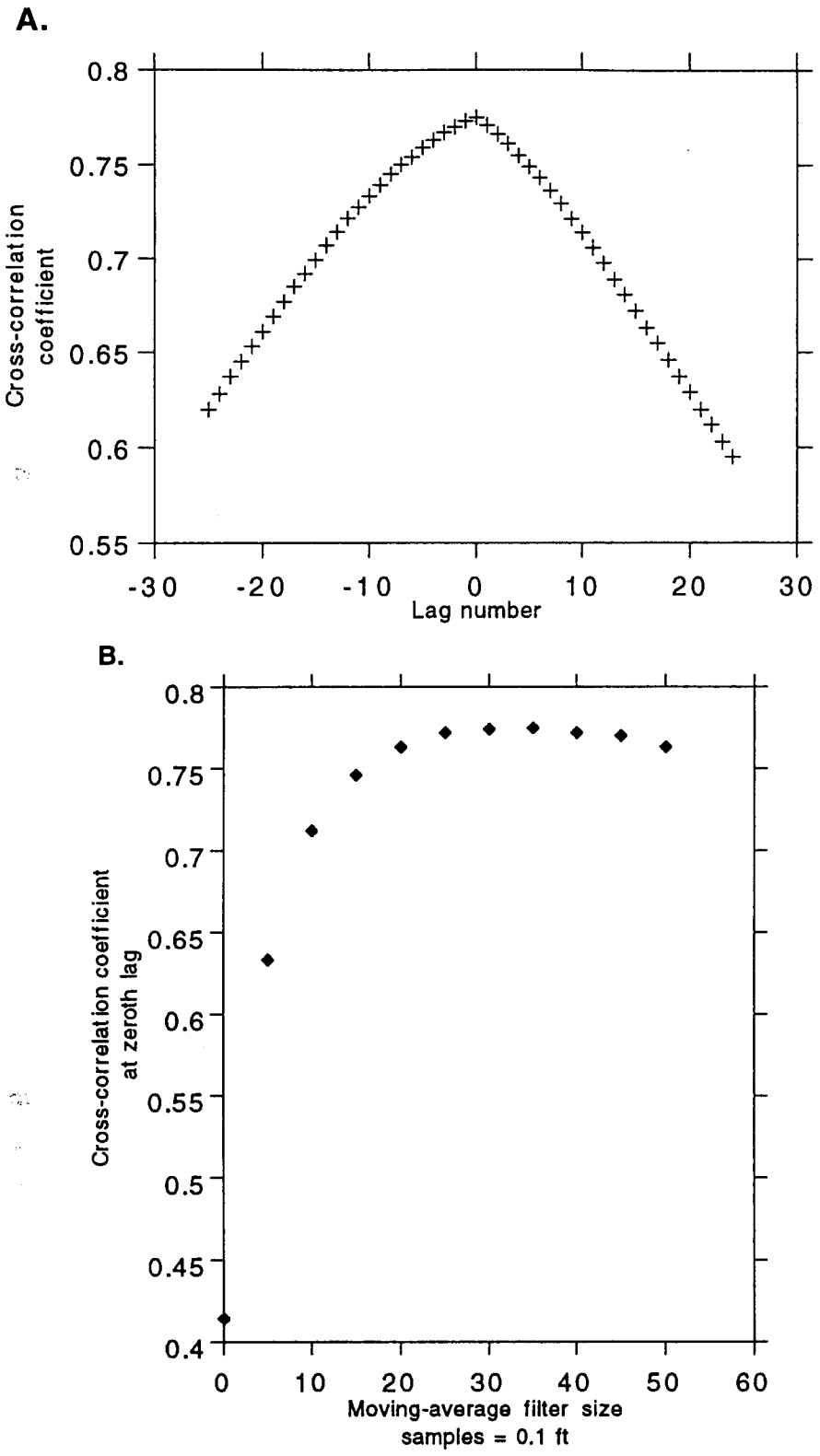

Figure 11. Cross correlation between gamma-ray and electromagnetic induction logs from a freshwater well (A). Optimization of cross correlation using a 35-sample moving average filter on the gamma-ray log (B).

obtained from analysis of logs in the fresh-water zone at sites 51 and 52. The EM and GR log cross correlation is thus assumed to be constant for the entire study area; this is consistent with the uniform GR log-to-lithology relationship inferred by Rosner (1988).

The cross correlation was optimized by adjusting the moving-average filter size for smoothing the GR log to achieve the highest correlation coefficient. Figure 11B shows that the optimum cross correlation is achieved using a filter size of between 30 and 35 samples. A moving-average filter of 35 samples ("boxcar" filter) was selected for this study because the rate of decrease of the correlation coefficient is less with a larger filter as compared to a smaller filter size (Figure 11B). Figure 12 parts A to C illustrates the results of GR log processing.

Shaly-sand EM signal correction

The following method of shaly-sand or lithologic background "noise" correction represents an adaptation of standard techniques applied in digital image processing. The reduction of non-periodic and stationary coherent noise in an image scene can be accomplished by subtraction of another image containing just the noise pattern (Castleman, 1979). The EM log is simply a one-dimensional image scene containing the non-periodic and stationary coherent shaly-sand noise pattern. The GR log is a one-dimensional image of just the noise pattern. The amplitude distributions of the EM and GR log noise patterns must be matched to optimize the removal by subtraction because the "images" were obtained from different sensors. Statistical matching of digital images for subtraction can be accomplished by standard amplitude histogram operations. The mean and standard deviation of one image histogram are matched to the histogram statistics of another image by standardization and renormalization (Castleman, 1979). The applications of GR log averaging (stacking) and moving-average filtering, described in the previous section, are also standard digital image processing techniques (Castleman, 1979).

The shaly-sand signal correction applied to well logs for this study was accomplished by conversion of the filtered GR log (GR_f) into

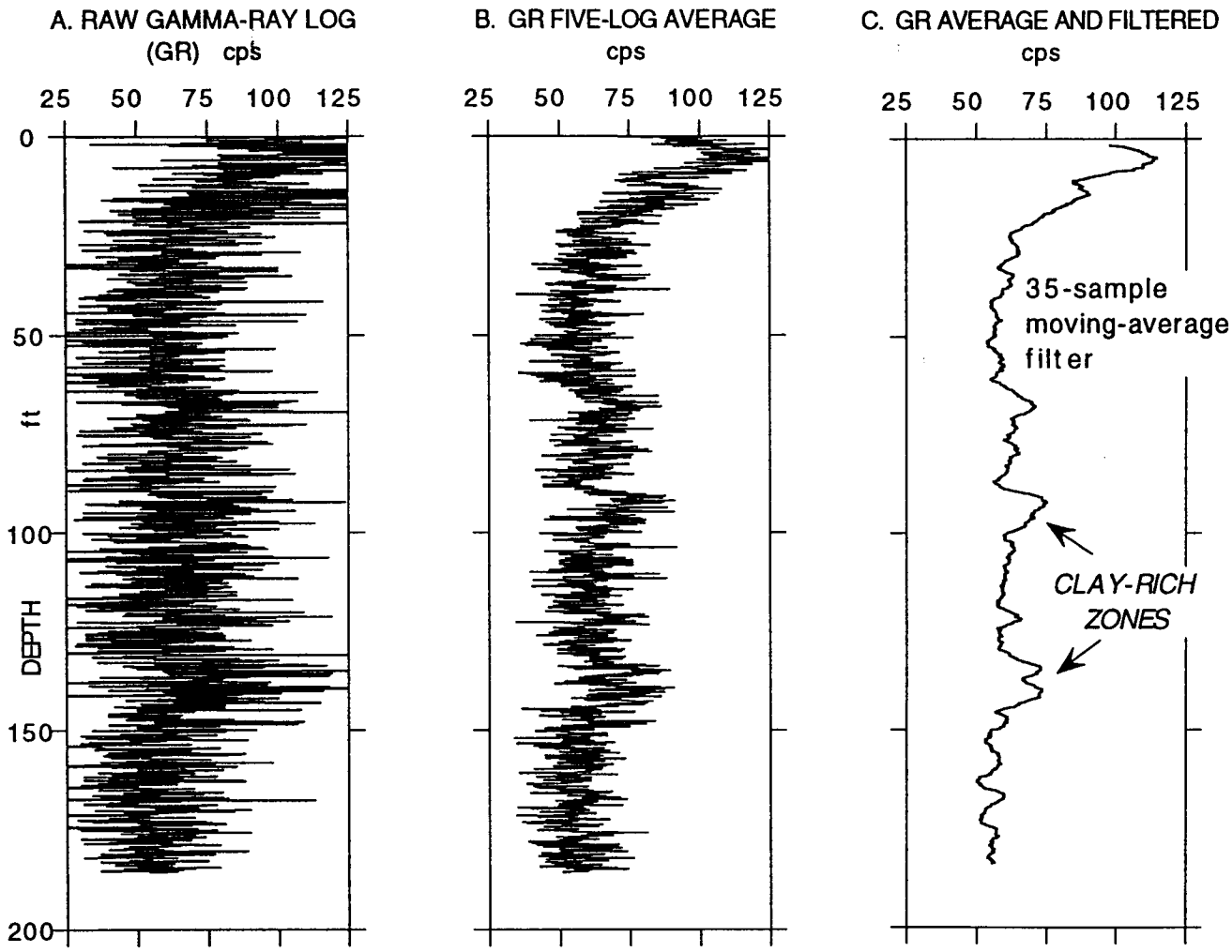

Figure 12 A-C. Steps in gamma-ray (GR) log processing.

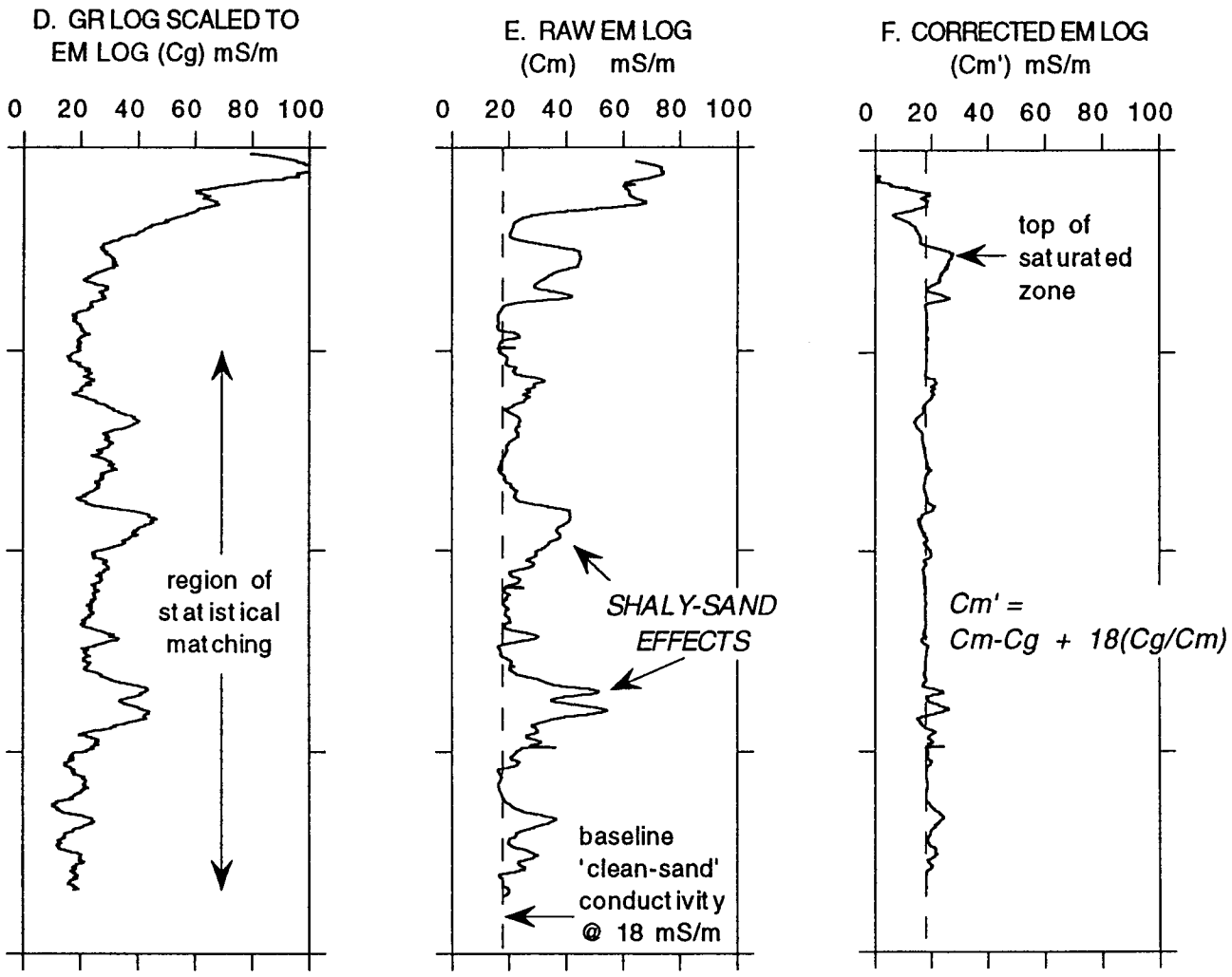

Figure 12 D-F. Steps in electromagnetic (EM) log shaly-sand correction.

conductivity units (millisiemens per meter or mS/m) with the same mean and standard deviation as the EM log. The conversion of the GR log (C_g) is made using the equation

$$C_g = \left[\frac{GR_f - GR_{fmean}}{GR_{fstdv}}\right] * EM_{stdv} + EM_{mean} \qquad (6)$$

where: GR_f is the 35-sample moving-average filtered GR log value, GR_{fmean}, GR_{fstdv}, EM_{mean}, and EM_{stdv} are the means and standard deviations of the site 50 GR (averaged and filtered) and EM logs. The statistics used in equation (6) were determined in the depth range of between 50 and 186 ft to avoid any effects of changes in the position of the water table.

Equation (6) accomplishes both the standardization and renormalization of the GR log. The terms within the brackets of equation (6) standardize the filtered GR log which results in a dimensionless series with a zero mean and a standard deviation equal to one. The GR log is then renormalized or statistically matched to the EM log by multiplying the dimensionless GR log series by the standard deviation and adding the mean of the EM log series. The two series now have the identical mean and standard deviation in addition to the spatial (cross) correlation and are logically considered to be in the same units (mS/m).

The renormalized GR log can now be subtracted from the spatially correlated EM-log to correct for the shaly-sand effects in the aquifer. The averaged, filtered, standardized, and matched GR log value (C_g; Figure 12D) is used to correct the EM log values sample-to-sample by the equation

$$C_{m'} = (C_m - C_g) + 18\left(\frac{C_g}{C_m}\right) \qquad (7)$$

where C_m is the raw EM log value (adjusted for any instrument drift) and the constant 18, in the second term, represents the empirical baseline (or "clean sand") conductivity at site 50 (Figure 12E). The second right-hand side (or "addback") term of equation (7) ideally maintains a positive baseline conductivity level of the corrected EM log. The 18 mS/m baseline is maintained because if C_m = 18 or if $C_m = C_g$ then $C_{m'}$= 18. Where the logs do

not match (i.e. $C_m \neq C_g$) the addback term limits over-correction of the EM log (creation of spurious negative values) at samples where $C_m < C_g$. The value of the addback term tends toward zero as the EM log value increases in response to increases of ground water conductivity; when $C_m >> C_g$ the conductivity of the porewater overwhelms the shaly-sand effects. Figure 12 parts D to F show the steps in EM-log background signal or shaly-sand correction.

Figure 12F shows that the corrected EM log from site 50 closely approximates the idealized flat response, at 18 mS/m, expected in a situation of uniformly fresh water permeating a uniformly conductive matrix. The corrected log ($C_{m'}$) is therefore a representation of a typical "clean" (clay-free) sand fully saturated with water with an average chloride concentration of approximately 40 mg/L (Whittemore, 1993) within the Great Bend Prairie aquifer.

The shaly-sand correction, based on the statistics determined at site 50, was then applied to all other pairs of logs collected at the other monitoring well sites. Figure 13 is an example of the correction applied to the EM log from a monitoring site (Siefkes Site; Figure. 3) that exhibits a distinct transition from fresh to saline water. This example demonstrates that the correction method maintains the EM response in the salt-water portion of the aquifer while significantly reducing the shaly-sand effects in the fresh-water portion. Reduction of the shaly-sand effects allows improved resolution of the important transition from fresh to brackish ground water.

The correction method developed in this thesis represents an *ad hoc* statistical approach to reduce apparent variations on the EM logs caused by factors independent of water quality in the aquifer. Therefore, the correction method must also maintain the primary electromagnetic response of the logging probe to the ionic strength of the porewater. The use of the GR log as proxy measure of the independent factors is similar in approach to the methods associated with other traditional empirical log analysis methods typified by equation (5). However, the correction method developed here also represents a straightforward linear approach that avoids the uncertainties associated with the estimation of aquifer

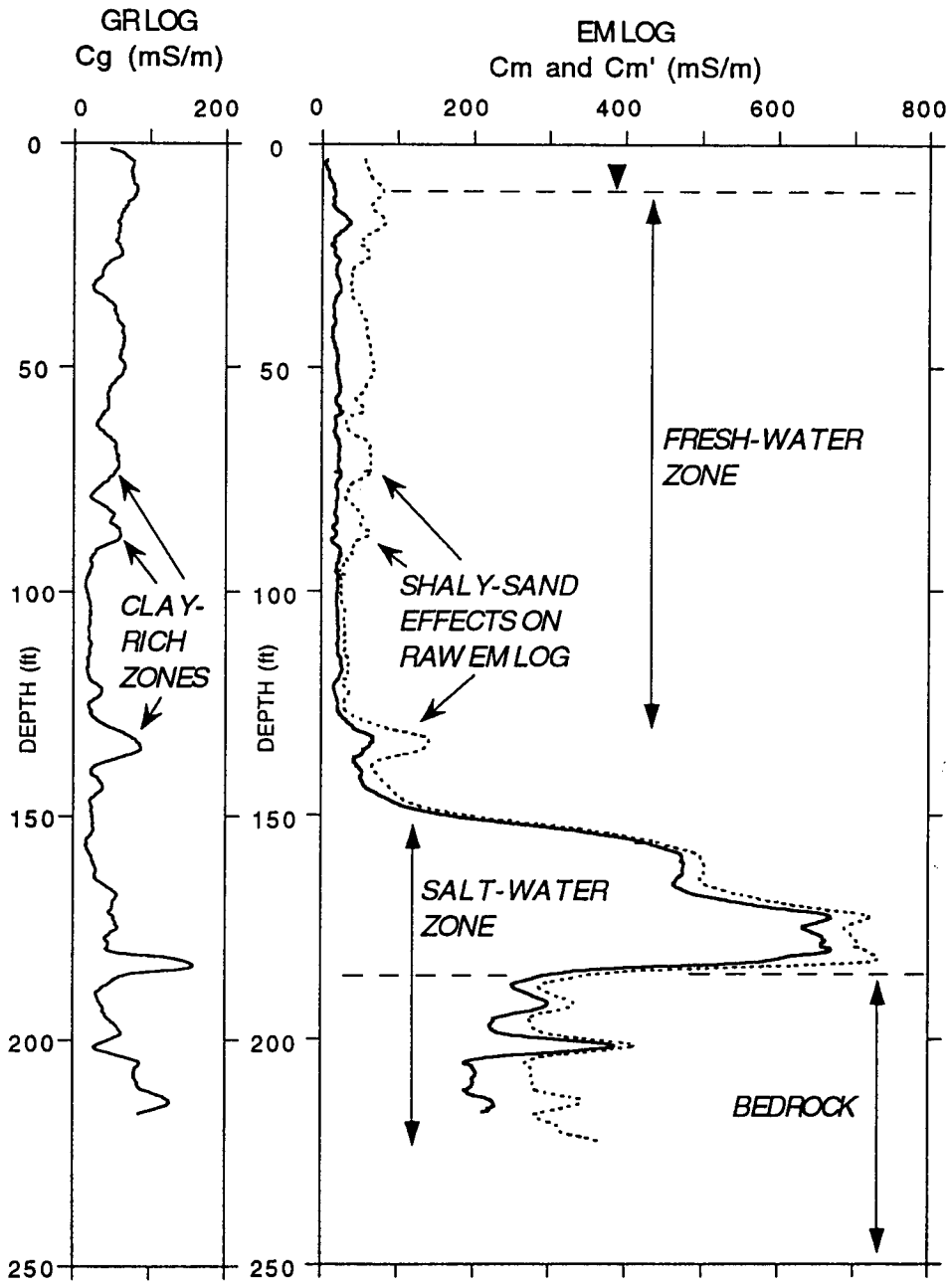

Figure 13. Example of shaly-sand correction applied to an EM log (dashed line) from a site (Siefkes) with a distinct transition from fresh to salt water.
Significant attenuation of shaly-sand effects is apparent on the corrected EM log (solid line) within the fresh water zone.
Attenuation is achieved through use of the matched GR log (see text) and preserves the primary EM signal response to salinity (conductivity) of the ground water.
The large decrease on the EM log below the transition from the aquifer to the bedrock is due to a decrease of porosity and the volume of salt water within the formation.

properties, such as porosity, required by traditional methods. Despite the *ad hoc* nature of this method, the techniques can be generalized for application to other settings given a comparable level of cross correlation between the GR and EM logs.

An alternative approach to the correction method of equations (6) and (7) would be to conduct a regression analysis of the GR and EM log relationship at site 50. This approach was not attempted here because of the difficult and arbitrary nature of the selection of weighting functions necessary for optimization of a regression function. Weighting functions are necessary in this case because of the presence of the baseline level (at 18 mS/m) or signal "pedestal" upon which the EM and GR log amplitude variations exist. A regression-based weighting function must somehow emphasize the highly-correlated amplitude variations while at the same time de-emphasize low amplitudes which are also highly correlated. The "addback" term used in equation (7) represents a very simple and deterministic weighting function that preserves both the amplitude attenuation and the baseline signal. This addback term also has an analog in standard image processing techniques. The application of scene-dependent filtering to images involves adding back some deterministic function of the original scene to the filter-modulated one (Castleman, 1979).

Calibration of corrected EM logs to chloride concentration

The corrected EM logs were compared directly and calibrated to parameters of water quality. The median conductance values of the corrected EM logs across the screened intervals (usually 5 ft) of wells completed in the lower Great Bend Prairie aquifer were compared to the specific conductance and chloride concentration values determined from the water-sample chemistry survey reported by Whittemore (1993). Only data from wells in the lower part of the aquifer were used for the calibration because these data are expected to be the least altered by dynamic processes in the aquifer. Figure 14 shows the linear regression relationships between the corrected EM log values (C_m') and both specific

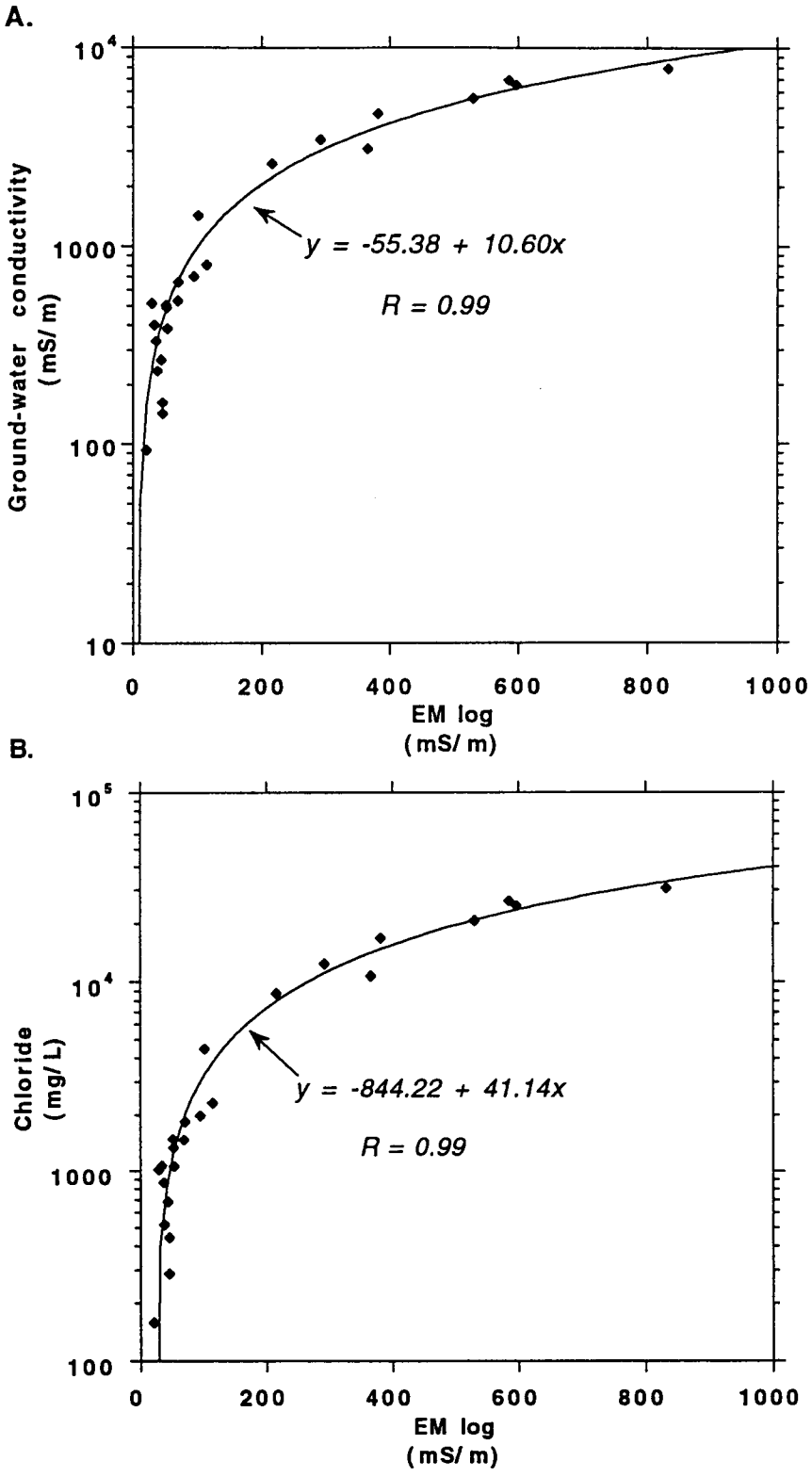

Figure 14. Linear regression relationships between the corrected EM log and ground-water conductivity (A) and chloride concentration (B).

conductance (1 mS/m = 10 mmho/cm) and chloride concentration (mg/L). The equivalent and highly significant correlations span the range (up to approximately 40,000 mg/L) of chloride concentrations encountered in the Great Bend Prairie aquifer.

The correlations of the corrected EM log data represented in Figure 14 do not vary significantly from correlations with uncorrected log data except for the offset caused by the shaly-sand correction (Young et al., 1993). This is because the monitoring wells were intentionally screened in the clean-sand portions of the aquifer where the shaly-sand correction should have a minimal effect. These equivalent correlations confirm that the shaly-sand correction does not alter the primary response of the EM log to ground-water conductivity while greatly reducing the spatial variability due to the shaly-sand effects.

The relationship between groundwater specific conductance (C_w) and the corrected EM log ($C_{m'}$) can be evaluated by use of the empirical Archie (1942) function because the correction method effectively eliminates the variable S or "shaly-sand" term in equation (3). By rearranging equations (1) and (2), taking $C_{m'} = C_o$, and assuming the pore geometry coefficient $a = 1$, then

$$\frac{C_w}{C_o} = \frac{1}{n^m} \qquad (8).$$

If the empirical cementation factor $m = 1.3$ for unconsolidated aquifer materials (Kwader, 1985) and $\frac{C_w}{C_o} = 10.60$ (the linear-regression slope coefficient from Fig. 14A), then solving for the porosity gives $n = 0.16$. This calculated porosity value is consistent with the typical midrange of 0.10-0.20 determined for the Great Bend Prairie aquifer (Bayne and O'Connor, 1968).

The other direct and significant relationship between chloride concentration (Cl) and $C_{m'}$ (Fig. 14B) allows conversion of the corrected EM logs into chloride concentration profiles with the equation

$$Cl = [41.14(C_{m'}-18)] + 40 \qquad (9)$$

where the numerical coefficients are: the baseline conductivity (18 mS/m) from site 50; the fresh-water chloride concentration (approximately 40 mg/L) from site 50; and the slope of the conductivity-chloride correlation linear regression from Figure 14B (41.14 mg/L per mS/m).

Chloride concentration profile curve fitting

Chloride concentration profiles were derived from the corrected EM logs using equation (9) and then processed by standard curve-fitting methods. The objective of the curve-fitting process is to reduce the large quantity of data represented by the corrected EM logs into a dataset of basic parameters which characterize the major freshwater-saltwater transition zone at each site. This dataset can then be used to compare fitted characteristics from site to site and to evaluate temporal changes in the freshwater-saltwater distribution. These characteristics include the transition zone thickness (width), the total concentration variation between fresh and saline water, and the depth to a threshold concentration or interface level between usable and unusable ground water. Significant temporal changes in these characteristics will indicate that salt water is undergoing vertical mass transport and is therefore not in steady-state conditions. The fitted profiles are thus idealized versions of reality related to an original source brine concentration and influenced by site-specific variations such as saturated thickness. Detailed salinity variations are therefore more accurately portrayed on the EM log-derived profiles as compared to the fitted profiles.

The transition zone profiles were fit to a mathematical model or paradigm associated with solute transport processes in a porous media -- the normal or Gaussian cumulative distribution function (Domenico and Schwartz, 1990). The normal distribution function (p) is defined by the frequency distribution mean (X) and standard deviation (σ) of a sampled variable (x):

$$p(x) = \frac{1}{\sigma\sqrt{2\pi}} e^{-\left[\frac{(x-X)^2}{2\sigma^2}\right]} \qquad (10).$$

The cumulative distribution function (CDF) of the normal distribution is obtained by integrating equation (10), and produces a characteristic *S*-shaped (sigmoidal) profile. The CDF profile is the archetypal representation of "breakthrough" curves generated by hydrodynamic dispersion or Fickian diffusion processes of solute transport in a porous medium. The fitted profiles can thus also be used to estimate aquifer characteristics such as dispersivity. The error function (*erf*) and complementary error function (*erfc*), which are often used to model solute distribution in a porous medium, are standardized (where: $X = 0$ and $\sigma = 1$) expressions of the CDF. The *erfc* profile represents the breakthrough curve or solute concentration transition zone produced as a result of column experiments conducted with a continuous source brine concentration (Domenico and Schwartz, 1990).

The transition zone profiles were fitted to CDFs by normalizing the chloride concentration values into percentages of the maximum concentration of salt water intruding into the aquifer within the study area. The value of 42,000 mg/L was chosen as the average maximum end-member concentration from the water sample concentrations reported by D. O. Whittemore (pers. comm.). Normalization of the transition zone profiles is required so that they may be plotted as normal probabilities versus depth. Schmorak and Mercado (1969) used equivalent methods to fit CDFs to freshwater-saltwater transition zone profiles for an investigation of salt-water intrusion into a coastal aquifer. In that investigation, the concentration in seawater was the obvious maximum end-member value for normalization. For this thesis, chloride percentage concentrations were calculated using the equation

$$Cl\% = \frac{MAX[40, Cl]}{420} \qquad (11)$$

where Cl is the derived chloride concentration from equation (9) and *MAX* is a function that selects the maximum log value of either 40 or Cl. Equation (11) sets the minimum concentration at 40 mg/L because this value represents the average freshwater concentration for the upper aquifer as was determined at site 50 (also from equation 9). The chloride concentration value is then divided by 420 to express the value as a percentage of 42,000 mg/L such that a value of 21,000 mg/L becomes 50%.

The transition zone region (D1 to D2; Fig. 15A) of the normalized chloride concentration profile is then plotted on depth-normal probability axes and fitted with a least-squares line (Fig. 15B). A straight line in normal probability coordinates plots as a CDF in linear coordinates. The transition zone limits D1 and D2 are selected (to the nearest foot) by visual inspection of the profiles such that D1 is the deepest part of the profile consistently below about 500 mg/L and D2 is either the depth of the greatest concentration on the profile within the aquifer or the bottom depth for incomplete logs. The equation for the fitted line (or CDF in linear coordinates), shown on Figure 15B, contains the mean (X) and standard deviation (σ) that define the normal distribution function of equation (10). The complete CDF profile is plotted in Figure 15C along with the normal distribution plotted as the derivative of the fitted CDF. The mean value (X) locates the depth of the inflection or mid-point on the fitted transition zone and the 50 percent probability value on the corresponding normal distribution curve (Figure 15C). Because the concentrations are all expressed as a percentage of 42,000 mg/L, the mean (X) estimates the depth of the 21,000 mg/L (50%) concentration of the idealized transition zone. The standard deviation (σ) provides a standardized measure of the width of the entire fitted transition zone (Figure 15C) because from normal-probability theory three standard deviations represents approximately 99.7 percent of the area enclosed by the normal distribution. Because the equation of the curve is fixed, the curve-fitting process can also be adapted to the characterization of the complete transition zone for wells that only partially penetrate the aquifer. The missing part of the transition zone is completed by extrapolation of the fitted curve, such as for the example of site 11 illustrated in Figure 15D.

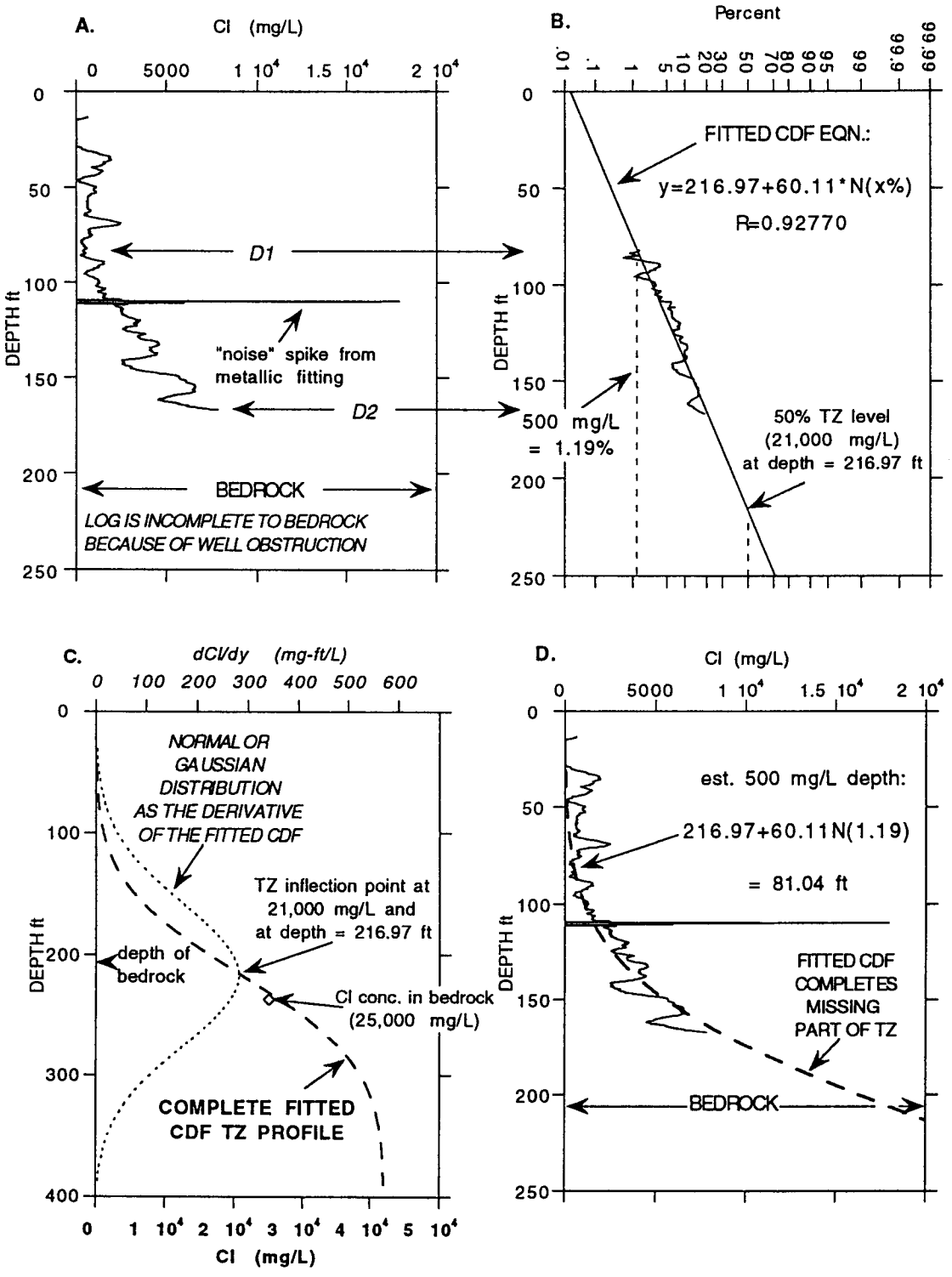

Figure 15. Example of a normal cumulative distribution function (CDF) fitted to the freshwater-saltwater transition zone (TZ) at site 11.

Site 11 is also an example of uncertainty in the location of an interface or threshold concentration value at levels of a few hundred mg/L within the upper 100 ft of the profile. The depth to the freshwater-saltwater interface at a concentration below about 3000 mg/L chloride cannot be determined directly on this and other transition zone profiles. These ambiguities may be shaly-sand effects that remain on the EM log after correction but more likely reflect actual variations of ground-water salinity within this zone. These salinity variations can be caused by both the downward movement of saline water from the surface or near-surface, and the lateral macrodispersion of saline water between alternating sand and clay layers. Areas of shallow downward movement of saline water may be locations of oil brine leakage from storage and transport facilities, or locations of salt build-up in soils. Areas of shallow macrodispersion may be located immediately down-regional gradient from areas of local discharging flow systems. Site 11 is down-gradient from where groundwater discharges to Rattlesnake Creek and Little Salt Marsh (Figure 3). Salt water brought up by the upward discharging flow may become perched or trapped between shallow sand and clay layers and then continue to flow down the regional gradient toward site 11.

The equations derived from the CDF curve-fitting process allow estimation of the depth to points with concentrations less than 3000 mg/L in the transition zone. For this thesis, the depth of the idealized 500 mg/L chloride interface is calculated for each of the sites with a transition zone with the curve-fit equation. For site 11, the 500 mg/L interface is calculated using the coefficients (X and σ) so that 216.97 + 60.11N(1.19) gives a value of 81.04 ft (Figure 15D). The value of N(1.19) equals approximately -2.26 (from standard statistical tables) and represents the normal probability of 500 mg/L expressed as a percentage of 42,000 mg/L (1.19%). Because of the selection criteria used to determine the fitted-curve endpoints (D1 and D2) described above, this calculated interface position estimates the first occurrence of fresh water (<500 mg/L chloride) in the aquifer above the bedrock.

The transition zone CDF fit typically represents an idealized freshwater-saltwater distribution unaffected by salt water intrusion from

surficial sources or shallow macrodispersive processes. At some sites the first occurrence of brackish water greater than 500 mg/L chloride below the water table will not be at the same depth as the fitted interface depth. The presence of shallow brackish water above the estimated interface is indicated on some of the profiles contained in Appendix I of this thesis and in the results of geochemical analyses of samples from the shallow monitoring wells (Whittemore, 1993) summarized in Figure 9.

The use of 42,000 mg/L as the average maximum brine chloride concentration for the study area provides a convenient value for the regional standardization of the transition zone profiles from site-to-site. However, the brine concentration at the base of the aquifer may be considerably less than 42,000 mg/L at a particular site. Using site 11 as an example again, the chloride concentration of the water sample from the bedrock well is 25,000 mg/L (Whittemore, 1993). Using this value to standardize the transition zone curve-fit for site 11 results in significant changes to the values of X (now the estimated depth to 12,500 mg/L) and σ yet the estimated depth to the 500 mg/L level shifts by less than 1 ft compared to the estimate using 42,000 mg/L. This small shift is considered well within the uncertainty of the estimate itself and justifies the use of 42,000 mg/L as a constant source brine concentration to standardize the transition zone parameters for the entire study area.

The means (X), standard deviations (σ), and correlation coefficients (R, Figure 15B) generated by the CDF curve-fitting process represent parameters which characterize the transition zone. These parameters provide an important dataset for regionalization of, and detection of systematic temporal changes in, the freshwater-saltwater distribution as it relates to other hydrologic factors. The values of D1, D2, X, σ, R, and the depth to the 500 mg/L chloride concentration interface are tabulated for all sites that have a transition zone in the RESULTS section.

Interface regionalization by trend surface analysis

Trend surface analysis is a geostatistical method by which map data, such as water table or stratigraphic elevations, are separated into regional

trends and local fluctuations (Davis, 1986). Both the water table and bedrock surfaces defining the saturated thickness of the Great Bend Prairie aquifer can be thought of as regional trend surfaces generally dipping toward the east.

Multiple-regression analysis of the elevations of the 500 mg/L chloride interface, determined from the curve-fitting process, with the elevations of both the water table and bedrock surfaces from Table I was conducted. Multiple regression is a method to test for a significant relationship between regional hydrologic trends and a potential trend surface defining regional salt water distribution in the Great Bend Prairie aquifer. A significant relationship allows regionalization of the 500 mg/L interface in between the monitoring well network sites but limited to areas of suspected mineral intrusion. Deviations from the multiple-regression interface trend surface may correspond to local fluctuations caused by local changes in the regional hydrologic trends. The results of the analysis are summarized in the RESULTS section, which follows.

RESULTS

Table I contains the results of the analytical methods applied to logs collected in the spring of 1993 and 1994 from monitoring well sites in the Mineral Intrusion study area that have a freshwater-saltwater transition zone (TZ). The estimated depth to the 500 mg/L chloride concentration level of the TZ is used to calculate the percent of saturated thickness occupied by saline water and is shown as contours (with a 20% interval) in Figure 16. Figure 16 shows one region of saline water exceeding 20% of saturated thickness occupying most of the study area and generally extending eastward from the western edge of contact with the Permian bedrock formations. Figure 16 represents a composite of results from 1993 and 1994 because there were only minor differences between the two sets of annual observations (see Table I).

Figure 16 also shows that within the main region of mineral intrusion there are three subregions that exceed 40% of the saturated thickness. The three subregions decrease in area from north to south and also coincide with the three largest streams flowing through the study area. The largest subregion occurs along the entire course of Rattlesnake Creek in the study area and extends beyond the stream to the eastern edge of the study area from where Rattlesnake Creek turns northward in the southeast portion of T22SR11W. This location is also the center of the area of greatest mineral intrusion (> 80%). The next largest subregion is centered in T25SR10W and is mainly just south of the North Fork of the Ninnescah River. The smallest and southernmost subregion is centered in the southeast part of T27SR12W and is mainly to the north of the South Fork of the Ninnescah River.

The largest subregion is the only part of the Great Bend Prairie aquifer with saline water that clearly and substantially extends to the west of the subcrop area of the Cedar Hills Sandstone hydrostratigraphic unit. This extension occurs along Rattlesnake Creek -- the only stream that flows for any significant distance west of the subcrop contact in the study area. The occurrence of saline water appears to be intimately connected with the hydrologic regime caused by stream-aquifer interaction. This type of

Table I.	Results of fitting cumulative distribution functions to the freshwater-saltwater transition zone at monitoring well sites for 1993 and 1994.						
Monitor Well Site.Year	D1 (ft)	D2 (ft)	X (ft) 21,000 mg/L	sigma (ft)	R	500 mg/L depth (ft)	change in depth (ft)
1.93	90	128	133.18	17.07	0.9909	94.6	
1.94	90	128	134.54	17.894	0.9892	94.1	-0.5
3.93	94	119	197.41	43.008	0.8229	100.15	
3.94	94	119	192.14	39.927	0.8102	101.85	1.7
4.93	80	100	177.57	49.714	0.764	65.144	
4.94	80	100	165.23	44.262	0.8814	65.127	-0.016998
5.93	66	106	98.876	12.641	0.972	68.288	
5.94	66	106	97.269	12.539	0.9754	68.912	0.624
6.93 bad data							
6.94	78	97	156.2	31.731	0.88445	84.445	
8.93 TZ @ BR						118	
8.94 TZ @ BR						118	0
9.93	40	79.5	90.065	17.336	0.5944	50.859	
9.94	40	79.5	88.037	16.182	0.5655	51.442	0.583
10.93	111	126	164.71	24.533	0.81843	109.23	
10.94	111	126	160.34	21.824	0.82634	110.99	1.76
11.93	82	167	216.97	60.108	0.9277	81.038	
11.94	82	167	226.16	66.184	0.912	76.429	-4.609
16.93	122	187	176.97	21.62	0.9691	128.08	
16.94	122	187	176.63	21.89	0.974	127.13	-0.95
17.93	61	100	111.1	20.366	0.9412	65.046	
17.94	61	100	111.02	20.488	0.9395	64.681	-0.365
18.93	107	172	182.26	31.753	0.8504	110.45	
18.94	107	172	181.63	31.233	0.8407	110.99	0.54
19.93	142	174	237.37	41.181	0.78367	144.23	
19.94	142	174	237.49	41.545	0.78048	143.54	-0.69
21.93	80	136	161.27	34.198	0.9653	83.934	
21.94	80	136	160.13	32.164	0.9642	87.387	3.453
22.93	133	204	198.15	25.648	0.9338	140.15	
22.94	133	204	197.82	24.549	0.9523	142.3	2.15
23.93	52.5	82	123.87	21.585	0.5614	75.05	
23.94	52.5	82	158.41	40.539	0.6778	66.732	-8.318
24.93	88	112	146.88	24.408	0.86403	91.68	
24.94	88	112	148.55	25.444	0.8805	91.008	-0.672
25.93	8	38	35.675	11.43	0.9346	9.827	
25.94	8	38	35.56	11.099	0.9477	10.46	0.633
26.93	64	102	102.11	12.625	0.9278	73.56	
26.94	64	102	106.61	17.432	0.9788	67.19	-6.37
27.93	53	66	78.229	7.5943	0.9907	61.054	
27.94	53	66	84.086	11.187	0.9905	58.788	-2.266
29.93	94	150	254.31	67.954	0.634	100.64	
29.94	94	150	248.73	64.379	0.6457	103.13	2.49
30.93	85	132	216.98	48.91	0.5368	106.36	
30.94	85	132	204.65	42.662	0.4906	108.17	1.81
31.93	73	90	196.27	52.737	0.8467	77.008	
31.94	73	90	192	50.257	0.8138	78.345	1.337
32.93	75	135	158.26	31.292	0.6085	87.497	
32.94	75	135	151.87	27.745	0.551	89.126	1.629
33.93	120	139	191.41	26.976	0.794	130.41	
33.94	120	139	176.71	18.718	0.8117	134.38	3.97

Table I. (cont.)							
Monitor Well	D1 (ft)	D2 (ft)	X (ft)	sigma (ft)	R	500 mg/L	change in
Site.Year			21,000 mg/L			depth (ft)	depth (ft)
35.93	115	142	186.37	27.447	0.8686	124.3	
35.94	115	142	188.79	28.937	0.8685	123.34	-0.96001
36.93	121	188	202.18	31.618	0.9544	130.67	
36.94	121	188	203.65	32.828	0.9462	129.41	-1.26
37.93	212	233	260.55	17.497	0.902	220.98	
37.94	212	233	259.04	16.663	0.9271	221.36	0.38
38.93	150	177	198.04	19.209	0.8461	154.6	
38.94	150	177	197.33	18.805	0.8577	154.8	0.2
39.93 TZ @ BR						55	
39.94 TZ @ BR						55	0
42.93	74	149	187.52	37.412	0.93	102.91	
42.94	74	149	188.01	37.263	0.9392	103.74	0.82999
43.93	40	55	61.092	7.1996	0.9387	44.81	
43.94	40	55	60.55	6.8257	0.938	45.113	0.303
49.93 no data							
49.94	40	70	87.128	17.603	0.9264	47.139	
SP.93	123	180	166.76	16.647	0.97414	129.12	
SP.94	123	180	166.18	17.069	0.97529	127.57	-1.55
SD.93	123	156	164.05	15.296	0.84618	129.46	
SD.94	123	156	164.27	15.454	0.80825	129.32	-0.14
NOTE: logs at sites 8 and 39 indicate major transition zone at base of aquifer.							

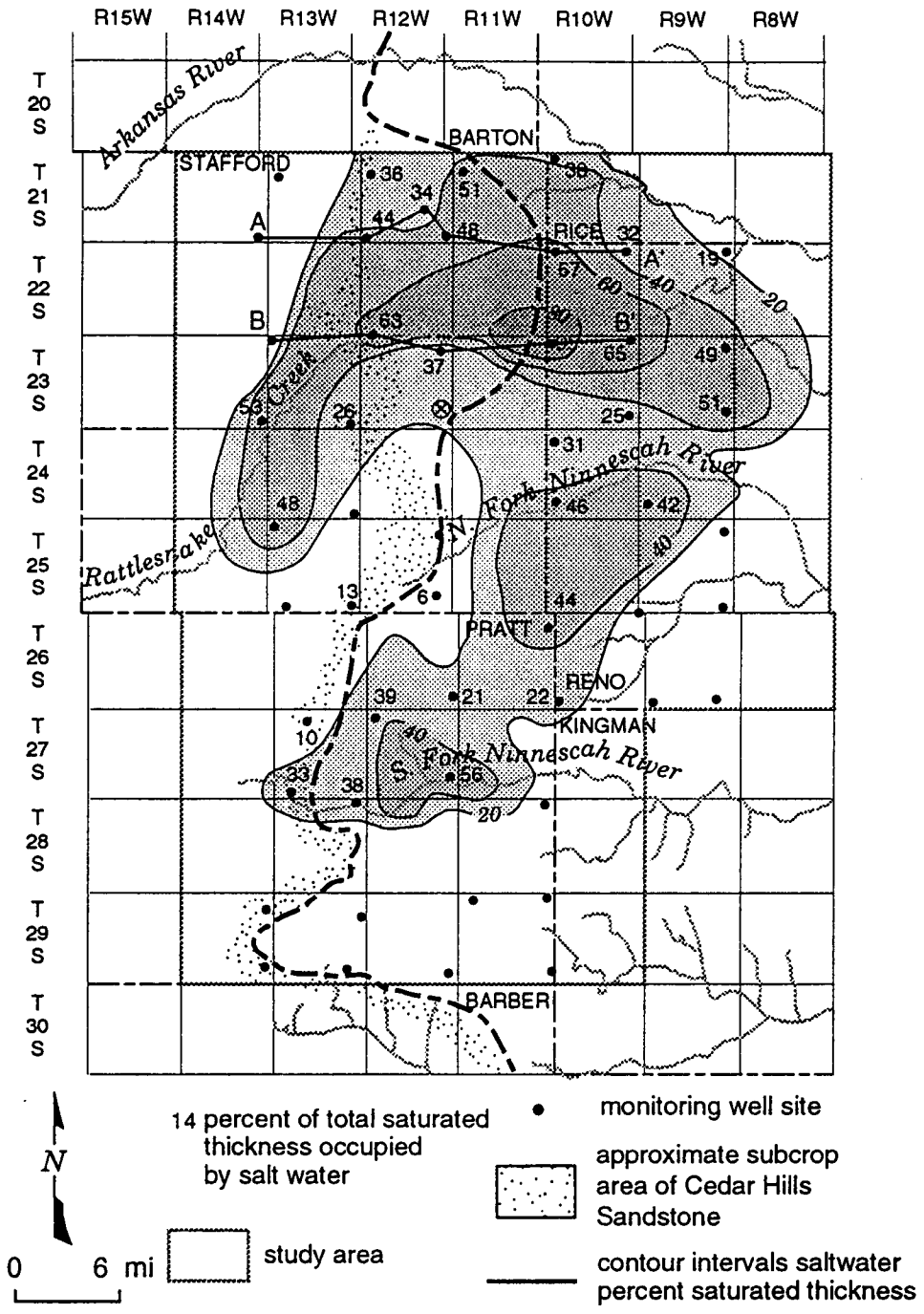

Figure 16. Percent of total Great Bend Prairie aquifer saturated thickness occupied by water with a chloride concentration greater than 500 mg/L, based on freshwater-saltwater transition zone estimates from cumulative distribution function curves fitted to the profiles. Composite of data from 1993 to 1994.

interaction is further illustrated by cross-sections through the largest area of mineral intrusion. Inferred on Figure 17A and shown on Figure 17B is the sharp increase of saline-water saturated thickness near Rattlesnake Creek indicating upconing caused by groundwater discharge to the stream. Discharge of saline ground water to Rattlesnake Creek and to the South Fork of the Ninnescah River was determined by previous studies (Cobb, 1980; Gillespie and Hargadine, 1994) to be the principal mechanism of stream water salinization. The discharge of saline water to streams is probably an important component in the over-all salt budget of the aquifer.

Figure 17B also shows the perching of saline water on clay lenses in the subregion to the east of where Rattlesnake Creek turns northward. At least three discrete, perched transition zone intervals occur within the aquifer at site 26. Other sites that appear to have perched saline water intervals within the general transition zone from fresh to salt water are 4, 11, 18, 19, 25, 33, 37, and 49 (see profiles in Appendix II). Most of these perched interval sites occur on the east side of the study area and are down-gradient from areas of salt-water upconing caused by discharge along Rattlesnake Creek. Perching of saline water on clay lenses complicates interpretation of the vertical distribution of water quality leading to underestimation of overall water quality and must be considered in order to accurately portray the regional distribution of salt water.

Figure 17A also suggests the freshwater-saltwater interface between sites 16, SP, and 17 is both smooth and flat compared to either the land or bedrock surfaces. This feature gives the salt water in this area the appearance of being 'ponded' such that the salt water approaches a horizontal static level between subcropping bedrock ridges on the west and east.

Trend surface analysis of the 500 mg/L chloride interface

Figure 18 shows that a significant multiple-regression relationship (R= 0.90) exists between the calculated 500 mg/L chloride concentration elevation in the transition zone and the elevations of the water table and

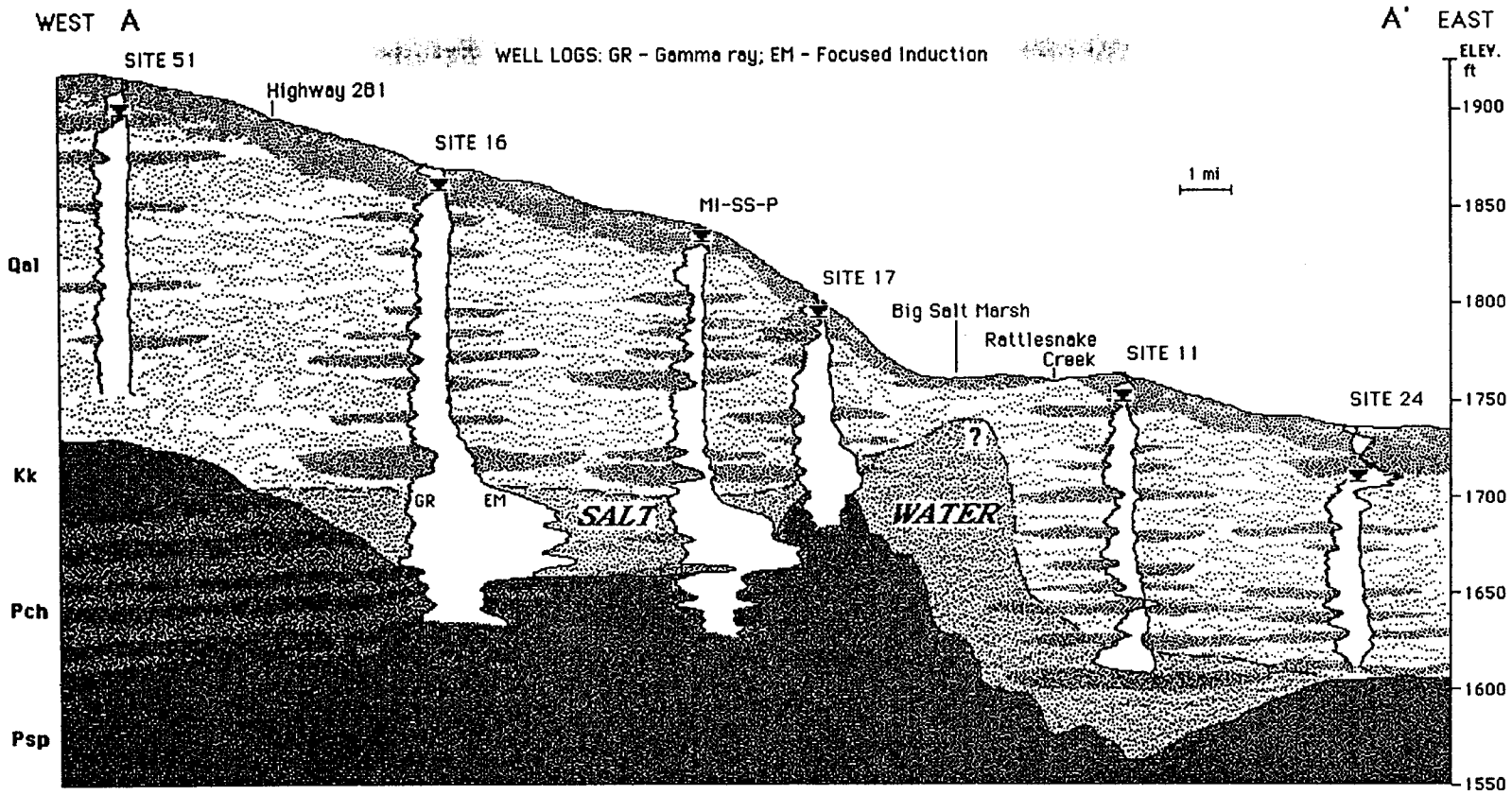

LITHOLOGY: Qal - Quaternary alluvium (fluvial and aeolian); Kk - Cretaceous Kiowa Formation (shale); Pch - Permian Cedar Hills Formation (siltstones and sandy siltstones); Psp - Permian Salt Plain Formation (sandy siltstones and fine-grained sandstones)

Figure 17A. Cross section AA' (Figure 16) showing estimates of clay lenses (dark stippling) inferred from gamma logs and of salt water distribution (light stippling) inferred from conductivity logs. The dashed line indicates the estimated elevation of the 100 mS/m (C'm) transition zone boundary. At each site the left-hand vertical trace is a reproduction of the gamma log and the right-hand trace a reproduction of the conductivity log.

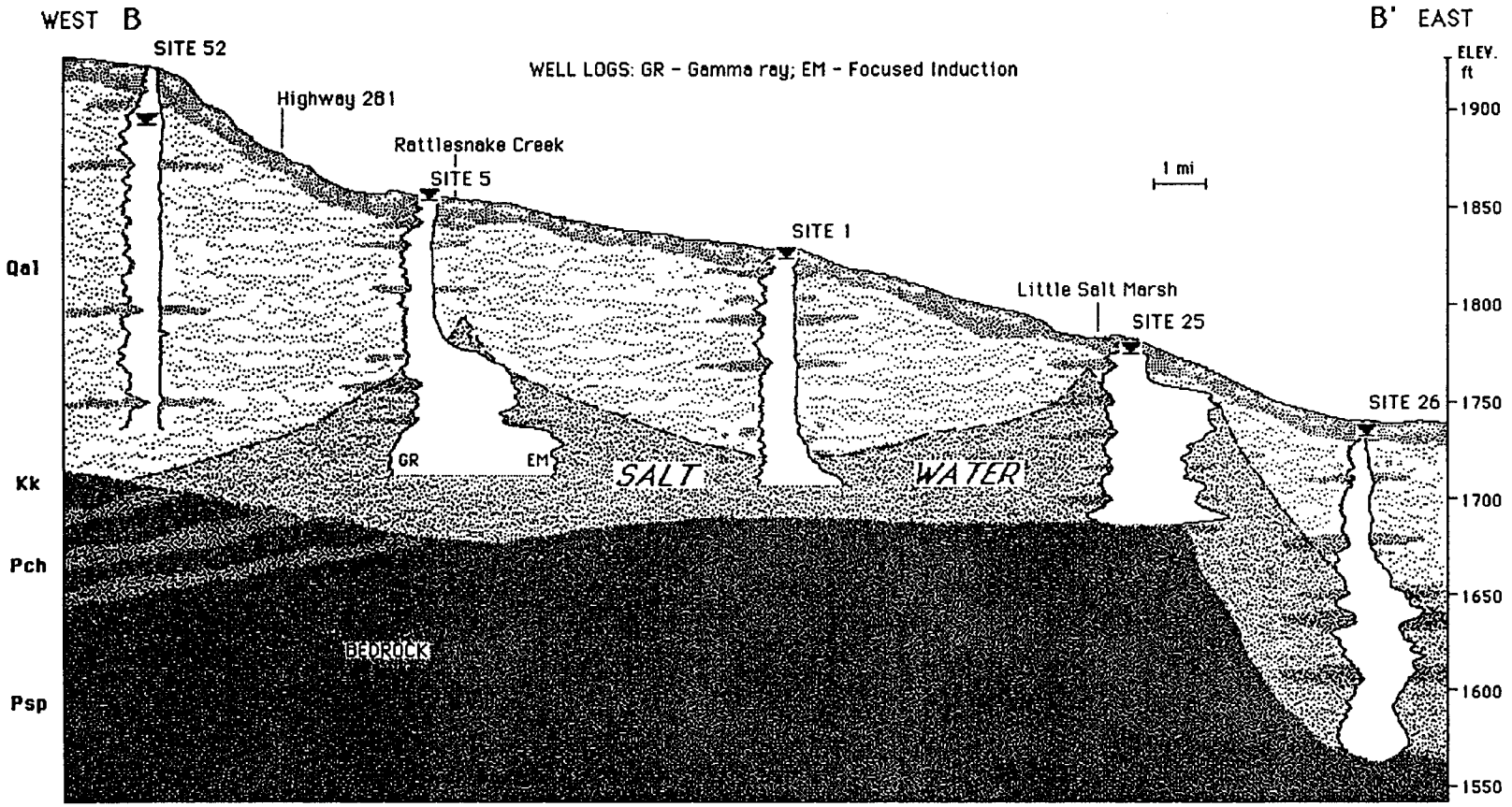

LITHOLOGY: Qal - Quaternary alluvium (fluvial and aeolian); Kk - Cretaceous Kiowa Formation (shale); Pch - Permian Cedar Hills Formation (siltstones and sandy siltstones); Psp - Permian Salt Plain Formation (sandy siltstones and fine-grained sandstones)

Figure 17B. Cross section BB' (Figure 16) showing estimates of clay lenses (dark stippling) inferred from gamma logs and of salt water distribution (light stippling) inferred from conductivity logs. The dashed line indicates the estimated elevation of the 100 mS/m (C'm) transition zone boundary. At each site the left-hand vertical trace is a reproduction of the gamma log and the right-hand trace a reproduction of the conductivity log.

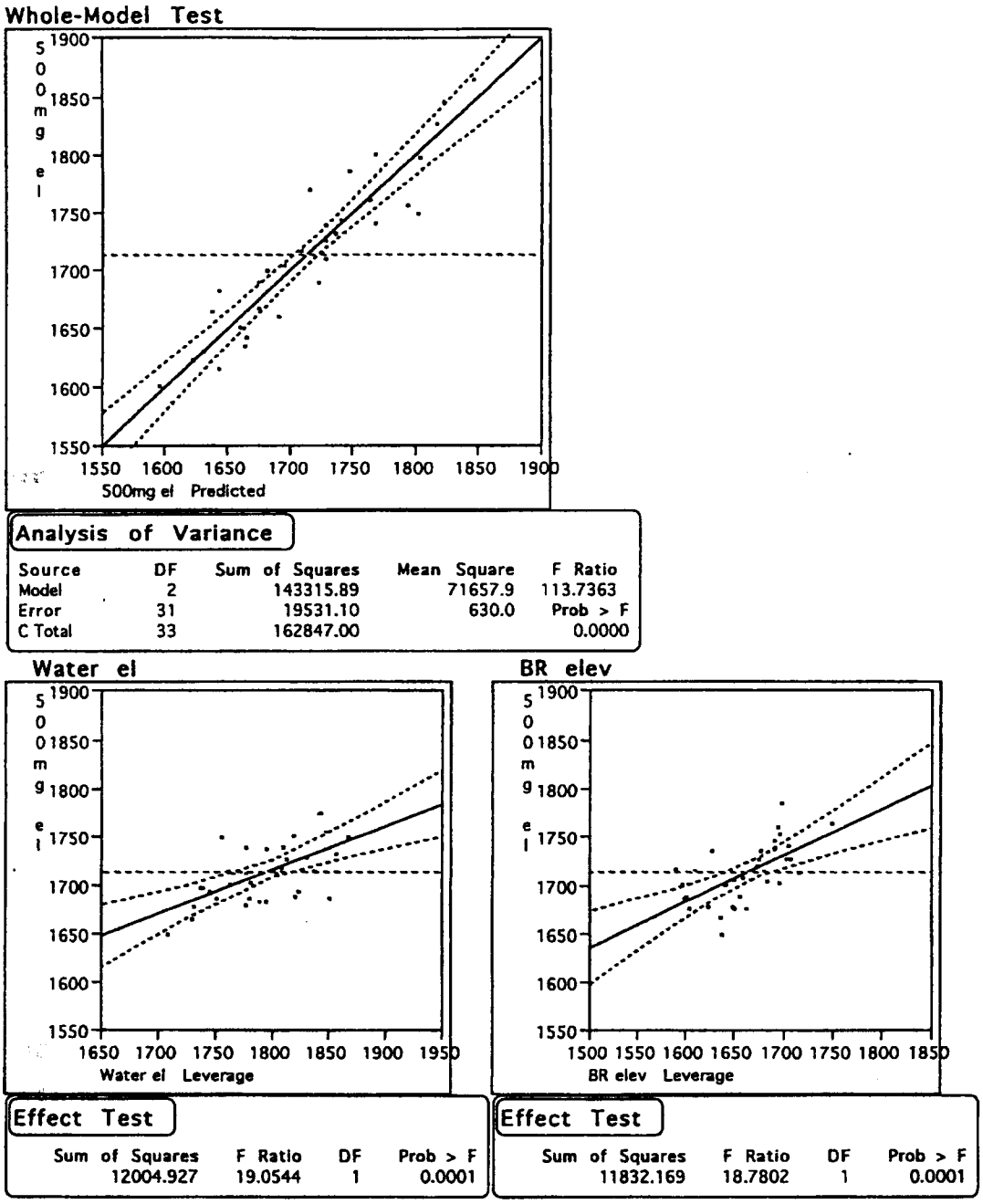

Figure 18. Multiple-regression analysis of the 500 mg/L chloride interface elevation with elevations of the water table and bedrock trend surfaces. Dashed lines indicate 95% confidence interval.

bedrock -- the upper and lower hydrologic trend surface boundaries of the aquifer system. This relationship supports the concept that the 500 mg/L interface forms a trend surface within the aquifer. A similar relationship was found by multiple-regression analysis of the 100 mS/m (~3400 mg/L chloride) transition zone elevation (Young et al., 1993).

From the multiple-regression analysis, the elevation of the 500 mg/L chloride concentration interface (TZ_{500}) can be predicted by the formula

$$TZ_{500} = 147.176 + 0.464WT + 0.441BR \qquad (12)$$

where WT and BR are the elevations (above mean sea level) of the water table and the bedrock, respectively. Equation (12) allows regionalization of the 500 mg/L chloride interface within the area of mineral intrusion delineated on Figure 16, within the uncertainties indicated by the statistical analysis on Figure 18. This relationship provides a convenient method of salt water regionalization because of the existence of both water table and bedrock (Figure 6) datasets that can be processed by Geographical Information Systems (GIS) software applications (Sophocleous and Stern, 1994).

Equation (12) indicates that the 500 mg/L chloride interface elevation is essentially represented by a weighted average of both the water table and bedrock elevations. Both the weights or multiplicative factors in Equation (12) and the F ratios for each of the elevation variables shown in Figure 18 are nearly equal. This indicates that the elevation of the 500 mg/L trend surface is controlled equally by both the elevations of the water table and the bedrock trend surfaces.

Changes in TZ characteristics from 1993 to 1994

The data in Table I show that there have been only minor and isolated changes to the regional distribution of saline water in the Great Bend Prairie aquifer between spring 1993 and spring 1994--despite the heavy rains and resulting flooding and recharge during the summer of 1993. These minor changes also indicate that the regional freshwater-

saltwater distribution is close to steady state on a time scale of years and that several years worth of observations are required to detect any systematic temporal changes in the distribution. The largest change of the 500 mg/L chloride interface (approximately an 8 ft rise) occurred at site 23 and may reflect the down-gradient transport (eastward) of saline water as a result of the heavy recharge.

Despite the apparent regional steady-state distribution of saline water, local fluxes in the vertical transition zone were detected in a monitoring well near a pumping irrigation well and at sites with perched transition zones. Figure 19A shows the systematic changes in the transition zone corresponding to the depth of the irrigation well screen (Figure 19B) at the Siefkes Intensive Study Site (Figure 3) during the summer and fall of 1993. The chloride concentration, just above a clay lens and just below the bottom of the pumping well, increased into October following pumping begun in July. The profile returned to approximate pre-pumping levels by March 1994. The build-up of salinity in this case appears to be a reversible process--salt water is flushed from the area of build-up during the winter and early spring months. These observations for 1993 and 1994 at the Siefkes Site are summarized in Appendix II.

Other local freshwater-saltwater transition zone changes occur within discrete vertical sections of the aquifer (see change plot figures in Appendix I) corresponding to the shallow, perched transition zones discussed previously (see site 26 as example). Heavier than normal recharge may have also affected the perched zones because of saline water moving through high hydraulic conductivity intervals between clay lenses influenced by macrodispersion.

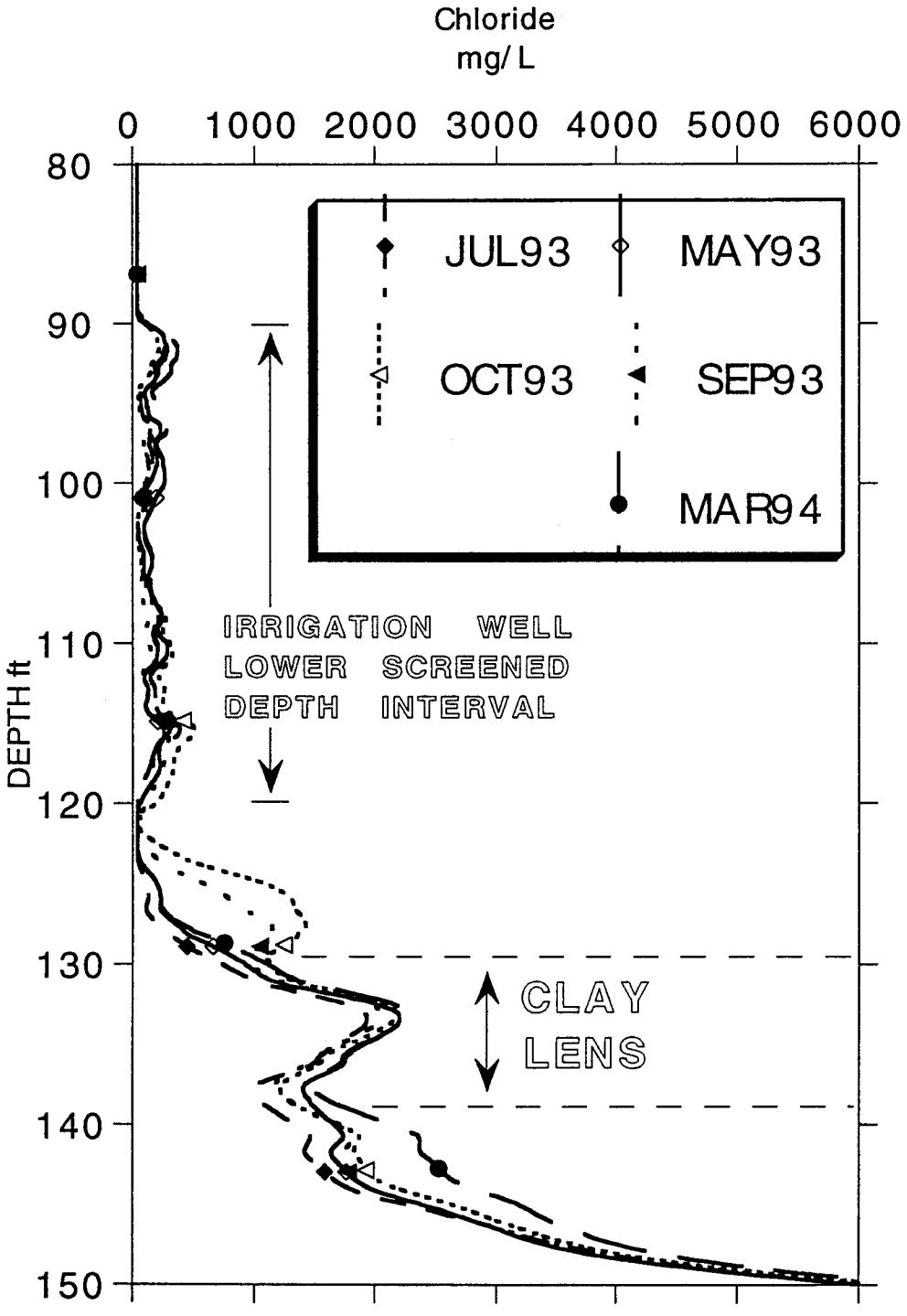

Figure 19A. Detail from sequence of vertical chloride concentration profiles from the Permian monitoring well showing seasonal build-up of salinity following pumping at the Siefkes Intensive Study Site.

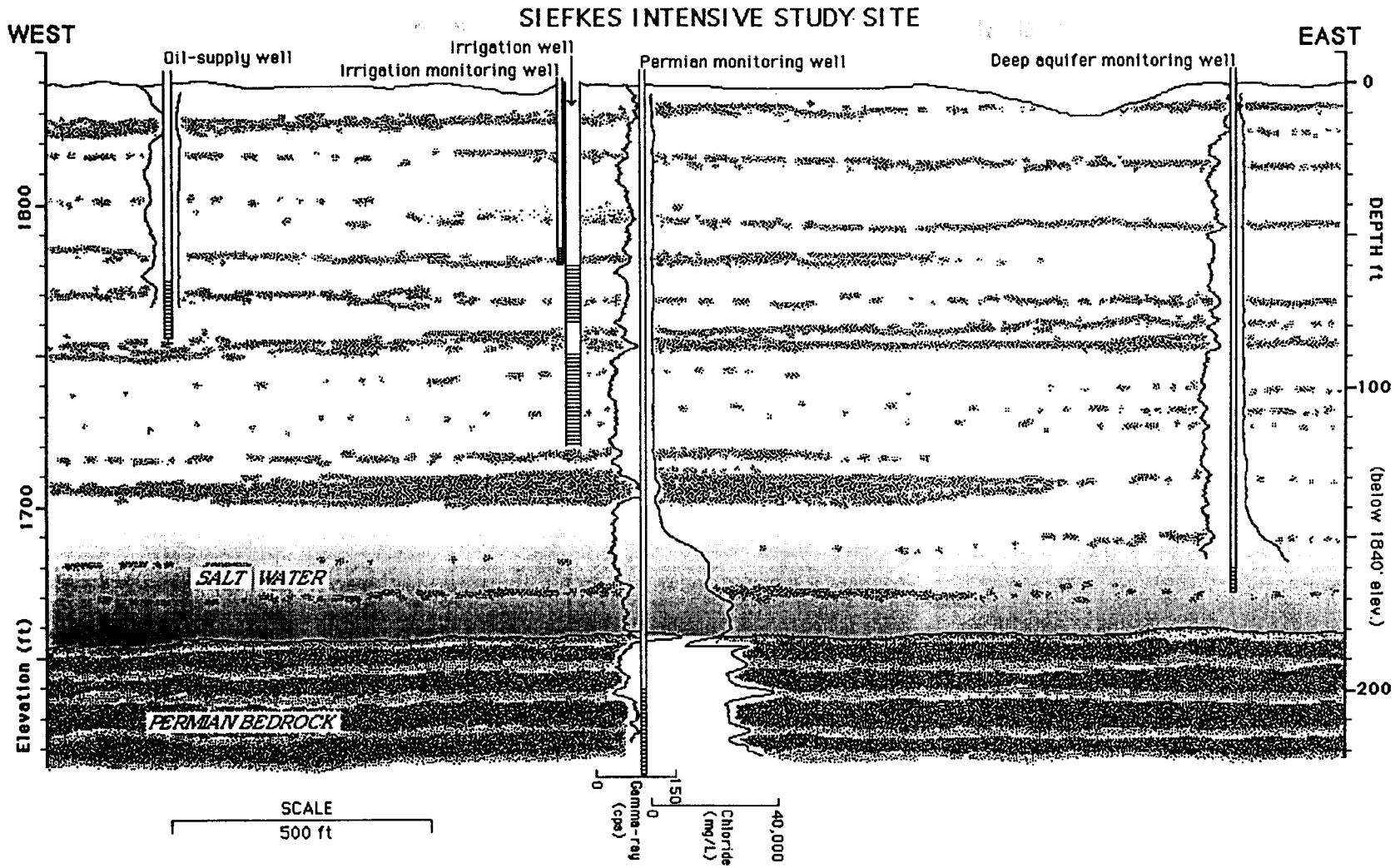

Figure 19B. Cross section of Siefkes Intensive Study Site; patterns and vertical traces as represented on Figures 17A and B.

APPLICATIONS AND DISCUSSION

The results of the freshwater-saltwater transition zone analysis presented above show the horizontal distribution of salt water based on the position of the 500 mg/L threshold (interface) value expressed as a percentage of the total saturated thickness (Figure 16). Figure 16 is a useful presentation of the horizontal distribution of saline water, however it contains no information on the vertical mass distribution of salt water in the aquifer. In addition to determining the location of the freshwater-saltwater interface, the chloride profiles generated by the methods developed in this thesis also permit quantification of the complete vertical saltwater distribution and salt inventory. Together, the horizontal and vertical salt-water distributions help to locate the possible sources of mineral intrusion and areas of advective and dispersive solute transport.

In order to develop a salt budget for the Mineral Intrusion study area of the Great Bend Prairie aquifer, a regional inventory of salt water, an accurate measure of the hydraulic potential flow fields, and the estimation of key parameters for solute transport modeling are required. The vertical chloride profiles developed by this thesis can be further analyzed to: (1) determine the mass of salt and chloride at each monitoring well site within the Great Bend Prairie aquifer and to express the mass as a percentage of total saturated thickness per unit area; (2) make adjustments to measured fluid levels for the effects of variable density; and (3) provide a calibration reference to estimate appropriate solute source supply rates and aquifer dispersivity parameters for transport modeling. Each of these three separate, yet related applications is presented with results and examples for discussion in the following sections.

Application 1: salt inventory

The integrated salt load within the aquifer at each site is determined by calculating the area underneath the chloride concentration profile between the water table (*wt*) and the bedrock (*br*). For sites lacking a complete profile to bedrock, the cumulative distribution function fitted to

the transition zone (described above in the Methods section) is used to estimate the missing section of the chloride concentration profile. Sites requiring extrapolation of the chloride profile were: 1, 5, 11, and 21. The example of site 11 shown in Figure 15C indicates that the extrapolated profile closely fits the actual chloride concentration in the bedrock immediately below the aquifer. The area (A) was calculated by using the curve integration function in KaleidaGraph™ software running on a Macintosh personal computer. The integrated area (A) under the curve is based on the Riemann sum

$$A = \sum_{wt}^{br} Cl(x)\Delta x \qquad (13)$$

where: Cl(x) is the concentration (mg/L) at depth x, and Δx = 0.1 ft. From the fundamental theorem of calculus

$$A = \lim_{\Delta x \to 0} \sum_{a}^{b} f(x)\Delta x = \int_{a}^{b} f(x)dx \qquad (14)$$

provided that $f(x)$ is continuous and its derivative exists between the limits of integration a and b. The total mass of chloride per unit aquifer surface area (m_{Cl}; units of mg/ft^2) is

$$m_{Cl} = 28.32An \qquad (15)$$

where: A is the area under the depth profile of chloride concentration (mg-ft/L), 28.32 is a volumetric conversion factor (L/ft^3), and n is the aquifer porosity (estimated to be 0.16 from the Archie (1942) relationship of equation 8). The total chloride mass is a measure of the salt load for that portion of the aquifer. This calculation ignores any chloride mass sorbed onto aquifer surfaces because chloride is usually considered to be a conservative species (Domenico and Schwartz, 1990). Table II includes the chloride mass (mg) per square foot of the aquifer surface and the equivalent saturated thickness of a brine with 42,000 mg/L chloride

Table II.	Salt inventory at monitoring well sites 1993 and 1994.							
Monitor Well	1993	1993	1993	1993	1994	1994	1994	1994
Site.Well No.	sat. thickness	mass chloride	42,000 mg/L	42k equivalent	sat. thickness	mass chloride	42,000 mg/L	42k equivalen
	(ft)	(mg/sq ft)	equiv. tk. (ft)	thickness %	(ft)	(mg/sq ft)	equiv. tk. (ft)	thickness %
1.1	140.7	2.91E+06	15.308	11	139.65	2.76E+06	14.517	10
3.1	104.27	1.52E+05	0.79907	0.77	109.46	1.49E+05	0.78138	0.71
4.1	120.3	8.66E+05	4.5492	3.8	121.13	9.82E+05	5.1603	4.3
5.1	179.23	1.39E+07	72.775	41	178.92	1.38E+07	72.522	41
6.1	128.63				132.58	5.93E+05	3.1181	2.4
7.1	128.28				133.08			
8.1	109.5	3.11E+05	1.6361	1.5	107.2	3.42E+05	1.7955	1.7
9.1	78	8.89E+05	4.6693	6	77.64	9.39E+05	4.9332	6.4
10.1	137.7	3.85E+05	2.0234	1.5	142.25	3.62E+05	1.9047	1.3
11.1	194.5	3.92E+06	20.592	11	196.61	3.64E+06	19.135	9.7
14.1	138.3	2.49E+05	1.3094	0.95	138.82			
15.1	98.3	92770	0.48746	0.5	99.98	89595	0.47078	0.47
16.1	208.02	7.60E+06	39.915	19	212.36	7.50E+06	39.412	19
17.1	102.4	1.13E+06	5.9393	5.8	103.46	1.16E+06	6.1104	5.9
18.1	194.75	3.86E+06	20.295	10	202.98	3.89E+06	20.454	10
19.1	151.35	4.43E+05	2.33	1.5	151.51	4.49E+05	2.3586	1.6
20.1	175.94	4.84E+05	2.5412	1.4	178.52			
21.1	115.4	1.21E+06	6.3524	5.5	113.93	9.80E+05	5.1505	4.5
22.1	198.9	3.66E+06	19.208	9.7	202.29	3.67E+06	19.267	9.5
23.1	72.58	1.88E+05	0.98698	1.4	71.6	1.85E+05	0.97055	1.4
24.1	102	1.66E+06	8.6993	8.5	99.1	1.16E+06	6.1079	6.2
25.1	91.7	5.95E+06	31.241	34	91.98	6.00E+06	31.535	34
26.1	170.2	4.31E+06	22.661	13	168.24	4.66E+06	24.47	15
27.1	93.88	3.76E+05	1.9739	2.1	92.78	4.92E+05	2.5833	2.8
28.1	89.73	72623	0.3816	0.43	91.54	82568	0.43386	0.47
29.1	111.4	3.53E+05	1.8548	1.7	114.01	3.32E+05	1.7433	1.5
30.1	123.46	2.58E+05	1.3542	1.1	120.81	2.15E+05	1.1308	0.94
31.1	79.35	1.69E+05	0.88746	1.1	77.94	1.60E+05	0.84096	1.1
32.1	169.4	1.12E+06	5.9067	3.5	162.9	1.18E+06	6.1963	3.8
33.1	106.3	1.89E+05	0.99304	0.93	108.77	1.35E+05	0.7078	0.65
34.1	27.06	66130	0.34748	1.3	25.74	59923	0.31487	1.2
35.1	133.61	2.20E+05	1.1548	0.86	134.59	2.32E+05	1.2208	0.91
36.1	167	1.93E+06	10.15	6.1	167.16	1.95E+06	10.249	6.1
37.1	181.37	4.34E+05	2.2787	1.3	182.9	4.21E+05	2.21	1.2
38.1	162.65	5.32E+05	2.795	1.7	163.19	5.46E+05	2.8711	1.8
39.1	53.08	36641	0.19253	0.36	51.87	42480	0.22321	0.43
40.1	101.15	43270	0.22737	0.22	104.69	59165	0.31088	0.3
41.1	80.5	91978	0.4833	0.6	80.82	91182	0.47912	0.59
42.1	146.97	6.91E+05	3.6311	2.5	146.99	6.79E+05	3.5671	2.4
43.1	60.13	3.25E+05	1.7071	2.8	59.86	3.67E+05	1.9294	3.2
45.1	130.23	1.49E+05	0.78398	0.6	132.31	1.62E+05	0.85085	0.64
46.1	129.72				132.43	1.43E+05	0.75111	0.57
47.1	105.56	1.50E+05	0.78812	0.75	106.96			
49.1	106				106	8.91E+05	4.6825	4.4
50.1	196.85	61885	0.32518	0.17	200.66	67271	0.35348	0.18
51.1	182.7	1.06E+05	0.5551	0.3	186.32	1.09E+05	0.57498	0.31
52.1	190.21	71667	0.37658	0.2	197.33	76390	0.40139	0.2
SP	177	3.61E+06	18.944	11	177	3.67E+06	19.282	11

required to equal the chloride mass at sites in the Mineral Intrusion study area.

Figure 20 is a contour map of the percent of saturated thickness that would be occupied if the total salt inventory were present in the form of a brine of 42,000 mg/L (Table II). Sites with one percent or less of the brine equivalent are indicated with a '1' and represent the ambient background level of chloride mass distribution. Whereas the contour map of Figure 16 shows the lateral distribution of saline water, Figure 20 shows the vertically integrated salt mass distribution in the aquifer. Figure 20 indicates three subregions of mineral intrusion related to those shown in Figure 16; however, it should be noted that the three subregions are now separated from one another and that the centers of areal mass are shifted back toward the west -- toward the subcrop area of the Permian Cedar Hills Sandstone hydrostratigraphic unit. The largest subregion in Stafford Co. and the southernmost subregion in Pratt Co. appear to broadly originate along the subcrop area while the central subregion appears to originate from a localized area of the subcrop near site 8 in southern Stafford Co. Figure 20 is a composite of data from 1993 and 1994 because there were only minor differences (one to two percent) between the observations in Table II.

The data used to construct the contour maps of Figures 16 and 20 can also be combined in the form of block diagrams arranged in a perspective format. Figure 21 shows the relative inventories (1993 and 1994) of brine and fresh water with the extent of mixing between the two (indicated by the 500 mg/L chloride interface value). The vertical extent of mixing does not have any salt-water budgetary significance but does show the general increase of dispersion towards the eastern part of the study area while the brine inventory decreases. Figure 21 also shows the very minor changes in inventories between 1993 and 1994.

Application 2: variable-density fluid level correction

In addition to the salt inventory application described above, the ability to generate complete vertical chloride concentration profiles

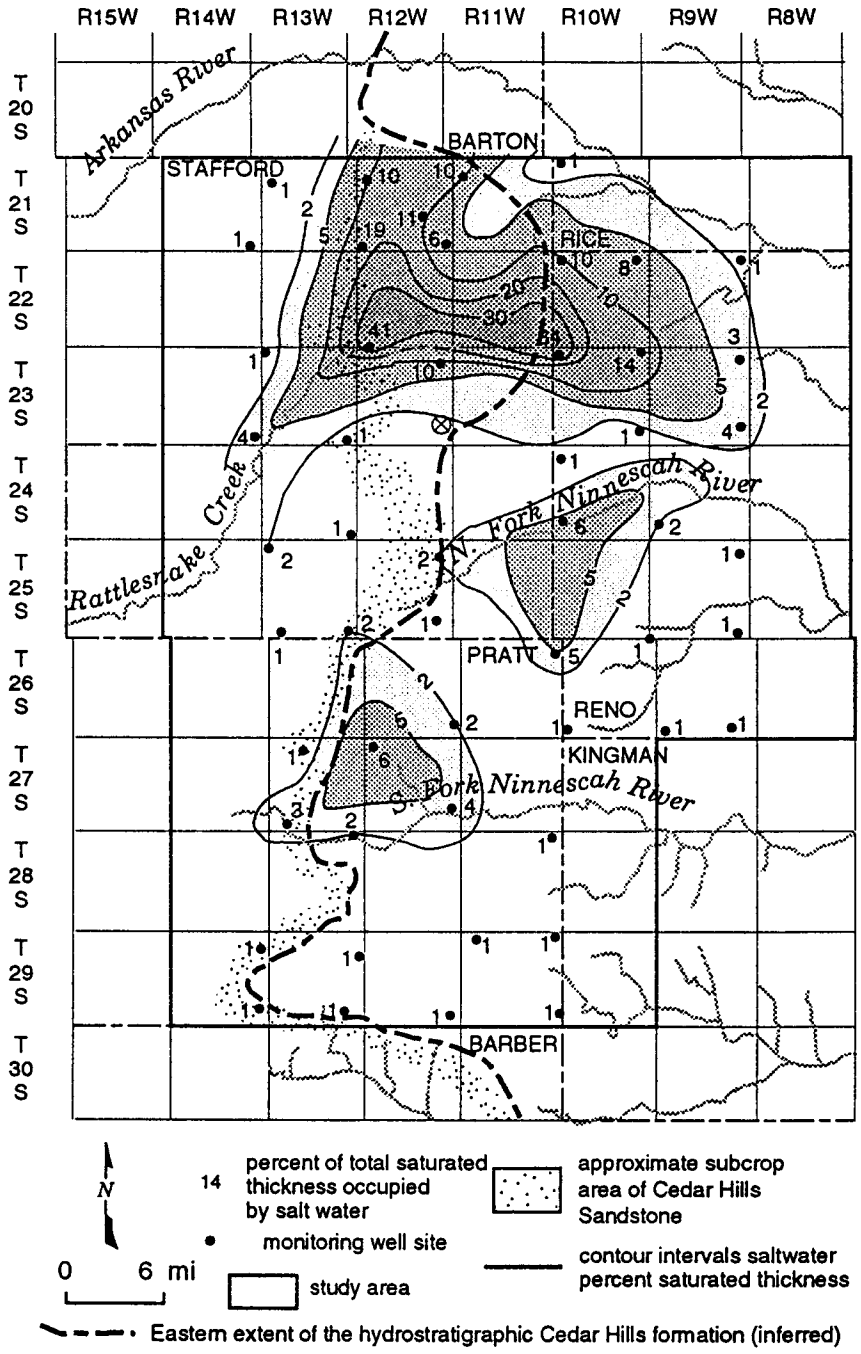

Figure 20. Distribution of total Great Bend Prairie aquifer salt load expressed as percent of saturated thickness that would be occupied by an equivalent volume of brine with 42,000 mg/L Cl (the average maximum brine concentration determined in water samples obtained from the upper Permian bedrock). Composite of data from 1993 and 1994.

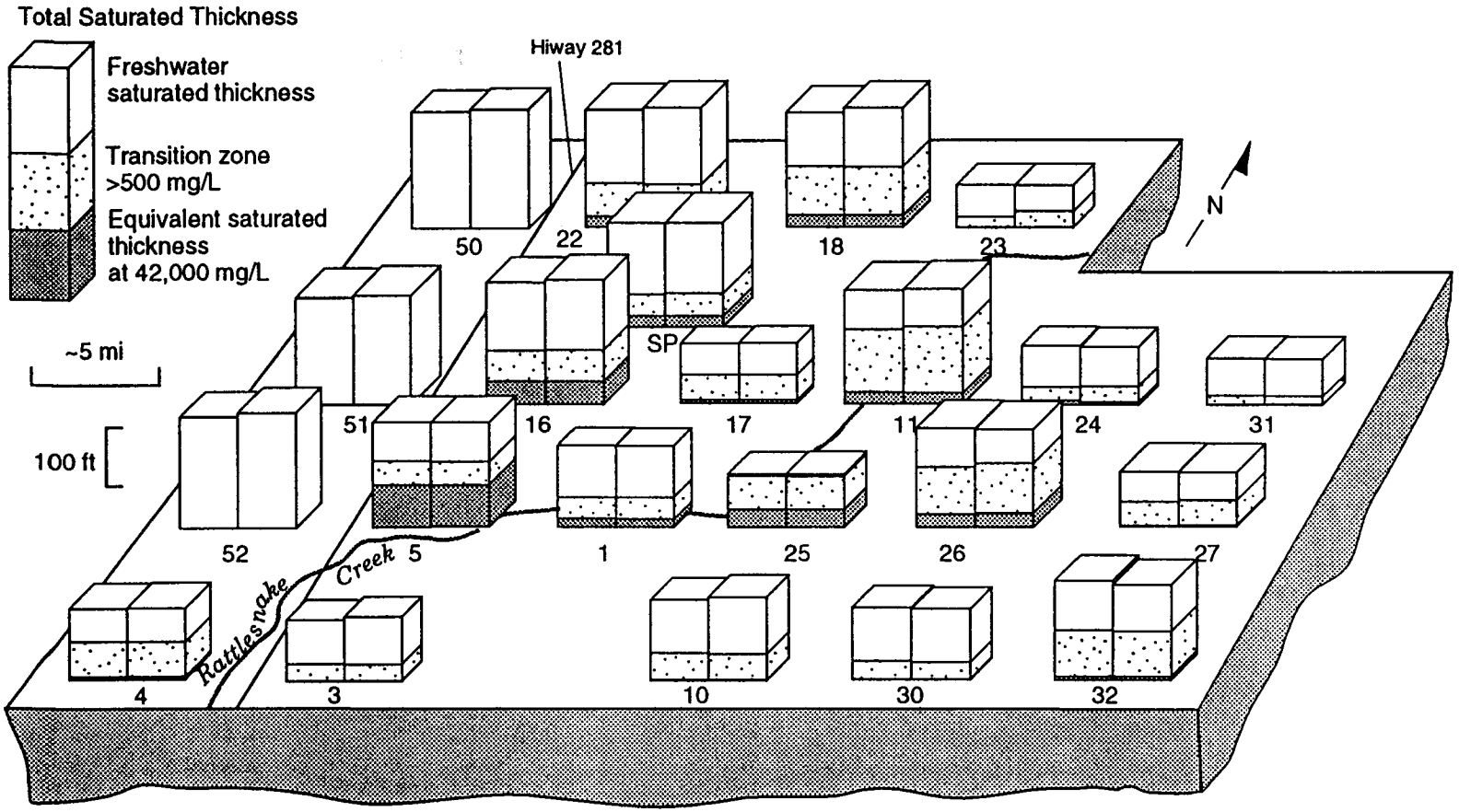

1993 (left block) 1994 (right block)

Figure 21. A representation of the total saturated thickness (height of column) and the saturated thickness that would be occupied by the volume of Permian brine equivalent to the salt content of the total water column (height of dark column). At each site, 1993 values are on the left, 1994 on the right. The height of 500 mg/L limit of the mixed zone is shown by light stippling; this has no budgetary significance, but shows the extent of vertical mixing and the amount of usable fresh water at each site.

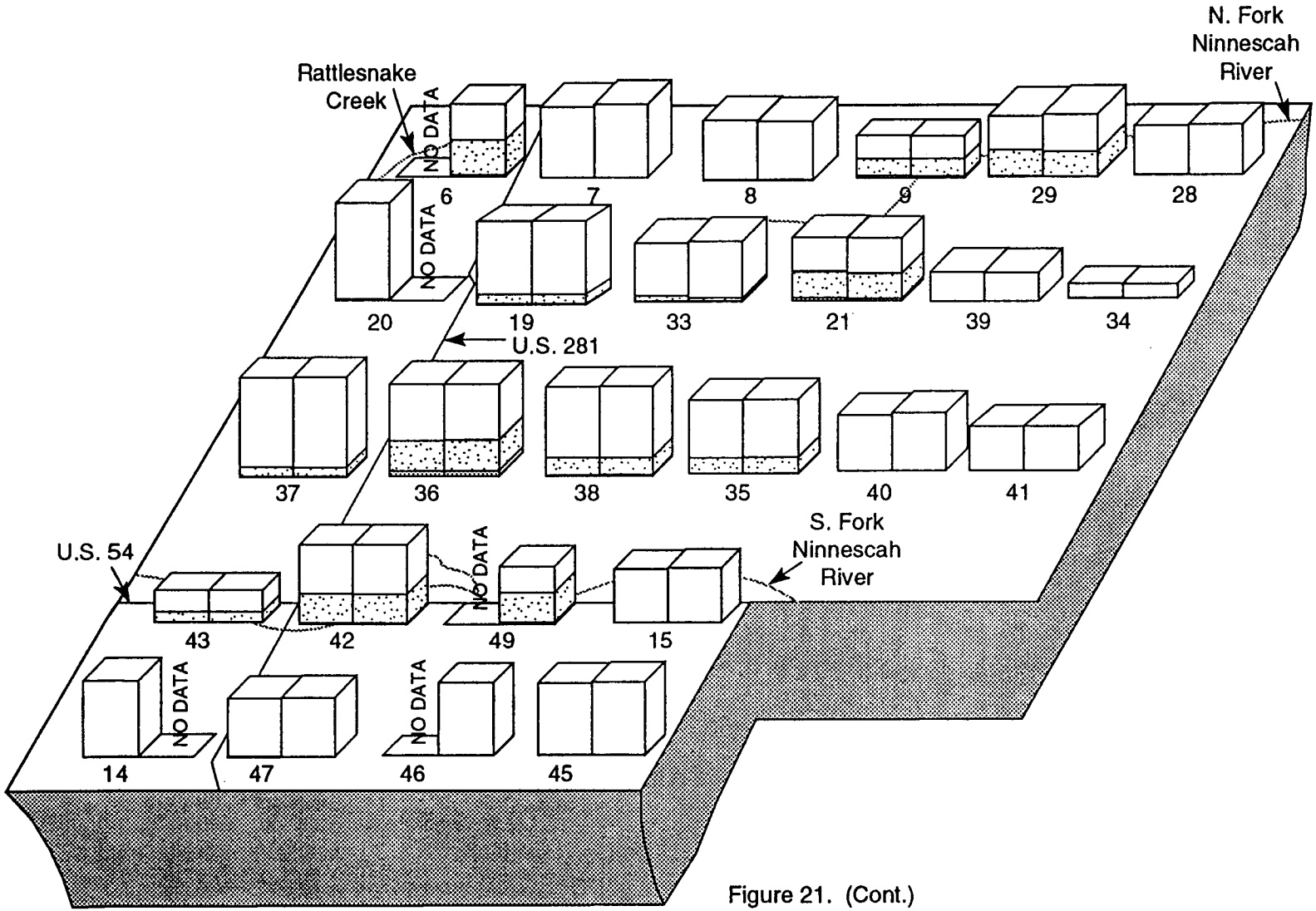

Figure 21. (Cont.)

permits the adjustment of measured fluid levels for the effects of variable density. This correction is used to explore regional relationships between the heads in the Great Bend Prairie and Permian aquifers and the present distribution of fresh and saline water. Accurate potentiometric fields are important to estimate the flow of saline water into and within the Great Bend Prairie aquifer.

The effect of increasing ground-water density with depth causes borehole fluid levels to be lower, compared to levels in fresh-water environments, because of the greater pressure required to support the greater weight of the saline water. Thus, the pressure (P), as a component of the pressure head of the system, is a function of density (ρ) such that if $P = \rho_1 g h_1 = \rho_2 g h_2$ and if $\rho_1 < \rho_2$, then $h_1 > h_2$. Various methods to correct for variable-density effects, and thus the development of accurate potentiometric fields for an aquifer containing saline water, are discussed by Jorgensen et al. (1982) and Bachu (1995). These methods typically involve the standardization of fluid levels to a reference water of uniform density, usually fresh water. The concept of fresh-water equivalent heads uses the standardized fluid levels to calculate a theoretical potentiometric surface with perpendicular streamlines for the flow field of the aquifer as if it contained fresh ground water.

The fresh-water equivalent correction may not be adequate to estimate horizontal potentiometric gradients in certain variable-density situations. Davies (1987) discusses the limitations of these approximation methods to remove the effects of variable density on horizontal ground-water flow calculations. A density-related error associated with the gravity-driven component of Darcian flow can be assessed by computing the ratio between the relative magnitude of the density-related error term and the magnitude of the freshwater-head term called the driving-force ratio or DFR (Davies, 1987)

$$DFR = \frac{\Delta\rho|\nabla E|}{\rho_f|\nabla H_{if}|} \qquad (16)$$

where: $\Delta\rho$ is the difference between the ground-water density at the well screen (or point-water density, ρ_i) and the fresh-water density (ρ_f); $|\nabla E|$ is the magnitude of the gradient of water table elevation; and $|\nabla H_{if}|$ is the magnitude of the equivalent fresh-water head gradient.

Figure 22 is a nomograph plot of the dimensionless DFR as a function of $|\nabla E|/|\nabla H_{if}|$ with lines representing fluid density curves ranging from brackish water (ρ=1.007 g/cm^3 or approximately 6000 mg/L chloride) to water fully saturated with respect to NaCl (ρ=1.200 g/cm^3 or over 150,000 mg/L chloride). Figure 22 also locates the DFR value of 0.5 as an approximate threshold where the error associated with the density-related gravity effect becomes important to head gradient calculations. From equation (16), it is apparent that this threshold value requires that the product of the density contrast ($\Delta\rho$) and the magnitude of the elevation gradient ($|\nabla E|$) be greater than or equal to half of the magnitude of the equivalent fresh-water gradient ($|\nabla H_{if}|$) for the error to become significant. Such extreme conditions can only be expected to occur within a sloping confined aquifer or within an unconfined aquifer in a state of unsteady flow. Calculations based on the maximum density contrast between sites with a maximum elevation gradient indicate that the DFR for the Great Bend Prairie aquifer is of the order of magnitude of 10^{-2} and therefore much less than the threshold value of 0.5. This result indicates that the fresh-water equivalent correction is adequate to estimate the horizontal potentiometric gradient in the mineral intrusion study area of the Great Bend Prairie aquifer.

Bond (1972) developed a method to adjust measured fluid levels for the effects of variable density in wells screened at different levels in an aquifer. This method assumes a linear variation of density with depth if the density is different between the wells. Application of this assumption would greatly over-estimate the general vertical distribution of ground-water density in the Great Bend Prairie aquifer. The results of this thesis show that salinity variation generally follows a normal cumulative distribution as a function of depth -- often with a narrow transition zone. Furthermore, some sites exhibit complex, multiple levels of transition from

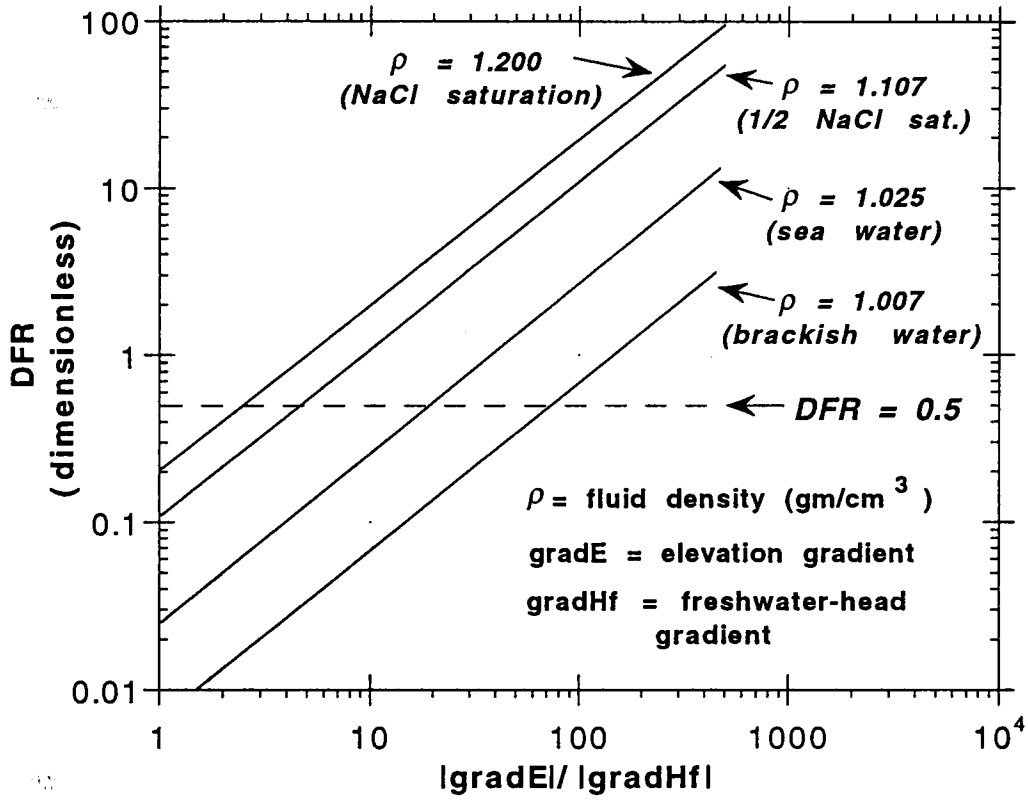

Figure 22. Driving-force ratio (DFR) as a funtion of |gradEl/|gradHf| for fluid density curves ranging from brackish water to brine fully saturated with respect to NaCl. The DFR=0.5 line is shown as the approximate threshold at which density-related gravity effects may become significant (after Davies, 1987).

fresh to saline water such as at site 26 (Figure 17B). The method of Bond (1972) should therefore be restricted to application in settings where the linear density assumption is generally valid such as in a homogeneous confined aquifer.

Figure 23 illustrates the concepts of hydraulic heads in variable density situations as described by Lusczynski (1961). This method was developed to adjust fluid levels measured in a nearly horizontal, unconfined coastal aquifer -- basically similar to the Great Bend Prairie aquifer except for the coastal setting. The point-water head (Figure 23A) is derived from the field-measured fluid level, which is assumed to reflect the pressure head of the well filled with water of uniform density equal to that occurring at the depth of the well screen. The fresh-water equivalent head (Figure 23B) is the hypothetical head of the same well filled with uniformly fresh water. This fresh-water equivalent head can be used to create a potentiometric surface for the horizontal flow-field calculations as described above. The environmental-water head (Figure 23C) is the hypothetical head of the same well filled with the variable density water reflecting the actual vertical density gradient in the aquifer. The environmental-water correction can also be thought of as the fresh-water correction reduced by an amount equivalent to the difference between the salt mass in fresh water and that in the actual (environmental) water in the interval from the top of the zone of saturation to the well screen (Luscynski, 1961). Because the environmental-water correction reflects the actual vertical mass distribution in the aquifer and thus an approximation of the density-related, gravity-driven component of flow, this correction is used for vertical potentiometric gradient calculations within the aquifer.

For assessing a probable flow rate of salt water from the Permian bedrock to the Great Bend Prairie aquifer, the critical gradient is across the bedrock interface. To estimate a vertical gradient value on the basis of consistently normalized densities, this investigation uses the difference between the calculated fresh-water head of the Permian bedrock well (H_{if}, assumed to represent the driving force for upward flow) and the environmental-water head at the bedrock datum (H_{in}, assumed to represent

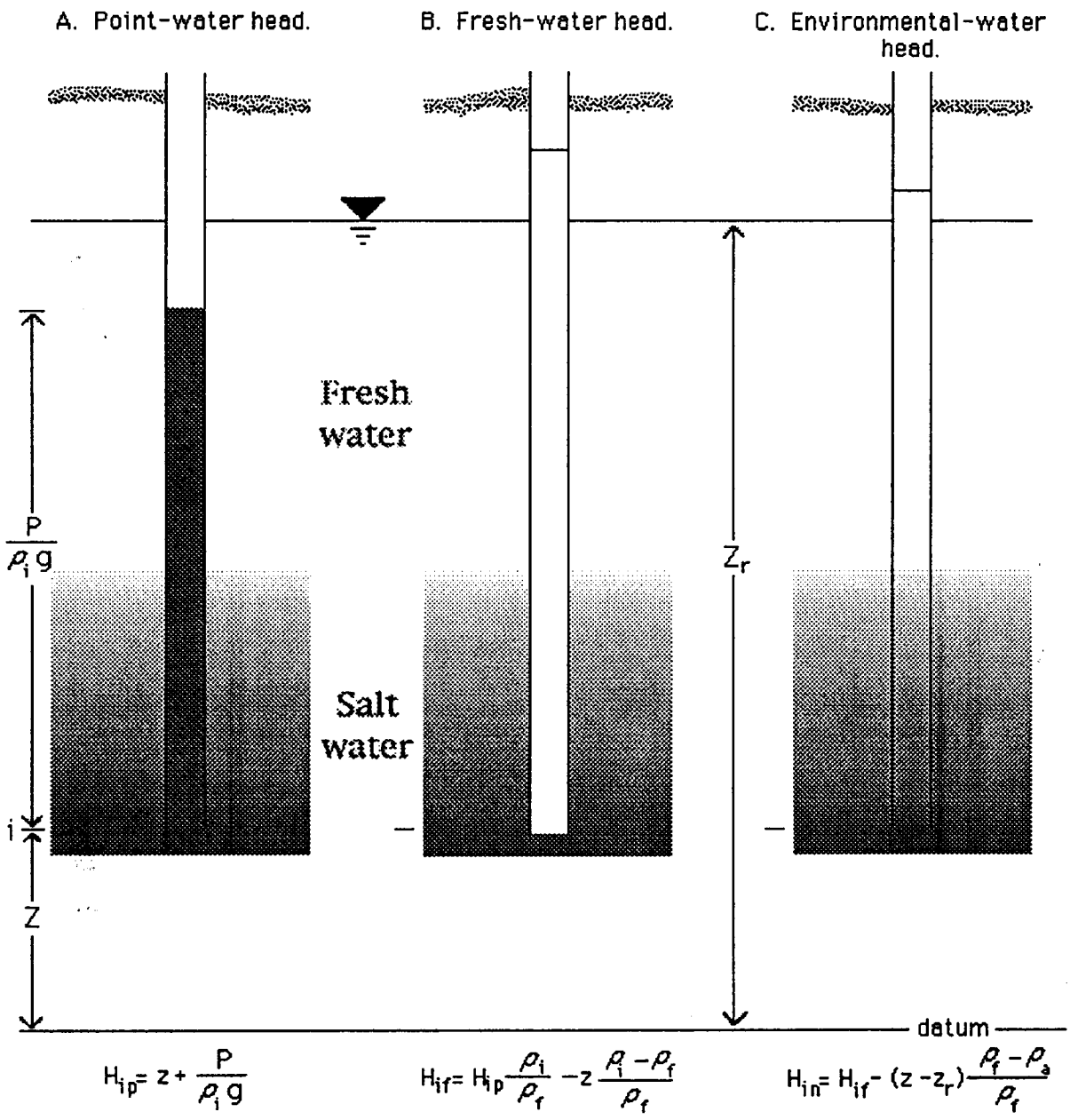

where: ρ_i = density at depth i ; ρ_f = fresh water density; ρ_a = average density.

Note: if well is screened in fresh water— $H_{ip} = H_{if} = H_{in}$

Figure 23. Heads in ground water of variable density (after Lusczynski, 1961).

the confining head of the overlying water column). This dimensionless gradient value is

$$GRAD_{br} = \frac{H_{if} - H_{in}}{\Delta z} \qquad (17)$$

where Δz is the distance from the bedrock-aquifer interface to the top of the screen of the bedrock well. The reader should be strongly cautioned that this gradient calculation is, to say the least, highly uncertain. The uncertainty is due to the necessary comparison between vastly different geohydrologic systems -- the Great Bend Prairie aquifer and the underlying Permian bedrock formations. An equivalent environmental-water correction cannot be applied to fluid levels measured in the wells screened in the bedrock. The environmental-water correction is limited to application only within the aquifer because the integrated density profiles are based on the processed EM logs which are only considered valid for the extent of aquifer saturated thickness. Other sources of uncertainty in the calculation of a probable bedrock-aquifer flow rate are factors that influence the relative permeability contrast between the hydrologic systems. These factors include the variable amount of bedrock weathering and fracturing and the relative exposures of sandy versus shaly subcropping units. Furthermore, most of the wells -- screened at variable depths in the bedrock -- have not been developed for several years. The borehole fluid has probably become stratified by density effects, yet measured fluid levels are still probably representative of the average density occurring in the upper bedrock at each site. The bedrock-aquifer interface gradient also assumes static conditions (no recharge or discharge gradient) in the aquifer. Although aquifer environmental-water gradients are generally small, they will also influence any flow rate across the interface from one system to the other. With all of these sources of uncertainty to consider, the bedrock-aquifer gradient calculation should not be compared quantitatively to any other previously described gradient.

In spite of the many uncertainties, both the bedrock fresh-water and aquifer environmental-water heads can be expressed in terms of

pressure. Referring to Figure 23, the pressure (P) at the well screen (i) as a function of the fresh-water head (H_{if}) is (Lusczynski, 1961)

$$P_i = \rho_f g(H_{if} - Z) \tag{18}$$

and as a function of the environmental-water head (H_{in}) is (Lusczynski, 1961)

$$P_i = \rho_f g(H_{in} - Z_r) + \rho_a g(Z_r - Z) \tag{19}.$$

Then the generalized Darcy equation for the vector velocity or specific discharge (q) in terms of the gradient of pressure is

$$\mathbf{q} = -\frac{k}{\mu}(\nabla P - \rho_i \mathbf{g}) \tag{20}$$

where k is the permeability of an isotropic medium, μ is the fluid viscosity, and g is the vector of gravitational acceleration. Here again the importance of permeability is apparent. The extremes of aquifer and bedrock permeabilities would bracket a range of possible specific discharge values. The uncertainty in the gradient of pressure (derived from either the fresh-water or the environmental-water heads) is probably insignificant compared to the uncertainty in permeability. It is beyond the scope of this thesis to attempt a full quantitative resolution of the many uncertainties inherent in these calculations. Only a semi-quantitative assessment of the probable distribution of fluid potentials can be made here.

Calculations for the variable-density fluid level corrections are accomplished by conversion of the EM-log derived vertical chloride profiles into density. Figure 24 demonstrates the relationship between chloride concentration and density of seawater at 15 deg. C (Williams, 1962), the typical ambient temperature of ground water in the Great Bend Prairie aquifer. The linear relationship must be extrapolated to concentrations of 42,000 mg/L (the average maximum groundwater concentration) because

S	ρ	Cl
0.0000	0.99913	-0.016606
5.0000	1.0030	2.7618
10.000	1.0068	5.5613
15.000	1.0107	8.3821
20.000	1.0145	11.224
25.000	1.0183	14.087
30.000	1.0222	16.972
35.000	1.0260	19.878
40.000	1.0299	22.805

where: S = salinity (parts per thousand); ρ = density (gm/cm^3) of seawater at 15 deg C; and Cl = [(S-0.03)/ 1.805] ρ(mg/ L)/ 1000.
From Williams (1962) Table III-1 and eqn. 3.1.

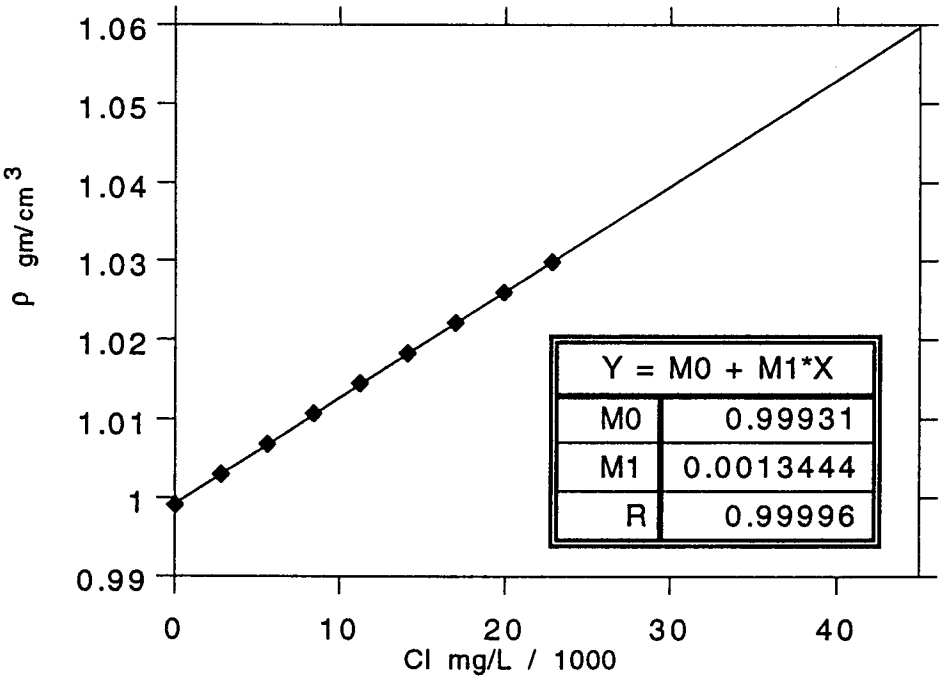

Figure 24. Conversion of chloride concentration to density.

the relationship shown was developed for seawater with typical chloride concentrations of less than 25,000 mg/L. Although there are slight differences between the ionic ratios of seawater and of the Permian formation brine, they are similar enough to justify the use of this relationship. The complete saturated-thickness density profiles allow integration, as was described in the previous section, for the variable-density correction calculations.

The results of the variable-density fluid level corrections for the monitoring well sites, with measurements from 1993 and 1994, are contained in Table III parts 1 and 2. The bedrock surface elevation was used as the datum for the adjusted heads at each site. Three examples from Table III clearly illustrate the necessity, precision, and congruity of the fluid level correction applications:

EXAMPLE (1). For site 5, the point-water heads indicate a recharge (downward) potential between the upper (number 3 well) and the lower (number 2 well) aquifer whereas the environmental-water corrected heads indicate a discharge (upward) potential. Because site 5 is located close to the gaining (discharge) Rattlesnake Creek and has an unusually thick and massive salt-water profile (Table II), a discharge gradient appears to be a more reasonable reflection of the actual fluid potential within the aquifer.

EXAMPLE (2). At site 8, the number 2 and 3 wells are both screened in the lower aquifer with only about 30 ft of vertical screen separation. The point-water heads for these two wells are approximately 0.3 ft different for both 1993 and 1994 measurements. After adjustments, the fresh-water and environmental-water corrected heads are brought into coincidence to within 0.06 ft for 1993 and to within 0.01 ft for 1994. The much smaller resultant gradients reflect the expected equilibrium of fluid potentials for this site.

EXAMPLE (3). Site 23 shows a complete reversal from a downward to an upward environmental-water gradient between 1993 and 1994. This change, the largest for all sites, is independently confirmed by the fact that this site also experienced the largest change in the depth of the 500 mg/L chloride interface--a depth decrease of over 8 ft (see Table I) which would likely be caused by upward flow. The reversal of gradient within the

Table III. part 1	Variable density corrections applied to fluid levels measured in monitoring wells during 1993.												
Monitor Well Site.Well No.	Elevation of land (ft)	Depth to bedrock (ft)	Depth to top of screen (ft)	Depth to wat table (ft)	Depth to wat in well (ft)	Dens. of wate at screen (g/	Avg. density water (g/cc)	Hip point-water head (	Hif fresh-water head (	Hin environ.-water head (	Aquifer vert. gradient	GRADbr aquifer-bedrock gradient	
1.1	1827	146	146	5.3	6.8	1.0171	1.0055	1820.2	1822.7	1821.8			
1.2	1827	146	106	5.3	5.7	1.0036	0.99973	1821.3	1821.7	1821.7	0.00010638		
1.3	1827	146	36	5.3	5.3	0.99936	0.9995	1821.7	1821.7	1821.7			
3.1	1898	130	120	25.73	28.31	1.0135	0.99974	1869.7	1871	1871	0.023972		
3.2	1898	130	65	25.73	25.73	0.9994	0.99941	1872.3	1872.3	1872.3			
4.1	1912	129	217	8.7	5.8	1.041	1.0015	1906.2	1915	1903.6		-0.12999	
4.2	1912	129	106	8.7	5.8	1.0004	1.0013	1906.2	1906.3	1906.1	-0.053204		
4.3	1912	129	53	8.7	8.7	1.0009	1.001	1903.3	1903.4	1903.3			
5.1	1855	181	193	1.77	1	1.0547	1.0222	1854	1864.6	1857.3		-0.60826	
5.2	1855	181	92	1.77	3.26	1.0282	1.0019	1851.7	1854.3	1854.1	-0.016456		
5.3	1855	181	40	1.77	1.77	0.99936	0.99973	1853.2	1853.2	1853.2			
6.1	1950	148	216	19.37	21.96	1.0566		1928	1939.2				
6.2	1950	148	135	19.37	14.13			1935.9					
6.3	1950	148	60	19.37	19.37			1930.6					
7.1	1906	150	230	21.72	39.54	1.0453		1866.5	1875.2				
7.2	1906	150	150	21.72	18.56			1887.4					
7.3	1906	150	56	21.72	21.72	0.99937	0.99937	1884.3	1884.3	1884.3			
8.1	1848	118	237	8.8	25.1	1.0582	1.0002	1822.9	1835.4	1839.3		0.032956	
8.2	1848	118	116	8.8	15.8	1.0024	1.0001	1832.2	1832.5	1832.4			
8.3	1848	118	87	8.8	15.5	1.0001	1.0002	1832.5	1832.6	1832.5	0.16412		
8.4	1848	118	46	8.8	8.8	0.99998	0.99955	1839.2	1839.2	1839.2			
9.1	1755	87	86	9	9	1.0037	1.0027	1746	1746.3	1746.1			
9.2	1755	87	62	9	8.8	1.0012	1.0004	1746.2	1746.3	1746.2	-0.010345		
9.3	1755	87	38	9	9	0.99936	0.99955	1746	1746	1746			
10.1	1790	156	160	18.3	22.9	1.0016	1.0001	1767.1	1767.4	1771.8		1.0997	
10.2	1790	156	143	18.3	22.7	1.0013	1	1767.3	1767.5	1767.5			
10.3	1790	156	100	18.3	20.8	1.0004	0.99961	1769.2	1769.3	1769.3	0.094177		
10.4	1790	156	74	18.3	18.3	0.99961	0.99942	1771.7	1771.7	1771.7			
11.1	1763	208	237	13.5	31.89	1.0329	1.0053	1731.1	1738	1750.7		0.43641	
11.2	1763	208	61	13.5	13.5	1.0002	1.0002	1749.5	1749.5	1749.5			
12.1	1776	142	166	22.68	24.32	0.99942	0.99941	1751.7	1751.7	1753.3		0.068247	
12.2	1776	142	130	22.68	22.17	0.99936	0.99941	1753.8	1753.8	1753.8	-0.0072405		
12.3	1776	142	60	22.68	22.68	0.99936	0.99942	1753.3	1753.3	1753.3			
13.1	1905	172	182	34.7	37.4	0.99934	1	1867.6	1867.6	1870.4		0.27906	
13.2	1905	172	120	34.7	34.8	1.001	0.99981	1870.2	1870.3	1870.3	-4.01E-05		
13.3	1905	172	53	34.7	34.7	0.99936	0.99943	1870.3	1870.3	1870.3			
14.1	1989	238	280	99.7	100.6	0.99936	0.99984	1888.4	1888.4	1889.4		0.023031	
14.2	1989	238	223	99.7	99.7	0.99936	0.9999	1889.3	1889.3	1889.2	0.00069173		
14.3	1989	238	115	99.7	99.7	1.0001	0.99957	1889.3	1889.3	1889.3			
15.1	1725	128	135	29.7	26.8	0.99994	0.99959	1698.2	1698.3	1695.3		-0.41997	
15.2	1725	128	116	29.7	30.7	0.99973	0.99951	1694.3	1694.3	1694.3	0.016657		
15.3	1725	128	57	29.7	29.7	0.99942	0.99937	1695.3	1695.3	1695.3			
16.1	1872	220	243	11.98	29.2	1.0461	1.0101	1842.8	1852.8	1862.3		0.41159	
16.2	1872	220	198	11.98	19.25	1.0452	1.0065	1852.8	1860.9	1859.6	0.0029162		
16.3	1872	220	80	11.98	11.98	0.99948	1.0003	1860	1860	1860			
17.1	1804	114	129	11.6	45.7	1.0126	1.0026	1758.3	1759.4	1792.7		2.2218	
17.2	1804	114	102	11.6	10.8	1.0105	1.002	1793.2	1794.2	1794	-0.025943		
17.3	1804	114	41	11.6	11.6	0.99936	0.99952	1792.4	1792.4	1792.4			
18.1	1810	214	231	19.25	34.32	1.0157	1.0052	1775.7	1778.9	1791.9		0.76405	
18.2	1810	214	197	19.25	32.76	1.0189	1.004	1777.2	1780.5	1779.6	0.073184		
18.3	1810	214	45	19.25	19.25	0.99961	0.99961	1790.7	1790.8	1790.7			
19.1	1901	163	180	11.65	19.52	0.99957	1.0002	1881.5	1881.5	1889.5		0.46846	
19.2	1901	163	145	11.65	14.59	1.0006	1.0001	1886.4	1886.6	1886.5	0.027929		
19.3	1901	163	42	11.65	11.65	0.99936	0.99937	1889.3	1889.3	1889.3			

Table III. (cont.)

part 1

Monitor Well Site.Well No.	Elevation of land (ft)	Depth to bedrock (ft)	Depth to top of screen (ft)	Depth to wat table (ft)	Depth to wat in well (ft)	Dens. of wate at screen (g/	Avg. density water (g/cc)	Hip point- water head (	Hif fresh- water head (	Hig environ.- water head (	Aquifer vert. gradient	GRADbr aquifer- bedrock gradient
20.1	1960	198	221	22.06	30.05	1.0063	1.0001	1929.9	1931.3	1938.1		0.29539
20.2	1960	198	189	22.06	21.08	0.99936	1.0002	1938.9	1938.9	1938.8	-0.0058782	
20.3	1960	198	46	22.06	22.06	0.99944	0.99948	1937.9	1937.9	1937.9		
21.1	1801	137	145	21.6	25.2	1.015	1.0024	1775.8	1777.7	1779.8		0.2592
21.2	1801	137	113	21.6	22.9	1.0047	1.0007	1778.1	1778.6	1778.5	0.013138	
21.3	1801	137	43	21.6	21.6	1.0003	1.0013	1779.4	1779.4	1779.4		
22.1	1855	215	231	16.1	29.3	1.043	1.0048	1825.7	1834.5	1840		0.34168
22.2	1855	215	206	16.1	24.7	1.0313	1.0036	1830.3	1836.1	1835.3	0.021119	
22.3	1855	215	35	16.1	16.1	0.99936	0.99936	1838.9	1838.9	1838.9		
23.1	1743	94	122	21.42	24.22	1.008	1.0001	1718.8	1719.6	1721.6		0.071594
23.2	1743	94	79	21.42	22.99	0.99905	1	1720	1720	1720	0.044036	
23.3	1743	94	44	21.42	21.42	0.99936	1.0008	1721.6	1721.6	1721.5		
24.1	1743	123	131	21	23.8	1.0018	1.0041	1719.2	1719.5	1722.5		0.37866
24.2	1743	123	86	21	21.2	0.99997	1.0056	1721.8	1721.8	1721.4		
25.1	1780	98	120	6.3	11.4	1.0227	1.0185	1768.6	1771.1	1775.5		0.19654
25.2	1780	98	95	6.3	12	1.0343	1.0181	1768	1770.9	1769.2	0.098058	
25.3	1780	98	44	6.3	6.3	1.0266	1.0123	1773.7	1774.7	1774.2		
26.1	1738	177	190	6.8	16.2	1.0174	1.0068	1721.8	1724.9	1732.5		0.57932
26.2	1738	177	118	6.8	11.1	1.0154	1.0038	1726.9	1728.6	1728.1	0.053056	
26.3	1738	177	60	6.8	6.8	0.99961	0.99963	1731.2	1731.2	1731.2		
27.1	1685	104	115	10.12	10.75	1.0018	1.0005	1674.3	1674.5	1675		0.04399
27.2	1685	104	60	10.12	10.1	1.0005	1.0001	1674.9	1675	1674.9	-0.0019043	
27.3	1685	104	30	10.12	10.12	0.99994	1.0008	1674.9	1674.9	1674.9		
28.1	1668	114	125	24.27	24.9	1.0005	0.99955	1643.1	1643.2	1643.7		0.048384
28.2	1668	114	85	24.27	24.37	0.99952	0.99941	1643.6	1643.6	1643.6	0.0018652	
28.3	1668	114	35	24.27	24.27	0.99937	0.99937	1643.7	1643.7	1643.7		
29.1	1732	150	176	38.6	50.3	1.0289	1.0003	1681.7	1685.4	1693.5		0.31119
29.2	1732	150	120	38.6	38	1.0009	0.99994	1694	1694.1	1694.1	-0.011721	
29.3	1732	150	62	38.6	38.6	0.99943	0.99946	1693.4	1693.4	1693.4		
30.1	1750	138	155	14.54	17.3	1.0026	0.99993	1732.7	1733.1	1735.5		0.14064
30.2	1750	138	123	14.54	14.57	1.0003	0.99986	1735.4	1735.5	1735.5	-0.0006937	
30.3	1750	138	60	14.54	14.54	0.99936	0.99993	1735.5	1735.5	1735.4		
31.1	1664	93	108	13.65	13.43	1.0017	0.99994	1650.6	1650.8	1650.4		-0.026294
31.2	1664	93	85	13.65	13.78	1.0004	0.9999	1650.2	1650.3	1650.3	0.0042358	
31.3	1664	93	55	13.65	13.65	1.0002	0.99941	1650.3	1650.4	1650.4		
32.1	1689	172	189	2.6	45.83	1.0018	1.0013	1643.2	1643.5	1686.7		2.5414
32.2	1689	172	161	2.6	45.88	1.0022	1.0012	1643.1	1643.4	1643.2	0.92917	
32.3	1689	172	113	2.6	1.48	1.0025	1.0004	1687.5	1687.9	1687.8		
32.4	1689	172	78	2.6	2.6	1.0002	0.99968	1686.4	1686.5	1686.4		
33.1	1872	141	157	34.7	35.01	1.0009	0.99984	1837	1837.2	1837.4		0.011047
33.2	1872	141	137	34.7	34.08	1.0004	0.99982	1837.9	1838	1838	-0.011628	
33.3	1872	141	78	34.7	34.7	0.99936	0.9995	1837.3	1837.3	1837.3		
34.1	1653	34	48	6.94	7.82	0.99941	1	1645.2	1645.2	1646.1		0.063947
34.2	1653	34	29	6.94	6.94	0.99945	1.0002	1646.1	1646.1	1646		
35.1	1760	153	168	19.39	24.88	1.0084	0.9998	1735.1	1736.4	1740.7		0.28376
35.2	1760	153	150	19.39	23.95	1.0013	0.99977	1736.1	1736.3	1736.2	0.051989	
35.3	1760	153	66	19.39	19.39	0.99938	0.99942	1740.6	1740.6	1740.6		
36.1	1892	195	210	28	29.9	1.0286	1.0027	1862.1	1867.4	1864.6		-0.18717
36.2	1892	195	191	28	27.8	1.022	1.0023	1864.2	1867.9	1867.4	-0.024539	
36.3	1892	195	146	28	26	1.0026	1	1866	1866.4	1866.3		
36.4	1892	195	85	28	28	1.0004	0.99969	1864	1864.1	1864		
37.1	1971	240	255	58.63	60.84	1.0024	1	1910.2	1910.8	1912.5		0.11573
37.2	1971	240	235	58.63		1.0023	0.99996					
37.3	1971	240	151	58.63	59.06	0.99947	0.99972	1911.9	1912	1911.9	0.0064591	

Table III. (cont.)

part 1

Monitor Well Site.Well No.	Elevation of land (ft)	Depth to bedrock (ft)	Depth to top of screen (ft)	Depth to wat table (ft)	Depth to wat in well (ft)	Dens. of wate at screen (g/	Avg. density water (g/cc)	Hip point- water head (	Hif fresh- water head (	Hin environ.- water head (	Aquifer vert. gradient	GRADbr aquifer- bedrock gradient
37.4	1871	240	82	58.63	58.63	0.99951	0.99983	1912.4	1912.4	1912.4		
38.1	1844	189	204	26.35	32.17	1.0019	1.0003	1811.8	1812.3	1817.8		0.36937
38.2	1844	189	187	26.35	31.7	1.003	1.0002	1812.3	1812.9	1812.7	0.046006	
38.3	1844	189	80	26.35	26.35	0.99996	0.9999	1817.7	1817.7	1817.7		
39.1	1679	55	73	1.92	4.98	1.0158	0.99952	1674	1675.1	1677.1		0.10813
39.2	1679	55	53	1.92	2.93	0.99984	0.99951	1676.1	1676.1	1676.1	0.026081	
39.3	1679	55	15	1.92	1.92	0.99936	0.99955	1677.1	1677.1	1677.1		
40.1	1735	158	176	56.85	57	1.0002	0.99944	1678	1678.1	1678.2		0.0032145
40.2	1735	158	156	56.85	56.77	0.99951	0.99944	1678.2	1678.2	1678.2	-0.0014793	
40.3	1735	158	97	56.85	56.85	0.99942	0.99943	1678.2	1678.2	1678.1		
41.1	1655	83	98	2.5	3.09	1.0013	0.99965	1651.9	1652.1	1652.5		0.028776
41.2	1655	83	78	2.5	2.55	1.0001	0.99962	1652.4	1652.5	1652.5	0.0003139	
41.3	1655	83	29	2.5	2.5	0.99944	0.99938	1652.5	1652.5	1652.5		
42.1	1829	160	178	13.03	21.28	1.0059	1.0007	1807.7	1808.7	1816.2		0.41237
42.2	1829	160	157	13.03	20.36	1.0042	1.0006	1808.6	1809.3	1809.1	0.12883	
42.3	1829	160	103	13.03	13.03	1.0007	0.99948	1816	1816.1	1816.1		
43.1	1872	65	88	4.87	5.4	1.0023	1.0009	1866.6	1866.8	1867.2		0.016665
43.2	1872	65	40	4.87	4.87	0.9996	0.99946	1867.1	1867.1	1867.1		
44.1	1891	186	203	76.48	68.57	0.99934		1822.4	1822.4			
44.2	1891	186	173	76.48	68.55	0.99933		1822.4	1822.4			
44.3	1891	186	121	76.48	76.48	0.9994	0.9995	1814.5	1814.5	1814.5		
44.4	1891	186	78	76.48		0.99956	0.99948					
45.1	1795	178	192	47.77	48.65	0.99946	0.99965	1746.3	1746.4	1747.3		0.064514
45.2	1795	178	150	47.77	48.69	0.99936	0.99972	1746.3	1746.3	1746.3	0.014463	
45.3	1795	178	85	47.77	47.77	0.99938	0.99983	1747.2	1747.2	1747.2		
46.1	1830	177	195	47.28	51.65	0.99973		1778.3	1778.4			
46.2	1830	177	164	47.28	47.37	0.99939		1782.6	1782.6			
46.3	1830	177	78	47.28	47.28	0.99955	0.9994	1782.7	1782.7	1782.7		
47.1	1900	177	188	71.44	77.05	0.99935	0.99973	1822.9	1822.9	1828.6		0.51364
47.2	1900	177	158	71.44	71.86	1.0016	0.99961	1828.1	1828.3	1828.3	0.00323	
47.3	1900	177	82	71.44	71.44	0.99941	0.99971	1828.6	1828.6	1828.6		
48.1	1842	178	187	56.59	62.85	0.99935	0.99955	1779.2	1779.1	1785.4		0.6982
48.2	1842	178	162	56.59	56.36	0.99936	0.99957	1785.6	1785.6	1785.6	-0.0044378	
48.3	1842	178	114	56.59	56.59	0.99939	0.99948	1785.4	1785.4	1785.4		
49.1	1737	106	116	-0.75		1.0433						
49.2	1737	106	89	-0.75								
49.3	1737	106	51	-0.75	0.33	1.0001		1736.7	1736.7			
49.4	1737	106	27	-0.75	-0.75	0.99936	0.99974	1737.8	1737.8	1737.7		
50.1	1912	223	190	26.15	25.94	0.99952	0.9994	1886.1	1886.1	1886.1	-0.0025164	
50.2	1912	223	120	26.15	26.09	0.99936	0.99943	1885.9	1885.9	1885.9		
50.3	1912	223	45	26.15	26.15	0.99936	0.99956	1885.8	1885.8	1885.8		
51.1	1915	200	170	17.3	17.83	1.0011	0.99948	1897.2	1897.4	1897.4	0.003597	
51.2	1915	200	95	17.3	17.3	0.99941	0.99954	1897.7	1897.7	1897.7		
52.1	1920	221	195	30.79	30.4	0.99952	0.99942	1889.6	1889.6	1889.6	-0.0040682	
52.2	1920	221	97	30.79	30.79	0.99954	0.99943	1889.2	1889.2	1889.2		
SP	1840	186	197	10.8	20.9	1.0352	1.0054	1819.1	1825.4	1830.3		0.44013

NOTE: Density at screen is median value from the processed EM logs for the screened interval except for wells screened in bedrock where density is determined from the chloride concentration (Whittemore, 1993).

NOTE: Average density is determined from EM logs between water table and lesser of depth to screen or bedrock.

Table III. part 2	Variable density corrections applied to fluid levels measured in monitoring wells during 1994.											
Monitor Well Site.Well No.	Elevation of land (ft)	Depth to bedrock (ft)	Depth to top of screen (ft)	Depth to wat table (ft)	Depth to wat in well (ft)	Dens. of wate at screen (g/	Avg. density water (g/cc)	Hip point-water head (	Hif fresh-water head (	Hin environ.-water head (	Aquifer vert. gradient	GRADbr aquifer-bedrock gradient
1.1	1827	146	146	6.35	6	1.0171	1.0052	1821	1823.5	1822.7		
1.2	1827	146	106	6.35	6.51	1.0036	0.99973	1820.5	1820.9	1820.9	-0.0032558	
1.3	1827	146	36	6.35	6.35	0.99936	0.99945	1820.7	1820.7	1820.6		
3.1	1898	130	120	20.54	23.31	1.0117	0.99971	1874.7	1875.9	1875.8	0.029279	
3.2	1898	130	65	20.54	20.54	0.99939	0.99941	1877.5	1877.5	1877.5		
4.1	1912	129	217	7.87	5.54	1.041	1.0017	1906.5	1915.3	1904.4		-0.12335
4.2	1912	129	106	7.87	3.16	1.0012	1.0015	1908.8	1909	1908.8	-0.088561	
4.3	1912	129	53	7.87	7.87	1.001	1.0011	1904.1	1904.2	1904.1		
5.1	1855	181	193	2.08	1.53	1.0547	1.0222	1853.5	1864.1	1857		-0.58867
5.2	1855	181	92	2.08	3.6	1.028	1.0017	1851.4	1853.9	1853.7	-0.015578	
5.3	1855	181	40	2.08	2.08	0.99936	0.99955	1852.9	1852.9	1852.9		
6.1	1950	148	216	15.42	21.66	1.0566	1.0006	1928.3	1939.5	1934.7		-0.069611
6.2	1950	148	135	15.42	10.45	0.99936	1.0003	1939.6	1939.6	1939.4	-0.064528	
6.3	1950	148	60	15.42	15.42	1.0005	1.0001	1934.6	1934.6	1934.6		
7.1	1906	150	230	16.92		1.0453						
7.2	1906	150	150	16.92	15.75			1890.3				
7.3	1906	150	56	16.92	16.92	0.99939	0.99939	1889.1	1889.1	1889.1		
8.1	1848	118	237	11.1	23.52	1.0582	1.0003	1824.5	1837	1837		-0.0004381
8.2	1848	118	116	11.1	17.19	1.0032	1.0002	1830.8	1831.2	1831.1		
8.3	1848	118	87	11.1	16.86	0.99999	1.0003	1831.1	1831.2	1831.1	0.14152	
8.4	1848	118	46	11.1	11.1	0.99998	0.99955	1836.9	1836.9	1836.9		
9.1	1755	87	86	9.36	9.34	1.0037	1.0029	1745.7	1746	1745.7		
9.2	1755	87	62	9.36	9.2	1.0013	1.0003	1745.8	1745.9	1745.9	-0.0089722	
9.3	1755	87	38	9.36	9.36	0.99936	0.99944	1745.6	1745.6	1745.6		
10.1	1790	156	160	13.75	20.4	1.0016	1.0001	1769.6	1769.9	1776.4		1.6091
10.2	1790	156	143	13.75	20.16	1.0012	0.99995	1769.8	1770.1	1770		
10.3	1790	156	100	13.75	18.12	1.0003	0.99959	1771.9	1772	1771.9	0.1662	
10.4	1790	156	74	13.75	13.75	0.99956	0.99942	1776.2	1776.3	1776.3		
11.1	1763	208	237	11.39	29.37	1.0329	1.0048	1733.6	1740.6	1752.7		0.41651
11.2	1763	208	61	11.39	11.39	1.0003	1.0003	1751.6	1751.7	1751.6		
12.1	1776	142	166	20.25	22.04	0.99942	0.99944	1754	1754	1755.8		0.074651
12.2	1776	142	130	20.25	19.87	0.99936	0.99944	1756.1	1756.1	1756.1	-0.0053833	
12.3	1776	142	60	20.25	20.25	0.99936	0.9995	1755.7	1755.7	1755.7		
13.1	1905	172	182	33.68	36.09	0.99934	1	1868.9	1868.9	1871.4		0.25013
13.2	1905	172	120	33.68	33.66	1.001	0.99981	1871.3	1871.5	1871.4	-0.0018547	
13.3	1905	172	53	33.68	33.68	0.99936	0.99943	1871.3	1871.3	1871.3		
14.1	1989	238	280	99.18	100.1	0.99936	0.99984	1888.9	1888.9	1889.9		0.023748
14.2	1989	238	223	99.18	99.3	0.99936	0.9999	1889.7	1889.7	1889.6	0.0018084	
14.3	1989	238	115	99.18	99.18	1.0001	0.99957	1889.8	1889.8	1889.8		
15.1	1725	128	135	28.02	25.19	0.99994	0.99958	1699.8	1699.9	1697		-0.41019
15.2	1725	128	116	28.02	29.16	0.9997	0.9995	1695.8	1695.9	1695.9	0.019051	
15.3	1725	128	57	28.02	28.02	0.99941	0.99937	1697	1697	1697		
16.1	1872	220	243	7.64	20.85	1.0461	1.0098	1851.2	1861.5	1866.6		0.21902
16.2	1872	220	198	7.64	14.93	1.0445	1.0063	1857.1	1865.3	1864	0.0026235	
16.3	1872	220	80	7.64	7.64	0.99936	0.99982	1864.4	1864.4	1864.3		
17.1	1804	114	129	10.54	44.06	1.0126	1.0026	1759.9	1761.1	1793.8		2.1824
17.2	1804	114	102	10.54	9.91	1.0106	1.002	1794.1	1795.1	1794.9	-0.023437	
17.3	1804	114	41	10.54	10.54	0.99936	0.99954	1793.5	1793.5	1793.5		
18.1	1810	214	231	11.02	26.44	1.0157	1.005	1783.6	1786.9	1800.1		0.77756
18.2	1810	214	197	11.02	26.97	1.0192	1.0038	1783	1786.4	1785.6	0.088169	
18.3	1810	214	45	11.02	11.02	0.99957	0.99954	1799	1799	1799		
19.1	1901	163	180	11.49	17.92	0.99957	1.0002	1883.1	1883.1	1889.6		0.38374
19.2	1901	163	145	11.49	13.32	1.0006	1.0001	1887.7	1887.8	1887.7	0.017141	
19.3	1901	163	42	11.49	11.49	0.99936	0.99936	1889.5	1889.5	1889.5		

Table III. (cont.)
part 2

Monitor Well Site.Well No.	Elevation of land (ft)	Depth to bedrock (ft)	Depth to top of screen (ft)	Depth to wat table (ft)	Depth to wat in well (ft)	Dens. of wate at screen (g/	Avg. density water (g/cc)	Hip point-water head (	Hif fresh-water head (	Hin environ.-water head (	Aquifer vert. gradient	GRADbr aquifer-bedrock gradient
20.1	1960	198	221	19.48	25.91	1.0063	1.0001	1934.1	1935.4	1940.7		0.2264
20.2	1960	198	189	19.48	18.46	0.99936	1.0002	1941.5	1941.5	1941.4	-0.0061436	
20.3	1960	198	46	19.48	19.48	0.99944	0.99948	1940.5	1940.5	1940.5		
21.1	1801	137	145	23.07	26.04	1.015	1.0019	1775	1776.8	1778.2		0.17361
21.2	1801	137	113	23.07	23.93	1.0042	1.0004	1777.1	1777.5	1777.4	0.0072283	
21.3	1801	137	43	23.07	23.07	0.99999	1.0008	1777.9	1777.9	1777.9		
22.1	1855	215	231	12.71	24.57	1.043	1.0047	1830.4	1839.4	1843.4		0.24522
22.2	1855	215	206	12.71	20.11	1.0305	1.0035	1834.9	1840.7	1839.9	0.014084	
22.3	1855	215	35	12.71	12.71	0.99936	0.99936	1842.3	1842.3	1842.3		
23.1	1743	94	122	22.4	23.93	1.008	1.0001	1719.1	1719.9	1720.7		0.026114
23.2	1743	94	79	22.4	21.95	1.0006	0.99969	1721.1	1721.1	1721.1	-0.014362	
23.3	1743	94	44	22.4	22.4	0.99939	0.99942	1720.6	1720.6	1720.6		
24.1	1743	123	131	23.9	25.94	1.0018	1.0028	1717.1	1717.3	1719.4		0.26602
24.2	1743	123	86	23.9	24.15	0.99991	1.0036	1718.8	1718.9	1718.6		
25.1	1780	98	120	6.02	11.8	1.0227	1.0187	1768.2	1770.7	1775.8		0.22863
25.2	1780	98	95	6.02	12.64	1.0318	1.0182	1767.4	1770	1768.4	0.12116	
25.3	1780	98	44	6.02	6.02	1.0267	1.0121	1774	1775	1774.5		
26.1	1738	177	190	8.76	16.72	1.0174	1.0075	1721.3	1724.4	1730.6		0.47714
26.2	1738	177	118	8.76	12.61	1.0166	1.0042	1725.4	1727.2	1726.7	0.04425	
26.3	1738	177	60	8.76	8.76	0.99994	0.99983	1729.2	1729.3	1729.2		
27.1	1685	104	115	11.22	11.52	1.0018	1.0009	1673.5	1673.7	1673.9		0.01729
27.2	1685	104	60	11.22	11.05	1.0008	1.0004	1673.9	1674	1674	-0.007015	
27.3	1685	104	30	11.22	11.22	1.0002	1.0013	1673.8	1673.8	1673.8		
28.1	1668	114	125	22.46	22.62	1.0005	0.99958	1645.4	1645.5	1645.6		0.005704
28.2	1668	114	85	22.46	22.55	0.99939	0.99954	1645.4	1645.5	1645.4	0.002019	
28.3	1668	114	35	22.46	22.46	0.99957	0.99944	1645.5	1645.5	1645.5		
29.1	1732	150	176	35.99	49.44	1.0289	1.0002	1682.6	1686.3	1696.1		0.37717
29.2	1732	150	120	35.99	35.49	1.0009	0.99988	1696.5	1696.6	1696.6	-0.010199	
29.3	1732	150	62	35.99	35.99	0.99937	0.99956	1696	1696	1696		
30.1	1750	138	155	17.19	18.59	1.0026	0.99984	1731.4	1731.8	1732.9		0.060138
30.2	1750	138	123	17.19	17.15	1.0002	0.99976	1732.8	1732.9	1732.9	-0.0016257	
30.3	1750	138	60	17.19	17.19	0.99937	0.99974	1732.8	1732.8	1732.8		
31.1	1664	93	108	15.06	14.3	1.0017	0.99992	1649.7	1649.9	1649		-0.062329
31.2	1664	93	85	15.06	14.6	1.0004	0.99988	1649.4	1649.5	1649.4	-0.015792	
31.3	1664	93	55	15.06	15.06	0.99998	0.9994	1648.9	1649	1649		
32.1	1689	172	189	9.1	48.64	1.0018	1.0015	1640.4	1640.7	1680.2		2.3257
32.2	1689	172	161	9.1	47.87	1.0023	1.0014	1641.1	1641.5	1641.2	0.89831	
32.3	1689	172	113	9.1	4.95	1.0026	1.0006	1684.1	1684.4	1684.3		
32.4	1689	172	78	9.1	9.1	1.0003	0.99981	1679.9	1680	1679.9		
33.1	1872	141	157	32.23	32.88	1.0009	0.99968	1839.1	1839.3	1839.8		0.031082
33.2	1872	141	137	32.23	32.71	1.0001	0.99966	1839.3	1839.4	1839.3	0.007289	
33.3	1872	141	78	32.23	32.23	0.99936	0.99945	1839.8	1839.8	1839.8		
34.1	1653	34	48	8.26	9.09	0.99941	1	1643.9	1643.9	1644.8		0.060329
34.2	1653	34	29	8.26	8.26	0.99943	1	1644.7	1644.7	1644.7		
35.1	1760	153	168	18.41	23.45	1.0084	0.99982	1736.6	1737.9	1741.7		0.25311
35.2	1760	153	150	18.41	22.59	1.0013	0.99979	1737.4	1737.7	1737.6	0.047469	
35.3	1760	153	66	18.41	18.41	0.9994	0.99944	1741.6	1741.6	1741.6		
36.1	1892	195	210	27.84	28.43	1.0286	1.0028	1863.6	1868.9	1864.7		-0.277
36.2	1892	195	191	27.84	27.65	1.0193	1.0024	1864.3	1867.6	1867.1	0.0080539	
36.3	1892	195	146	27.84	24.83	1.0026	1.0001	1867.2	1867.6	1867.5		
36.4	1892	195	85	27.84	27.84	1.0001	0.99971	1864.2	1864.2	1864.2		
37.1	1971	240	255	57.1	59.09	1.0024	0.99999	1911.9	1912.5	1914		0.10045
37.2	1971	240	235	57.1		1.0022	0.99993					
37.3	1971	240	151	57.1	57.53	0.99944	0.99971	1913.5	1913.5	1913.4	0.0064556	

Table III. (cont.)

part 2

Monitor Well Site.Well No.	Elevation of land (ft)	Depth to bedrock (ft)	Depth to top of screen (ft)	Depth to wat table (ft)	Depth to wat in well (ft)	Dens. of wate at screen (g/	Avg. density water (g/cc)	Hip point-water head (	Hif fresh-water head (	Hin environ.-water head (	Aquifer vert. gradient	GRADbr aquifer-bedrock gradient
37.4	1971	240	82	57.1	57.1	0.99944	0.99984	1913.9	1913.9	1913.9		
38.1	1844	189	204	25.81	30.95	1.0019	1.0003	1813.1	1813.5	1818.3		0.32386
38.2	1844	189	187	25.81	30.42	1.0031	1.0003	1813.6	1814.2	1814	0.039055	
38.3	1844	189	80	25.81	25.81	0.99997	0.99991	1818.2	1818.2	1818.2		
39.1	1679	55	73	3.13	6	1.0158	0.99956	1673	1674.1	1675.9		0.098619
39.2	1679	55	53	3.13	4.42	0.99996	0.99954	1674.6	1674.6	1674.6	0.033383	
39.3	1679	55	15	3.13	3.13	0.99936	0.99946	1675.9	1675.9	1675.9		
40.1	1735	158	176	53.31	53.55	1.0002	0.99948	1681.4	1681.6	1681.7		0.0083008
40.2	1735	158	156	53.31	54.41	0.99972	0.99947	1680.6	1680.6	1680.6	0.01829	
40.3	1735	158	97	53.31	53.31	0.99963	0.99953	1681.7	1681.7	1681.7		
41.1	1655	83	98	2.18	1.93	1.0013	0.99965	1653.1	1653.3	1652.8		-0.02736
41.2	1655	83	78	2.18	1.98	0.99996	0.99963	1653	1653.1	1653	-0.0045739	
41.3	1655	83	29	2.18	2.18	0.99944	0.9994	1652.8	1652.8	1652.8		
42.1	1829	160	178	13.01	18.48	1.0059	1.0007	1810.5	1811.6	1816.2		0.25671
42.2	1829	160	157	13.01	17.61	1.0039	1.0006	1811.4	1812	1811.8	0.078652	
42.3	1829	160	103	13.01	13.01	1.0006	0.99947	1816	1816.1	1816.1		
43.1	1872	65	88	5.14	5.19	1.0023	1.0011	1866.8	1867.1	1867		-0.003678
43.2	1872	65	40	5.14	5.14	0.99955	0.99979	1866.9	1866.9	1866.9		
44.1	1891	186	203	75.43	67.3	0.99934		1823.7	1823.7			
44.2	1891	186	173	75.43	67.25	0.99933		1823.8	1823.7			
44.3	1891	186	121	75.43	75.36	0.99945	0.99954	1815.6	1815.6	1815.6	-0.001533	
44.4	1891	186	78	75.43	75.43	0.9996	0.9996	1815.6	1815.6	1815.6		
45.1	1795	178	192	45.69	46.7	0.99946	0.99967	1748.3	1748.3	1749.4		0.074018
45.2	1795	178	150	45.69	46.73	0.99936	0.99974	1748.3	1748.3	1748.2	0.016369	
45.3	1795	178	85	45.69	45.69	0.99938	0.99978	1749.3	1749.3	1749.3		
46.1	1830	177	195	44.57	49.79	0.99973	0.99963	1780.2	1780.3	1785.5		0.28899
46.2	1830	177	164	44.57	44.62	1.0003	0.99957	1785.4	1785.5	1785.5	-0.0004358	
46.3	1830	177	78	44.57	44.57	0.99937	0.99938	1785.4	1785.4	1785.4		
47.1	1900	177	188	70.04	77.68	0.99935	0.99973	1822.3	1822.3	1830		0.69823
47.2	1900	177	158	70.04	70.56	1.0016	0.99961	1829.4	1829.6	1829.6	0.0045054	
47.3	1900	177	82	70.04	70.04	0.99941	0.99971	1830	1830	1830		
48.1	1842	178	187	55.18	62.52	0.99935	0.99957	1779.5	1779.5	1786.8		0.81851
48.2	1842	178	162	55.18	55.06	0.99936	0.99959	1786.9	1786.9	1786.9	-0.0019506	
48.3	1842	178	114	55.18	55.18	0.99942	0.99939	1786.8	1786.8	1786.8		
49.1	1737	106	116	-0.02		1.0433	1.0019			1737.3		
49.2	1737	106	89	-0.02		1.0013	1.0015					
49.3	1737	106	51	-0.02	1.02	1.0005	0.9999	1736	1736	1736	0.041423	
49.4	1737	106	27	-0.02	-0.02	0.99936	0.99997	1737	1737	1737		
50.1	1912	223	190	22.34	22.2	0.99952	0.99943	1889.8	1889.8	1889.8	-0.0016479	
50.2	1912	223	120	22.34	22.29	0.99936	0.99946	1889.7	1889.7	1889.7		
50.3	1912	223	45	22.34	22.34	0.99936	0.99956	1889.7	1889.7	1889.7		
51.1	1915	200	170	13.68	14.17	1.0011	0.99948	1900.8	1901.1	1901.1	0.0029818	
51.2	1915	200	95	13.68	13.68	0.99941	0.99954	1901.3	1901.3	1901.3		
52.1	1920	221	195	23.67	28.83	0.99952	0.99942	1891.2	1891.2	1891.2	0.052535	
52.2	1920	221	97	23.67	23.67	0.9995	0.99945	1896.3	1896.3	1896.3		
SP	1840	186	197	11.3	18.4	1.0352	1.0055	1821.6	1828	1829.8		0.1607

NOTE: Density at screen is median value from the processed EM logs for the screened interval except for wells screened in bedrock where density is determined from the chloride concentration (Whittemore, 1993).

NOTE: Average density is determined from EM logs between water table and lesser of depth to screen or bedrock.

aquifer may have been a consequence of the extreme recharge occurring in the upper Rattlesnake Creek basin during the summer of 1993. Similarly, the second largest rise of the interface (> 6 ft) at site 26 was accompanied by a significant decrease of the recharge gradient between 1993 and 1994.

Figures 25A and B show the fresh-water equivalent potentiometric surfaces derived from water levels measured in wells screened in the upper aquifer, lower aquifer, and bedrock for 1993 and 1994, respectively. Because the wells in the upper aquifer are typically in fresh water, there is essentially no correction to the fluid levels for these wells (Table III). These maps indicate that at this scale there is no significant difference between the shallow fresh-water and the deep fresh-water equivalent potentiometric surfaces for the Great Bend Prairie aquifer in the mineral intrusion study area. Only at sites 18 and 32 do the surfaces within the aquifer deviate significantly (over 10 ft) indicating possible confining conditions within the aquifer at these locations. Major clay layers in the aquifer at these sites may be responsible for the differences. The general pattern of hydraulic connectedness within the aquifer is also indicated by the highly correlated well hydrographs reported by Young et al. (1993). These results indicate that horizontal flow in the aquifer can be generally characterized by potentiometric surface maps developed from observation wells screened only in the upper part of the aquifer.

The maps of Figures 25A and B also indicate that the fresh-water equivalent potentiometric surface for the wells screened in the bedrock has a similar pattern of flow and apparent hydraulic connectedness between the bedrock and aquifer. Similar differences between the surfaces occur at sites 18 and 32 as described above. Differences are also apparent where the aquifer surface is significantly above the bedrock surface in the north-central part of the study area. This area corresponds with a major decrease of aquifer saturated thickness caused by a topographic high of the subcropping (and outcropping) bedrock surface (Figure 6). Other differences are apparent along Rattlesnake Creek in the western part of the study area where the bedrock potentiometric surface is above the aquifer surface. This area corresponds to the area of greatest

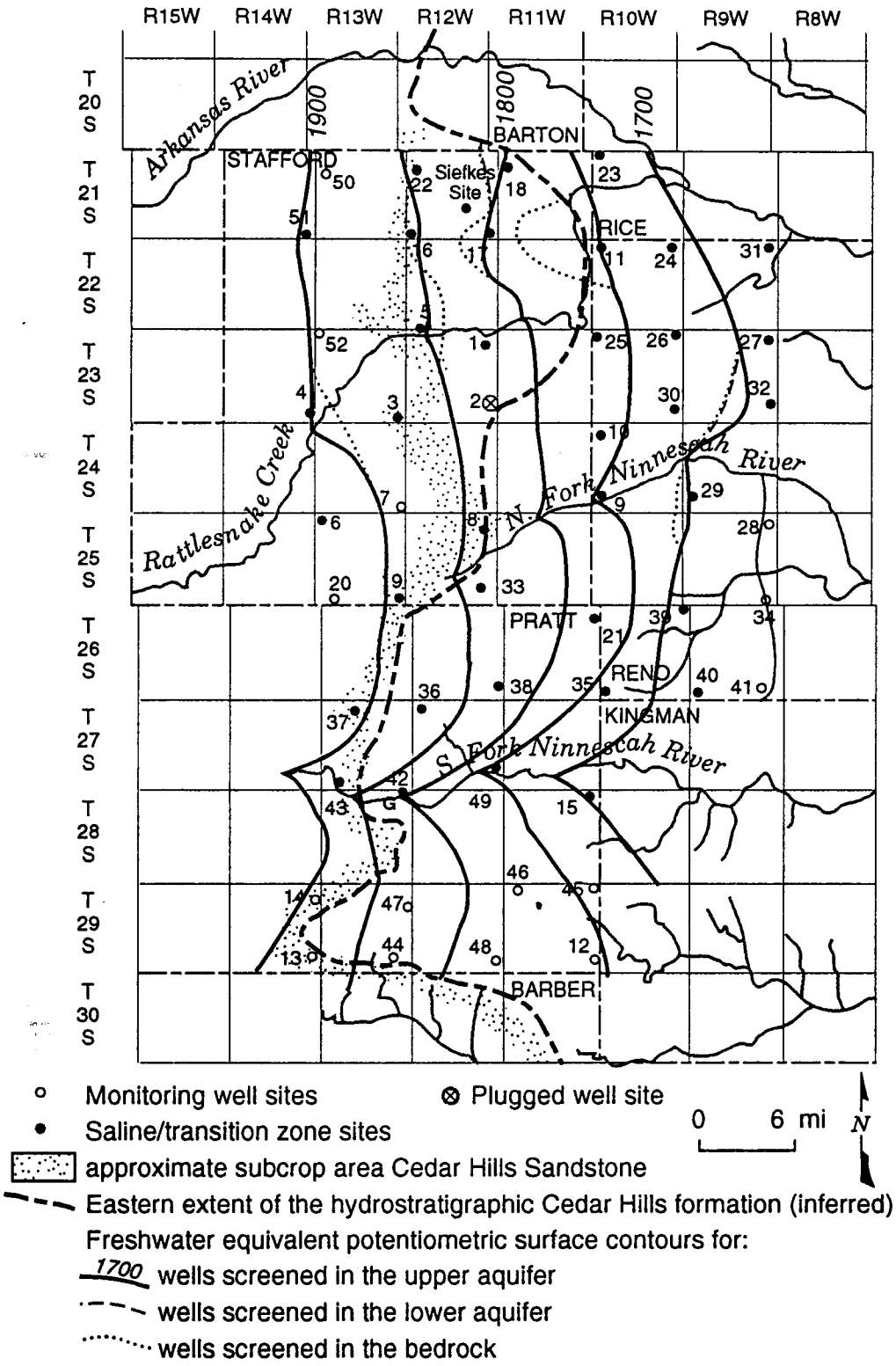

Figure 25A. Fresh-water equivalent potentiometric surfaces for the mineral intrusion study area of the Great Bend Prairie aquifer (1993).

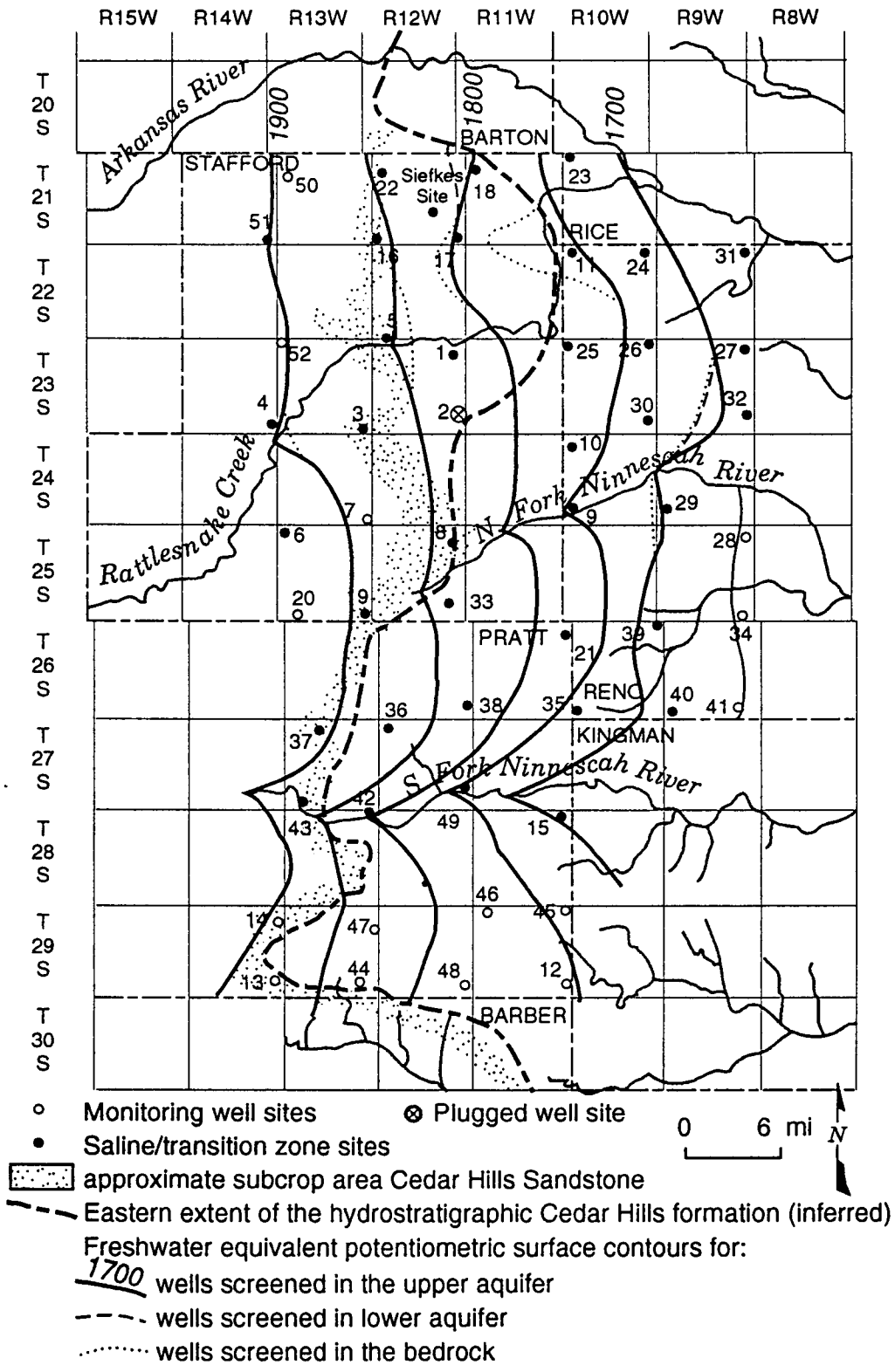

Figure 25B. Fresh-water equivalent potentiometric surfaces for the mineral intrusion study area of the Great Bend Prairie aquifer (1994).

mineral intrusion into the Great Bend Prairie aquifer as indicated by Figure 20.

Figures 26A and B show the boundary between upward and downward vertical (environmental-water) gradients between wells screened in the upper and lower alluvial aquifer for 1993 and 1994, respectively. Figures 26A and B also show where the bedrock-aquifer gradient is upward (shaded areas) calculated using equation (17) for 1993 and 1994, respectively. Figure 26 parts A and B indicates the regional vertical hydraulic connectedness of the Great Bend Prairie aquifer. The vertical environmental-water potentiometric gradient forms an extremely subtle, yet consistent pattern of vertical-flow potential distributed within the aquifer. The only significant temporal change occurred at site 23 (T21S R10W) where a reversal of gradient was accompanied by the largest upward shift in the depth of the 500 mg/L chloride interface, as was discussed previously. The pattern of vertical gradient distribution also appears to be highly correlated with the maps showing the distribution of both saline water and salt mass within the aquifer (Figures 16 and 20, respectively). The centers of saline water and salt mass distribution all coincide with areas of upward flow either directly over or immediately to the east of the Cedar Hills Sandstone hydrostratigraphic unit subcrop and where the three major streams (Rattlesnake Creek, and the North and South Forks of the Ninnescah River) flow across the Great Bend Prairie. The general eastward decrease in saline water and salt mass distribution typically coincides with transitions from an upward to a downward flow gradient or where upward flow terminates with discharge to a gaining stream.

Figure 26 parts A and B also depict a very consistent pattern of vertical flow potential between the bedrock and the Great Bend Prairie aquifer. Once again there is a correspondence between the three areas of greatest mineral intrusion (as shown in Figure 20) with areas of greatest potential for upward flow or near neutral flow (sites 8 and 33; Table III) at or adjacent to the subcrop of the Cedar Hills Sandstone hydrostratigraphic unit. In spite of the lack of actual fluid-level measurements for adjustment, the area around site 49 is also shown as a probable location of upward flow

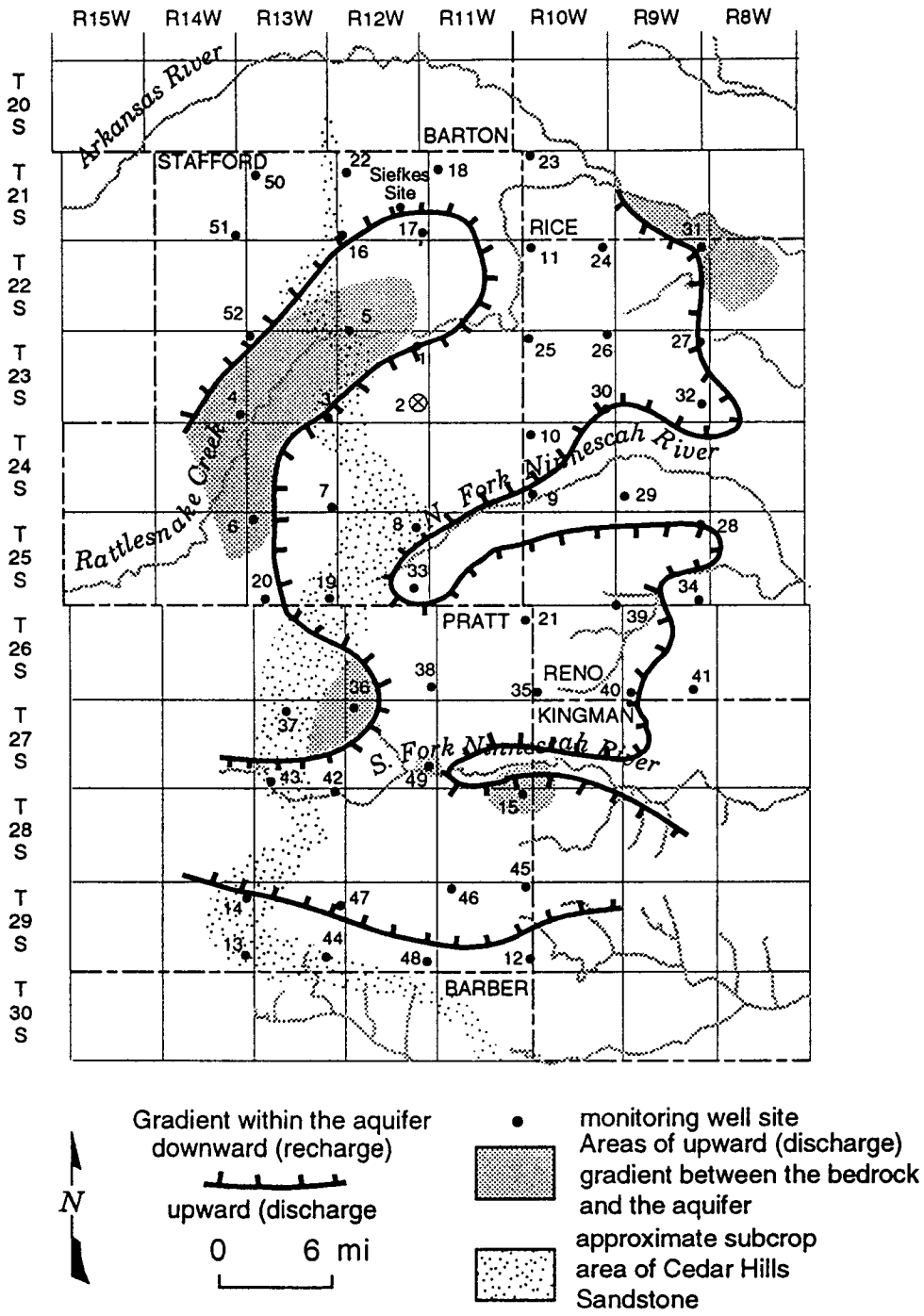

Figure 26A. Vertical environmental-water gradient between shallow and deep wells screened within the Great Bend Prairie aquifer, 1993. Contour lines indicated transition from recharge (hachured) to discharge gradient. Shaded regions indicate areas where gradient (GRADbr, Table 111A) from bedrock to aquifer is upward.

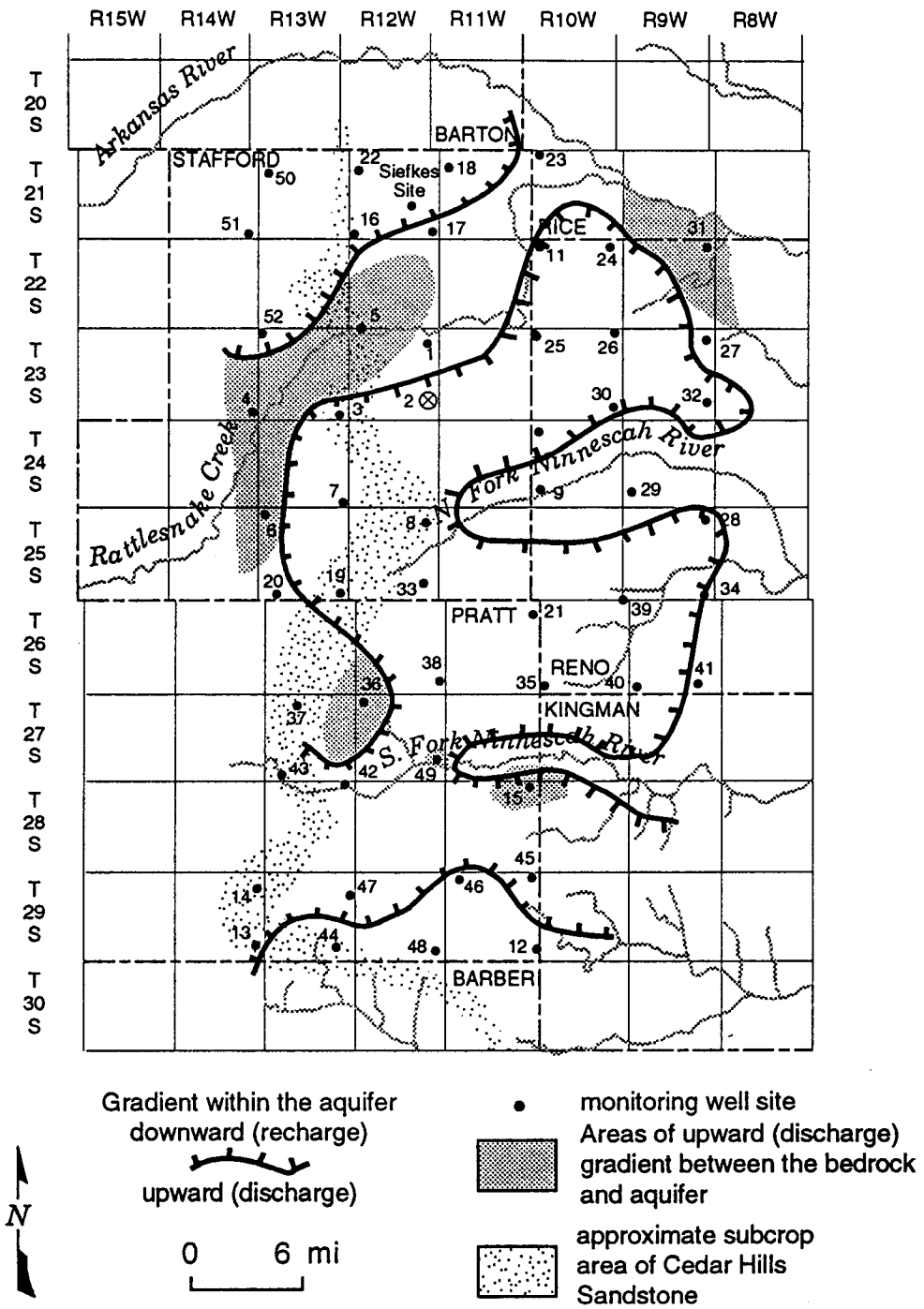

Figure 26B. Vertical environmental-water gradient between shallow and deep wells screened within the Great Bend Prairie aquifer, 1994. Contour lines indicate transition from recharge (hachured) to discharge gradient. Shaded regions indicate areas where gradient (GRADbr, Table 111B) from bedrock to aquifer is upward.

potential from the bedrock. The bedrock well at site 49 has been observed to have fluid levels above land surface and thus required installation of a casing extension and sealed cap (D. O. Whittemore, pers. comm.).

The combination of upward flow potential from the bedrock with upward flow potential in the aquifer appears to identify the three primary locations of mineral intrusion into the Great Bend Prairie aquifer. One broad area is defined by the subcrop of the Cedar Hills Sandstone hydrostratigraphic unit under the Rattlesnake Creek watershed; another broad area extends north along the Cedar Hills subcrop from the South Fork of the Ninnescah River; and one, much less broad than the other two, from the Cedar Hills subcrop in the vicinity of site 8 where the subcrop makes a dogleg bend to the east. These three potential source areas account for the three areas of salt mass distribution shown in Figure 20 -- all apparently originating at the Cedar Hills subcrop. The results from the analysis of the adjustments to fluid levels for the effects of variable density indicate that salt water seeps into the aquifer primarily where the Permian Cedar Hills Sandstone hydrostratigraphic unit subcrops, is then dispersed down-gradient, and discharges to the streams or is further dispersed laterally and vertically into the aquifer, often perching on clay lenses.

These results also indicate that the mode of seepage from the bedrock may vary. Both the well driller's lithologic and geophysical logs at site 8 of the monitoring well network record the apparent chaotic lithology characteristic of a brecciated zone produced as a consequence of bedrock collapse (Buddemeier et al., 1993). Site 8 also has the highest chloride concentration (43,800 mg/L; Whittemore, 1993) of the network indicating the presence of a possible conduit for the upward flow of highly saline water. Figure 27 shows that the thickness of salt beds in the Permian Ninnescah Shale exceeds 50 ft in areas within 4 to 5 mi south and east of site 8 (A. Martinez, unpublished data).

If the area around site 8 is a collapsed zone as a consequence of salt dissolution in the bedrock, this may explain the localized nature of this source area compared to the other apparent bedrock source areas.

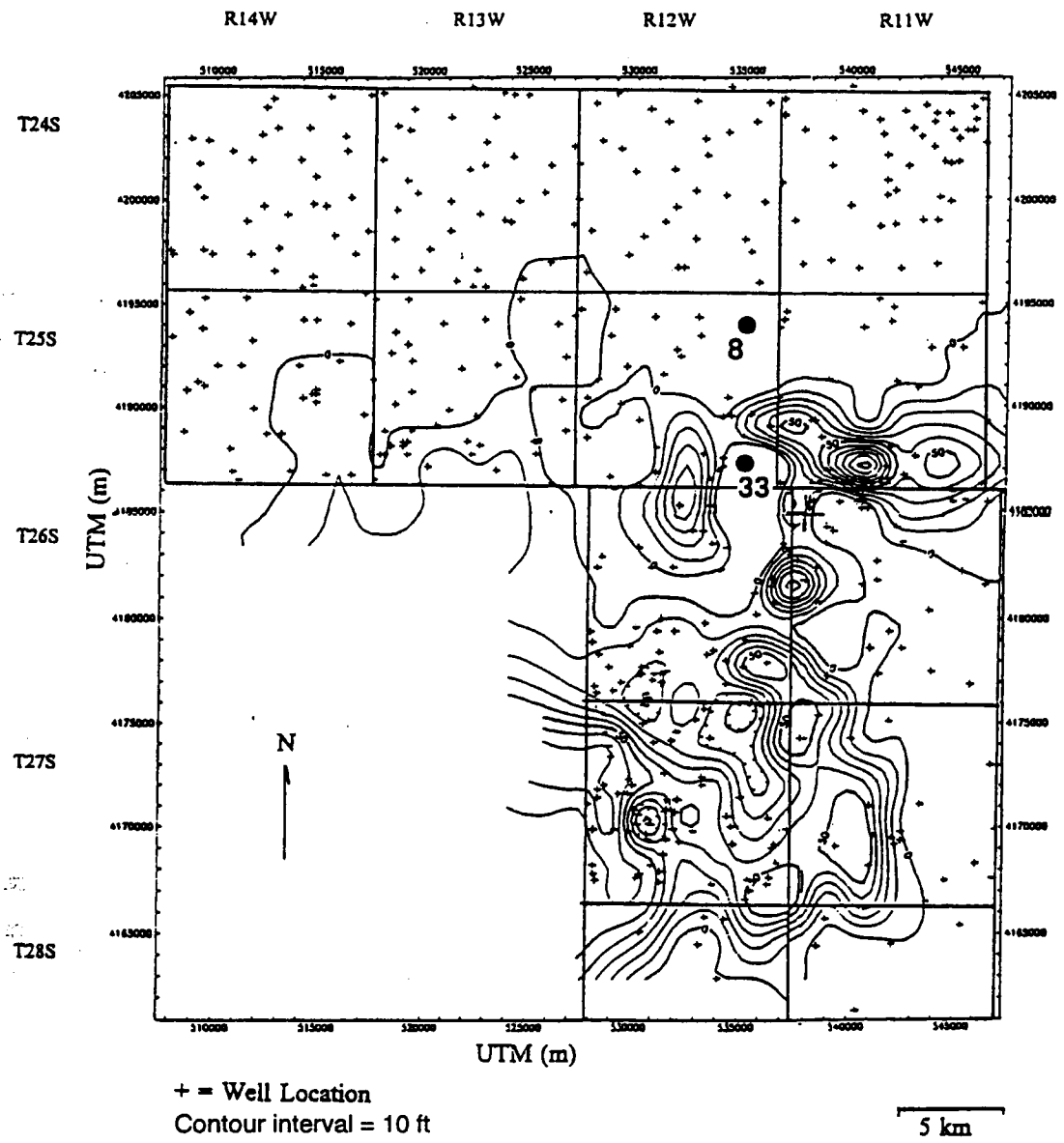

Figure 27. Isopach map of the Lower Cimmaronian Salt (Permian Ninnescah Shale). After A. Martinez (unpublished map).

Application 3: solute transport model calibration

The characteristics of the vertical freshwater-saltwater transition zone profiles represent the results of advective and dispersive solute transport in the Great Bend Prairie aquifer. Another application that can be used to analyze the freshwater-saltwater profiles is the calibration of solute transport models. The governing equation for advective and dispersive solute transport in two dimensions is (Domenico and Schwartz, 1990)

$$D_L \frac{\partial^2 C}{\partial x^2} + D_T \frac{\partial^2 C}{\partial y^2} - V_x \frac{\partial C}{\partial x} = \frac{\partial C}{\partial t} \qquad (21).$$

The first two left-hand terms of equation (21) represent the longitudinal (horizontal, along-gradient) and transverse (vertical) dispersive components, respectively. The third left-hand term represents advective transport as a function of pore velocity (V_x). Because V_x is assumed to be horizontal and uniformly distributed in the vertical direction, equation (21) represents an application of the Dupuit approximation. The dispersion coefficients (D_L and D_T) control the longitudinal and transverse spreading of solute in the modeled aquifer as functions of the corresponding dimensional dispersivities.

Equation (21) does not include a third dispersive term for lateral (horizontal, across-gradient) spreading for this application because the source of salinity is assumed to be infinite in the lateral direction for all practical purposes. The assumption is made here that the Permian Cedar Hills hydrostratigraphic unit represents a single, laterally extensive source for salt water intrusion into the Great Bend Prairie aquifer. Figure 20 shows that this assumption is probably valid for most of the study area.

Various analytical methods have been developed to solve forms of equation (21). Domenico and Schwartz (1990) present analytical solutions for multi-dimensional transport with continuous or instantaneous solute sources spreading from source areas of different geometries. These analytical solutions are generally formed as the product of solutions

derived for each dimension. These solutions are somewhat limited in application because of problems associated with the scale of the modeled aquifer. If the aquifer is shallow, vertical spreading of the solute must logically be limited to the saturated thickness. Unfortunately, transverse dispersivity must therefore often be arbitrarily adjusted to produce the desired vertical spreading dependent on the scale of the simulation. Ideally, dispersivity values should be aquifer parameters that are independent of model scale. Furthermore, most analytical solutions do not account for the synergistic effects of mass redistribution engendered by solute transport such as gravity and density effects. The distribution of mass has been demonstrated by the preceding data analyses in this thesis to be of great importance in identifying the locations and mechanisms of mineral intrusion in the Great Bend Prairie aquifer.

The top specified boundary layer (TSBL) model approach was recently developed by Rubin and Buddemeier (1994) to conceptualize the mineral intrusion process in the Great Bend Prairie aquifer. The source of mineral intrusion is considered to be a laterally extensive discontinuity in an aquitard that allows contact between fresh and saline ground water. Figure 28 shows the basic elements of the TSBL conceptual model. The width of the aquitard discontinuity is given by X_e; x being the horizontal, along-gradient dimension. The vertical (transverse) dimension is represented by the y-axis. In this basic framework, the modeled aquifer is considered to be horizontal and with a uniform but indeterminate saturated thickness.

The TSBL model approaches the analytical solution of equation (21) by establishing two boundary layers wherein the distribution of solute mass is considered. Figure 28 shows the two boundary layers: the inner layer of thickness δ_u and the outer layer of thickness δ_o-δ_u. The shaded area on Figure 28 represents the solute mass distribution at an arbitrary down-gradient point. The vertical concentration profile at this point is represented by a cumulative distribution function. The conservation of mass within the boundary layers allows the layers to spread down-gradient as a function of transverse dispersivity; yet the rate of expansion is moderated with increasing distance from the source area.

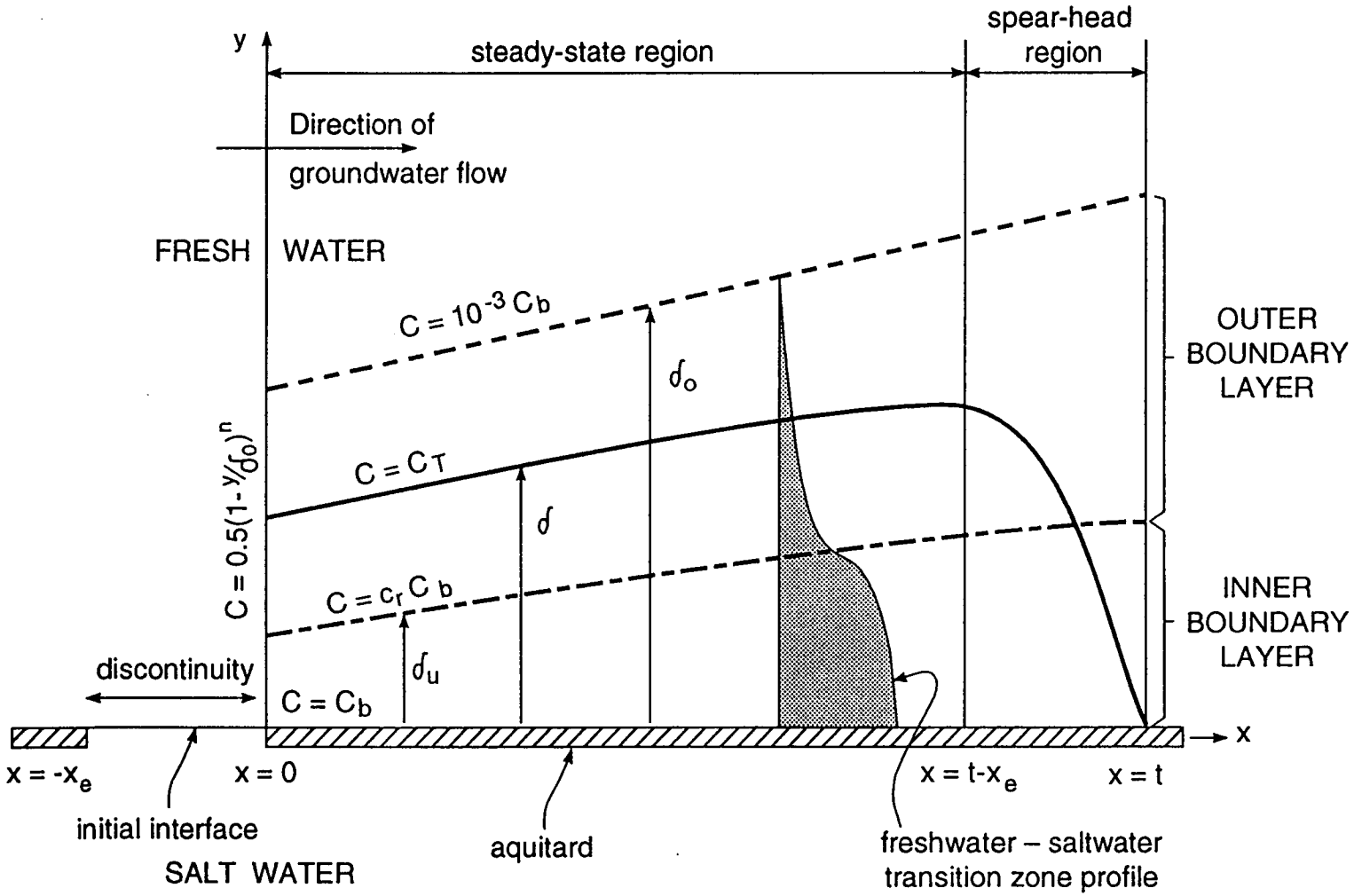

Figure 28. Basic conceptual framework of the Top Specified Boundary Layer (TSBL) model. See text for explanation of symbols.

Figure 28 also shows the position (δ) of a constant threshold concentration (where $C=C_T$) or freshwater-saltwater interface within the outer boundary layer. Because mass is conserved within the outer boundary layer, the interface position also expands (i.e. δ increases) down-gradient from the source area until at a distance that marks the boundary between the steady-state and spear-head regions. The spear-head region thus locates the area of salinity build-up from zero (or ambient) concentration to the maximum vertical spread of a given interface concentration.

A preliminary manuscript detailing the conceptual elements and derivation of the TSBL model has been published as an Open-file Report of the Kansas Geological Survey (Rubin and Buddemeier, 1994) and is also reproduced here as an appendix (Appendix III) to this thesis with the kind permission of the authors. The following two sections conduct initial experiments with the TSBL model approach (with reference to equations and formulae contained in Appendix III) to simulate both regional mineral intrusion and the localized process of upward saline water penetration near a pumping well. The TSBL model is first calibrated by determining a range of transverse dispersivity values from the fitted freshwater-saltwater transition zone profiles at sites that are within the assumed source area: the Permian Cedar Hills hydrostratigraphic unit.

Dispersivity as determined by the TSBL model approach

Using the TSBL model approach and some basic assumptions regarding the salt-water source dimensions and concentration, a range of values for transverse dispersivity can be determined. These values can then be applied in the model to simulate the regional advection and dispersion of salinity in the Great Bend Prairie aquifer. Schmorak and Mercado (1969) used statistics garnered from fitting cumulative distribution functions (CDFs) to the freshwater-saltwater transition zone profiles to estimate transverse dispersivity in a coastal aquifer. In a similar fashion, the results from fitting CDFs to the transition zone profiles in the Great Bend Prairie aquifer, shown in this thesis, are applied to

determine a possible range of transverse dispersivity values for the Great Bend Prairie aquifer.

Figure 29A shows a west-to-east cross-sectional profile through a portion of the aquifer in the mineral intrusion study area. The profile shows the elevations of the water table and bedrock surfaces as well as the elevations of the estimated 500 mg/L and 21,000 mg/L chloride concentration levels. The concentration elevations are based on the freshwater-saltwater transition zone profile curve-fitting (CDF) methods described previously in this thesis. Also shown on Figure 29A is the predicted elevation of the 500 mg/L chloride concentration based on the previously demonstrated multiple-regression analysis (see Figure 18 and Equation 12) of the water table and bedrock elevations. At site 51 the 500 mg/L elevations are set equal to the bedrock elevation and the 21,000 mg/L elevation is set equal to the corresponding elevation at the next eastward site (16) because site 51 lacked sufficient data to determine these points directly.

Based on the assumption that the subcrop of the Cedar Hills Sandstone hydrostratigraphic unit represents a laterally extensive, cumulative source area (probably an aggregate of several discrete sources) for mineral intrusion into the Great Bend Prairie aquifer, characteristics of transition zones from sites within the source area are used to determine a possible range of values of transverse dispersivity. The TSBL model can then be used to simulate the advection and dispersion of salinity from the source area and compared to actual transition zone profiles at down-gradient sites. The elevation of transition-zone points from sites 16, SP, and 17 are used for the calibration because these sites are located within the suspected source area.

Equation (12) (App. III) is solved for transverse dispersivity (a) by: determining the vertical distance (y) between the elevations of the 500 (from CDF fit estimate) and 21,000 mg/L points (ft; Table I); assuming the source area dimension (X_e) to be 10,000 ft (as an order-of-magnitude approximation for the aggregate source); and normalizing the solute (chloride) concentration (C) using equation (5) (App. III) with the fresh-water concentration (C^*_f) of 40 mg/L and salt-water concentration (C^*_s) of

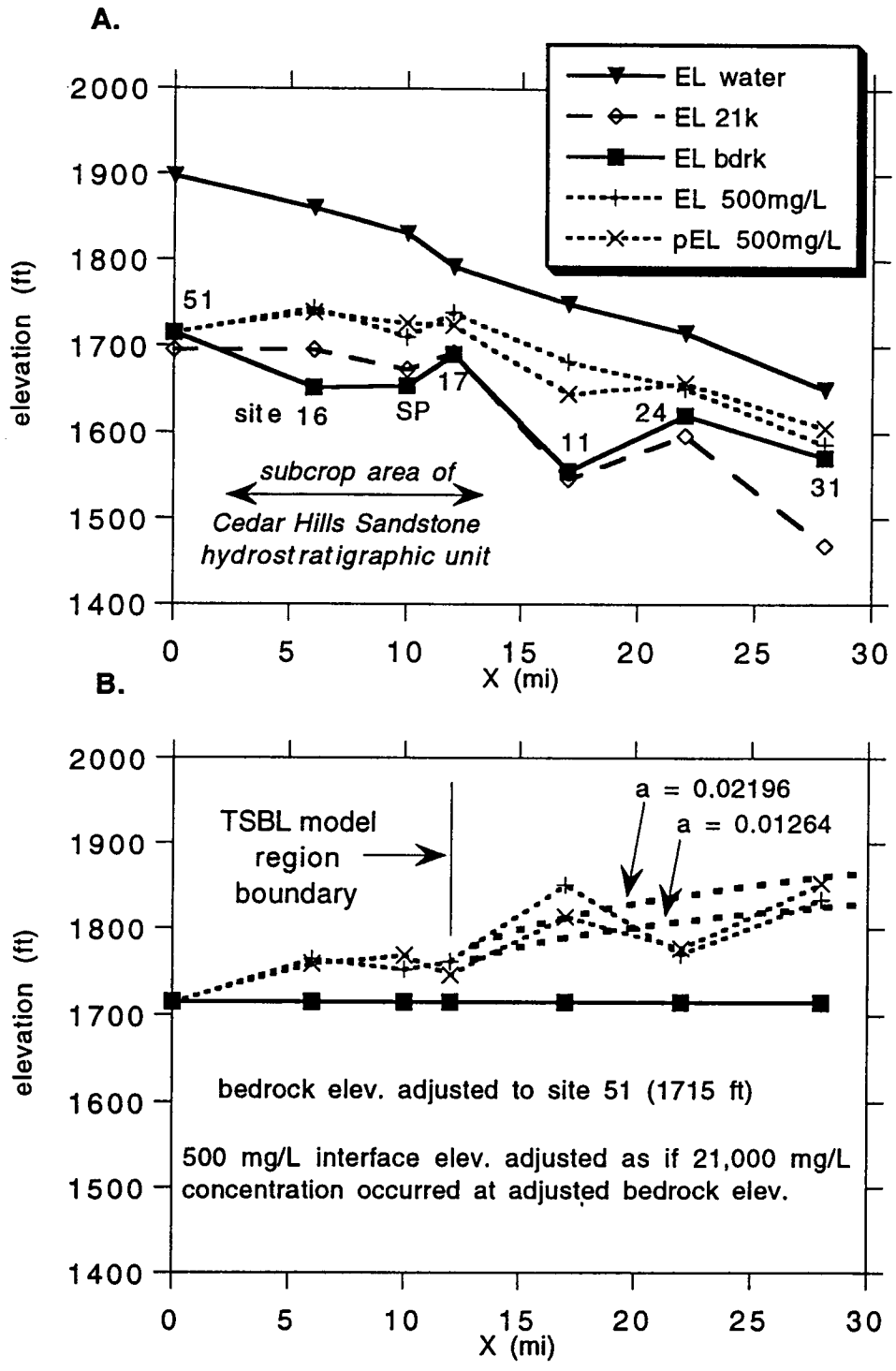

Figure 29. (A) cross section showing elevation of the 500 mg/L chloride interface relative to elevation of the water table and bedrock surfaces. (B) the adjusted interface elevations compared to TSBL model interface profiles (heavy dashed lines) using a range of transverse dispersivity values (a).

42,000 mg/L. Site 16 yields the highest value for transverse dispersivity of 0.02196 ft; the lowest value of 0.01264 ft is from site SP. The fact that these values range within only a factor of two indicates that these sites are likely within the probable source area (at steady-state conditions) for mineral intrusion.

Figure 29B shows the same profile as Figure 29A with the bedrock elevations all adjusted to a constant value (1715 ft at site 51). Adjustments are made to place the profile into the same basic conceptual framework of the TSBL model as shown in Figure 28; where the initial concentration at the saltwater interface at the base of the source area is half the source brine concentration (assumed to be 42,000 mg/L). Therefore, the 500 mg/L elevations on Figure 29B have been adjusted relative to the elevation of the 21,000 mg/L level as if the latter concentration was now everywhere coincident with the adjusted bedrock (or aquitard) elevation. These adjustments are intended to reduce any influence on the relative position of the interface by changes of the saturated thickness apparent on the original cross section (Figure 29A) and also the depth to the source brine.

Figure 29B also shows the modeled positions of the 500 mg/L concentration interface using the TSBL approach. Two 500 mg/L interface profiles are shown representing the use of the maximum and minimum calibrated values for transverse dispersivity. These values were determined from the fitted concentration profiles at site 16 (a = 0.02196 ft) and at site SP (a = 0.01264 ft) with the methods described previously in this section. The boundary of the model region, or eastern edge of the source area, was placed at site 17. The position of the modeled 500 mg/L interface was determined using the boundary layer relationships expressed in equations (13), (28), (37) through (40), and the dimensional interrelationships expressed in equations (47) through (50) (App. III).

Figure 29B shows that the TSBL model profiles underestimate the elevation of the 500 mg/L interface at site 11 and overestimate the elevation at site 24. The difference at site 11 may be caused by discharge to Rattlesnake Creek (just west of site 11) and the resultant perching (macrodispersion) of saline water on clay lenses immediately down gradient as shown on Figure 17. The difference at site 24 may be caused by

the eastward and down-gradient decrease of saturated thickness that probably restricts ground-water flow--especially the flow of dense saline water at the base of the aquifer. These differences emphasize the importance of local flow systems and the bedrock topography on the distribution of salt water in the aquifer. Whatever the probable cause of these differences, the difference between the observed interface and the modeled interface is only about the same as the difference between the two TSBL model profiles. The deviation of site-specific interface elevations from the TSBL model elevations is also probably comparable to uncertainties in the methods of determination of the elevations of the 21,000 mg/L concentration level that were used to make the profile adjustments shown on Figure 28B and calibration of transverse dispersivity values.

TSBL model comparison to an observed local salinization process

This section applies the TSBL model again using the same calibrated values for transverse dispersivity to compare the conceptual salt-water penetration to observed dynamic variations within the Great Bend Prairie aquifer. In this next experimental case, the TSBL approach is used to model the penetration of saline water through a suspected discontinuity between clay lenses within the aquifer. The penetration is a response to the seasonal pumping of one or more irrigation wells in the vicinity of the discontinuity.

Figure 19A shows the build-up of salinity directly above a clay layer in a monitoring well that is near a seasonally pumped irrigation well. Figure 19B shows that the clay layer is probably discontinuous to the east of the monitoring and irrigation wells. The sequential chloride concentration profiles (Figure 19A) show that the saline water builds-up at chloride concentrations above approximately 100 mg/L within the depth range of 120 to 130 ft.

This localized build-up of salinity can also be simulated using the TSBL model approach. Interface profiles can be generated using the same values for transverse dispersivity that were calibrated in the previous

section. Additionally, the source area discontinuity width must be estimated for this situation. Figure 30A shows the TSBL model boundary layer and 100 mg/L interface profiles spreading down-gradient from a discontinuity width (X_e) of 100 ft using the maximum (0.02196 ft) and minimum (0.01264 ft) values of transverse dispersivity. These profiles were generated using the same methods described in the previous section -- using the equations and relationships derived within Appendix III (Rubin and Buddemeier, 1994). Chloride concentration values were normalized using 40 mg/L for the fresh water (C^*_f) and 2000 mg/L for the saline source water (C^*_s) by inspection of Figure 19A. Figure 30A shows that at a horizontal distance of approximately 1200 ft, the interface and the upper edge of the inner boundary layer meet, i.e. where $\delta = \delta_u$. This distance is therefore considered to be within the region of salinity build-up, or "spear-head" region, at concentrations above that of the interface (100 mg/L in this simulation). The spear-head region is shown on Figure 27 and is defined in the TSBL model derivation within Appendix III.

Figure 30A also shows the ultimate position of the 100 mg/L interface in the spear-head region as a function of transverse dispersivity. The highest position of this modeled interface above the top of the aquitard (clay layer) surface ranges between approximately 8 to 11 ft. This range of distance closely matches the observed vertical expansion of the 100 mg/L interface from inspection of Figure 19A.

Figure 30A indicates that the horizontal distance from the clay-layer discontinuity to the spear-head region is insensitive to the range of transverse dispersivity values used in this simulation. Figure 30B shows the effect of increasing the discontinuity width (X_e) on the distance to the spear-head region. Doubling the width causes a doubling of the distance such that a discontinuity of X_e = 200 ft results in the spear-head region occurring at approximately 2400 ft. This result indicates a possible range of distances for the clay-layer discontinuity from the monitoring well given a range of discontinuity widths and using the range of transverse dispersivity values that were determined in the previous regional model simulation.

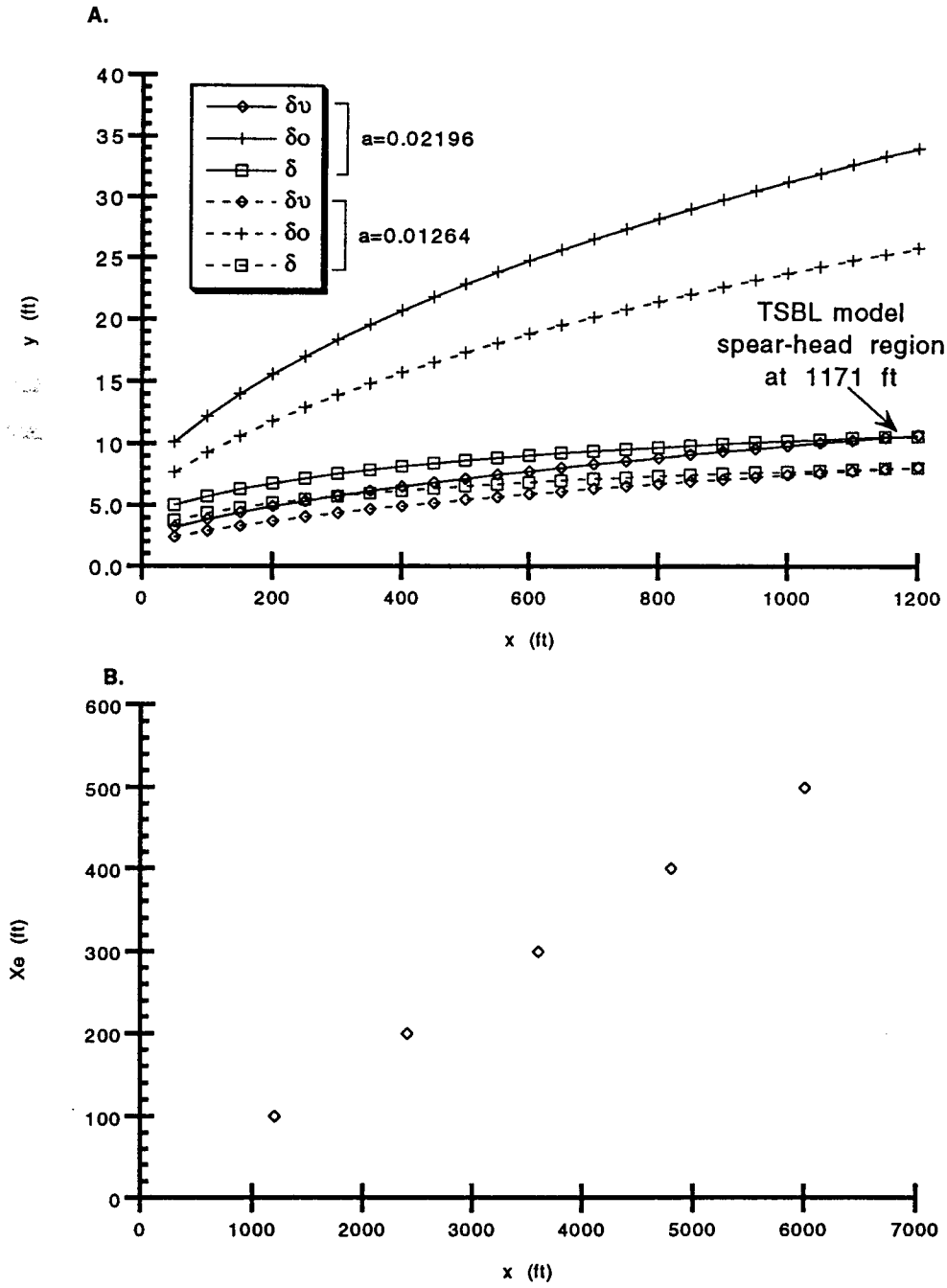

Figure 29. TSBL model profiles for 100 mg/L chloride interface position (δ) spreading from source of dimension Xe = 100 ft. (A) Spear-head region of salinity build-up is reached at approximately 1200 ft where δ = δυ.
(B) Distance to the spear-head region as a linear function of source width Xe.

The results from these basic experiments with the TSBL model indicate that this technique provides a robust simulation of mineral intrusion into the Great Bend Prairie aquifer at both regional and local scales. Transverse dispersivity, calibrated from observed freshwater-saltwater transition zones, can apparently be used as an aquifer parameter that is independent of model scale. The results further indicate that the use of simplifying assumptions regarding aquifer saturated thickness and solute source dimensions allows general comparisons between observed and simulated advective and dispersive solute transport. More detailed regional simulations will require the consideration of the effects of local flow systems and changes of saturated thickness on the distribution of solute in the aquifer.

SUMMARY

The log analysis methods developed and described herein provide a simple and effective technique for the detection and evaluation of mineral intrusion into the alluvial Great Bend Prairie aquifer and similar hydrologic systems. The cross correlation between gamma-ray and electromagnetic induction logs provides a method to significantly reduce background lithologic noise or shaly-sand effects, allowing standard curve-fitting techniques to estimate ground water quality to within a few hundred mg/L of chloride concentration. This technique makes unnecessary the determination of porosity or other complex formation factors required for traditional log analysis methods developed for hydrocarbon exploration. This technique provides the critical resolution necessary in many environmental investigations and is easily adaptable to other locations provided there is a comparable level of cross correlation.

The correction method developed by this thesis provides a simple, linear approach to the shaly-sand problem. The log cross correlation was optimized by selection of an appropriate moving-average filter size for pre-processing of the gamma-ray log. Future experiments may show that the cross correlation can be marginally improved by use of a non-linear operator such as a median or modal-type filter. However, examples in this thesis show that significant attenuation of the shaly-sand effects is presently achieved while maintaining the primary induction log response to water quality variation. This method provides an unprecedented view of the vertical variation of ground-water quality in the Great Bend Prairie aquifer.

The results of the induction log analysis provide a database for monitoring temporal changes of the regional and local saltwater distribution. The database also provides a means by which the saltwater distribution may be regionalized by trend surface analyses. The results from two years worth of measurements indicates only minor and localized changes of the saltwater distribution. This indicates that the present regional salt-water distribution approaches steady state and requires sustained monitoring to detect any significant systematic changes.

The products of the log analysis also provide elements for the development of a necessary salt budget for the aquifer. These elements include a salt mass inventory, methods to correct for variable density effects on measured fluid levels, and the calibration of transverse dispersivity for solute transport modeling. Maps generated from analysis of the salt inventory indicate that brine seeps into the Great Bend Prairie aquifer primarily from the subcropping bedrock coinciding with the Permian Cedar Hills Sandstone hydrostratigraphic unit. Analysis of the results from variable-density correction indicate that the brine is then laterally dispersed into the aquifer under regional flow control with vertical dispersion controlled by subtle but persistent local flow systems connected to discharge areas. Initial experiments were conducted using the recently developed top specified boundary layer (TSBL) model to simulate the two-dimensional advective and dispersive solute transport in the aquifer. The experimental results indicate that the TSBL model is a useful approach to simulate both regional and local mineral intrusion processes by using a narrow range (a factor of two) of values for transverse dispersivity.

Despite the apparent prevailing regional steady-state conditions for salt distribution in the Great Bend Prairie aquifer, results from a monitoring well installed near a seasonally pumped irrigation well demonstrate that local disturbances to the fresh-water flow regime cause saline water to penetrate upward through discontinuities in clay layers within the aquifer. This upconing phenomenon clearly demonstrates the importance of maintaining the hydrologic balance between fresh and saline water, particularly in areas already regionally contaminated by mineral intrusion and lacking extensive confining clay layers. In many cases, distributed, shallow irrigation pumping may alleviate upconing caused by localized, deep pumping. While brine probably continues to seep into the aquifer, the brine that has already penetrated into the aquifer from the bedrock poses the immediate threat to the fresh-water resource.

The future development of a comprehensive salt budget for the Great Bend Prairie aquifer requires detailed understanding of stream-aquifer interactions. Monitoring of stream-aquifer interaction, particularly in the

high mineral intrusion area along Rattlesnake Creek, would produce important data toward the understanding of the salt-water upconing phenomenon. The discharge of salt water to streams is of important budgetary concern because this is probably an important salt-loss mechanism.

Future work may also consider possible engineering solutions to mineral intrusion. The apparent broad discharge of brine from the Cedar Hills Sandstone hydrostratigraphic unit in most areas would seem to make any engineering solution impractical. However, if some areas of brine discharge are restricted to discrete features such as bedrock collapse or subsidence zones, then the installation of relief wells may be useful to intercept brine before it can be dispersed into the aquifer. The precise location of such zones would require extensive geophysical exploration such as with reflection seismic and/or surface electromagnetic methods.

REFERENCES

Alger, R. P., 1966. Interpretation of electric logs in fresh water wells in unconsolidated formations. Paper CC, 7th Annual SPWLA Symposium Trans., p. 1-25.

Allen, J. R. L., 1974. Studies in fluviatile sedimentation: implications of pedogenic carbonate units, Lower Old Red Sandstone, Anglo-Welsh outcrop. Geol. Jour., v. 9, p. 181-208.

Allen, P. A., and J. D. Collinson, 1986. Lakes; in: Sedimentary Environments and Facies, 2nd Edition; ed. H. G. Reading, Blackwell Scientific Pub., Oxford, p. 63-94.

Archie, G. E., 1942. The electrical resistivity log as an aid in determining some reservoir characteristics. Jour. Pet. Tech., v. 5, n. 1.

Bachu, S., 1995. Flow of variable-density formation water in deep sloping aquifers: review of methods of representation with case studies. Jour. of Hydrology, v. 164/1-4, p. 19-39.

Bayne, C. K., and H. G. O'Connor, 1968. Quaternary System; in, The Stratigraphic Succession in Kansas, D. E. Zeller, ed.: Kansas Geological Survey, Bulletin 189, p. 59-67.

Boellstorff, J., 1976. The succession of late Cenozoic volcanic ashes in the Great Plains: A progress report. In: Stratigraphy and faunal sequences -- Meade Co., Kansas. Kansas Geological Survey Guidebook Ser. 1., p. 37-38.

Bond, D. C., 1972. Hydrodynamics in deep aquifers of the Illinois Basin. Illinois State Geological Survey Circular 470, 50 pp.

Buddemeier, R. W., M. A. Sophocleous, and D. O. Whittemore, 1992. Mineral Intrusion: investigation of salt contamination of ground water in the eastern Great Bend Prairie Aquifer. Kansas Geological Survey, Open-File Report 92-25, 47 pp.

Buddemeier, R. W., G. W. Garneau, J. M. Healey, T.-S. Ma, M. A. Sophocleous, D. O. Whittemore, D. P. Young, and D. Zehr, 1993. The Mineral Intrusion Project: Report of progress during fiscal year 1993. Kansas Geological Survey Open-file Report 93-23, 59 pp.

Buddemeier, R. W., S. Falk, G. W. Garneau, J. Lanterman, T.-S. Ma, M. A. Sophocleous, D. O. Whittemore, D. P. Young, and D. Zehr, 1994. The Mineral Intrusion Project: investigation of salt contamination of ground water in the eastern Great Bend Prairie aquifer; progress and activities during fiscal year 1994. Kansas Geological Survey Open-file Report 94-28.

Castleman, K. R., 1979. Algebraic operations, in: Digital Image Processing, Prentice-Hall Signal Processing Series, New Jersey, 429 pp.

Cobb, P. M., 1980. The distribution and mechanisms of salt water intrusion in the fresh water aquifer and Rattlesnake Creek, Stafford County, Kansas. Kansas Geological Survey Open-file Report 80-17, ? pp.

Cobb, P. M., S. J. Colarullo, and M. Heidari, 1983. A ground-water flow model for the Great Bend Aquifer, south-central Kansas. Kansas Geological Survey, Open-File Report 83-20, 229 pp.

Collinson, J. D., 1986. Alluvial sediments; in: Sedimentary Environments and Facies, 2nd Edition; ed. H. G. Reading, Blackwell Scientific Pub., Oxford, p. 20-62.

Davies, P. B., 1987. Modeling areal, variable-density, ground-water flow using equivalent freshwater head -- analysis of potentially significant errors. In: Proceedings of the NWWA/IGWMC Conference - Solving groundwater problems with models; National Water Well Assoc., Dublin, Ohio, pp. 888-903.

Davis, J. C., 1986. Trend surfaces; in: Statistics and Data Analysis in Geology, 2nd Edition. John Wiley and Sons, New York, p. 405-430.

Desbarats, A. J., 1990. Macrodispersion in sand-shale sequences. Water Res. Res. v. 26, p. 153-163.

Domenico, P. A., and F. W. Schwartz, 1990. Physical and Chemical Hydrogeology. John Wiley and Sons, New York.

Dresser Atlas, 1979. Dresser Industries, Inc., Houston, Texas.

Fader, S. W., and L. E. Stullken, 1978. Geohydrology of the Great Bend Prairie, south-central Kansas. Kansas Geological Survey Irrigation Series 4, 19 pp.

Gaither, B. E., 1994. Some considerations in the application of wireline logging to environmental investigations. Amer. Assoc. Pet. Geol., v. 78, n. 9, p. 1458.

Gillespie, J. B., and G. D. Hargadine, 1994. Geohydrology and saline ground-water discharge to the South Fork Ninnescah River in Pratt and Kingman Counties, south-central Kansas. U.S. Geological Survey Water-Resources Investigations Report 93-4177, 51 pp.

Gustavson, T. C., R. J. Finley, and K. A. McGillis, 1980. Regional dissolution of Permian salt in the Anadarko, Dalhart and Palo Duro Basins of the Texas Panhandle. Texas Bur. Econ. Geol., Rep. Invest. 106, 39 pp.

Gustavson, T. C., A. J. Avakian, S. D. Hovorka, J. G. Paine, and B. C. Richter, 1994. Using electromagnetic geophysical surveys to locate nonpoint sources of natural salt water pollution of the Canadian River, Texas and New Mexico; in: Annual Report 1993 Texas Bureau of Economic Geology, p. 22.

Hallam, A., 1981. Facies Interpretation and the Stratigraphic Record. W. H. Freeman and Co., San Francisco.

Hallenburg, J. K., 1992. Nonhydrocarbon logging. The Log Analyst May-June, p. 259-269.

Holdoway, K. A., 1978. Deposition of evaporites and red beds of the Nippewalla group (Permian), western Kansas. Kansas Geological Survey Bull. 215, 45 pp.

Jenkins, E. D., 1983. Ground-water management in western Kansas. Jour. Hydraulic Eng. v. 109, n. 10, p. 1314-1322.

Johnson, K. S., 1981. Dissolution of salt on the east flank of the Permian Basin in the southwestern U.S.A. J. Hydrol., v. 54, p. 75-94.

Jordan, L., and D. L. Vosburg, 1963. Permian salt in the Anadarko Basin Oklahoma and Texas. Oklahoma Geological Survey Bulletin 102, 76 pp.

Jorgensen, D. G., T. Gogel, and D. C. Signor, 1982. Determination of flow in aquifers containing variable-density water. Ground Water Mon. Rev., v. 2, n. 2, p. 40-45.

Kwader, T., 1985. Estimating aquifer permeability from formation resistivity factors. Groundwater v. 23, n. 6, p. 762-766.

Layton, D. W., and D. W. Berry, 1973. Geology and ground-water resources Pratt County south-central Kansas. Kansas Geological Survey Bulletin 205, 33 p.

Lusczynski, N. J., 1961. Head and flow of ground water of variable density. Jour. Geophys. Res., v. 66, n. 12, p. 4247-4256.

Macfarlane, A., J. Combes, S. Turbek, D. Kirshen, and S. Yoder, 1993. Shallow subsurface bedrock geology and hydrostratigraphy of southwest Kansas. Kansas Geological Survey Open-file Report 93-1A, 13 pp. and 18 maps.

Martinez, A., no date. Isopach map of lower Cimmaronian salt in south-central Kansas. Kansas Geological Survey [unpublished map].

McElwee, C. D., 1984. A model study of salt-water intrusion to a river using the sharp interface approximation. Groundwater, v. 23, n. 4, p.465-475.

Morton, R. B., 1986. Effects of brine on the chemical quality of water in parts of Creek, Lincoln, Okfuskee, Payne, Pottawatomie, and Seminole Counties, Okahoma. Oklahoma Geological Survey, Circular 89, 20 pp.

Moya, P., 1985. Stream-aquifer system of the South Fork Ninnescah River Basin in Pratt County, Kansas. MS Thesis, Univ. of Kansas, 216 pp.

Richter, B. C., A. R. Dutton, and C. W. Kreitler, 1990. Identification of sources and mechanisms of salt-water pollution affecting ground-water quality: a case study, west Texas. Texas Bureau of Economic Geology, Report of Investigations No. 191, 43 pp.

Rosner, M. L., 1988. The stratigraphy of the Quaternary alluvium in the Great Bend Prairie, Kansas. M.S. Thesis, Dept. of Geology, Univ. of Kansas, 183 pp.

Rubin, H., and R. W. Buddemeier, 1994. The effect of local discontinuities on the mineralization of groundwater Part 1: Mineralization due to complete exposure and direct contact between fresh and saltwater. [unpublished]

Schmorak, S., and A. Mercado, 1969. Upconing of freshwater-seawater interface below pumping wells. Water Resources Res., v. 5, p. 1290-1311.

Smith, Z. A., 1989. Groundwater in the West: Kansas. Academic Press, Inc., N.Y., p. 107-116.

Sophocleous, M. A., 1992. Groundwater recharge estimation and regionalization: the Great Bend Prairie of central Kansas and its recharge statistics. Jour. of Hydrology 107:113-140.

Sophocleous, M. A., and J. A. McAllister, 1990. Hydrologic-balance modeling of the Rattlesnake Creek watershed, Kansas. Kansas Geological Survey Ground Water Series 11, 72 pp.

Sophocleous, M. A., and S. P. Perkins, 1992. Stream-aquifer and mineral intrusion modeling of the lower Rattlesnake Creek basin with emphasis on the Quivira National Wildlife Refuge. Kansas Geological Survey Open-file Report 92-6, 204 pp.

Sophocleous, M. A., and A. Stern, 1993. Fifteen GIS hydrologic maps of the Big Bend Ground-water Management Disctrict No. 5 (GMD5). Kansas Geological Survey Open-file Report 93-3, 8 pp., 15 plates.

Stullken, L. E., and S. W. Fader, 1976. Hydrogeologic data from the Great Bend Prairie, south-central Kansas. Kansas Geological Survey Basic Data Series, Ground-water Release No. 5, 50 pp.

Ward, P. A., B. J. Carter, and B. Weaver, 1993. Volcanic ashes: time markers in soil parent materials of the southern Plains. Soil Sci. Soc. Am. Jour. v. 57:453-460.

Walters, R. F., 1978. Land subsidence in central Kansas related to salt dissolution. Kansas Geological Survey Bulletin 214, 82 pp.

Welch, J. E., and J. M. Hale, 1987. Pleistocene loess in Kansas -- status, present problems, and future considerations. Kansas Geological Survey Guidebook Series 5, p. 67-84.

Whittemore, D. O., 1993. Ground-water geochemistry in the mineral intrusion area of Groundwater Management District No. 5, south-central Kansas. Kansas Geological Survey Open-File Report 93-2, 36+ pp.

Williams, J., 1962. Oceanography. Little, Brown and Co., Boston.

Worthington, P. F., 1976. Hydrogeophysical equivalence of water salinity, porosity and matrix conduction in arenaceous aquifers. Groundwater v. 14 n. 4, p. 224-232.

Worthington, P. F., 1985. The evolution of shaly-sand concepts in reservoir evaluation. The Log Analyst, Jan-Feb, p. 23-40.

Young, D. P., 1992. Mineral Intrusion: description of Permian Bedrock and its hydrologic relation to the overlying Great Bend Prairie Aquifer. Kansas Geological Survey Open-File Report 92-44, 47 pp.

Young, D. P., G. W. Garneau, R. W. Buddemeier, D. Zehr, and J. Lanterman, 1993. Elevation and variability of the freshwater-saltwater interface in the Great Bend Prairie aquifer, south-central Kansas. Kansas Geological Survey, Open-file Report 93-55, 60 pp.

APPENDIX I. Freshwater-saltwater transition zone profile changes (1993-1994)

This appendix contains plots showing the changes in the freshwater-saltwater transition zone profiles between spring 1993 and spring 1994. These plots are shown side-by-side with the actual profiles from the sites listed in Table I for 1994. The change plots (left plot) show where in the profile that ground water has become saltier (positive) or fresher (negative). The depth of the 500 mg/L chloride interface--listed in Table I-- is shown with arrowheads: solid (1993) and open (1994) on the change plots.

These plots demonstrate the very minor changes in the freshwater-saltwater distribution between 1993 and 1994. These minor changes occurred during the extraordinary precipitation and subsequent recharge during the summer of 1993. The two sites that had the largest change in the depth of the 500 mg/L interface--site 23 (>8 ft rise) and site 26 (>6 ft rise)--also show obvious systematic increases in salininty in the depth range of the transition zone. Both of theses sites are down-gradient from the areas of mineral intrusion in the Rattlesnake Creek basin. These increases were probably the result of the extraordinary recharge that flushed saline water toward these sites during the summer of 1993.

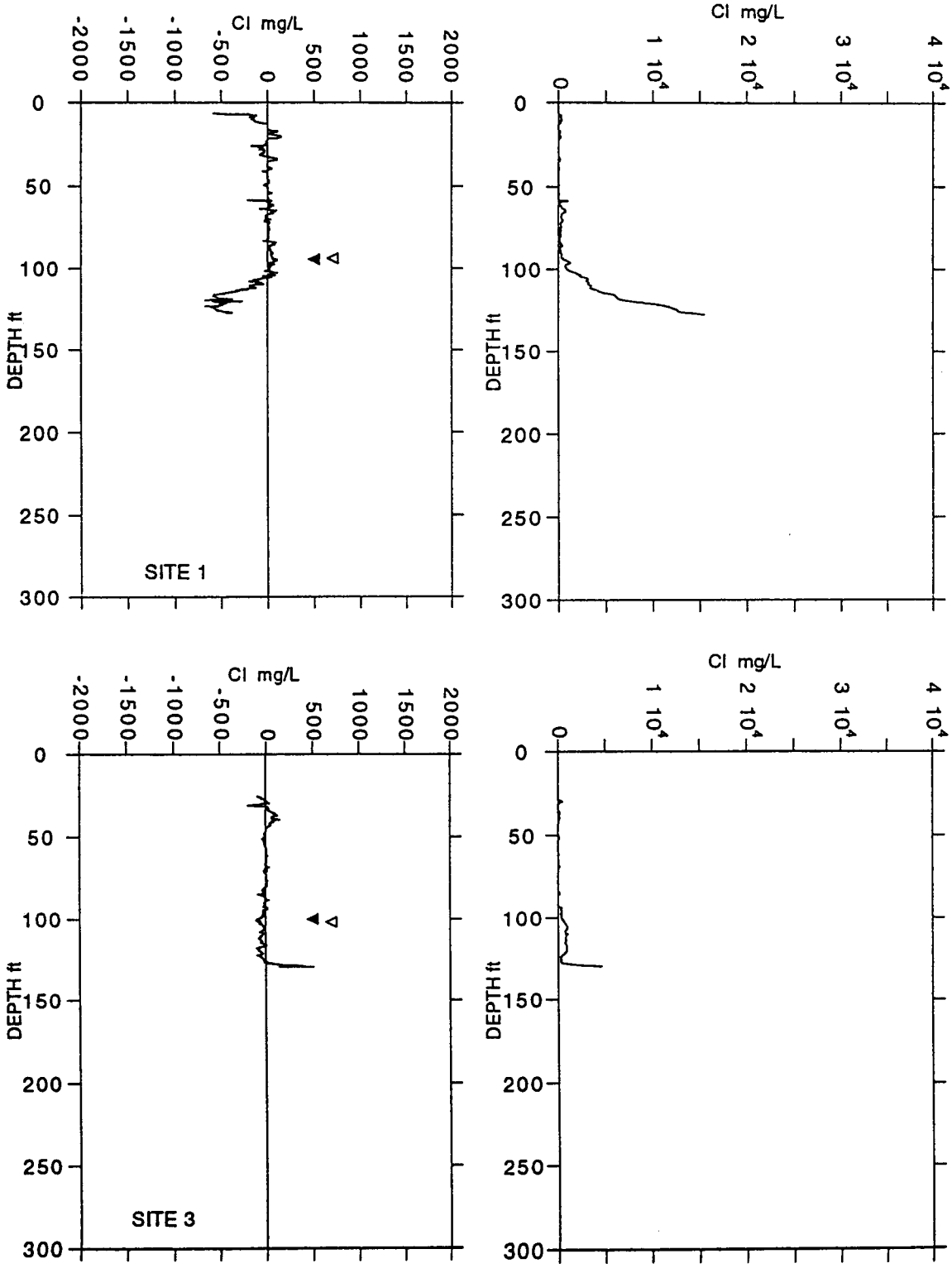
Cl mg/L
-2000
-1500
-1000
-500
0
500
1000
1500
2000
0
50
100
150
200
250
300
DEPTH ft
SITE 1
Cl mg/L
0
1 10^4
2 10^4
3 10^4
4 10^4
DEPTH ft
Cl mg/L
SITE 3
DEPTH ft
Cl mg/L
DEPTH ft

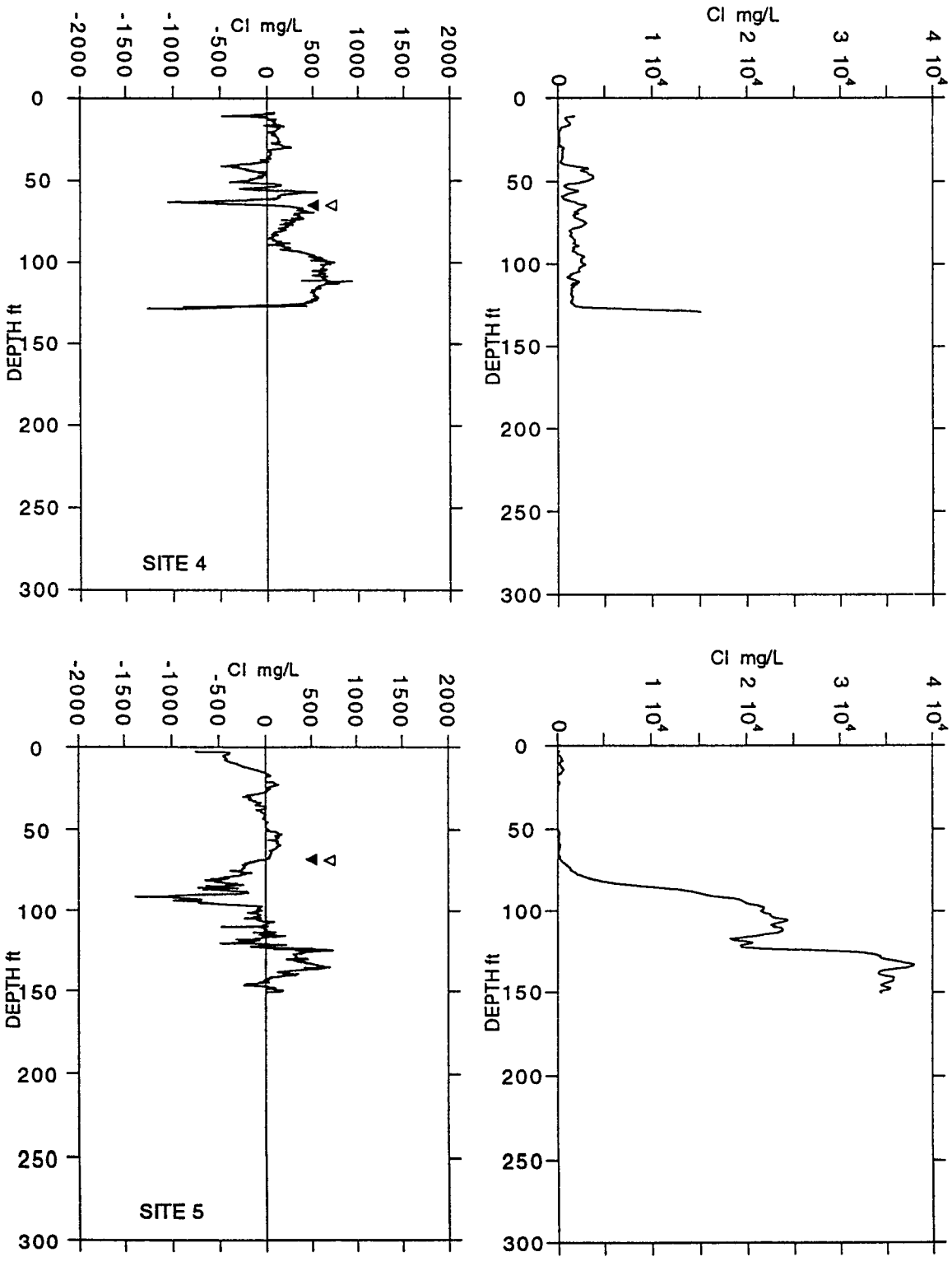
Cl mg/L
-2000
-1500
-1000
-500
0
500
1000
1500
2000
DEPTH ft
0
50
100
150
200
250
300
SITE 4
Cl mg/L
0
1 10⁴
2 10⁴
3 10⁴
4 10⁴
DEPTH ft
SITE 5

SITE 6
(no log for 1993)

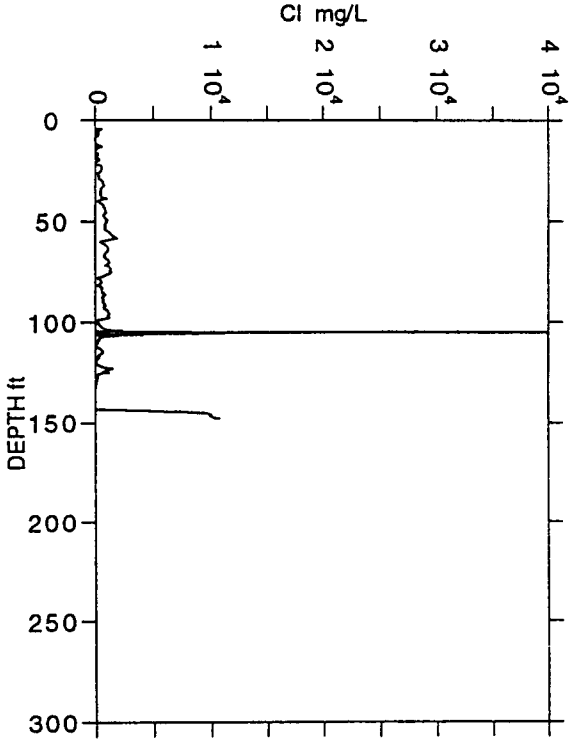

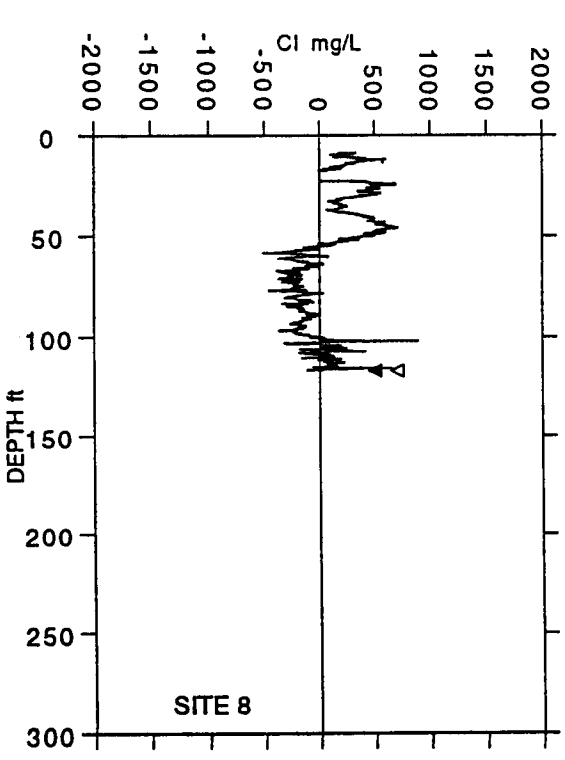

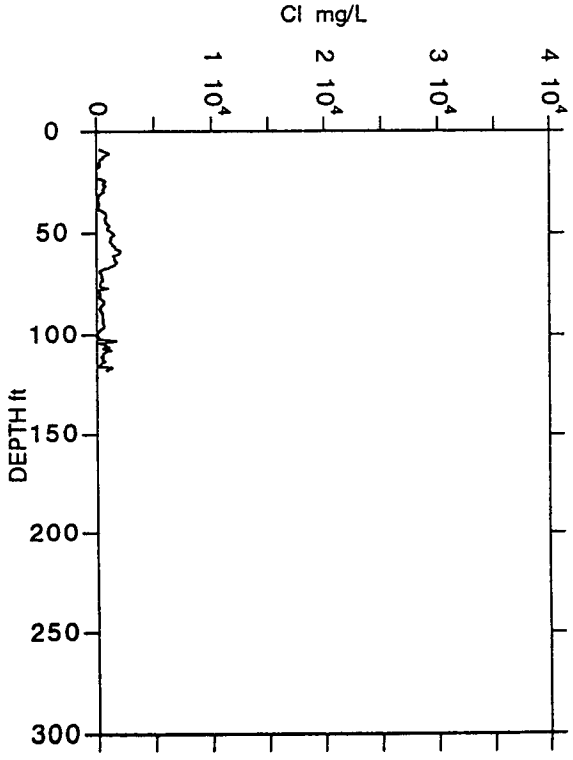

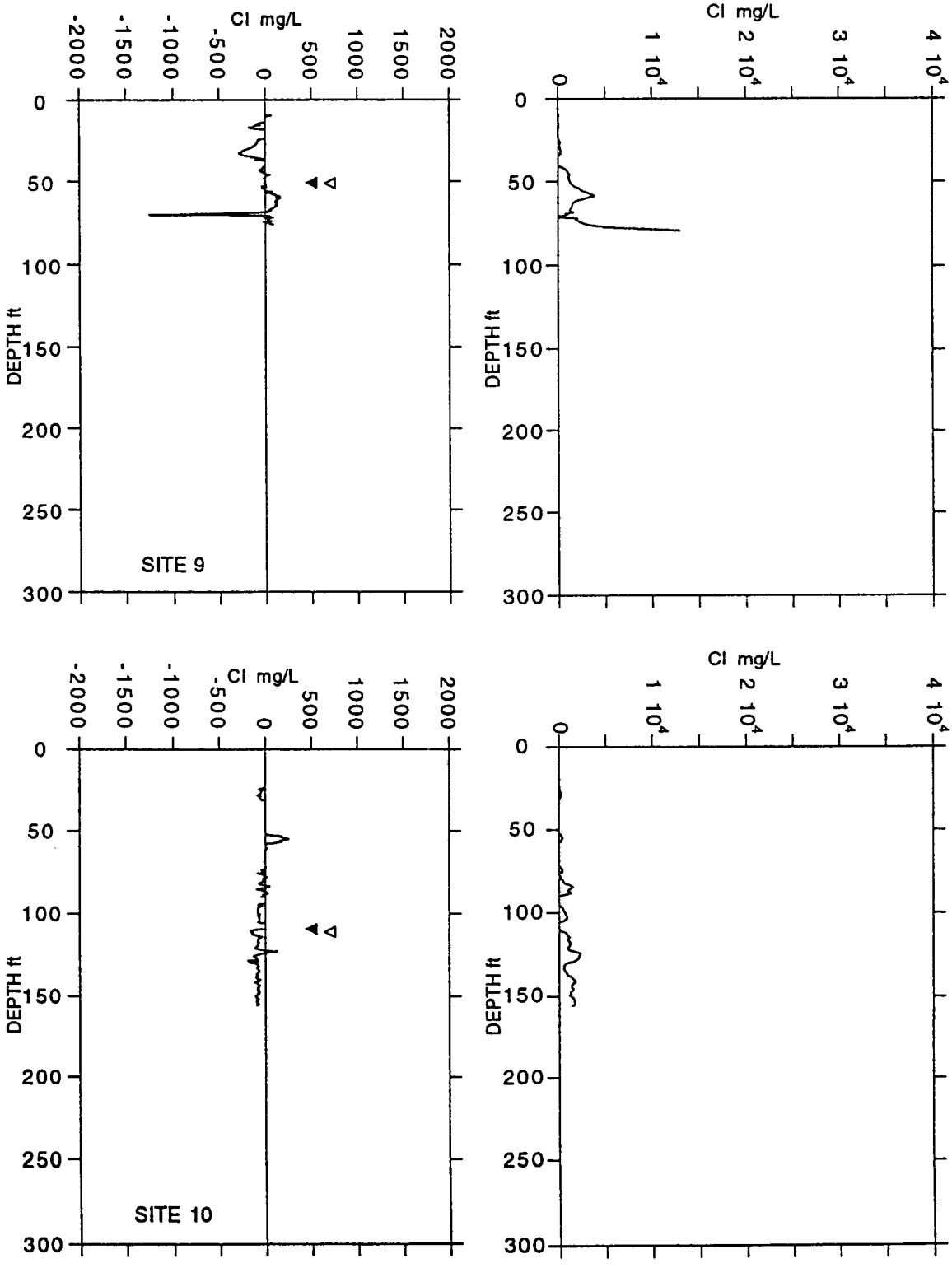
Cl mg/L
-2000
-1500
-1000
-500
0
500
1000
1500
2000
1 10^4
2 10^4
3 10^4
4 10^4
DEPTH ft
0
50
100
150
200
250
300
SITE 9
SITE 10

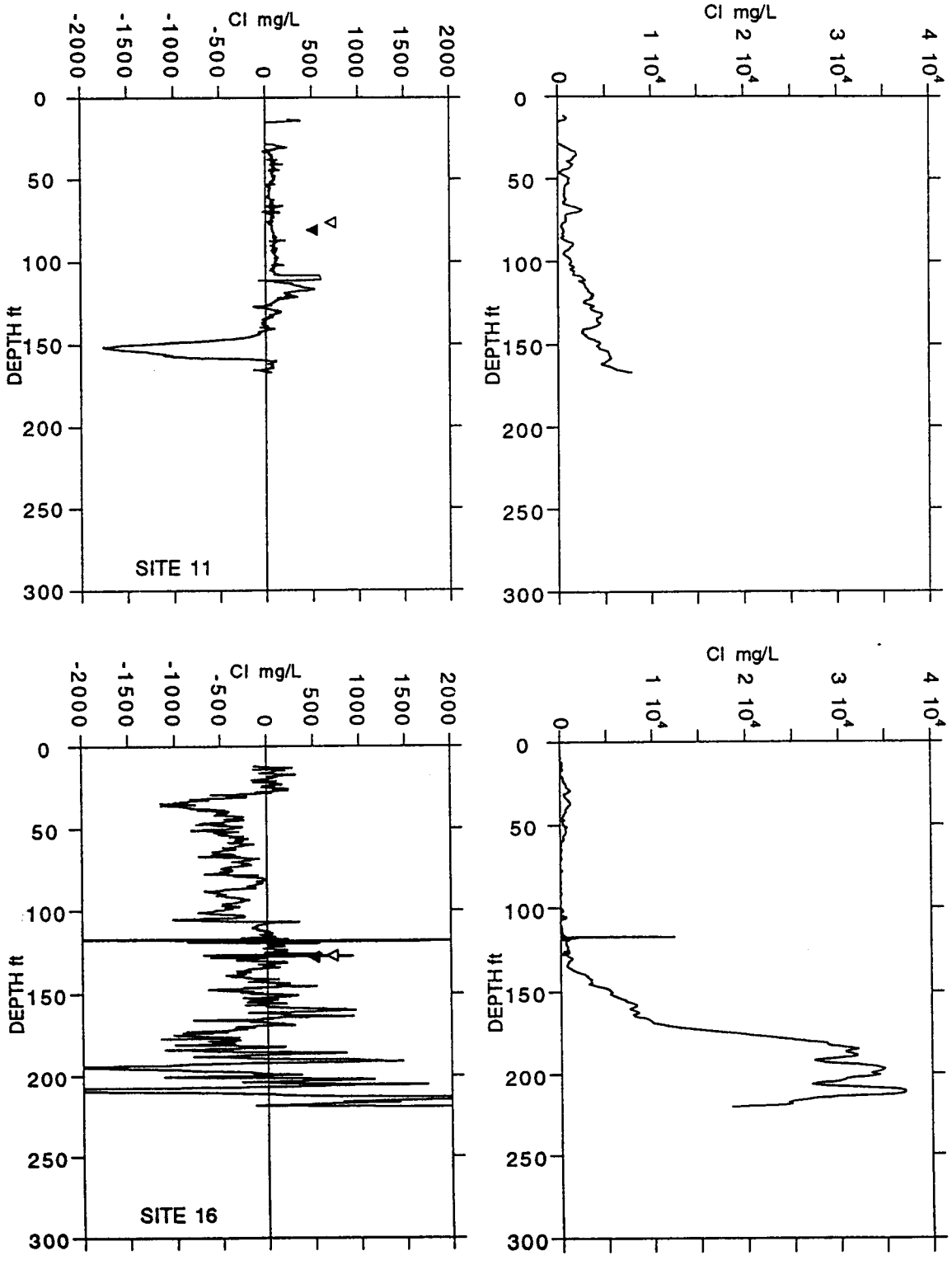
Cl mg/L
-2000
-1500
-1000
-500
0
500
1000
1500
2000
DEPTH ft
0
50
100
150
200
250
300
SITE 11
Cl mg/L
0
1 10⁴
2 10⁴
3 10⁴
4 10⁴
DEPTH ft
SITE 16

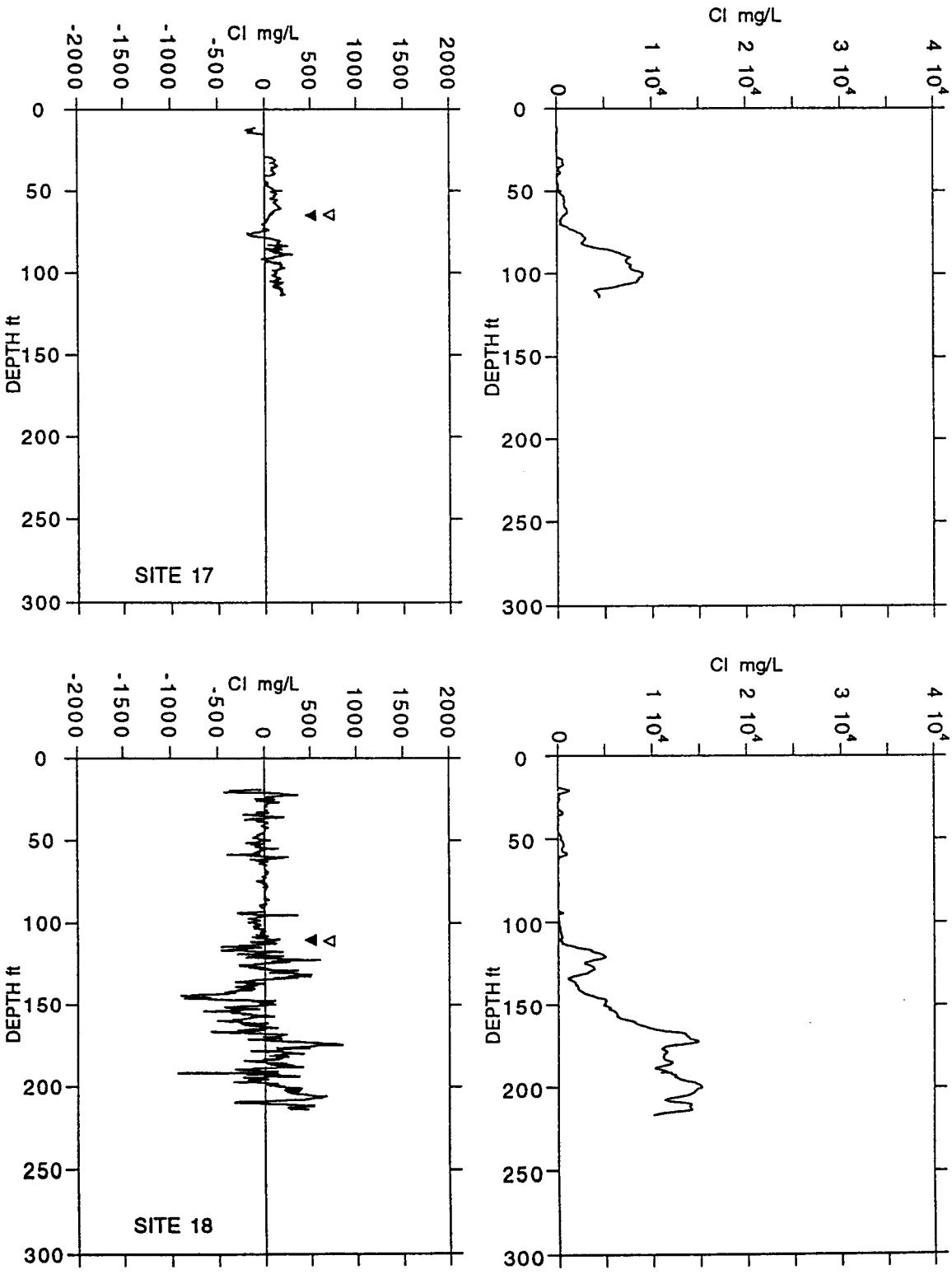
Cl mg/L
-2000
-1500
-1000
-500
0
500
1000
1500
2000
1 10⁴
2 10⁴
3 10⁴
4 10⁴
DEPTH ft
0
50
100
150
200
250
300
SITE 17
SITE 18

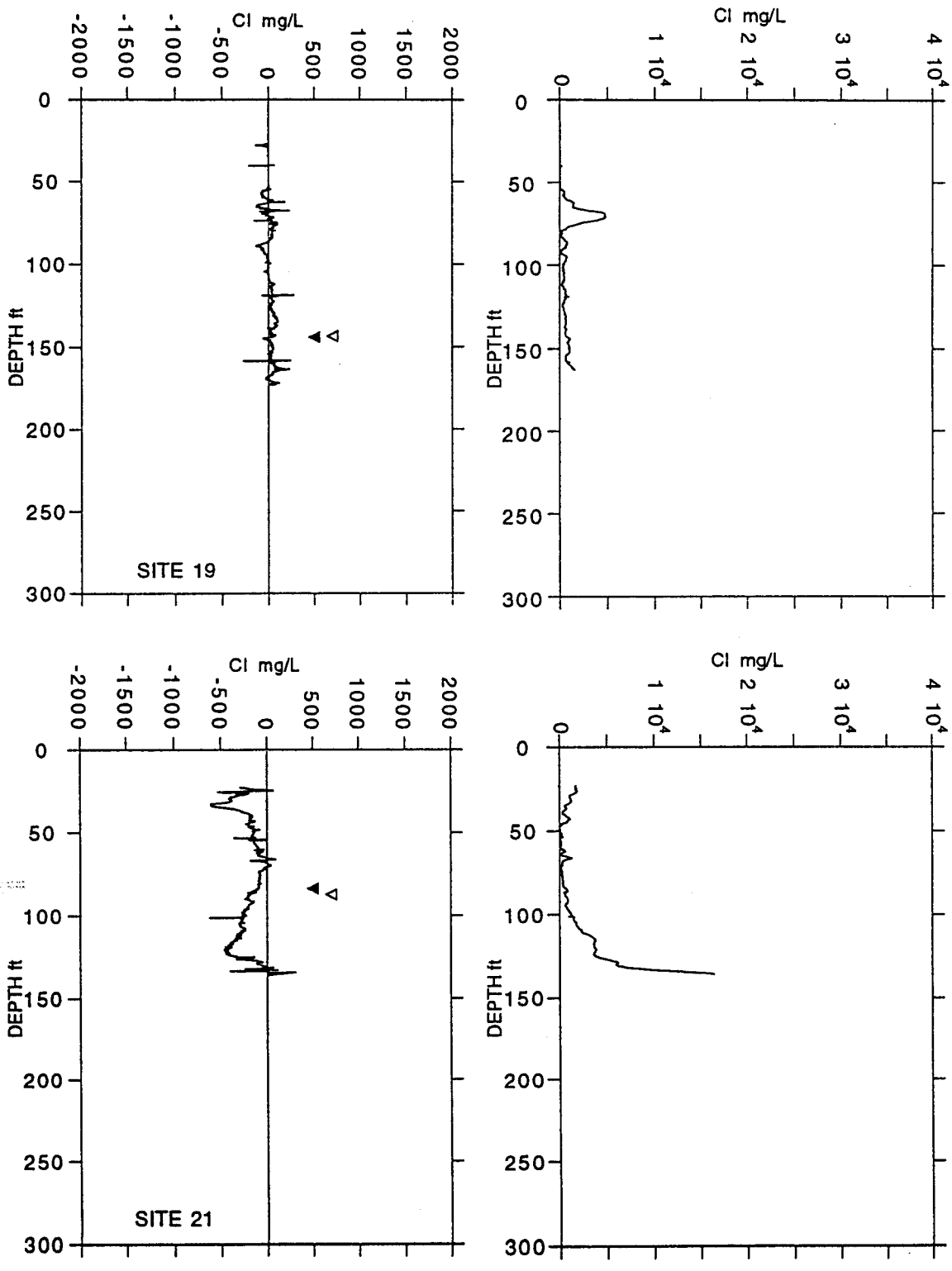
Cl mg/L
-2000
-1500
-1000
-500
0
500
1000
1500
2000
DEPTH ft
0
50
100
150
200
250
300
SITE 19
Cl mg/L
0
1 10⁴
2 10⁴
3 10⁴
4 10⁴
DEPTH ft
SITE 21

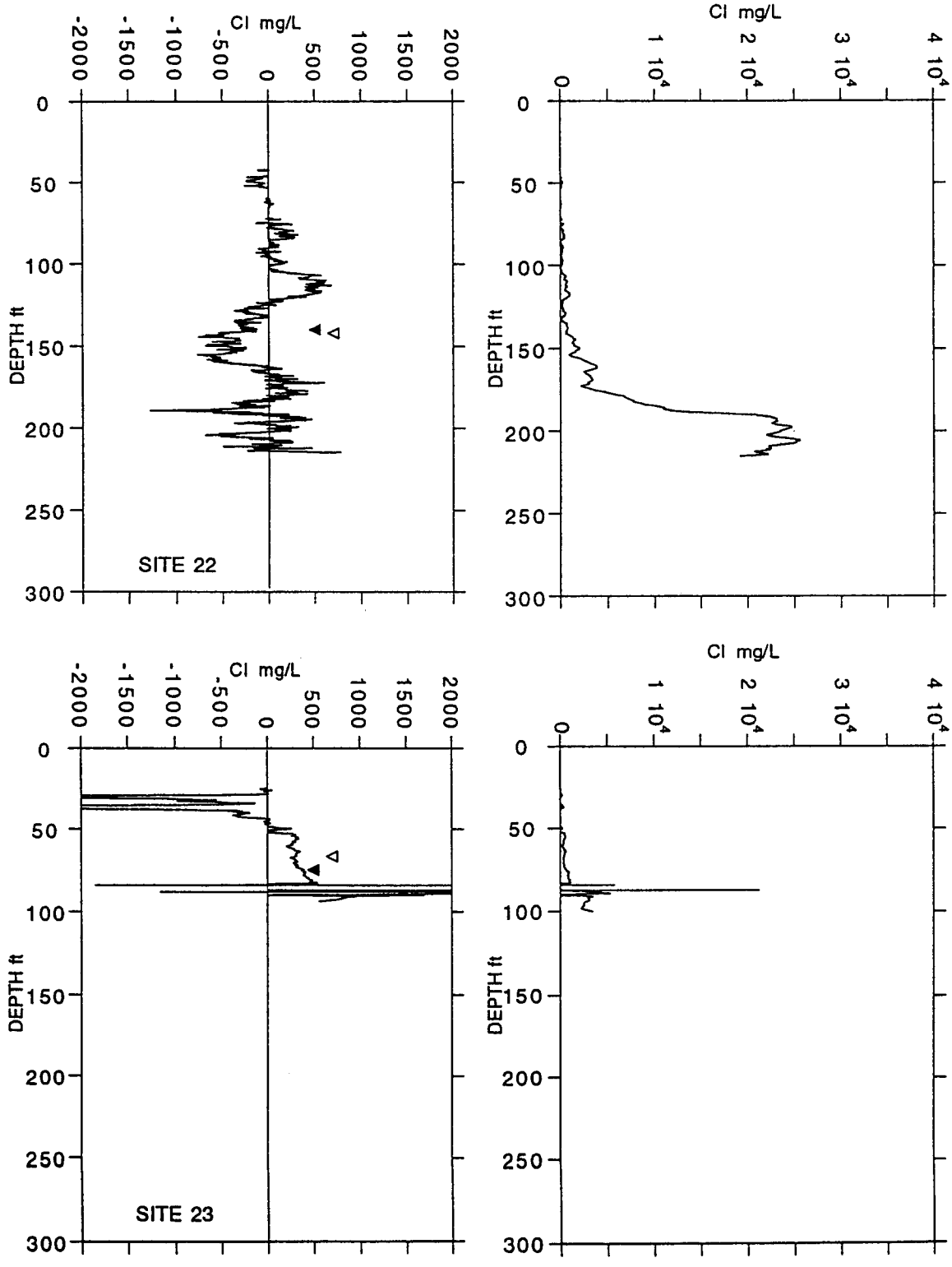
Cl mg/L
-2000
-1500
-1000
-500
0
500
1000
1500
2000
DEPTH ft
0
50
100
150
200
250
300
SITE 22
Cl mg/L
0
1 10^4
2 10^4
3 10^4
4 10^4
DEPTH ft
SITE 23

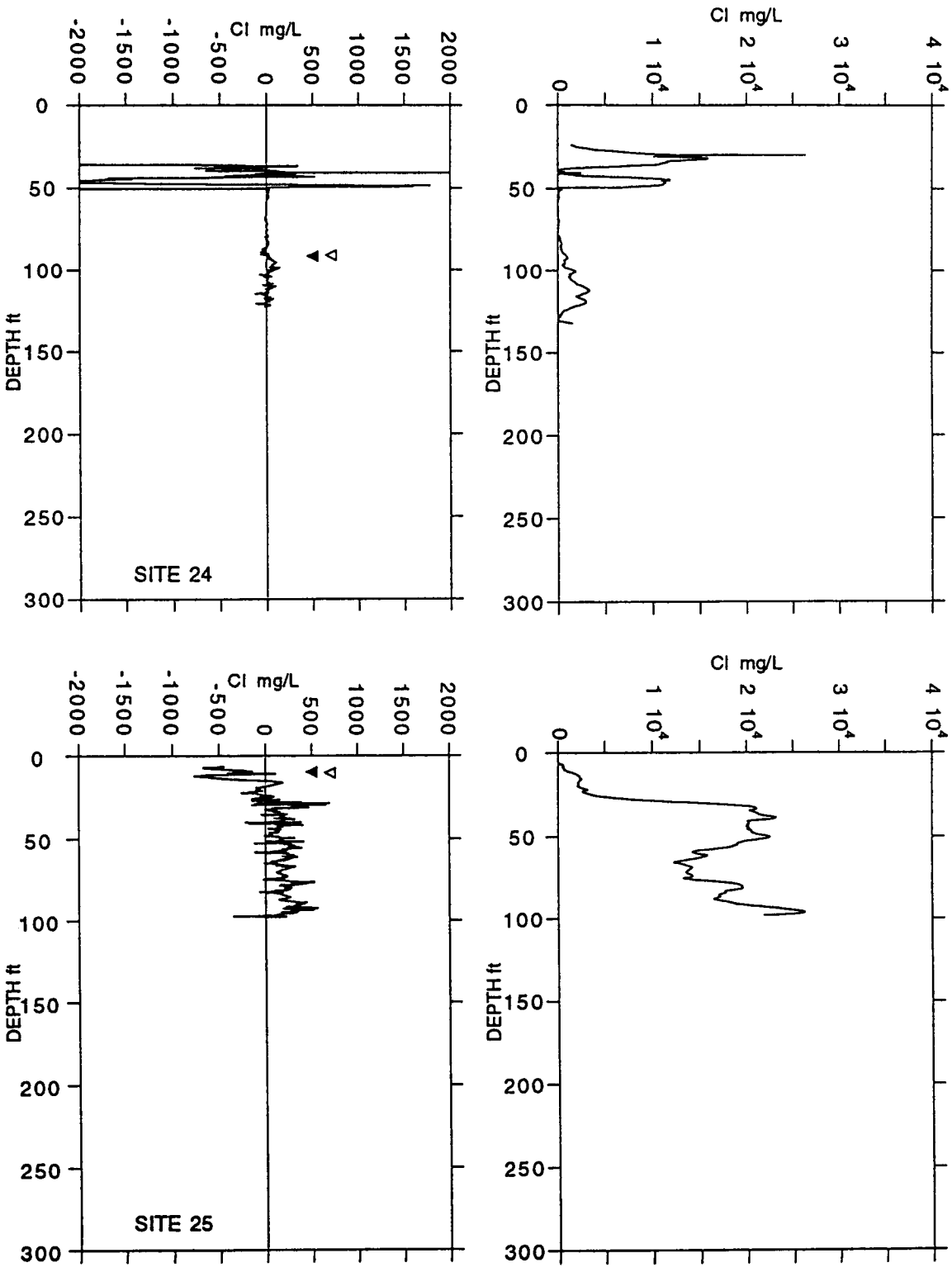
Cl mg/L
-2000
-1500
-1000
-500
0
500
1000
1500
2000
1 10⁴
2 10⁴
3 10⁴
4 10⁴
DEPTH ft
0
50
100
150
200
250
300
SITE 24
SITE 25

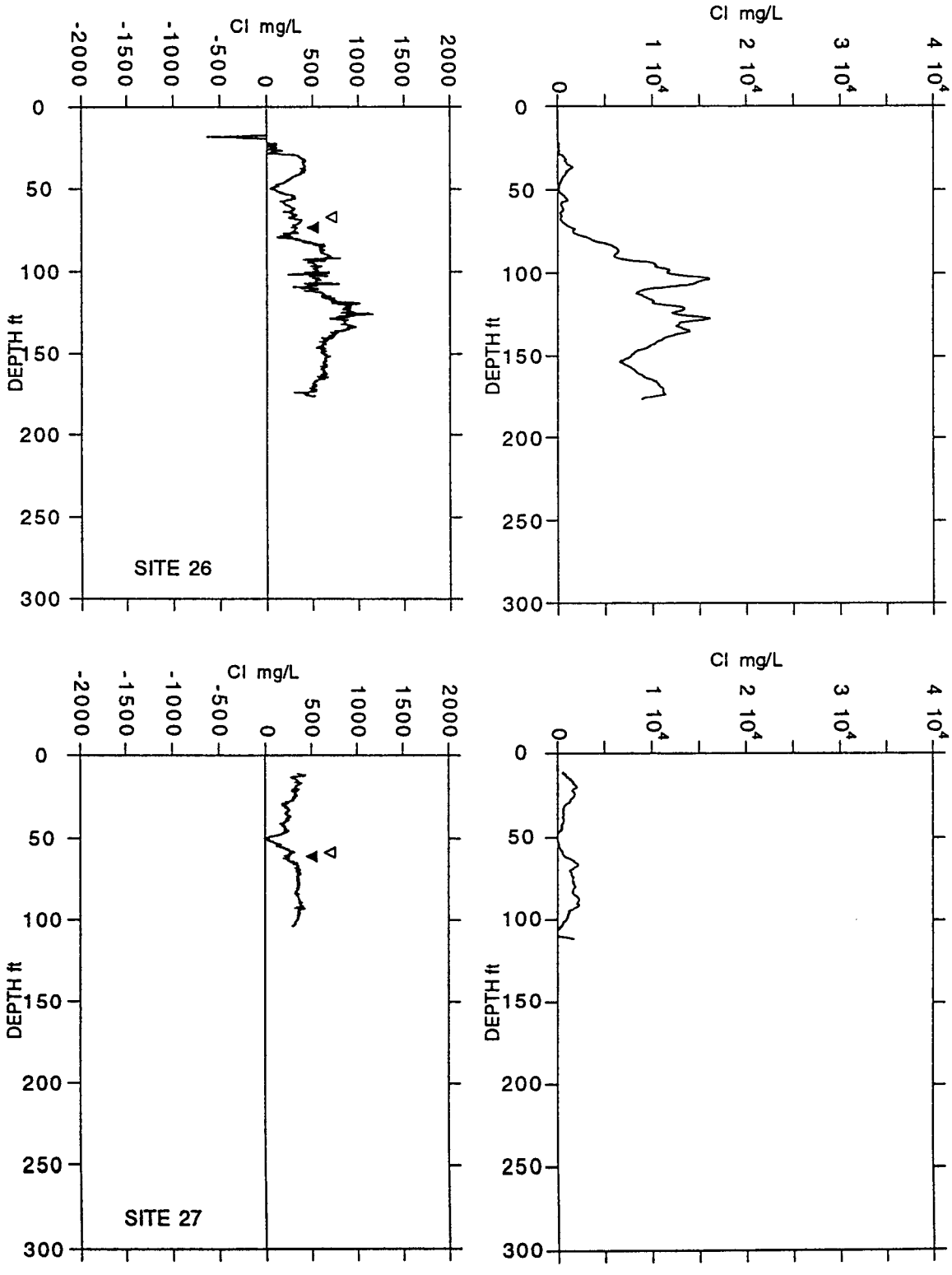
Cl mg/L
-2000
-1500
-1000
-500
0
500
1000
1500
2000
0
50
100
150
200
250
300
DEPTH ft
SITE 26
Cl mg/L
0
1 10^4
2 10^4
3 10^4
4 10^4
DEPTH ft
SITE 27

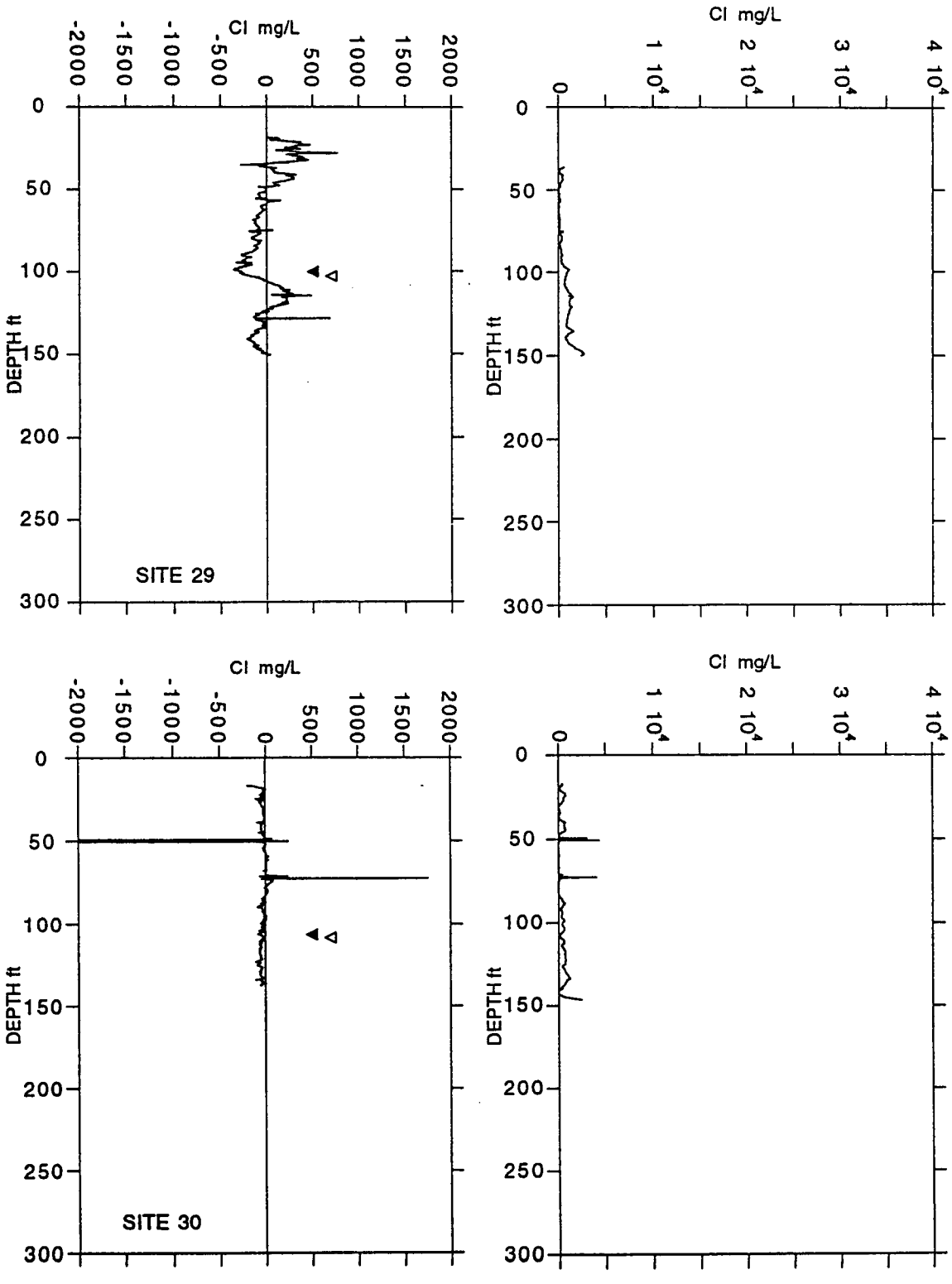
Cl mg/L
-2000
-1500
-1000
-500
0
500
1000
1500
2000
1 10⁴
2 10⁴
3 10⁴
4 10⁴
DEPTH ft
0
50
100
150
200
250
300
SITE 29
SITE 30

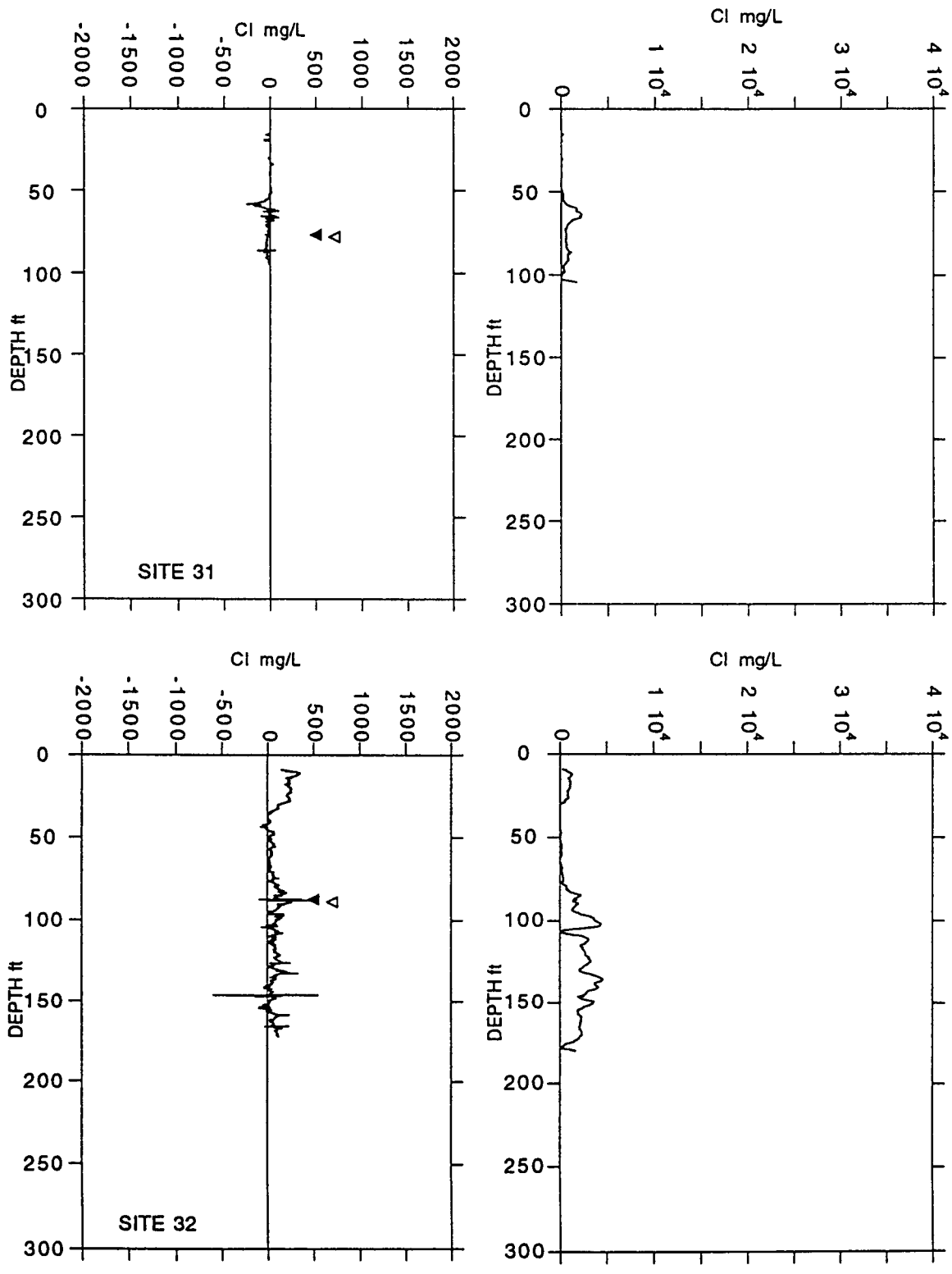
Cl mg/L
-2000
-1500
-1000
-500
0
500
1000
1500
2000
0
50
100
150
200
250
300
DEPTH ft
SITE 31
Cl mg/L
0
1 10^4
2 10^4
3 10^4
4 10^4
0
50
100
150
200
250
300
DEPTH ft
Cl mg/L
-2000
-1500
-1000
-500
0
500
1000
1500
2000
0
50
100
150
200
250
300
DEPTH ft
SITE 32
Cl mg/L
0
1 10^4
2 10^4
3 10^4
4 10^4
0
50
100
150
200
250
300
DEPTH ft

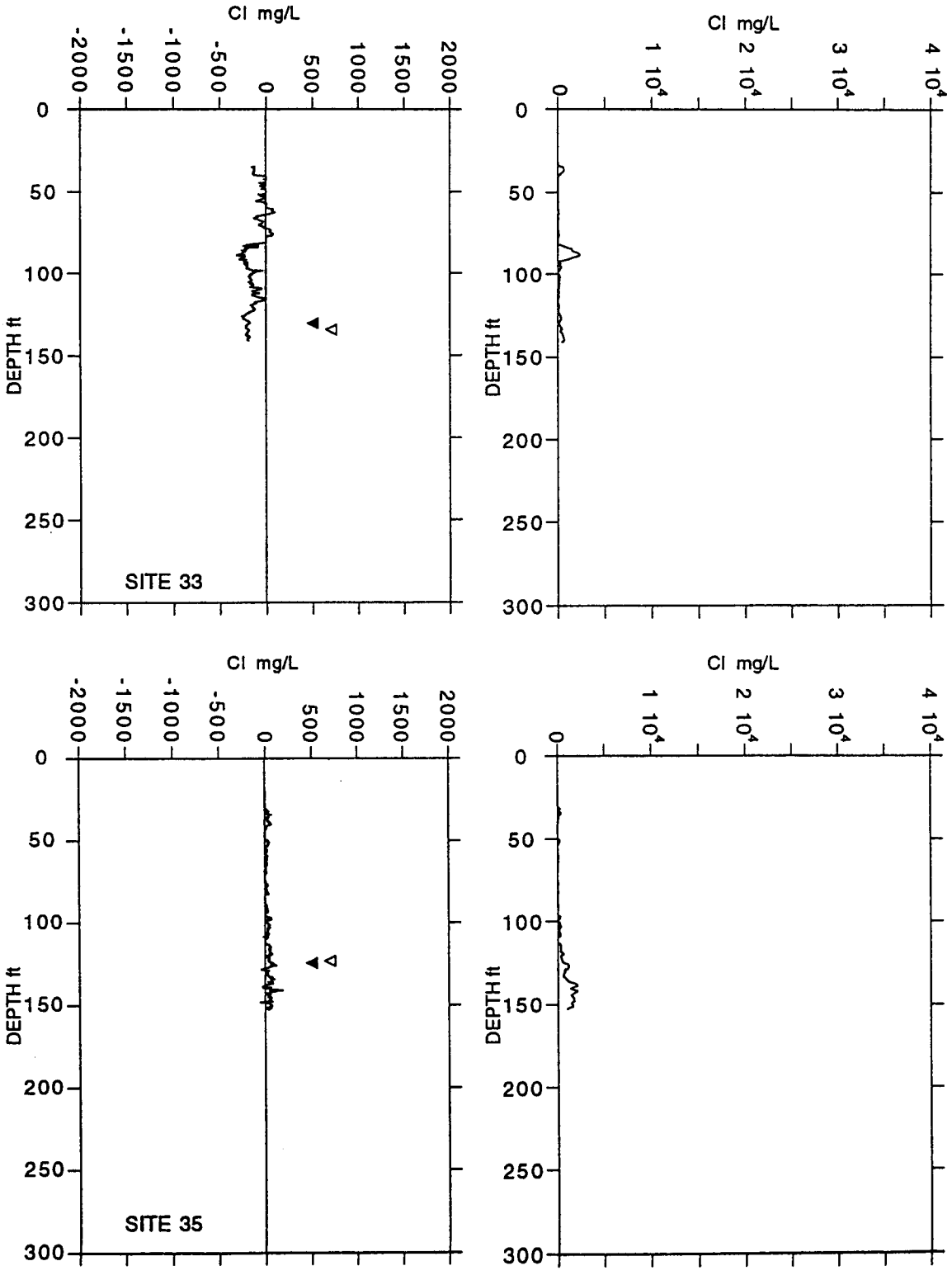
Cl mg/L
-2000
-1500
-1000
-500
0
500
1000
1500
2000
0
50
100
150
200
250
300
DEPTH ft
SITE 33
Cl mg/L
0
1 10⁴
2 10⁴
3 10⁴
4 10⁴
0
50
100
150
200
250
300
DEPTH ft
Cl mg/L
-2000
-1500
-1000
-500
0
500
1000
1500
2000
0
50
100
150
200
250
300
DEPTH ft
SITE 35
Cl mg/L
0
1 10⁴
2 10⁴
3 10⁴
4 10⁴
0
50
100
150
200
250
300
DEPTH ft

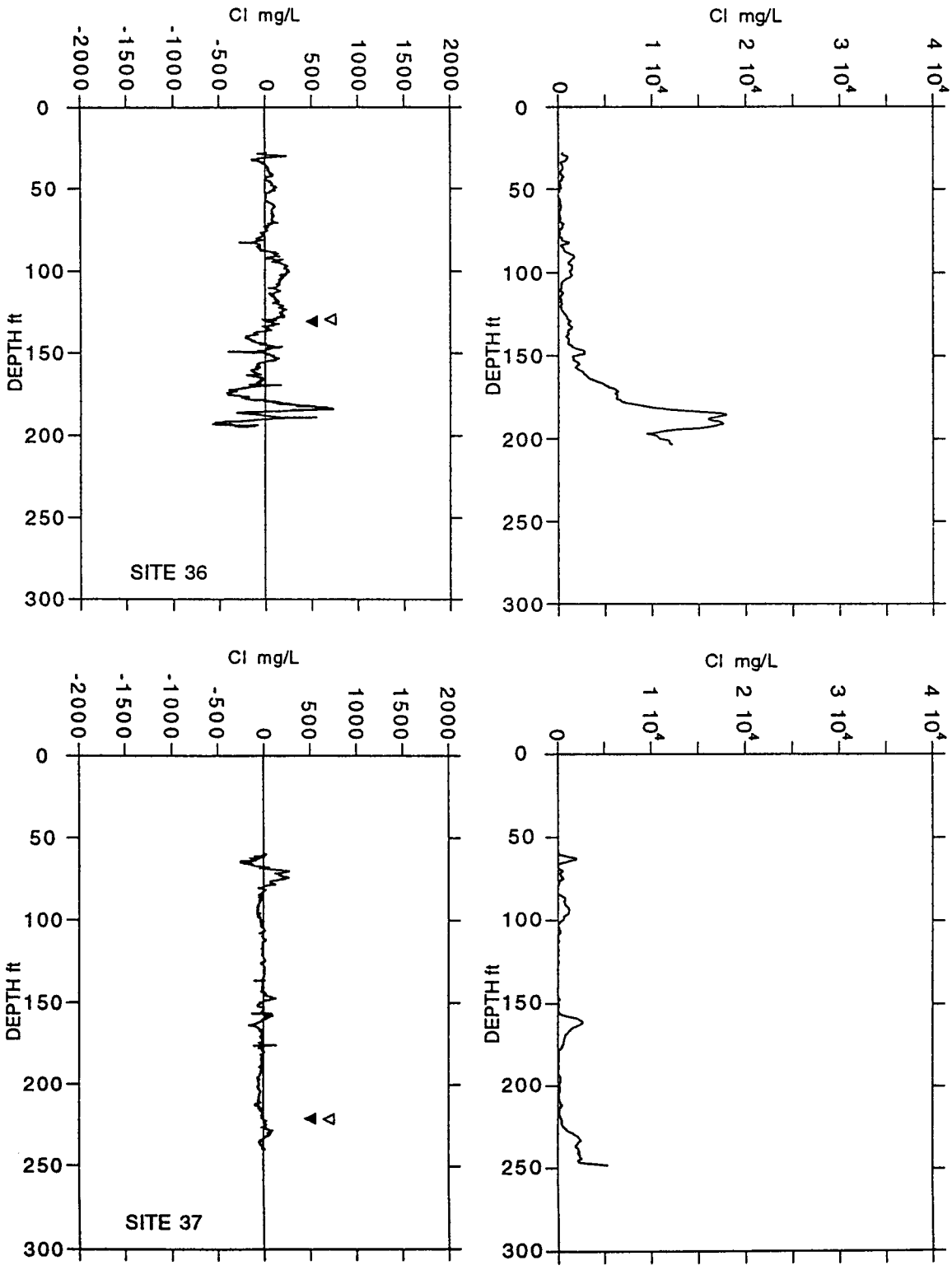
Cl mg/L
-2000
-1500
-1000
-500
0
500
1000
1500
2000
DEPTH ft
0
50
100
150
200
250
300
SITE 36
Cl mg/L
0
1 10⁴
2 10⁴
3 10⁴
4 10⁴
DEPTH ft
SITE 37

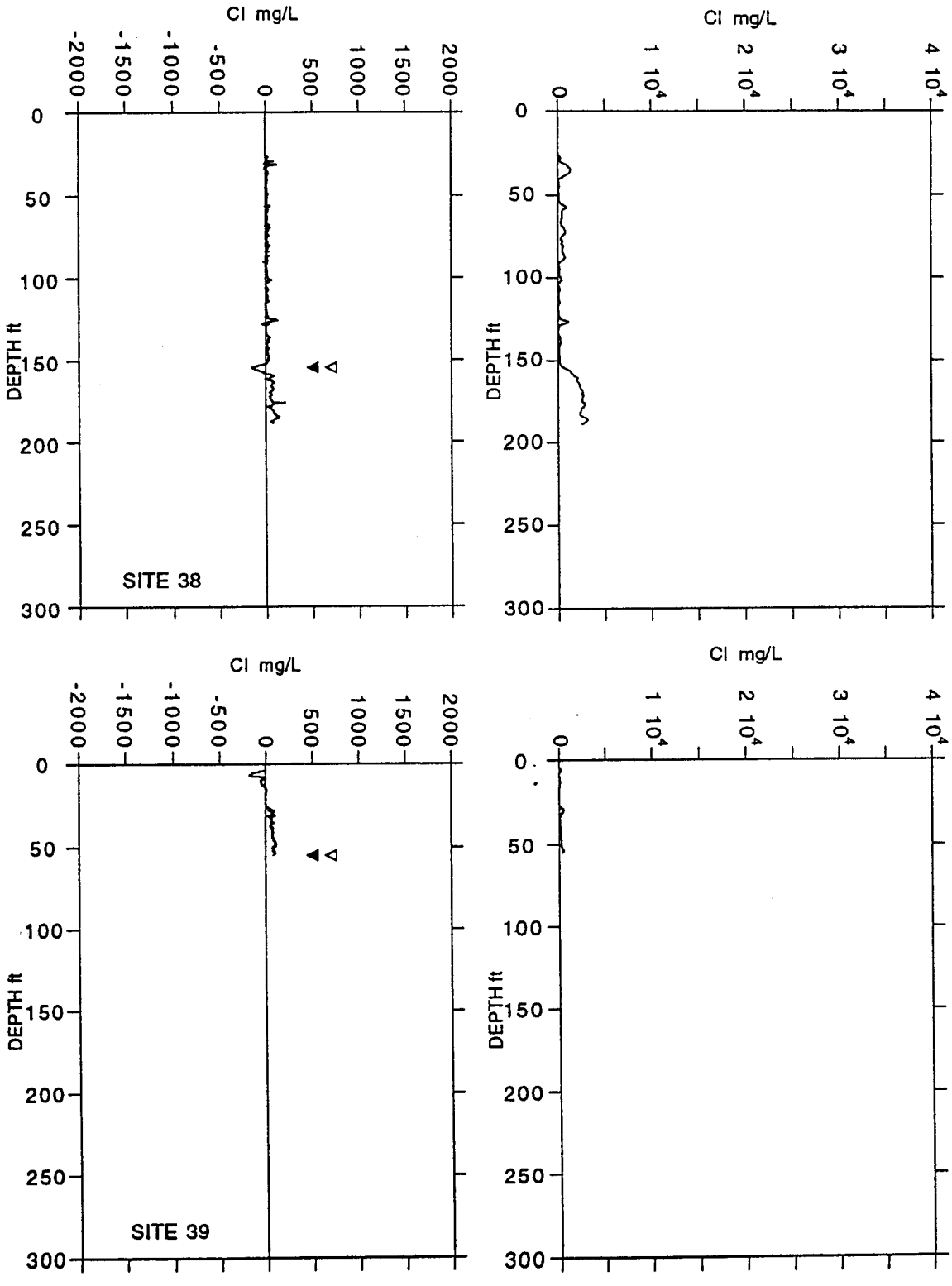
Cl mg/L
-2000
-1500
-1000
-500
0
500
1000
1500
2000
1 10⁴
2 10⁴
3 10⁴
4 10⁴
DEPTH ft
0
50
100
150
200
250
300
SITE 38
SITE 39

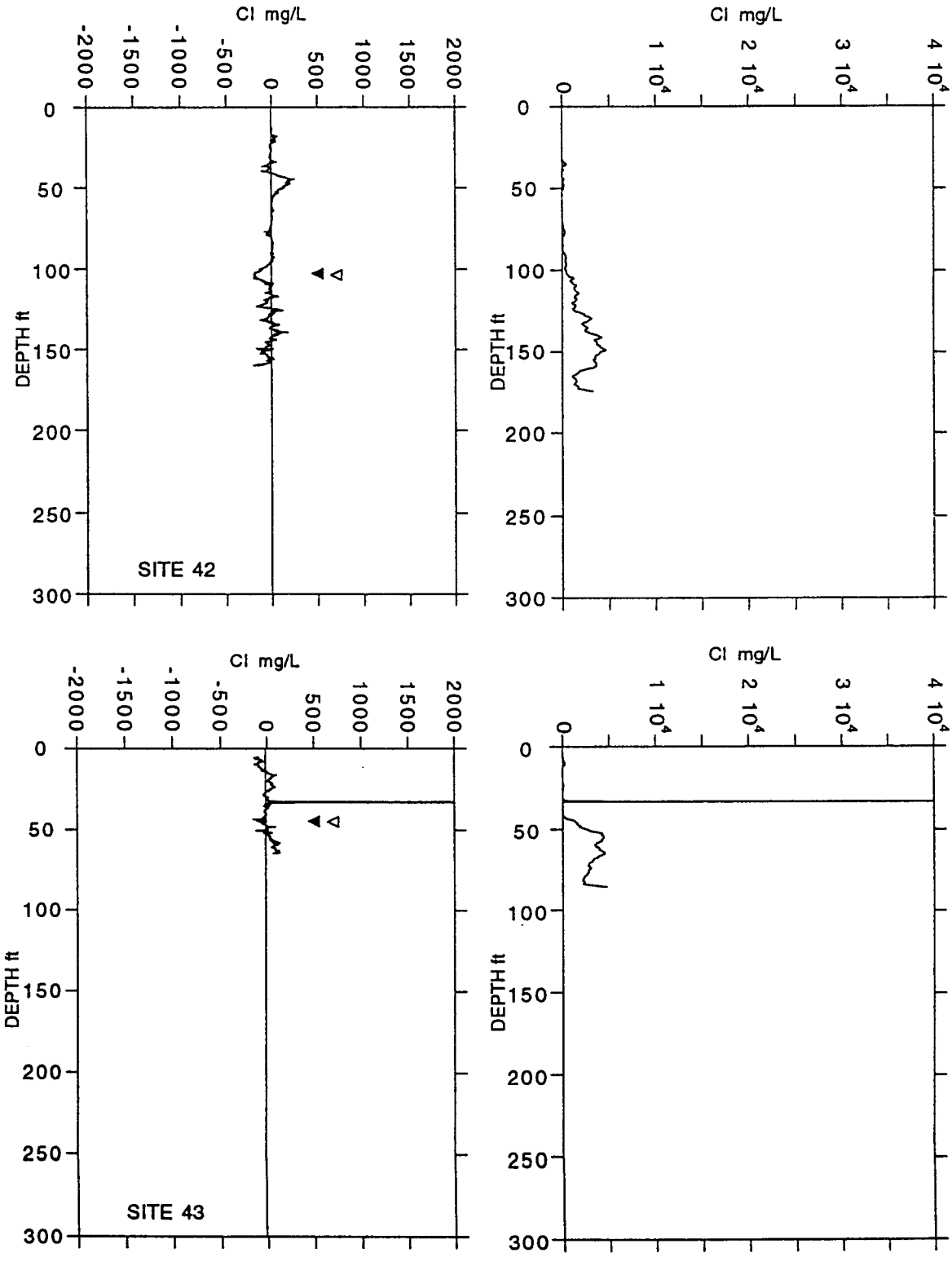
Cl mg/L
-2000
-1500
-1000
-500
0
500
1000
1500
2000
1 10⁴
2 10⁴
3 10⁴
4 10⁴
DEPTH ft
0
50
100
150
200
250
300
SITE 42
SITE 43

SITE 49
(no log for 1993)

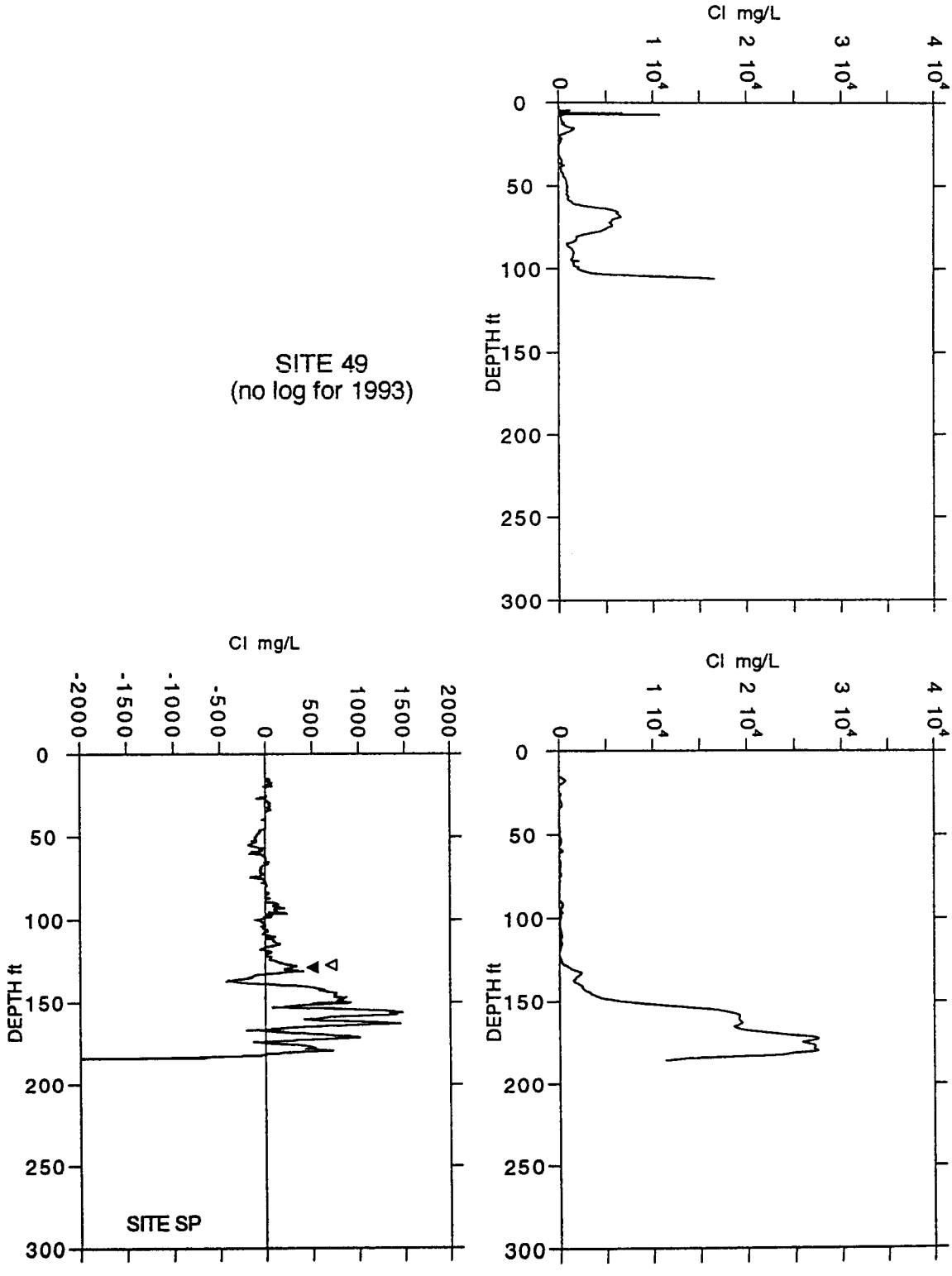

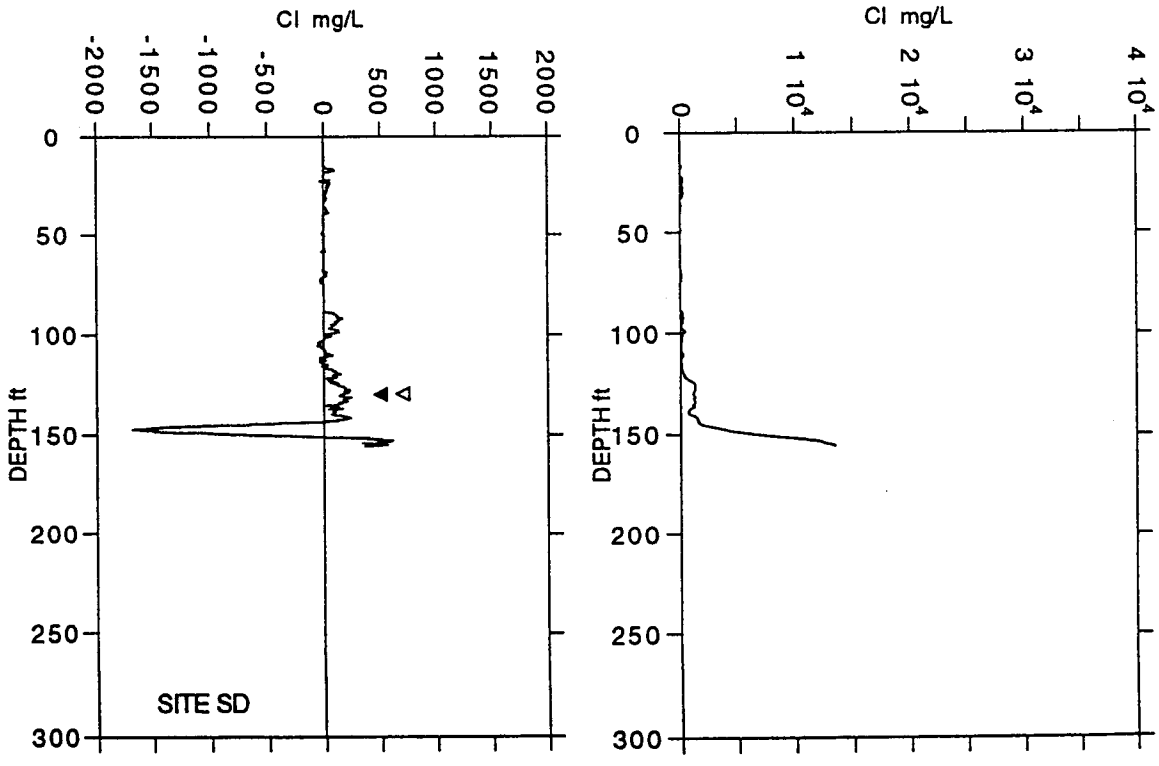
Cl mg/L
-2000
-1500
-1000
-500
0
500
1000
1500
2000
0
50
100
150
200
250
300
DEPTH ft
SITE SD
Cl mg/L
0
1 10^4
2 10^4
3 10^4
4 10^4
0
50
100
150
200
250
300
DEPTH ft

APPENDIX II. Summary of freshwater-saltwater distribution changes at the Siefkes Intensive Study Site (1993 and 1994).

This appendix summarizes the results of observations at the Siefkes Intensive Study Site (SISS) during 1993 and 1994. Figure 20A of this thesis graphically shows the variations of the freshwater-saltwater transition zone profiles in the bedrock monitoring well at the SISS. These changes are suspected to be the direct result of pumping of the nearby irrigation well (see Fig. 20B) and possibly other adjacent irrigation wells.

Table IIA and Figure IIA summarize the observed build-up of salinity at the monitoring well within the depth range of 90 to 130 ft. The transition zone profiles were integrated between this range--top of lower screened interval and top of the clay lens (see Fig. 20A)--to determine the mass of chloride per unit area in the region of saline water build-up. The methods of integration are the same as were previously described in this thesis (equations 13 and 15). Note that the cumulative changes of the chloride mass are a full order of magnitude less than the total saturated-thickness mass shown in Table 2.

A flow meter was installed on the irrigation well between the 1993 and 1994 pumping seasons. The meter now allows direct comparisons between water usage and the build-up of salinity. Figure IIA compares the cumulative water use and the cumulative build-up of salinity. The cumulative salinity values for each year were set to zero at the date coinciding with the onset of pumping.

The results for 1994 confirm the influence of the pumping well on salinity build-up. The build-up of salinity closely follows the water usage with a time lag. A decrease of the water usage rate in April and May results in a decrease of salinity build-up in June. The time lag appears to expand on Figure IIA, but this is somewhat of an artifact of the scales used to present these data. Exact comparative scaling of the salinity build-up curve would require year-round monthly logging to capture the trailing edge of the salinity curve. The data from 1993 suggests that the recovery (trailing edge) from the build-up following the 1992 pumping season was still occurring in July--well after the usual onset of pumping. Similarly,

the data from 1994 shows the recovery between March and April. The data from 1994 also indicates that the inflection point or peak of salinity build-up occurred in November; approximately three months following the peak of water usage in August. These results and future observations at the SISS would easily comprise another thesis project.

Figure IIA

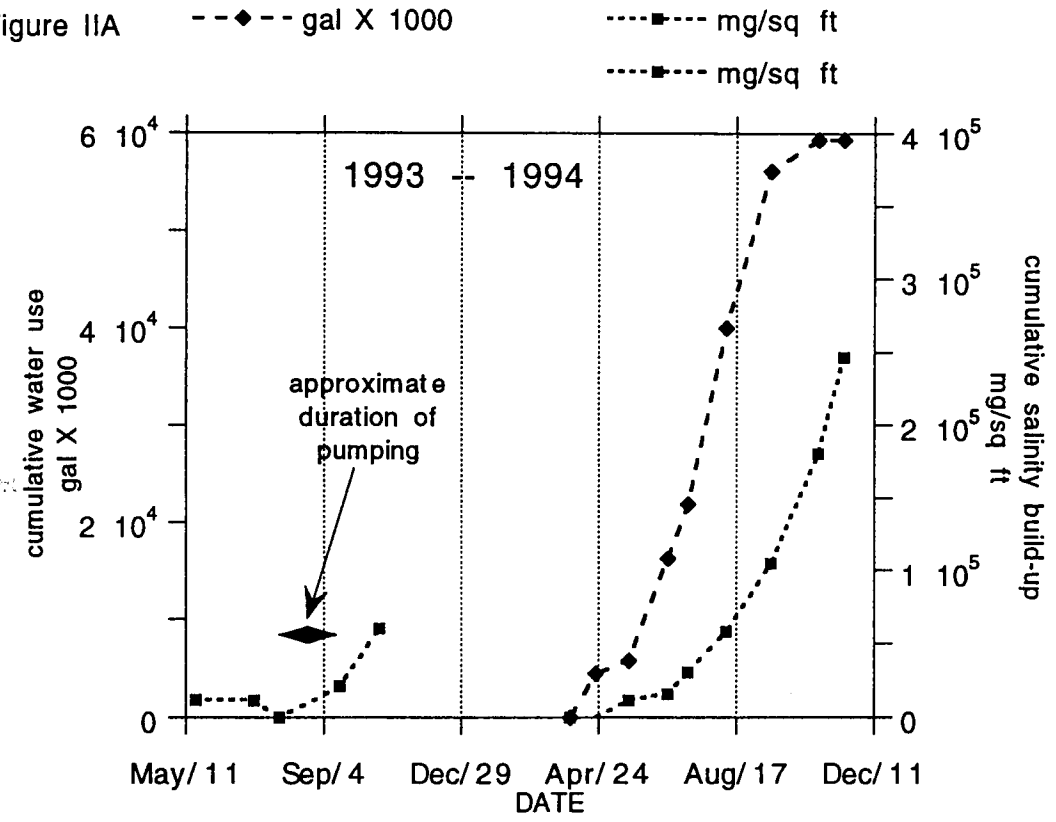

Table IIA

DATE	gal X1000 (1)	mg/sq ft
20-5-1993		12019
8-7-1993		11649
29-7-1993		0.0000
18-9-1993		21177
21-10-1993		60140
31-3-1994	0.0000	0.0000
21-4-1994	4426.0	-237.43
19-5-1994	5772.0	11397
21-6-1994	16236	15768
8-7-1994	21842	30079
9-8-1994	39955	58240
16-9-1994	56063	1.0445e+05
26-10-1994	59328	1.8032e+05
16-11-1994	59328	2.4636e+05

(1) Source: D. P. Young, Kansas Geol. Surv. fieldnotes

APPENDIX III.

The Effect of Local Discontinuities in Aquitards on the Mineralization of Groundwater
Part 1: Mineralization Due to Complete Exposure and Direct Contact Between Fresh and Saltwater

by
Hillel Rubin* and Robert W. Buddemeier
Kansas Geological Survey, The University of Kansas
Lawrence, KS 66047

Abstract

This paper represents a basic study carried out in the framework of comprehensive research concerning the understanding of major mechanisms and phenomena involved in the mineralization of groundwater of the Great Bend Prairie aquifer in Kansas by saltwater originating from a deeper Permian bedrock formation. The conceptual model of this study considers that mineralization of the aquifer is attributed to local discontinuities in the aquitards and direct contact between the fresh and saline water.

Calculations are made with regard to a single discontinuity. Salinity penetrates into the freshwater aquifer through that discontinuity in the aquitard. Downstream from that discontinuity, the salinity is subject to advection and dispersion processes. A boundary layer method developed in the framework of this study provides a simple but robust approach for the initial evaluation of mineralization processes taking place downstream of the local discontinuity in the aquitard.

*On leave from the Department of Civil Engineering, Technion—Israel Institute of Technology, Haifa 32000, Israel.

Introduction

This paper concerns the interest in understanding major mechanisms and phenomena involved in the mineralization of the Great Bend Prairie aquifer of south central Kansas. The Great Bend Prairie aquifer overlies bedrock of Cretaceous and Permian age. Various publications provide information concerning the geology of the region (e.g. Latta, 1950; Layton and Berry, 1973; Fader and Stullken, 1978; Cobb, 1980). During the last few years significant efforts have been invested in measuring salinity distribution in the region (Young, 1992; Whittemore, 1993; Buddemeier et al. 1992; 1994). These measurements are analyzed and used for the identification of sources of salinity (Whittemore, 1993) as well as mechanisms involved in the mineralization processes (Buddemeier et al., 1994). In the framework of these efforts the authors (Rubin and Buddemeier, 1994a; b) have developed some conceptual and modeling approaches which provide some quantitative estimates of phenomena and mechanisms leading to mineralization of the Great Bend Prairie aquifer. Generally, it seems that salinity penetration into the freshwater aquifer occurs in some locations due to direct contact between the fresh and saline water, or due to infiltration of saline water from the deep formation into the freshwater aquifer. In most places clay and shale layers effectively separate the freshwater aquifer from the saline water of the deep formations. Salinity penetrations are probably local phenomena. However, once it penetrates into the freshwater aquifer, the salinity is advected, disperses and thereby contaminates the freshwater resources of the region. In the framework of the present study we refer to salinity penetration into the freshwater aquifer due to direct contact between the freshwater and the saline water of the deeper formation (Rubin and Buddemeier, 1994a). We consider such a mechanism of salinity penetration into

the aquifer, and analyze phenomena of mineralization where the fresh and saline zones are separated by aquitards.

The Conceptual Model and Basic Formulation

We refer to the simplified conceptual model shown in fig. 1. It basically describes a local discontinuity in the aquitard. This discontinuity causes direct contact between fresh and saline water along the exposure length, x_e^*.

Flow conditions and salinity transport in the complete domain of fig. 1 are governed by the following set of differential equations.

$$\vec{q} = -\frac{k}{\mu}\left(\nabla p - \rho \vec{g}\right) \tag{1}$$

$$\frac{\partial C^*}{\partial t^*} + \vec{V}\cdot\nabla C^* = \nabla\cdot(\tilde{D}\cdot\nabla C^*) \tag{2}$$

where $\vec{q}$ is the specific discharge vector, k is the permeability; μ is the fluid viscosity; p is the pressure; ρ is the fluid density; g is the gravitational acceleration; C^* is the salt concentration (salinity); V is the interstitial flow velocity; $\tilde{D}$ is the dispersion tensor; t is time.

The set of differential eqs. (1) and (2) can be solved by various types of numerical procedures. However, the simultaneous solution of eqs. (1) and (2) is quite complicated; the non linearity stemming from the dependence of ρ on C^* introduces simulation difficulties, and there are problems of stability of the numerical solution, numerical dispersion etc. Therefore, an introduction of some simplifications into the calculation of salinity transport in the domain of fig. 1 is very desirable. Such simplification should be consistent with a methodology of groundwater quality simulation in stages. The initial stage, according to such a methodology, consists of general quantitative evaluation of phenomena, time scales of contamination and reclamation, as well as initial risk analysis. This paper addresses to such a limited stage. Some possible simplifications introduced into eqs. (1) and (2) for the initial

stage of groundwater quality calculation in the domain of fig. 1 are given in the following paragraphs.

Initially, the upper part of the domain, represented by $y^* \geq 0$, is occupied by freshwater, and a sharp interface between the fresh and saline water exists at the discontinuity exposure length, x_e^*; namely at

$$y^* = 0, \quad -x_e^* \leq x^* \leq 0 \tag{3}$$

The density and total dissolved solids (TDS) of the saltwater present in the Permian zone are very similar to those of sea water (Whittemore, 1993). Therefore, effects of salinity on the groundwater viscosity and thereby the hydraulic conductivity of the domain shown in fig. 1 is uniform. We also employ the Dupuit approximation and consider that streamlines are horizontal. Then eq. (1) indicates that the velocity V is uniformly distributed in the domain, and it has only a component in the x^* direction. Therefore, salinity transport in the domain is governed by

$$\frac{\partial C^*}{\partial t^*} + V\frac{\partial C^*}{\partial x^*} = D_x\frac{\partial^2 C^*}{\partial x^{*2}} + D_y\frac{\partial^2 C^*}{\partial y^{*2}} \tag{4}$$

where x^* and y^* are the longitudinal and vertical coordinates, respectively; D_x and D_y are the longitudinal and transverse dispersion coefficients, respectively.

The uniformity of the physical parameters in the domain of fig. 1 causes a complete asymmetry of the salinity distribution in that domain. We may also apply dimensionless quantities instead of the physical coordinates and variables, defined by

$$x = x^*/l_0;\ y = y^*/l_0;\ t = t^*V/l_0$$
$$C = \left(C^* - C_f^*\right)/\left(C_s^* - C_f^*\right) \tag{5}$$

where l_0 is an adopted unit length along the initial interface; C_s^* is the salinity of the saltwater, and C_f^* is the salinity of the freshwater.

Introducing the dimensionless variables of eq. (5) into eq. (4) we obtain

$$\frac{\partial C}{\partial t} + \frac{\partial C}{\partial x} = a_L\frac{\partial^2 C}{\partial x^2} + a\frac{\partial^2 C}{\partial y^2} \tag{6}$$

where a_L and a are the dimensionless longitudinal and transverse dispersivities which are defined by

$$a_L = D_x/(l_0 V); \quad a = D_y/(l_0 V) \tag{7}$$

The mineralization process in the region

$$y \geq 0; \quad -x_e \leq x \leq 0 \tag{8}$$

where $x_e = x_e^*/l_0$, has been analyzed by Rubin and Buddemeier (1994a). We can apply results obtained in that study and concentrate our effort in simulating the salinity transport in the region

$$x, y \geq 0 \tag{9}$$

The study of Rubin and Buddemeier (1994a) indicates that the initial interface at the aquitard discontinuity represents the isohaline $C = 0.5$. On both sides of that isohaline a transition zone (TZ) develops. The transition zone that develops in the domain part given by eq. (9) is called the region of interest (ROI) in which salinity exceeds the acceptable value. Applying the results of Rubin and Buddemeier (1994a) we infer that in the region specified by eq. (8) steady state conditions are obtained at $t = x_e$. During the time interval

$$0 \leq t \leq x_e \tag{10}$$

a time dependent boundary condition develops at

$$0 \leq y \leq \infty, \quad x = 0 \tag{11}$$

Referring to eq. (6), it is possible to ignore the first-right-hand side term of eq. (6) and obtain the following expression for the steady state salinity distribution at the boundary of eq. (11).

$$C = 0.5 \ erfc\left(\frac{y}{2\sqrt{a x_e}}\right) \tag{12}$$

where *erfc* is the complementary error function.

This expression can be applied to the simulation of steady state salinity distribution in the domain specified by (9), provided that the longitudinal extent of the domain is limited ($x \leq x_{max}$), and steady state conditions are established. However, by applying the top specified boundary layer (TSBL) approach Rubin and Buddemeier (1994a) conclude that at the boundary of eq. (11) the salinity distribution is

$$C = 0.5(1 - y/\delta_0)^n \tag{13}$$

$$\left(\delta_0^2\right)_{x=0} = 2an(n+1)\left[t - (t - x_e)u(t - x_e)\right] \tag{14}$$

where

$$u(t - x_e) = \begin{cases} 1 & t > x_e \\ 0 & t < x_e \end{cases} \tag{15}$$

The parameter δ_0 represents the value of y at which the salinity is smaller by at least an order of magnitude than the acceptable value. For the purpose of this derivation, the acceptable value of salinity defining the top of the ROI is considered to be $C_T = 0.005$, namely one percent of the salinity at the initial interface. For a wide range of values of the transverse dispersivity Rubin and Buddemeier (1994a) showed that the power coefficient of eq. (13) should be $n = 3$.

In the domain of eq. (9) the salinity distribution is determined by the boundary condition of eq. (12) or (13) as well as by the boundary conditions

$$\begin{aligned} &\frac{\partial C}{\partial y} = 0 \quad at \quad y = 0 \\ &C \to 0 \quad at \quad y \to \infty \\ &C = 0 \quad at \quad x = x_{max} \quad (x_{max} > t) \end{aligned} \tag{16}$$

The last boundary condition of eq. (16) is needed if the first right-hand-side term of eq. (6) is significant and x_{max} is larger than t. If reference is made to steady state conditions, then the last boundary condition should be replaced by

$$\frac{\partial C}{\partial x} \to 0 \quad at \quad x = x_{max} \quad (x_{max} < t) \tag{17}$$

If interest is concentrated on the penetration of the salinity into the domain of eq. (9) and build-up of the ROI, then besides the boundary conditions of eq. (16) we have to consider the following initial conditions

$$C = 0 \quad at \quad t = 0,\ x, y \geq 0 \quad except\ for\ the\ point\ x, y = 0$$
$$C = 0.5 \quad at \quad x, y = 0 \tag{18}$$

We intend to develop a quantitative modeling approach which describes the salinity distribution and build-up of the ROI in the domain of eq. (9) by applying the TSBL approach. Fig. 2 represents the basic domain structure considered for the salinity distribution.

It is assumed that the salinity profile, at each cross-section perpendicular to the x axis, can be described by a combination of two boundary layers taking place in adjacent ranges of the y coordinate. The inner boundary layer is represented by the salinity distribution.

$$C = C_b\left[1 - (1 - c_r)(1 - \xi)^{n_1}\right];\ \xi = \frac{\delta_u - y}{\delta_u};\ 0 \leq y \leq \delta_u \tag{19}$$

where n_1 is a power coefficient; ξ is the inner boundary layer coordinate; c_r is the ratio between the salinity at $y = \delta_u$ and the salinity C_b, at $y = 0$.

The outer boundary layer is represented by the salinity distribution

$$C = c_r C_b (1 - \eta)^{n_2};\ \eta = \frac{y - \delta_u}{\delta_0 - \delta_u};\ \delta_u \leq y \leq \delta_0 \tag{20}$$

where n_2 is a power coefficient; η is the outer boundary layer coordinate.

We are especially interested in the identification of a possible constant value of c_r which is involved with negligible salinity transfer between the two boundary layers specified by eqs. (19) and (20), respectively. We adopted such a approach following numerous numerical experiments in which we solved eq. (6) subject to the

boundary and initial condition of eqs. (13)–(18). In these experiments we have calculated salinity fluxes through isohalines normalized with regard to C_b values. The experiments showed very minor salinity fluxes from the outer boundary layer into the inner one through normalized isohalines. Therefore, we decided to identify the value of the normalized isohaline, namely c_r, associated with the minimum and almost negligible salinity flux crossing that normalized isohaline.

The ROI is considered as a top specified boundary layer (TSBL). At the top of the ROI

$y = \delta$ and the value of C is C_T, where C_T is the acceptable value of salinity, namely $C_T = 0.005$ as considered by Rubin and Buddemeier (1994a).

Continuity of the slope of the salinity profile at $y = \delta_u$ requires, according to eqs. (19) and (20),

$$\frac{\delta_0}{\delta_u} = \frac{c_r n_2}{(1-c_r)n_1} + 1 \tag{21}$$

Conservation of mass implies for the inner boundary layer

$$\frac{\partial}{\partial t}\left(\int_0^{\delta_u} C dy\right) + \frac{\partial}{\partial x}\left(\int_0^{\delta_u} C dy\right) = 0 \tag{22}$$

Referring to a moving coordinate system we obtain

$$\frac{d}{dt}(C_b \delta_u) = 0 \tag{23}$$

Therefore

$$(C_b \delta_u)_{x,t} = (C_b \delta_u)_{x=0,\ t_0 = t-x} \tag{24}$$

If we consider that the vertical salinity gradient does not lead to salinity transport between the inner and outer boundary layers, but leads to the expansion of the boundary layers, we obtain for the inner boundary layer

$$C_{avu} \frac{d\delta_u}{dt} = -\alpha_1 a \left(\frac{\partial C}{\partial y}\right)_{y=\delta_u} \tag{25}$$

where α_1 is a coefficient; C_{avu} is the average salinity of the inner boundary layer

$$C_{avu} = \frac{1}{\delta_u}\int_0^{\delta_u} C dy \tag{26}$$

Introducing eq. (19) into eq (26) we obtain

$$C_{avu} = C_b \frac{n_1 + c_r}{n_1 + 1} \tag{27}$$

Considering that at $x = 0$ the value of $C_b = 0.5$, we apply eq. (13) to obtain

$$\left(\frac{\delta_u}{\delta_0}\right)_{x=0} = 1 - c_r^{\frac{1}{n}} \tag{28}$$

Differences between this expression and eq. (21) stem from the adaptation of the salinity distribution to the first boundary condition of eq. (16).

Introducing eqs. (19) and (27) into eq. (25) we obtain

$$\frac{d\delta_u^2}{dt} = \alpha_1 \frac{2a(1-c_r)n_1(n_1+1)}{n_1 + c_r} \tag{29}$$

Direct integration of this expression yields

$$\left(\delta_u^2\right)_{x,t} = \left(\delta_u^2\right)_{x=0,t_0=t-x} + \alpha_1 \frac{2a(1-c_r)n_1(n_1+1)}{n_1 + c_r} x \tag{30}$$

Equations (14), (28), (30), and (24) fully determine the distribution of δ_u and C_b in the domain.

Equations (14), (28), and (24) imply that eq. (30) can be used at

$$0 \le x \le t \tag{31}$$

For $x > t$ the boundary layers vanish.

Steady state conditions are established in the region

$$0 \le x \le t - x_e \tag{32}$$

provided that $t > x_e$

Principles similar to those leading to eqs. (22)–(30), are also used with regard to the outer boundary layer.

We again consider that salinity gradients in the outer boundary layer lead to its expansion and obtain

$$C_{avo}\frac{d}{dt}(\delta_0-\delta_u)=-\alpha_2 a\left(\frac{\partial C}{\partial y}\right)_{y=\delta_u} \tag{33}$$

where α_2 is a coefficient; C_{avo} is the average salt concentration in the outer boundary layer.

$$C_{avo}=\frac{1}{\delta_0-\delta_u}\int_{\delta_u}^{\delta_0} C dy \tag{34}$$

Introducing eq. (20) into eq. (34) we obtain

$$C_{avo}=C_b\frac{c_r}{n_2+1} \tag{35}$$

Introducing eq. (20) and (35) into eq. (33) we obtain

$$\frac{d}{dt}(\delta_0-\delta_u)^2=2\alpha_2 a n_2(n_2+1) \tag{36}$$

Direct integration of this expression and reference to the initial and boundary conditions of eqs. (14) and (28) yield

$$(\delta_0-\delta_u)^2_{x,t}=(\delta_0-\delta_u)^2_{x=0,t_0=t-x}+2\alpha_2 a n_2(n_2+1)x \tag{37}$$

Again, only x-values smaller than t should be considered.

Following the determination of δ_u, C_b and δ_0, the thickness , δ, of the ROI defined as the top specified boundary layer, can be calculated. The value of this parameter is associated with the isohaline $C = C_T$. The value of δ can be either in the range of y values at the outer boundary layer, provided that $C_T \le c_r C_b$, or at the inner boundary layer, provided that $C_T > c_r C_b$.

If $\delta_u < \delta < \delta_0$ then according to eq. (20)

$$C_T=c_r C_b(1+\eta_T)^{n_2} \tag{38}$$

where η_T represents the value of $y = \delta$.

Equation (38) yields

$$\eta_T=1-\left(\frac{C_T}{c_r C_b}\right)^{\frac{1}{n_2}} \tag{39}$$

$$\delta=\eta_T(\delta_0-\delta_u)+\delta_u \tag{40}$$

If $0 < \delta < \delta_u$ then according to eq. (19)

$$C_T = C_b\left[1-(1-c_r)(1-\xi_T)^{n_1}\right] \tag{41}$$

where ξ_T represents the value $y = \delta$.

Equation (41) yields

$$\xi_T = 1-\left(\frac{1-C_T/C_b}{1-c_r}\right)^{\frac{1}{n_1}} \tag{42}$$

$$\delta = \delta_u(1-\xi_T) \tag{43}$$

Equations (14), (28), (30), (24), (37), and (40) or (43) provide a complete closed form analytical solution for the determination of δ_u, C_b, δ_0 and δ. Thereby, salinity transport and distribution in the domain $x, y \geq 0$ is fully determined, and the build-up of the ROI can be followed.

Although the general method of calculation given in this section seems quite simple and attractive, it requires some preliminary tests indicating that: it is possible to divide salinity profiles into two boundary layers; there is no salt mass transfer between the two boundary layers; salinity profiles in each boundary layer obey some laws of similarity; and the ratio between the thickness of the two boundary layers becomes constant at a certain comparatively small value of x.

The following section reports the performance and evaluation of some preliminary tests aimed at the consideration of these issues.

Preliminary Tests

Due to the build-up of the boundary condition at $x = 0$ as given by eq. (14) it seems that a spearhead front of salinity penetrates into the domain $x, y \geq 0$ from its left-hand-side boundary. At the penetrating front of the salinity some longitudinal dispersion probably takes place. Longitudinal dispersion probably has also some

effect at the left-hand-side boundary of the domain where the salinity profile is adopted from Dirichlet-type boundary conditions at $y = 0$, $-x_e \le x \le 0$ to Neumann type with zero flux at $y = 0, x > 0$. This phenomenon is represented by the transition from the relationship given by eq. (28) to that given by eq. (21). However, for most parts of the domain $x, y \ge 0$ we may assume that longitudinal dispersion effects are very minor in comparison to salinity advection in the longitudinal direction.

Calculations of the preceding section indicate that steady state conditions gradually develop in the simulated domain $x, y \ge 0$. If we refer to limited region of the domain $0 \le x \le x_{max}$ were $x_{max} < t - x_e$ then this region is subject to steady state conditions. As a preliminary set of tests we consider it appropriate to refer to all issues identified at the end of the preceding section by comparing the boundary layer methodology with the solution of the steady state version of eq. (6) in which effects of longitudinal dispersion are ignored. Therefore, the reference is to the differential equation

$$\frac{\partial C}{\partial x} = a \frac{\partial^2 C}{\partial y^2} \tag{44}$$

This equation is subject to the relevant boundary conditions of eqs. (12) and (16), namely

$$\begin{aligned} &\frac{\partial C}{\partial y} = 0 \quad at \ y = 0 \\ &C \to 0 \quad at \ y \to \infty \\ &C = 0.5 \ erfc\left(\frac{y}{2\sqrt{a x_e}}\right) \quad at \ x = 0 \end{aligned} \tag{45}$$

The problem of salinity transport represented by eqs. (44) and (45) is analogous to heat conduction in an insulated semi-infinite domain subject to an initial

temperature distribution. We apply the following Crank-Nicolson implicit finite difference scheme

$$-C_{r+1,s-1}\frac{a\Delta x}{2(\Delta y)^2}+C_{r+1,s}\left[1+\frac{a\Delta x}{(\Delta y)^2}\right]-C_{r+1,s+1}\frac{a\Delta x}{2(\Delta y)^2}$$
$$=C_{r,s-1}\frac{a\Delta x}{2(\Delta y)^2}+C_{r,s}\left[1-\frac{a\Delta x}{(\Delta y)^2}\right]+C_{r,s+1}\frac{a\Delta x}{2(\Delta y)^2} \tag{46}$$

where r and s represent nodal point numbers in the x and y directions, respectively.

Figure 3 shows how the steep salinity profile at $x = 0$ progressively becomes milder with increasing values of x. The decrease of the vertical salinity gradient is associated with penetration of the salinity to increasing values of the y coordinate. This penetration is more significant for larger dispersivity values.

Figure 4 provides information about the variation of C_b with the x coordinate. Various values of a and x_e are considered.

Figure 5 compares profiles of C_b obtained with various x_e-values and a single dispersivity. We have performed numerous experiments aiming at the identification of possible values of c_r and n_2. In these experiments, for various x-values, the values of δ_u and δ_0 have been identified according to the criteria shown in fig. 2. Then we calculate the value of

$$\delta_R = \delta_0 / \delta_u \tag{47}$$

By introducing the value of this parameter and a best fit value of n_2 into eq. (21) the value of n_1 is calculated.

Our numerical experiments showed that a very reasonable value for c_r is

$$c_r = 0.5 \tag{48}$$

We have also found best fit of salinity profiles when considering

$$n_2 = 4 \tag{49}$$

Figure 6 shows how the value of δ_R changes in a short distance from the quantity defined by eq. (28) to a constant value independent of x. When the constant value of δ_R is established then n_1 also reaches a constant value. We also find best fit values of α_1 and α_2

$$n_1 = 1.84;\ \alpha_1 = 1.25;\ \alpha_2 = 0.5 \tag{50}$$

The coefficient α_1 is larger than unity, probably due to the minor flux of salinity transferred from the outer boundary layer to the inner one.

Our experiments have been performed for quite wide ranges of the parameters x_e and a:

$$\begin{aligned} 10 \le x_e \le 100 \\ 0.01 \le a \le 1.0 \end{aligned} \tag{51}$$

For the ranges of values given by eq. (51) best fit values for the salinity profile are identical to those given by eq. (48)–(50). Fig. 7 exemplifies the determination of the appropriate value of n_2. In this figure we have applied the calculated C profiles at $x = 500$, 1000 and checked the adequacy of eqs. (19) and (20) as well as (21) with various values of n_2. Fig. 7 indicates that the values given by eqs. (49) and (50) provide the best fit C profiles when $a = 0.5$ and $x_e = 100$.

Figure 8 exemplifies the tests considering the applicability of the boundary layer methodology for $a = 0.1$, $x_e = 100$ and different x-values. Fig. 8 eventually indicates that for the range of x-values

$$10 \le x \le 1000 \tag{52}$$

the boundary layer approach of this study with quantities given by eqs. (48)–(50) provides a quite accurate description of salinity transport and distribution in the domain of $x, y \ge 0$. We have not observed any limitation on the maximum value of x to which the boundary layer approach could be applied.

In the next stage we have compared the steady state simulations obtained by using eq. (44) with those obtained by using the boundary layer approach with quantities given by eqs. (48)–(50).

Figure 9 provides a comparison between values of δ_u, δ and δ_0 obtained by both methods. Generally, differences between values of the various parameters are not significant, and they are definitely acceptable from the point of view of practical application.

Figure 10 provides a comparison between steady state profiles of C_b obtained by applying eq. (44) and those obtained by using the boundary layer approach with quantities given by eqs. (48)(50). Again, differences are small.

Characterizing the Mineralization Process

Equation (14) indicates that the boundary condition at the left hand side of the domain

$x, y \geq 0$ is subject to changes until $t = x_e$. Therefore, for t-values larger than x_e we identify in the domain two regions as represented by fig. 11: (a) the spear-head region at $t - x_e \leq x \leq t$, and (b) the steady state region at $0 \leq x \leq t - x_e$.

As indicated by eqs. (30) and (37) as well as fig. 11, values of δ_u and δ_0 progressively increase with x. The expansion of these layers decreases their average salinity. Therefore, the value of δ, associated with a constant salinity value $C = C_T$, does not increase at the same rate as δ_0 and δ_u. Fig. 12(a) refers to $t = 100$. It represents only the spear-head region. In this case the value of δ decreases only over the last twenty units of the x-values, namely at $80 \leq x \leq 100$. Fig. 12(b) refers to $t =$ 1000. The salinity penetration is shown for the spear-head region as well as the steady state region. Fig. 12(c) describes the various boundary layers in the spear-head region at $t = 1000$. In this case the value of δ decreases along the whole spear-head region.

The spear-head region represents the first x_e units of the salinity penetration into the aquifer.

Figure 13 indicates that the decrease in values of δ with increasing x-values is limited to the spear-head region even at a significant distance from the aquitard discontinuity. Fig. 14 shows conditions at a very large distance from the aquitard discontinuity. However, again the decrease of δ with the increase of x-values is limited to the spear-head region. Values of δ_u and δ_0 in the spear-head region are kept almost constant at large distances from the aquitard discontinuity.

Figure 15 demonstrates the effects of the exposure length, x_e, and the dispersivity, a, on the development of the various boundary layers in the steady state region. As indicated by eq. (12) the effect of x_e is identical to that of the dispersivity, a, with regard to the build-up of the left hand side boundary, at $x = 0$, of the domain x, $y \geq 0$. However, eqs. (30) and (37) indicate that the rate of growth of δ_u and δ_0 with increasing x-values depends solely on the dispersivity, a. Fig. 15 exemplifies this phenomenon.

We may expect a comparatively large effect of longitudinal dispersion in the spear-head region. Therefore, we have performed a series of comparative simulations aimed at the evaluation of such an effect. We have simulated the salinity penetration at consecutive time intervals by employing the boundary layer simulation approach as well as finite difference explicit schemes of eq. (6). The numerical scheme used by us represents a combination of the explicit-implicit approach for first order hyperbolic equations (e.g. Lapidus and Pinder, 1982) and the explicit approach for the solution of parabolic differential equations. The numerical scheme obtained by such an arrangement is

$$C_{r,s}^{m+1}\left(1+\frac{\Delta t}{\Delta x}\right)=C_{r,s}^{m}+C_{r-1,s}^{m+1}\frac{\Delta t}{\Delta x}+a\frac{\Delta t}{(\Delta y)^2}\left(C_{r,s+1}^{m}-2C_{r,s}^{m}+C_{r,s-1}^{m}\right)$$
$$+a_L\frac{\Delta t}{(\Delta x)^2}\left(C_{r+1,s}^{m}-2C_{r,s}^{m}+C_{r-1,s}^{m}\right) \tag{53}$$

where m is the number of the time step.

Equation (53) is associated with the finite difference presentation of the boundary and initial conditions given by eqs. (13)–(18). Von Neumann's stability analysis of the numerical scheme given by eq. (53), indicates that this scheme is stable provided that the following criteria are satisfied (Rubin, 1994).

$$\frac{2a_L\Delta t}{(\Delta x)^2}+\frac{2a\Delta t}{(\Delta y)^2}\le 1+\frac{\Delta t}{\Delta x}$$
$$\frac{2a\Delta t}{(\Delta y)^2}\le 1 \tag{54}$$

We have also performed simulations with the short version of eq. (53), in which the last term of this expression is neglected, namely neglecting the effect of the longitudinal dispersion on transport and distribution of salt in the simulated domain. In this short version only the last stability criterion of eq. (54) is applicable.

Results of both types of simulations are compared with results obtained by the use of the boundary layer approach in fig. 16. There are some differences between the boundary layer simulations and results obtained by the employment of the numerical schemes. However, numerical results of the complete and short versions are very similar. Therefore, it seems that differences between the boundary layer and the numerical results are very much affected by numerical dispersion. Generally, the boundary layer approach and the numerical simulations represent almost identical phenomena of salinity penetration into the freshwater aquifer. All approaches indicate that the region of interest (ROI), namely $0 \le y \le \delta$ increases with increasing

x-values in the steady state region, even for very large values of x, and it decreases with increasing x-values in the spear-head region. The dimensionless horizontal extent of the salinity penetration is identical to the dimensionless time period of advection of the mineralized fluid particles.

Summary and Conclusions

Recent field measurements in south-central Kansas as well as some quantitative calculations have indicated that phenomena of groundwater mineralization probably originate from local discontinuities in the clay layers and other types of aquitards. In much of the western part of Kansas, such aquitards completely separate the freshwater aquifer from the deep Permian formation which is saturated with saline water.

Previous studies of the authors (Rubin and Buddemeier, 1994a; b; c) concern the development and possible use of the top specified boundary layer (TSBL) approach for the simulation of contaminant hydrology issues. Special interest has been given to cases of groundwater mineralization due to direct contact between fresh and saltwater, as well as due to seepage of saltwater into the freshwater aquifer.

Traditional or classical uses of the boundary layer approach consider that the region of interest (ROI), in which the value of the transported quantity varies from significant to negligible, behaves as a boundary layer. In that region boundary layer laws of similarity are applicable. Due to this requirement of identity between the ROI and the region in which boundary layer laws of similarity take place, the traditional boundary layer approach can only be applied to Dirichlet type problems, namely cases in which the quantity value is specified at the boundary of the domain. By separating the definition of the ROI from the region in which boundary layer similarity laws apply, the TSBL approach can be applied to various types of Dirichlet and Neumann problems as well as combinations of such boundary conditions. However, in any particular case of study the appropriate definition of the ROI should be given, and regions of boundary layer similarity laws should be identified. Furthermore, laws of similarity in such regions should be identified, and appropriate

formulations for each similarity region should be adopted. We define the thickness of the ROI as δ. The thickness δ is measured in the direction perpendicular to the flow direction and the streamlines.

The present study concerns the penetration of salinity into the freshwater aquifer due to discontinuity in the aquitard which leads to direct contact between the fresh and saltwater. The direct contact between the fresh and saltwater causes penetration of the salinity to freshwater regions in which the local aquitard completely separates the freshwater aquifer from the deep saltwater aquifer. Simulation of this salinity penetration is achieved by dividing the vertical salinity profile into two boundary layers: (a) the inner boundary layer—located close to the impermeable bottom of the aquifer, and (b) the outer boundary layer—built on top of the inner boundary layer.

The calculations indicate that the salinity penetration can be represented as a build-up of the ROI whose thickness is δ and the longitudinal extent is identical to the advection length of the mineralized fluid particles. It is possible to identify two regions in the horizontal extent of the salinity penetration: (a) the steady state region, and (b) the spear-head region. In the steady state region the thickness of the ROI increases moderately with increasing x-values. The horizontal extent of the spear-head region is identical to that of the discontinuity that exposes the freshwater to direct contact with saltwater. Even at large distances from the exposure, any decrease of the ROI thickness with increasing values of x is limited to the spear-head region. At the downstream end of the spear-head region the thickness of the ROI vanishes.

Comparative simulations with the boundary layer method as well as with various types of finite difference numerical schemes have indicated the adequacy of the TSBL approach for the simulation of the salinity penetration into regions of

complete separation at the fresh- and salt-water aquifers by impermeable aquitard between them.

The method developed in this study is applied for a completely uniform domain. However, the application to various types of non-uniformity can be made with a little effort. In such cases simple numerical schemes should be employed for the solution of the transport equation which is basically converted to a first order hyperbolic equation.

Notation

a dimensionless transverse dispersivity

a_L dimensionless longitudinal dispersivity

(bl) subscript referring to boundary layer value

c_r ratio between C and C_b at the boundary between the inner and outer boundary layers

C dimensionless salinity

C_b dimensionless salinity at the bottom of the aquifer

C_T dimensionless salinity at the top of the ROI

C_{avo} dimensionless average salinity at the outer boundary layer

C_{avu} dimensionless average salinity at the inner boundary layer

C^* salt concentration – salinity [ML^{-3}]

C_f^* salinity of the freshwater aquifer [ML^{-3}]

C_s^* salinity of the saltwater [ML^{-3}]

d represents δ in figures

d_0 represents δ_0 in figures

d_u represents δ_u in figures

d_R represents δ_R in figures

$\tilde{D}$ dispersion tensor [L^2T^{-1}]

D_x longitudinal dispersion coefficient [L^2T^{-1}]

D_y transverse dispersion coefficient [L^2T^{-1}]

g gravitational acceleration [LT^{-2}]

k permeability [L^2]

l_0 length scale[L]

m number of the time step

n power coefficient of boundary layer series expansion at $-x_e \leq x \leq 0$

n_1 power coefficient of inner boundary layer

n_2 power coefficient of outer boundary layer

(nu) subscript referring to numerical value

p pressure [$ML^{-1}T^{-2}$]

q specific discharge [LT^{-1}]

r number of nodal point in the x-direction

ROI region of interest

s number of nodal point in the y-direction

t dimensionless time

t_0 dimensionless time at which the mineralized fluid particle is at $x = 0$

t^* time (T)

TSBL top specified boundary layer

TZ transition zone

u unit step function

V interstitial flow velocity [LT^{-1}]

x dimensionless longitudinal coordinate

x_e dimensionless extent of the aquitard discontinuity

x_{max} dimensionless extent of the simulated domain

x^* longitudinal coordinate [L]

x_e^* length of the aquitard discontinuity [L]

y dimensionless vertical coordinate

y^* vertical coordinate [L]

α_1 coefficient defined in eq. (25)

α_2 coefficient defined in eq. (33)

δ dimensionless thickness of the ROI

δ_u dimensionless thickness of the inner boundary layer

δ_0 dimensionless thickness of the inner and outer boundary layers

δ_R ratio between δ_0 and δ_u

Δt time step

Δx longitudinal interval

Δy vertical interval

η outer boundary layer coordinate

η_T value of η at $y = \delta$ (provided that $\delta_u < \delta < \delta_0$)

μ viscosity [$ML^{-1}T^{-1}$]

ξ inner boundary layer coordinate

ξ_T value of ξ at $y = \delta$ (provided that $0 < \delta < \delta_u$)

ρ fluid density [ML^{-3}]

References

Buddemeier, R.W., Sophocleous, M.A. and Whittemore, D.O., 1992. Mineral intrusion—Investigation of salt contamination of groundwater in the Eastern Great Bend Prairie Aquifer, Open-File Rept. 92-25, Geohydrology, Kansas Geological Survey, The University of Kansas, Lawrence, KS.

Buddemeier, R.W., Garneau, G.W., Young, D.P., Whittemore, D.O., Zehr, D., Lanterman, J., Ma, T.S., and Falk, S., 1994. The mineral intrusion project: Progress and activities during fiscal year 1994, Open-File Rept. 94-28, Geohydrology, Kansas Geological Survey, The University of Kansas, Lawrence, KS.

Cobb, P.M., 1980. The distribution and mechanisms of salt water intrusion in the fresh water aquifer and in Rattlesnake Creek Stafford County Kansas, M.S. thesis, Department of Civil Engineering, The University of Kansas, Lawrence, KS.

Fader, S.W. and Sutullken, L.E., 1978. Geohydrology of the Great Bend Prairie South-Central Kansas, Irrigation Series 4, Kansas Geological Survey.

Lapidus, L. and Pinder, G.F., 1982. "Numerical solution of Partial Differential Equations in Science and Engineering, " John-Wiley & Sons, NY.

Latta, B., 1950. Geology and groundwater resources of Barton and Stafford Counties, Kansas Bulletin 88, Kansas Geological Survey.

Layton, D.W. and Berry, D.W., 1973. Geology and ground-water resources of Pratt County, South-Central Kansas, Bulletin 205, Kansas Geological Survey.

Rubin, H., 1994. Numerical schemes applicable in contaminant hydrology, Open-File Rept. 94-8, Geohydrology, Kansas Geological Survey, The University of Kansas, Lawrence, KS.

Rubin, H. and Buddemeier, R.W., 1994a. Application of the top specified boundary layer (TSBL) approximation to initial characterization of an inland aquifer mineralization, (to be published).

Rubin, H. and Buddemeier, R.W., 1994b. Initial characterization of groundwater mineralization due to seepage of saline water through semiconfining layers, (to be published).

Rubin, H. and Buddemeier, R.W., 1994c. A top specified boundary layer (TSBL) approximation approach for the simulation of groundwater contamination processes, (to be published)

Whittemore, D.O., 1993. Ground water geochemistry in the mineral intrusion area of groundwater management district no. 5, South-Central Kansas, Kansas Geological Survey, The University of Kansas, Lawrence, KS.

Young, D.P., 1992. Mineral intrusion: Geohydrology of Permian bedrock underlying the Great Bend Prairie aquifer in south-central Kansas, Open-File Rept. 92-44, Geohydrology, Kansas Geological Survey, The University of Kansas, Lawrence, KS.

Figure Captions

Fig. 1 Conceptual model representing the localized salinity penetration and the mineralized region.

Fig. 2 Schematic specifying salinity values at the domain boundaries as well as at the edges of the various boundary layers.

Fig. 3 Steady state salinity profiles at various x-values ($x_e = 100$)

(a) $a = 0.5$ (b) $a = 0.1$ (c) $a = 0.01$

Fig. 4 Profiles of C_b for various values of a

(a) $x_e = 100$ (b) $x_e = 50$ (c) $x_e = 10$

Fig. 5 Profiles of C_b for various x_e-values ($a = 0.1$)

Fig. 6 Values of δ_R and n_1 versus x ($a = 0.1, x_e = 100, n_2 = 4$)

Fig. 7 Determination of the value of n_2

($a = 0.5, x_e = 100, c_r = 0.5$) – $C_{(bl)}$ – boundary layer value.

(a) $n_2 = 3$ (b) $n_2 = 4$ (c) $n_2 = 5$

Fig. 8 Comparison between profiles of C and $C(bl)$ versus y at various x-values ($a = 0.1, x_e = 100, n_2 = 4$) – $C_{(bl)}$ – boundary layer value.

(a) $x = 10, 20$ (b) $x = 50, 100$ (c) $x = 500, 1000$

Fig. 9 Comparison between steady state values of boundary layer thickness ($a = 0.1, x_e = 100$) – (bl) – boundary layer value.

Fig. 10 Comparison between steady state profiles of C_b and $C_b(bl)$ for various x_e-values

($a = 0.1$) – (bl) – boundary layer value.

Fig. 11 Schematics of the boundary layers and the typical salinity profile.

Fig. 12 Shape of the boundary layer at various t-values ($a = 0.1, 0.5, x_e = 100$)

(a) $t = 100$ (b) $t = 1000$ (c) $t = 1000$; the spear-head region

Fig. 13 Shape of the various boundary layers at $t = 1000$ for various x_e-values ($a = 0.1$)

Fig. 14 Shape of the various boundary layers at $t = 5000$ ($a = 0.1$, $x_e = 100$)

(a) the complete domain (b) the spear-head region

Fig. 15 Shape of the various boundary layers in the steady state region for various x_e-values

(a) $a = 0.1$ (b) $a = 0.5$

Fig. 16 Comparison between the salinity penetration according to the boundary layer and numerical simulations

(a) comparison when longitudinal dispersion is neglected

(b) comparison while considering longitudinal dispersion

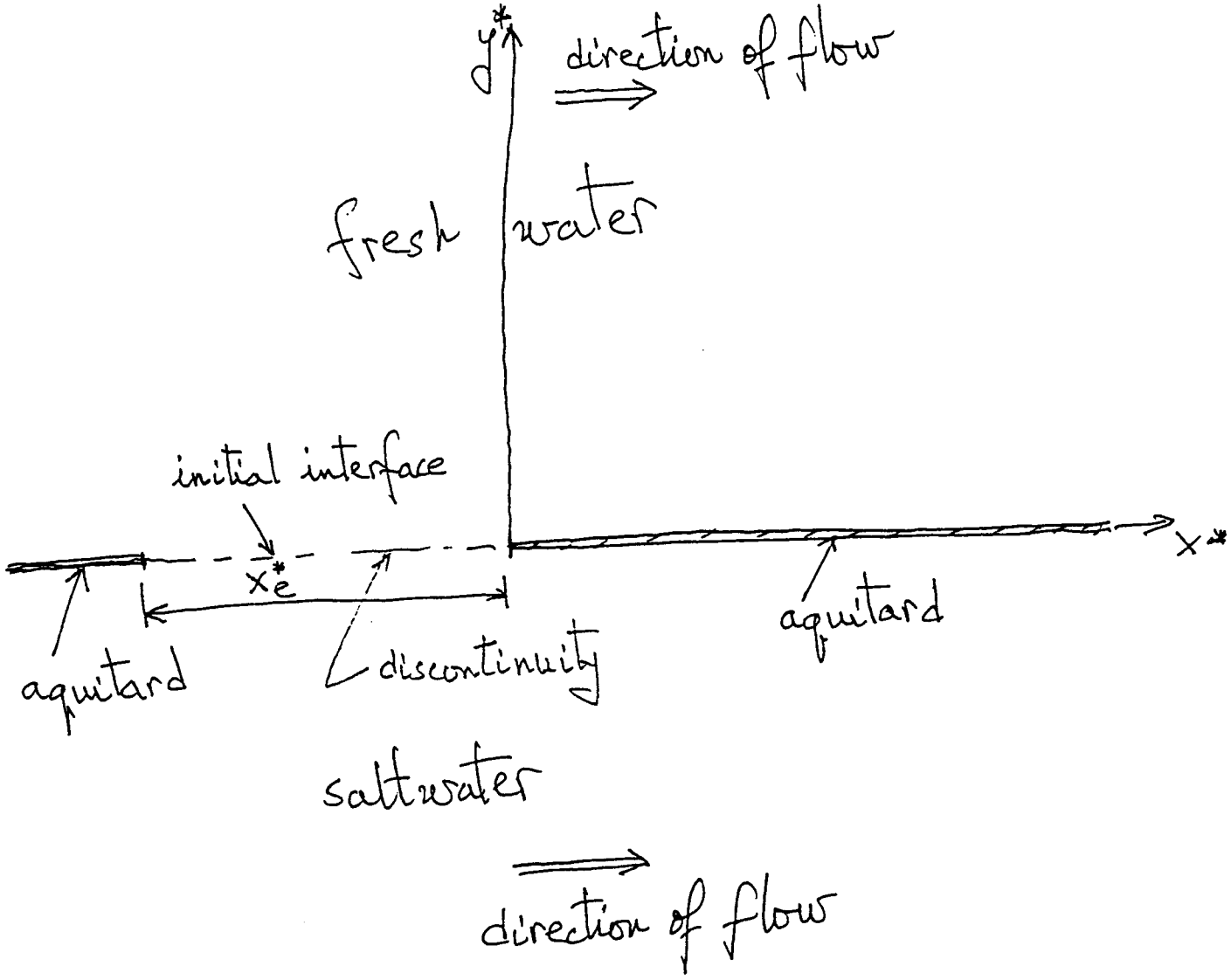
y*
direction of flow
fresh water
initial interface
x*
x*e
aquitard
discontinuity
aquitard
saltwater
direction of flow

Fig. 1

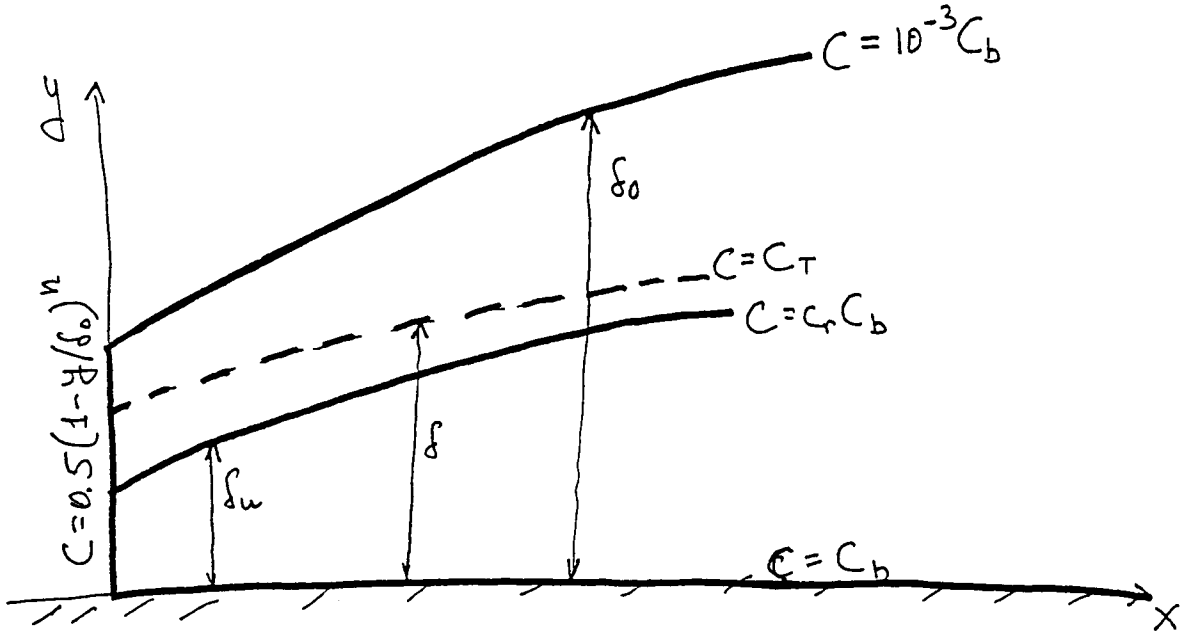

Fig. 2

Fig. 3(a)

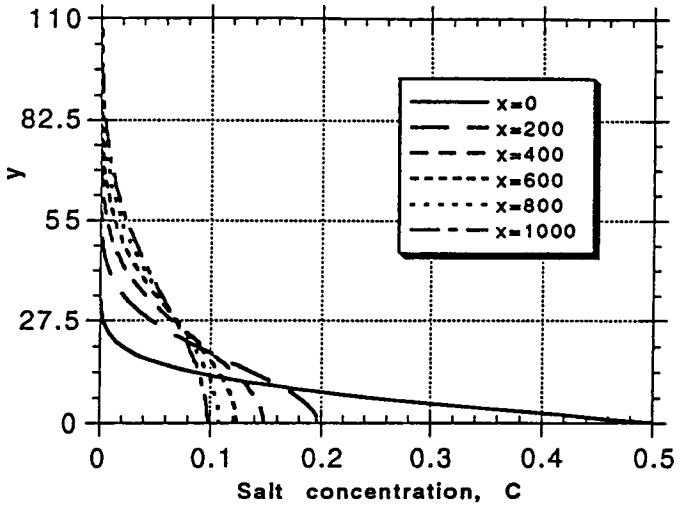

Fig. 3(b)

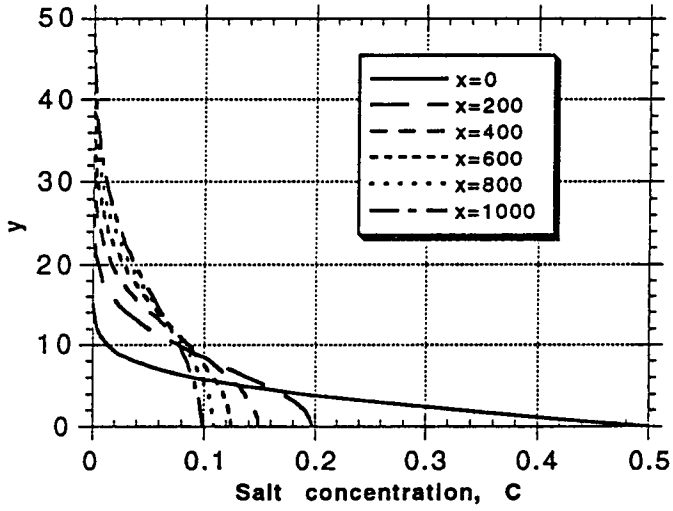

Fig. 3(c)

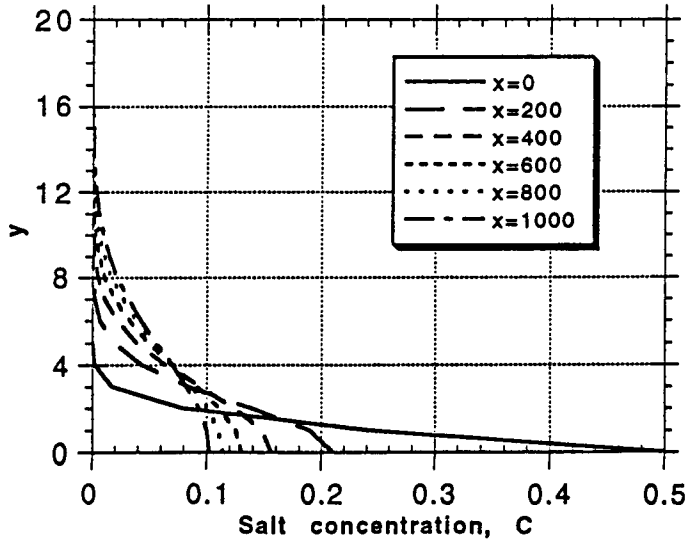

Fig. 4(a)

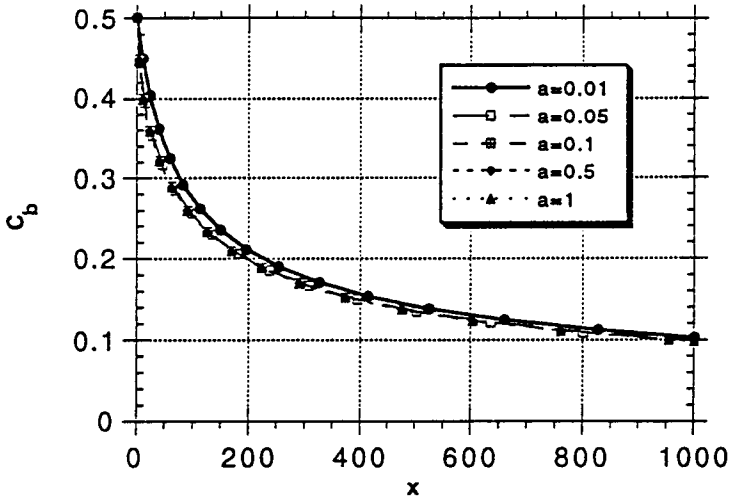

Fig. 4(b)

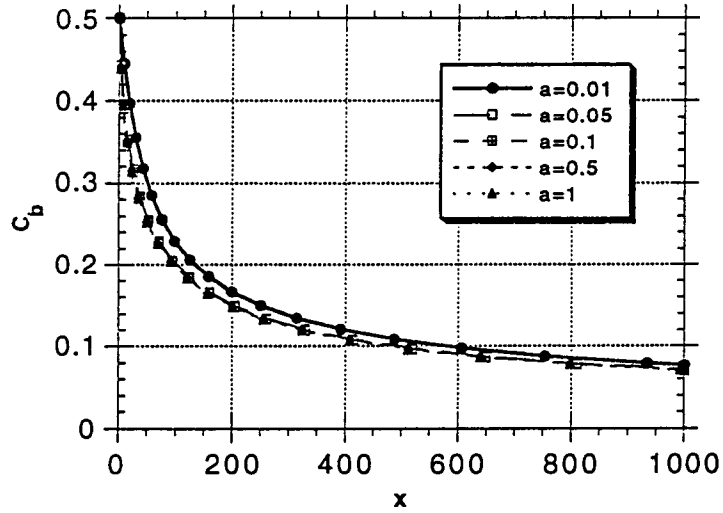

Fig. 4(c)

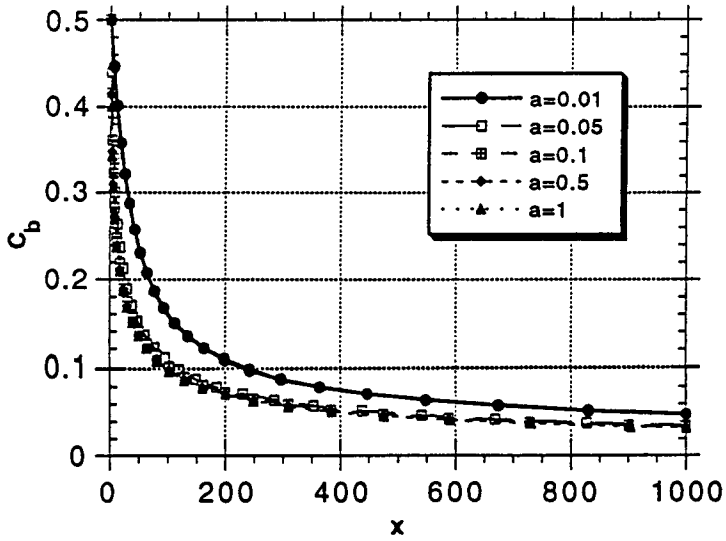

Fig. 5

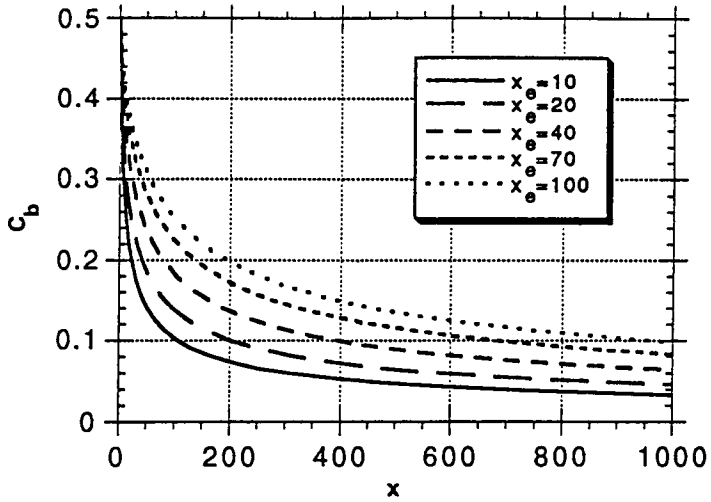
0.5
0.4
0.3
0.2
0.1
0
C_b
x_e=10
x_e=20
x_e=40
x_e=70
x_e=100
0
200
400
600
800
1000
x

Fig. 6

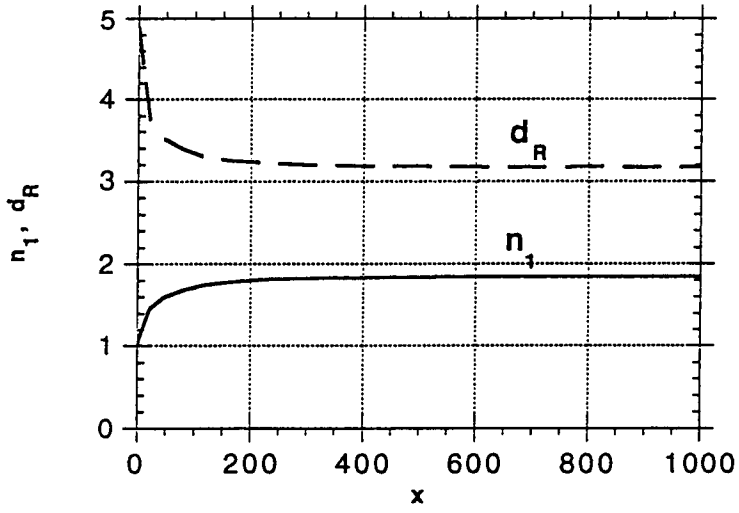
5
4
3
2
1
0
n_1, d_R
d_R
n_1
0
200
400
600
800
1000
x

Fig. 7(a)

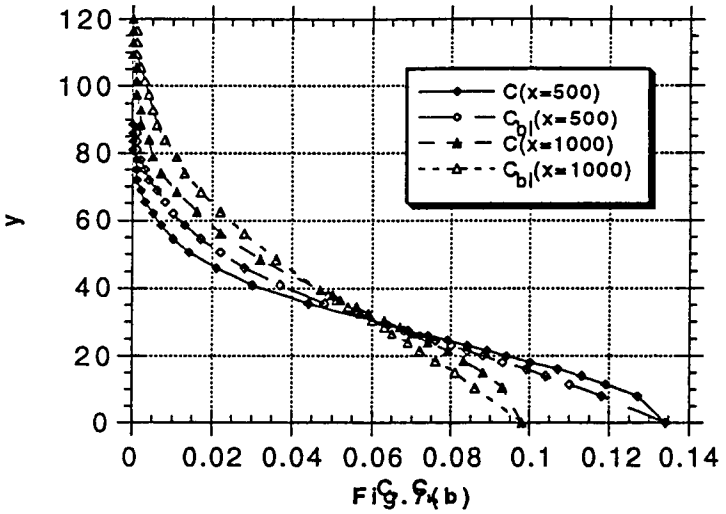

Fig. 7(b)

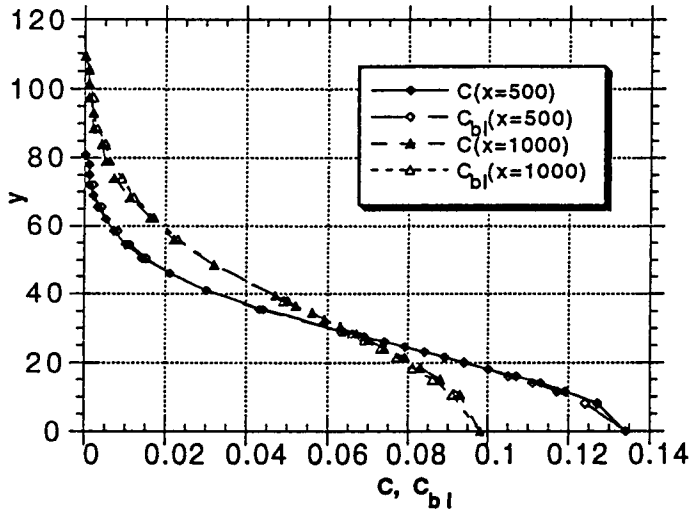

Fig. 7(c)

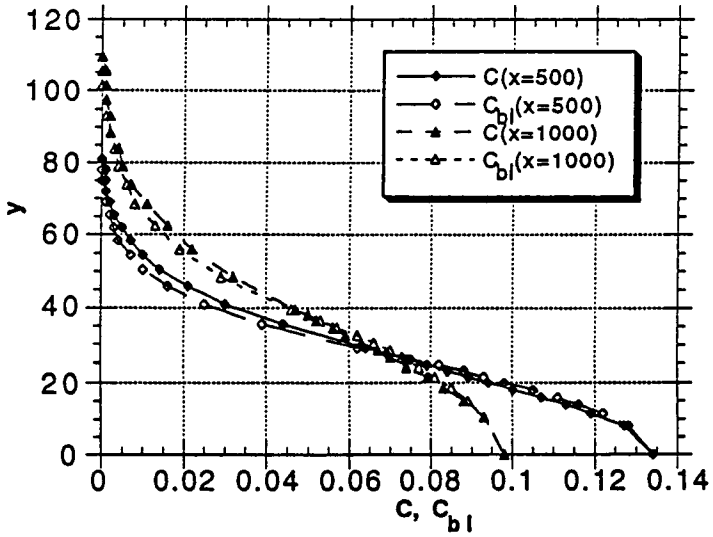

Fig. 8(a)

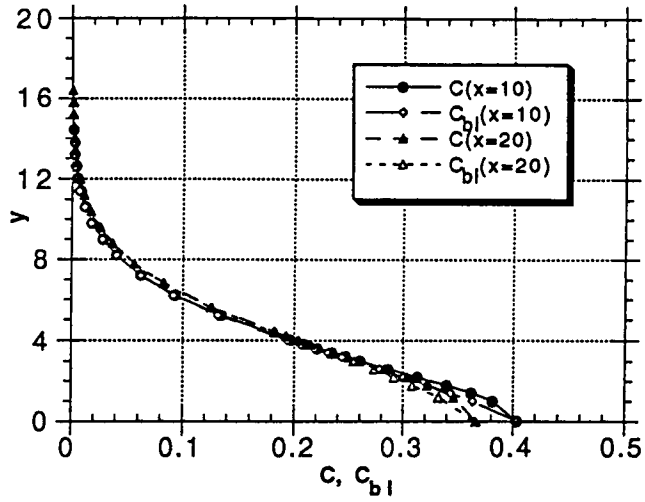

Fig. 8(b)

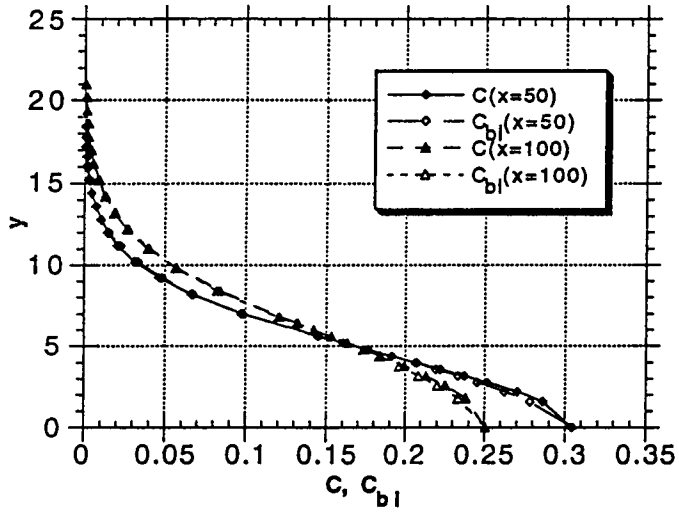

Fig. 8(c)

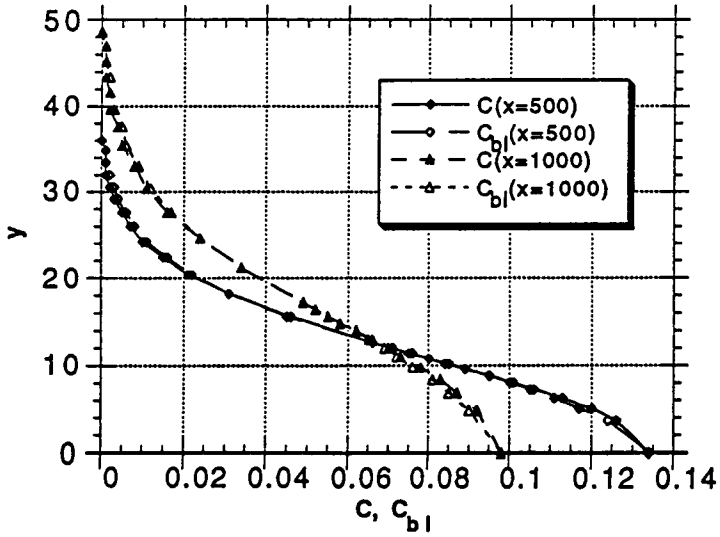

Fig. 9

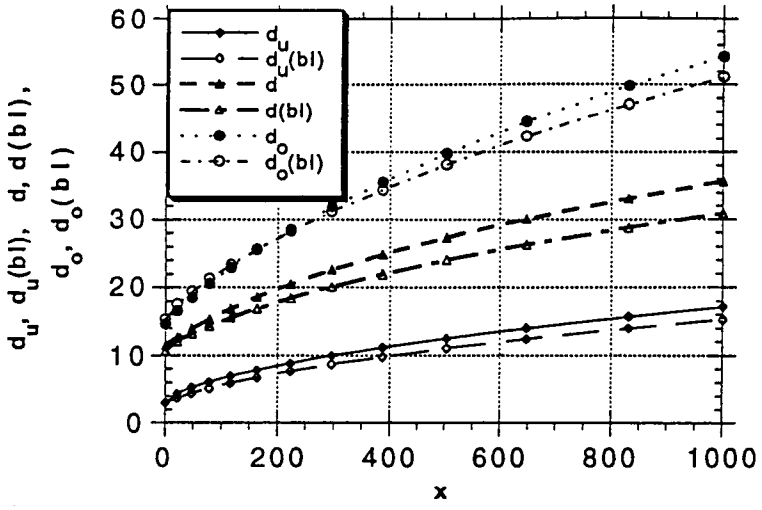
d_u
$d_u(bl)$
d
$d(bl)$
d_o
$d_o(bl)$
d_u, $d_u(bl)$, d, $d(bl)$, d_o, $d_o(bl)$
0
10
20
30
40
50
60
0
200
400
600
800
1000
x

Fig. 10

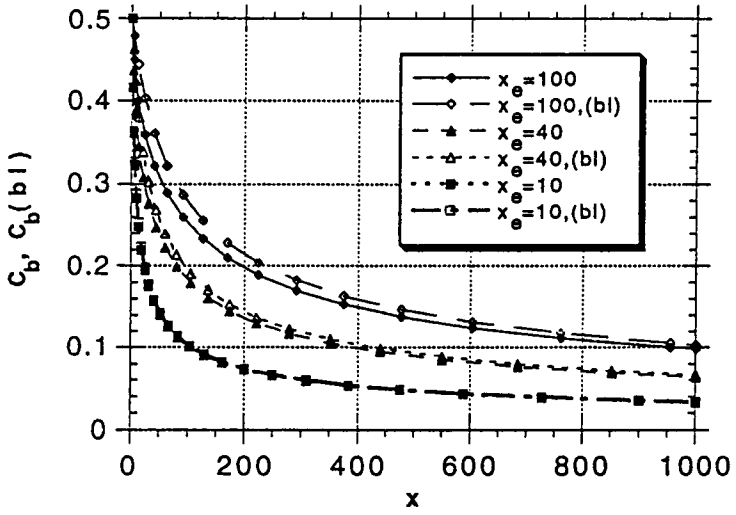
x_e=100
x_e=100,(bl)
x_e=40
x_e=40,(bl)
x_e=10
x_e=10,(bl)
C_b, $C_b(bl)$
0
0.1
0.2
0.3
0.4
0.5
0
200
400
600
800
1000
x

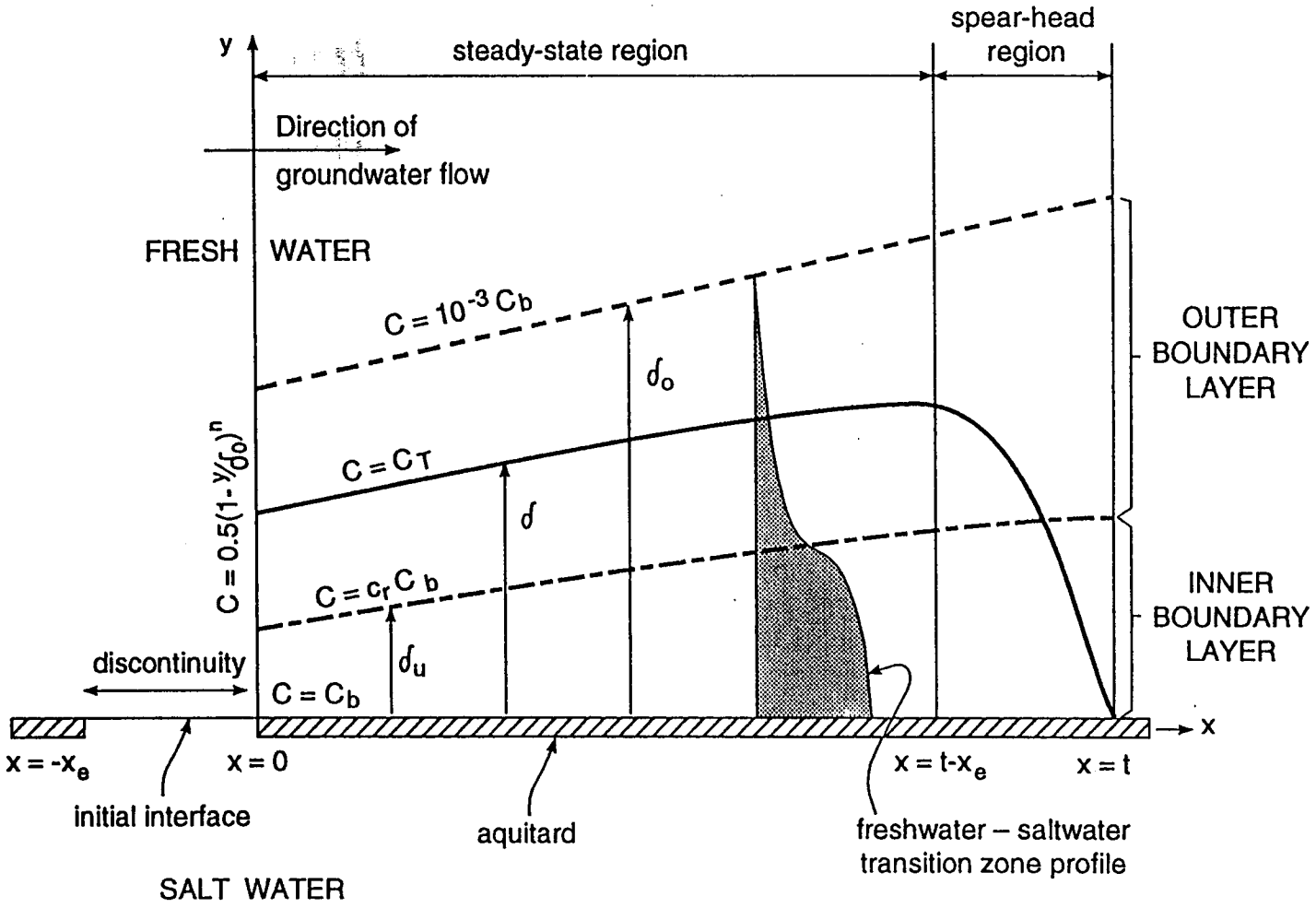

Figure 11. Basic conceptual framework of the Top Specified Boundary Layer (TSBL) model. See text for explanation of symbols.

Fig. 12(a)

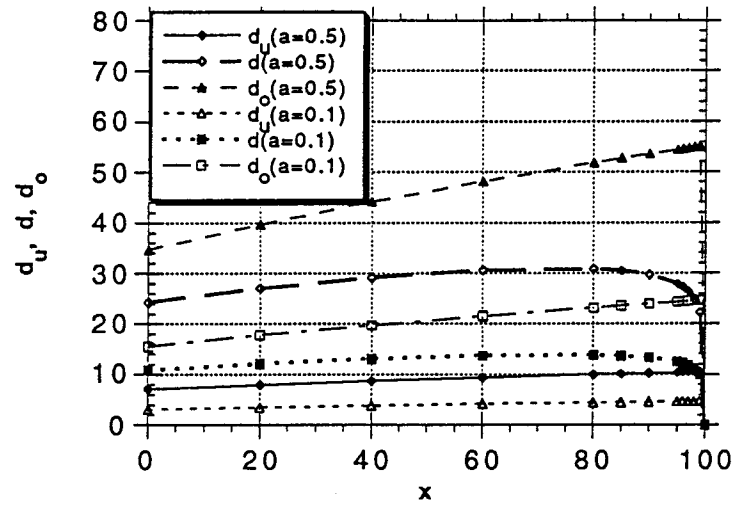

Fig. 12(b)

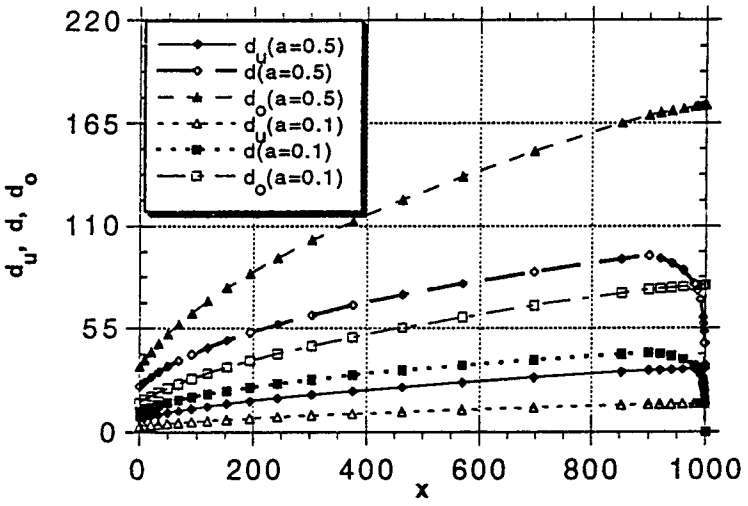

Fig. 12(c)

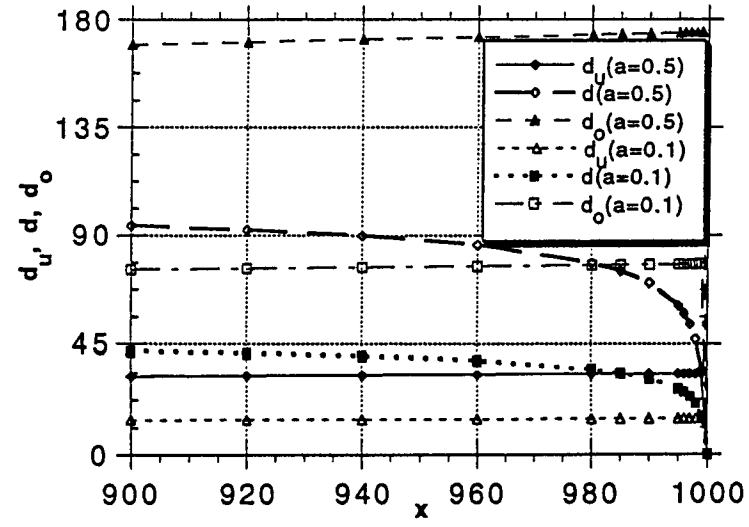

Fig. 13

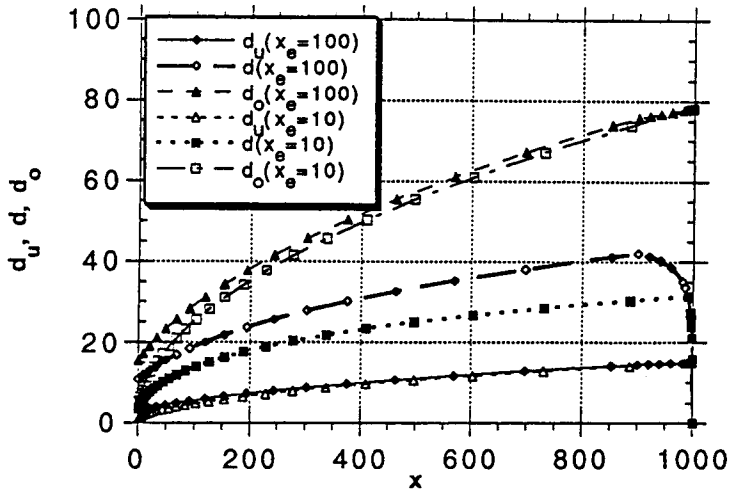

Fig. 14(a)

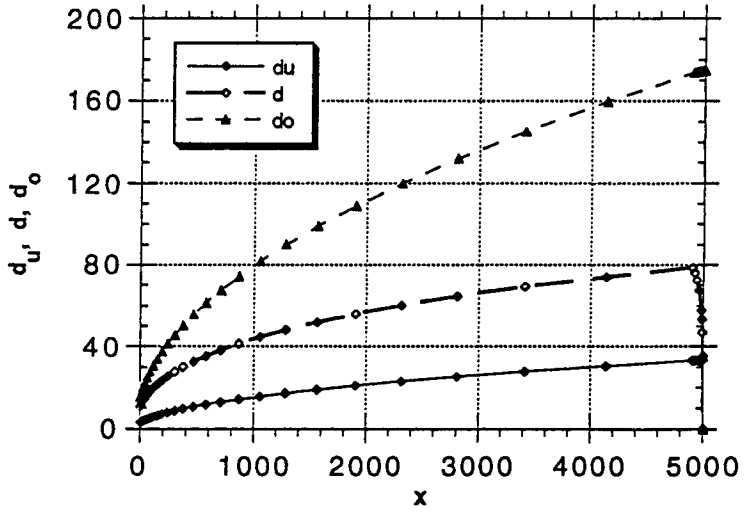

Fig. 14(b)

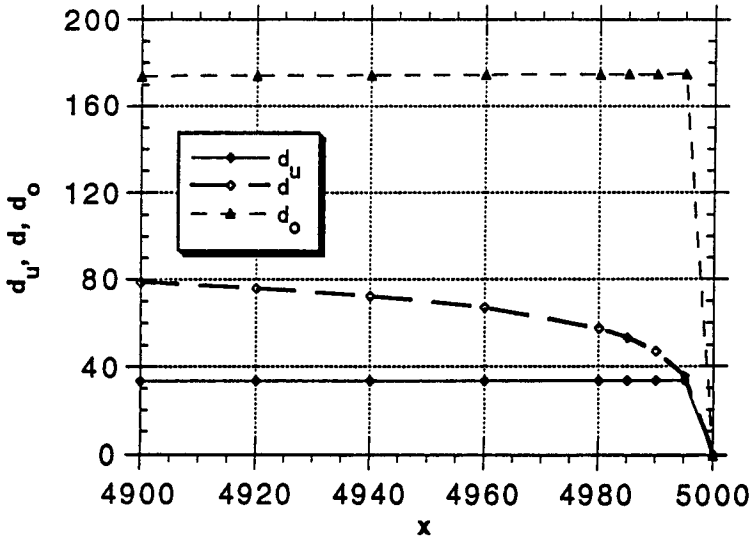

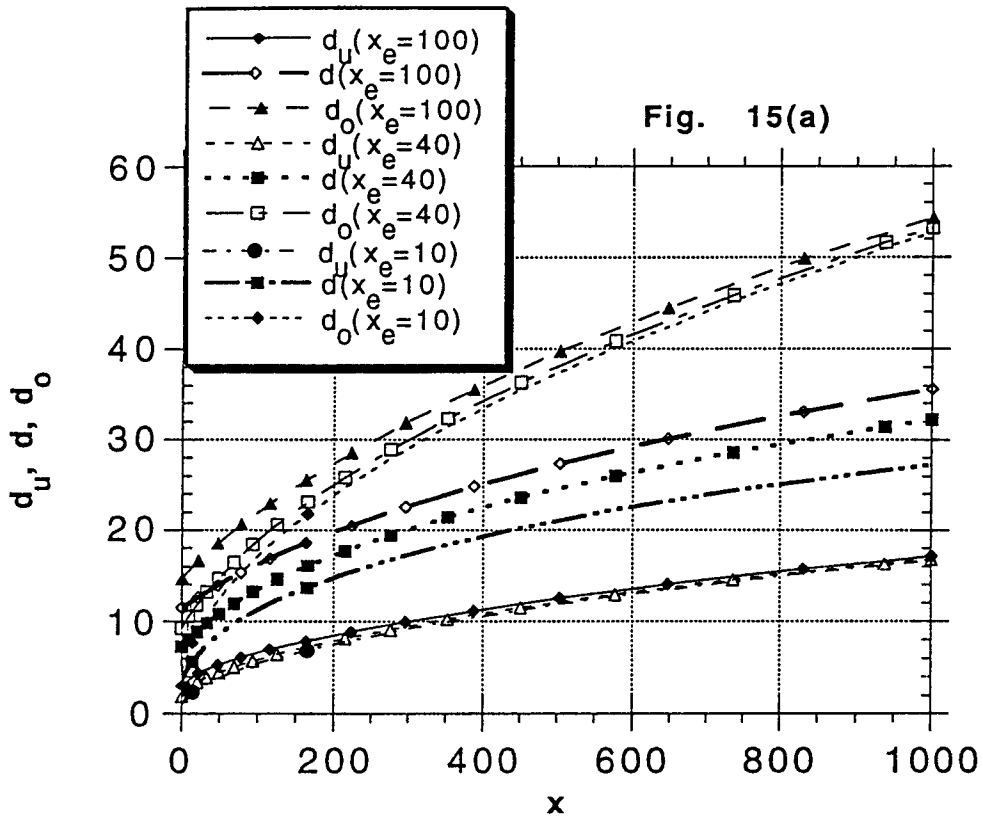

Fig. 15(a)

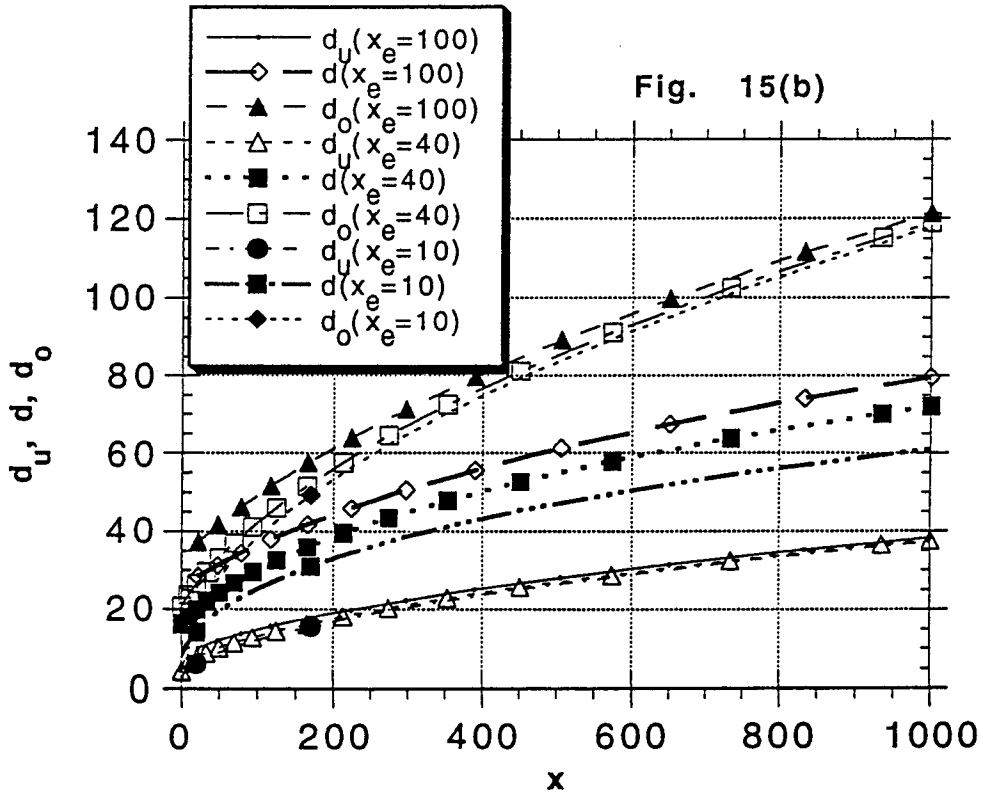

Fig. 15(b)

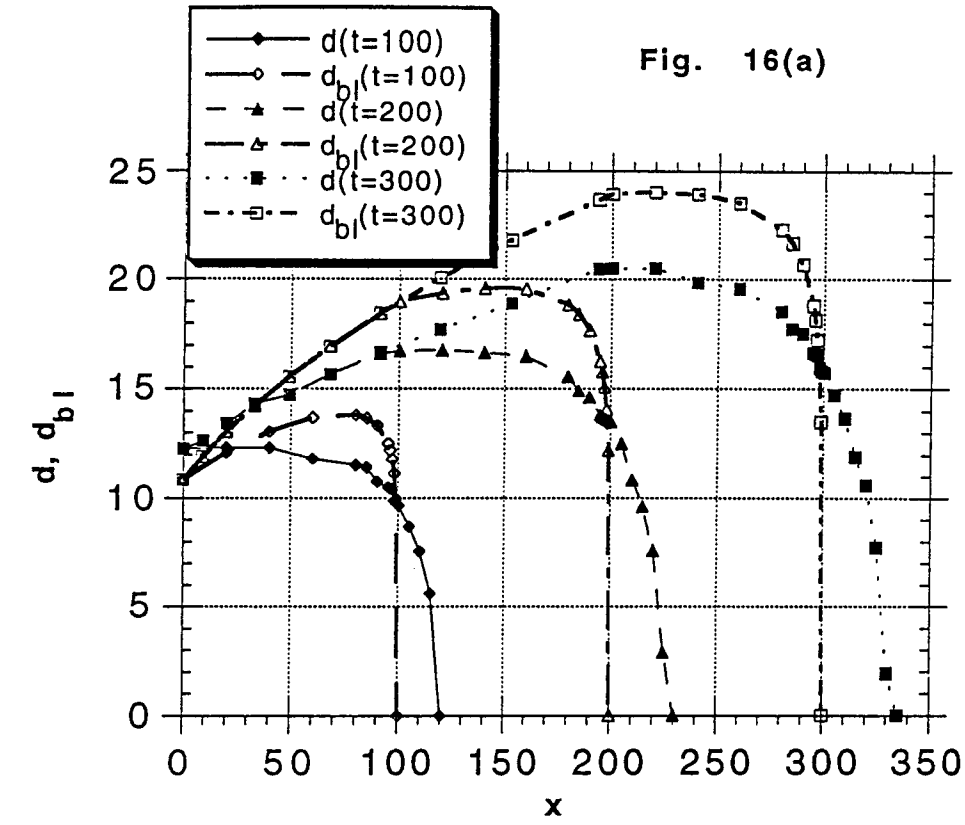

Fig. 16(a)

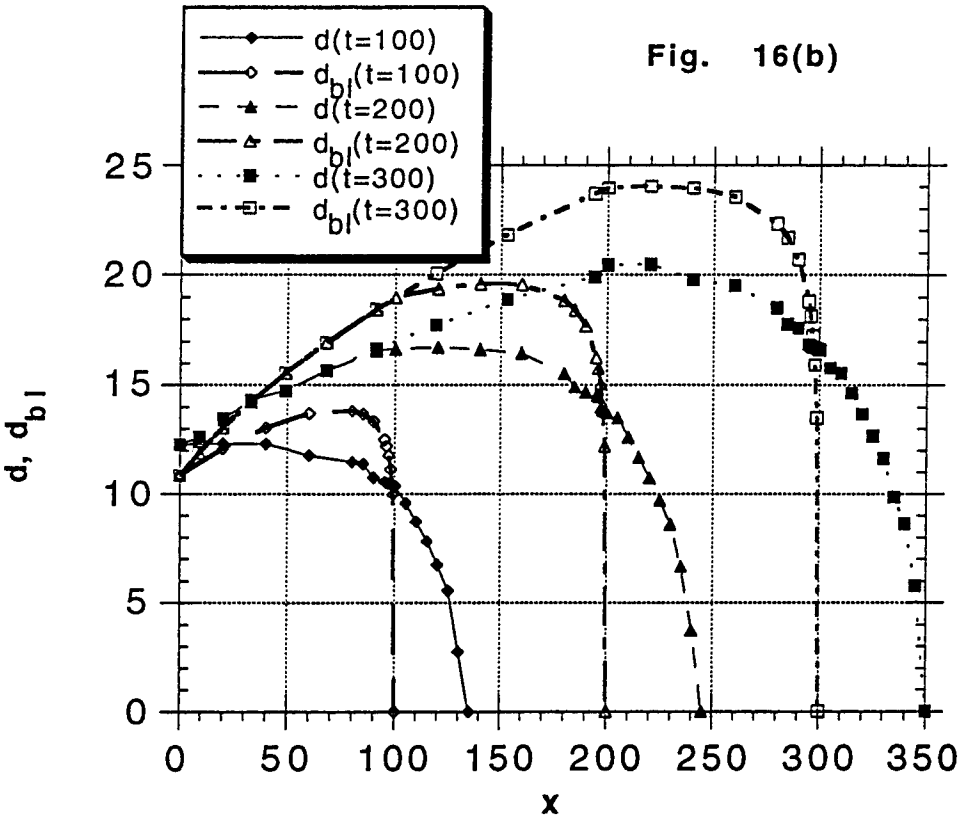

Fig. 16(b)